DOI: 10.14750/ME.2021.004

UNIVERSITY OF MISKOLC
Mikoviny Sámuel Doctoral School
of Earth Sciences

FACULTY OF
EARTH SCIENCE
AND ENGINEERING

Institute of Mineralogy and Geology

Complex geochemical-mineralogical behaviour of sulphidic mine wastes - a case study based on sampling from Bolivian mine sites and Recsk, Hungary

PHD DISSERTATION

FERENC MÓRICZ

Internal consultant: Dr. Ferenc Mádai, associate professor, University of Miskolc

External consultant: Dr. Ingar Walder, associate professor, New Mexico Tech, USA

Head of the doctoral school: Prof. Dr. Péter Szűcs, professor, University of Miskolc

2020. December
Miskolc, Hungary

DOI: 10.14750/ME.2021.004

TABLE OF CONTENT

DOI: 10.14750/ME.2021.004

DOI: 10.14750/ME.2021.004

OBJECTIVES

The mining activities are as old as human history, it started with the Stone Age and then by the discovery of metals, which can be strongly linked to ancient mineral exploitation. The mining-related serious environmental problems are dominantly modern. The manual mining technique produced such a small amount of mining waste material, which can be handled by natural processes. This fragile balance changed as modern mining techniques started to produce huge amount of waste during a short time. Globally acidic rock drainage (ARD) effects are recorded after several years of deposition as the unstable iron sulphides started oxidizing under surface conditions.

In this PhD dissertation, the different chapters are focusing on different types of characterization of the oxidizing system from different point of views. The common in them is the mineralogical or geochemical characterization using several new methods. They show much further than regular characterization, moreover, they can be adaptable and used in other cases and studies on other areas of geochemistry.

The guiding principle of this dissertation was to make new specific theses and calculations, via testing and proving them on samples in case studies. I wanted to reflect that these sulphidic oxidizing systems can result in serious or even catastrophic environmental impacts or contaminations, which frequently cannot be reversed, stopped or even mitigated.

With the correctly chosen methods it can be characterized from point of long term behaviour, so all the above mentioned impacts can be prevented by well-established mining waste material management and handling.

The first in this to reflect that the ARD effect apparently not always creates acidic condition. In presence of sufficient neutralizing minerals, the acidic condition is buffered, so acidic impacts will be not seen. Theoretically, even if the system has circumneutral pH, the sulphide oxidation can strongly take place. This should indicate a necessary change of thinking in waste management, if the monitoring of the pH value is not enough, because in spite of the circumneutral pH, strong oxidation reactions can be formed. If the system contains polymetallic sulphidic ores, such as galena, sphalerite, chalcopyrite, arsenopyrite, etc., the weathering of them can discharge to a huge load of heavy metals (Pb, Zn, Cd, Cu, As, etc.) into nature, through the (ground)water to the biosphere. The hazard of these heavy metals, that most of them stay dissolved form even in circumneutral pH condition.

To understand the oxidizing system well, it is essential to know the exact mineralogical composition of the sample. A new method, which is based on the combination of X-ray powder diffraction (XRD) and sequential chemical extraction (SCE), can be the key in the sharp determination of mineralogical composition, even in case of tiny concentration. My aim is to describe and show the method in details. Moreover, via case studies, the applicability of the combined method for altered sulphidic mine waste

DOI: 10.14750/ME.2021.004

materials will be proved. A further aim is to prove the presence of sulphides by calculation even if they are in extremely low concentrations.

Besides knowing the mineralogical composition the determination of the sulphide oxidizing rate is also indispensable. Based on the parameters of the seepage, resulting in humidity cell test, different modes of calculations will be made. The pH, the dissolved sulphate and iron content defines the pyrite oxidation. Thus by the use of these equations will be defined, which can be used and adaptable in all kinds of column and humidity cell tests. Apart from the seepage based modes, another solution will be also created, which is based on the oxygen consumption of the pyrite oxidation. The applicability of these equations, which can be determined the oxidation rate with, show further than the border of this PhD thesis.

It is also my objective to show how much additional information can get out from the humidity cell test if it is used several times on the same sample in consecutive years. The trends point much more forward than the results in the individual years. The comparison of them can give a reliable forecast of the real long term behaviour for the sample, showing the changes in the function of the long term future.

Further analysis shows how mineralogical inhomogeneity can be formed in the filling of the humidity cells in case of relatively fine-grained samples. Moreover, it will be shown, that the appearance of the inhomogeneity is a self-driven process, as the porosity and permeability changes significantly, more inhomogeneity will be created. In the case studies, it is pointed out that not every sample is suitable for humidity cell test, as the grain size is a limiting factor.

I would like to highlight also the possible applicability of these methods, in different other areas of geochemistry. Moreover, also important is to remind the necessity of the proper mining waste management to be able to avoid at least those pollutions which can be forecasted by modelling, simulation or calculation.

DOI: 10.14750/ME.2021.004

I. SULPHIDE - SULPHATE ALTERATION IN SULPHIDIC MINING WASTES

1.1. Introduction

Before the presentation of the measuring, results and discussions, necessary to take an insight, especially from point of chemistry. Without the information of which reactions can appear and what processes can come into existence, the oxidizing system cannot be characterized. Also essential to locate the individual parts of the system in the circle of the dissolution - (transportation) - precipitation. To be able to do this, necessary to well understand the chemical reactions and their moving forces in details. Because of the topic of this PhD thesis, the main focus will be only on the sulphide alterations.

In the last four decades, the pyrite oxidation caused Acid Rock Drainage (ARD) has become the leading environmental problem in the sulphidic mining industry. In the sulphidic mine wastes, the principal weathering process is the sulphide oxidation, which results low pH. This acidic environment creates a much more serious effect – than the low pH itself – as the heavy metal mobility increases dramatically. (Evangelou and Zhang 1995) Further, an aggravating circumstance can be if the heavy or toxic metals are in the structure of the oxidizing sulphides, because in this case by the alteration of the sulphides directly lead to quick and high rate of heavy or toxic metal mass load on nature. (Ferguson and Robertson 1994; Jambor 2000; Jennings and Dollhoph 1995; Plumlee 1999; Price 2003)

In the mining wastes the most common iron-bearing sulphides are the pyrite and pyrrhotite, which are usually stored in dumps, where are exposed to atmospheric water and oxygen, thus (quick) oxidation processes could take place. However, if neutralizing minerals are available, the acid production can be buffered, so the heavy metal mobility would be reduced. However, in the porous of the waste rock material in the presence of water and oxygen, the surface of the pyrite starts oxidizing thus creating an acidic micro-environment. Although in presence of enough calcite, which is the quickest neutralizing mineral, the material does not show acid production, till the calcite is able to maintain the pH, but the sulphide oxidation can be still present. (Al et al. 2000; Jambor et al. 2003; Jurjovec et al. 2002)

In this chapter not only the sulphide-sulphate alteration linked to the material of the mining wastes will be described, but also that type of precipitation, where the pH is high enough to let the formation of sulphate, hydroxide, oxy-hydroxide, oxide or a mixture of them.

1.2. Sulphide oxidation

The sulphides are the most important ore minerals, which are created in magmatic or postmagmatic processes. Various forms of sulphate can be formed, as the cation position consists of one, like pyrite or marcasite (FeS_2), or two, such as chalcopyrite ($CuFeS_2$). From point of ARD the pyrrhotite ($Fe_{1-x}S$), galena (PbS) and sphalerite (ZnS) are also important. Although the last two are not liable for acid production, but their prevalence makes them notable. In this chapter, those will be taken consideration,

DOI: 10.14750/ME.2021.004

which are responsible for ARD or could cause other environmental problem by their alterations. Ore beneficiation processes selectively extract minerals of commercial value and exclude minerals that cannot be economically recovered. The most abundant sulphide minerals in most tailings impoundments are pyrite (FeS_2) and pyrrhotite ($Fe_{(1-x)}S$). Other Fe-sulphide minerals, including marcasite (orthorhombic FeS_2), are encountered rarely. Because these minerals are the most abundant, they are the most common source of acidic drainage. (Blowes et al. 2003/a; Jambor 1994; Mikhlin et al. 2002)

Mill tailings can contain very large accumulations of these Fe-sulphide minerals, such as pyrite and pyrrhotite, but other sulphide minerals are also, such as sphalerite (ZnS), chalcopyrite ($CuFeS_2$), galena (PbS) and arsenopyrite (FeAsS), which can cause toxic or strongly toxic metal mass load. The presence of some of these minerals may be attributed to inefficiencies in recovery processes, or commonly, these minerals are deposited as waste because they are under the cut off grade. (Blowes et al. 2003/a)

In the sulphidic ore bodies the amount of arsenopyrite, chalcopyrite, galena and sphalerite are conditionally not as significant as pyrite or pyrrhotite. Moreover except the iron-containing sulphides, such as arsenopyrite or chalcopyrite, are not acid producers, if they start oxidizing in presence of O_2 and H_2O. But if the oxidizer agent is the Fe^{3+} in the oxidation process, all of these minerals work as acid generators, independently wether they contain iron or not in their mineral structure. (USEPA 1994)

1.2.1. Abiotic and biotic type of pyrite and sulphide oxidation

Although the pyrite weathering on surface condition, if the oxidizer is the oxygen, could be described with a quite simple equation, the parameters of the oxidizing system depend on several physical, chemical and biological processes (described in further topics). One of the first equation of the pyrite oxidation (Eq. 1) was created by Nordstrom in 1982, but this was made for abiotic condition:

$$FeS_2 + \frac{7}{2}O_2 + H_2O \rightarrow Fe^{2+} + 2SO_4^{2-} + 2H^+ \quad (1)$$

When the pH of the solution exceeds 7, low concentrations of ions derived from the partial oxidation of sulphide-sulphur (e.g. sulphite /SO_3^{2-}/ and thiosulphate /$S_2O_3^{2-}$/) are detected in solution. (Goldhaber 1983) These partial oxidation products are subsequently oxidized to SO_4^{2-}. (Moses et al. 1997) Under low pH conditions, these partial oxidation products are not detected. (Bonnissel-Gissinger et al. 1998)

By the chemical behaviour and the type of the end products, the sulphide oxidation can be divided into two reaction types. If the pH is above 3-4, the free Fe ions can form secondary iron hydroxides, oxy-hydroxides or oxides. But if the pH is under pH 3-4 the free iron ion cannot form the species above, only secondary sulphate phases. This is the real process of alteration of sulphides to sulphate, but the sulphide alteration to oxides is also an important process in nature, as well as in the mine wastes. If the iron-hydroxide, iron-oxy-hydroxides or iron-oxides form in significant amount, gossan can be formed. The Fe^{2+} released by pyrite oxidation may be further oxidized to Fe^{3+}, decreasing the acidity by consuming H^+ (Eq. 2). For this alteration, the Fe^{2+} ion needs special conditions, such as low pH (under

DOI: 10.14750/ME.2021.004

2-2.5), although the Fe^{2+}-Fe^{3+} alteration is only redox potential dependent. Moreover, this alteration is strongly catalysed by the Acidobacillus Ferrooxidans, which is discussed in detail later, in this chapter. Moreover, because the high acidity (Edvards et al. 1999, 2000; Schleper et al. 1996) high dissolved metal concentration can be in the seepage, as a result of the dramatically increased metal mobility.

$$Fe^{2+} + \frac{1}{4}O_2 + H^+ \rightarrow Fe^{3+} + \frac{1}{2}H_2O \quad (2)$$

If the pH is above 4, the Fe^{3+} may be hydrolysed and precipitate as Fe^{3+}-hydroxide, through reaction (Eq. 3) of the form, although the limit pH for precipitation depends on the concentration of the Fe^{3+} in the drainage, but in general the Fe^{3+}-hydroxide only can form, if the pH is higher than 3-3.5.

$$Fe^{3+} + 3H_2O \rightarrow Fe(OH)_3 + 3H^+ \quad (3)$$

Summarizing equations (Eq. 1, 2 and 3), a more complex reaction (Eq. 4) can be described:

$$FeS_2 + \frac{7}{2}O_2 + H_2O \rightarrow Fe(OH)_3 + 2SO_4^{2-} + 2H^+ \quad (4)$$

Although iron hydroxide appears as a byproduct of sulphide oxidation, the formation of goethite (Eq. 5) is much more common, thus the importance in weathering of tailings is higher. It surrounds the primary grains of pyrite or pyrrhotite and replaces these minerals' surface. (Jambor 1994; Jambor 2003)

$$Fe^{3+} + 2H_2O \rightarrow FeOOH + 3H^+ \quad (5)$$

From point of geochemistry, there is no difference whether Fe^{3+}-hydroxide ($Fe(OH)_3$) or goethite (FeOOH) is formed, because during precipitation, in both reaction (Eq. 3 and 5) one mole of Fe^{3+} produces 3 moles of acid (H^+). On the other hand, the Fe^{3+}-hydroxide can be transferred to oxy-hydroxide (Eq. 6), as goethite by water loss and even further to oxide, as hematite (Eq. 7).

$$Fe(OH)_3 \rightarrow FeOOH + H_2O \quad (6)$$

$$2FeOOH \rightarrow Fe_2O_3 + H_2O \quad (7)$$

Bonnissel-Gissinger et al. (1998) made surface analyses of oxidizing pyrite. This indicates that precipitates containing Fe+O+OH with a stoichiometry similar to FeOOH are the predominant form of Fe^{3+} on the surface of freshly oxidized pyrite. Electron microprobe analysis measurements proved that this secondary produced precipitation is really built up from Fe, O and OH. This mineral has no real crystal structure (amorphous), thus it is not detectable by XRD analysis. This fact is proved by us as well in Chapter 10.2.2, as on strongly oxidized, reddish-brown samples none of the secondary iron minerals were detected, but about 7 % of amorphous content was measured.

The Fe^{3+} generated by oxidation of Fe^{2+} also reacts with pyrite through a reaction (Eq. 8), moreover, it will be the primer oxidizer agent and not the O_2. (Singer and Stumm 1970) The Fe^{3+} type of pyrite oxidation is biotic because the Fe^{2+} - Fe^{3+} alteration (Eq. 2) is catalysed by bacterial activity.

$$FeS_2 + 14Fe^{3+} + 8H_2O \rightarrow 15Fe^{2+} + 2SO_4^{2-} + 16H^+ \quad (8)$$

DOI: 10.14750/ME.2021.004

Whether pyrite oxidation proceeds on abiotic (Eq. 1) or biotic (Eq. 8) depends on the chemical conditions in solution and the pyrite surface. Singer and Stumm (1970) published that Fe^{3+} is the dominant oxidant under low pH conditions. This hypothesis is supported by more studies of the surface chemistry of oxidizing pyrite, which indicate the presence of Fe^{3+} on the pyrite surface and an absence of O_2, suggesting that Fe^{3+} is the primary oxidant. (Bonnissel-Gissinger et al. 1998) Under these conditions, abiotic oxidation of Fe^{2+} to Fe^{3+} is slow and the rate of Fe^{2+} oxidation becomes the rate-limiting step in sulphide oxidation. (Blowes et al. 2003/a; Singer and Stumm 1970) Later, in Chapter 8, the differences of the two equations will be discussed from point of the oxidation rate calculation.

The chemistry of drainage from a mine site is the result of the competing processes of acid generation and acid neutralization, if there is at all. In nature, the chemical properties, the reacting surface and the oxidation of sulphide minerals proceeds with either dissolved oxygen (O_2) or ferric iron (Fe^{3+}) acting as the oxidizing agents. From point of ARD effect the iron-containing sulphides, such as pyrite, marcasite, pyrrhotite, chalcopyrite or arsenopyrite, and the iron not containing ones, like sphalerite or galena, have different behaviour (Table 1). They can oxidize on both ways, through oxidizing agent of O_2 or Fe^{3+}, but the first types are more unstable than the second. The iron-containing sulphides produce acidity in both types of reactions. Those sulphides, which have no iron in their structure, like galena, sphalerite, etc., are not acid producers if O_2 is the oxidizer agent. The situation turns, if the Fe^{3+} acts as the oxidizer, because even the iron non containing sulphides become acid producers, thus they will be also responsible for acidic environment. (Jambor et al. 2003; Jurjovec et al. 2002; Rimstidt and Vaughan 2003)

	Iron containing sulphides (pyrite, marcasite, arsenopyrite, etc..)	***Iron not containing sulphides*** (galena, sphalerite, etc..)
$\boldsymbol{O_2}$, as oxidizer agent	acid production	no acid production
$\boldsymbol{Fe^{3+}}$, as oxidizer agent	acid production	acid production

Table 1: Outcome of the oxidizing reactions in the function of the two different oxidizer agent (O_2 and Fe^{3+})

If the chemical parameters are appropriate, such as high enough concentration, ideal pH and redox potential, the dissolved ions can form different types of solid secondary minerals. These vary from hydrated or crystal water free sulphates, hydroxides, oxy-hydroxides to oxides or some type of mixture of them. If the toxic heavy metals stay in dissolved form in solution or in solid phase, but as easily soluble sulphates, can be biologically hazardous. (INAP 2009) If they can find a pathway toward living organisms, plants, animals or humans, cause health injury or even death. The situation is even worse if the pH is too low for the dissolved ions to form solid phases. In this case the possibility of further transport is higher even in larger doses, moreover, the pathway for living bodies is easier.

Near pyrite, other iron-containing sulphides can be oxidized on the abiotic way, so by O2. The most important are the pyrrhotite (Eq. 9) and the arsenopyrite (Eq. 10). (Seal et al. 2000) The pyrrhotite because of its unstable crystal structure, resulted in no constant chemical composition is very sensitive against weathering, thus it will oxidize quickly. (Becker et al. 1997; Janzen et al. 2000; Pratt et al. 1994)

DOI: 10.14750/ME.2021.004

$$Fe_{1-x}S + \frac{2-x}{2}O_2 + xH_2O \rightarrow (1-x)Fe^{2+} + SO_4^{2-} + 2xH^+ \quad (9)$$

$$4FeAsS + 13O_2 + 6H_2O \rightarrow 4H_2AsO_4 + 4H^+ + 4SO_4^{2-} + 4Fe^{3+} \quad (10)$$

If the Fe^{3+} is the oxidizer agent (abiotic condition), near the acid producers by O^2, such as pyrrhotite (Eq. 11) and chalcopyrite (Eq. 12), all of the sulphides, which does not contain Fe became acid producers, such as galena (Eq. 13) and sphalerite or wurtzite (Eq. 14). Although the lead sulphide is absolutely free of iron, in the zinc sulphide some iron can build in, but the amount of this mineral is much lower than pyrite, and usually, it is separated because of its Zn content, thus it usually not part of the minerals of the waste dumps. This fact justifies that it is not considered as acid producer mineral, however, it produces some because of its iron content. (Jennings et al. 2000; Show et al. 1998; Thomas et al. 2003) Nevertheless, its Fe content makes it more sensitive against weathering, compared with galena.

$$Fe_{1-x}S + (8-2x)Fe^{3+} + 4H_2O \rightarrow (9-3x)Fe^{2+} + SO_4^{2-} + 8H^+ \quad (11)$$

$$CuFeS_2 + 16Fe^{3+} + 8H_2O \rightarrow Cu^{2+} + 17Fe^{2+} + 2SO_4^{2-} + 16H^+ \quad (12)$$

$$PbS + 8Fe^{3+} + 4H_2O \rightarrow Pb^{2+} + 8Fe^{2+} + SO_4^{2-} + 8H^+ \quad (13)$$

$$ZnS + 8Fe^{3+} + 4H_2O \rightarrow Zn^{2+} + 8Fe^{2+} + SO_4^{2-} + 8H^+ \quad (14)$$

If the redox potential state is low, the pyrrhotite could work as an acid consuming mineral, it eats up some H^+ (Eq. 15), so the pH will increase. Although if the net effect is considered, pyrite and Fe^{2+} is produced, which could be oxidized again, thus the system is continuous. At low energy state the galena (Eq. 16) and sphalerite or wurtzite (Eq. 17) work similarly, thus it could be acid-neutralizing minerals producing toxic hydrogen sulphide gas (H_2S), during the reaction. (Seal and Hammarstrom 2003)

$$2Fe_{1-x}S + \frac{1}{2-x}O_2 + (2-4x)H^+ \rightarrow FeS_2 + (1-2x)Fe^{2+} + (1-2x)H_2O \quad (15)$$

$$PbS + 2H^+ \rightarrow Pb^{2+} + H_2S \quad (16)$$

$$ZnS + 2H^+ \rightarrow Zn^{2+} + H_2S \quad (17)$$

The situation becomes even worse if the equation (Eq. 18) takes place because the H_2S will create an even strongerly oxidizing system. (Seal and Hammarstrom 2003)

$$Fe_{1-x}S + (2-2x)H^+ + xH_2O \rightarrow (1-x)Fe^{2+} + H_2S \quad (18)$$

In some of these sulphides contain replacing elements, such as Ni and Co in pyrrhotite or Cd in sphalerite / wurtzite. For example, between sphalerite or wurtzite (ZnS) and greenockite (CdS) have solid solution, so the Cd content can easily reach the 4-6 %.

1.2.2. Alteration products

When an unstable sulphide starts oxidizing on the surface or inside the waste dumps (Jambor and Blowes 1998), or even in deeper regions by Fe^{3+} oxidation, the dissolved ions have two possibilities. If

DOI: 10.14750/ME.2021.004

the chemical conditions are not ideal for precipitation, it can stay in dissolved form and can be transported to shorter or longer distances. It will be transported to that environment, where chemical parameters become acceptable for the precipitation, so from the dissolved form it can make solid phase. The type of this phase, whether it became a sulphate or an oxide, depends on the chemical environment.

Only specific Fe-mineral groups can be linked to the producing environments (FIG. 1), which are clearly symbolized by the graph below. The Eh-pH diagram was made with HSC Chemistry 7.0 geochemical modelling programme, by the author. Firstly, on the lowest pH (<3), but on redox potential lower than 0.8V in presence of sulphate ion hydrated ***sulphates*** will be formed – marked as ***zone "a"*** (FIG. 1) –, such as ***melanterite ($FeSO_4$*7H_2O)*** after equation 19, which is one of the most common iron sulphate. (Jamor and Traill 1963) This mineral has ionic chemical bond, thus by this weak bondage, it can be dissolved easily, as it is water-soluble sulphate (marked with double head arrow in Eq. 19). (Balarew et al. 1973; Bayless and Olyphant 1993; Siebke et al. 1983)

In lack of dissolved sulphate in the system, the iron stays in dissolved ferrous so Fe^{2+} form, until it will oxidize to ferric (Fe^{3+}) ion. Another possibility, that it will be able to create Fe^{2+} or Fe^{3+}-hydroxide, but it needs much higher pH and much lower redox potential. (Nesbit and Muir 1994) Often a mixture of ferrihydrite and goethite is formed, but the identification ot them is difficult as they are weekly crsytallized ot not at all. (Dold 2003; Golden et al. 1994; Rhoton et al. 1981; Schwermann et al. 1982)

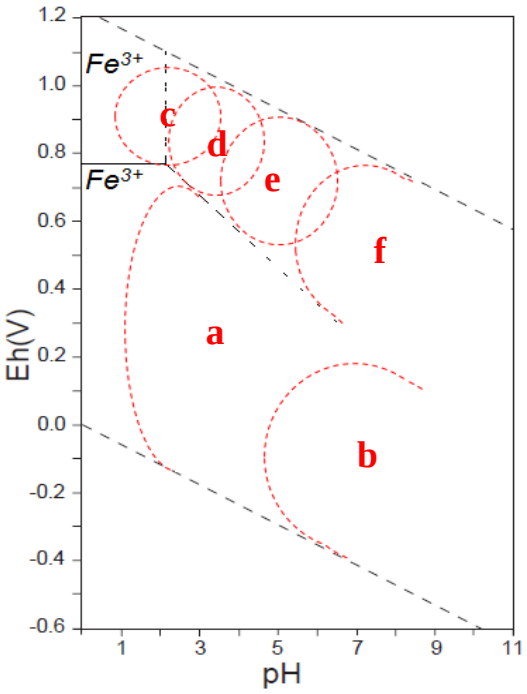

FIG. 1: Fe-minerals in the function of pH and redox potential. Abbr.: a: Fe^{2+}-sulphate; b: Fe^{2+}-hydroxide; c: jarosite; d: Fe^{3+}-hydroxide; e: Fe^{3+}-oxyhydroxide (goethite); f: Fe^{3+}-oxide (hematite)(author's own modelling)

The large variety even of the iron-sulphates (zone "a") highlights that fact, that they can appear from one crystal water, such as szomolnokite ($FeSO_4$*H_2O), even up to 22 crystal water containing member, via the melanterite ($FeSO_4$*7H_2O). (Frau 2000; Jambor et al. 2000/a; Jamieson et al. 1999)

DOI: 10.14750/ME.2021.004

$$Fe^{2+} + SO_4^{2-} + 7H_2O \leftrightarrow FeSO_4 * 7H_2O \quad (19)$$

When the melanterite starts to oxidize (Eq. 20) on surface environment in presence of water, it will form acid near the formation of Fe-hydroxide and dissolved sulphate root.

$$FeSO_4 * 7H_2O + \frac{1}{4}O_2 \rightarrow Fe(OH)_3 + SO_4^{2-} + \frac{9}{2}H_2O + 2H^+ \quad (20)$$

Usually because of the high variety of sulphides in the mine waste materials, not only iron sulphates will be formed. The high number of different cations - comes from the oxidation of the sulphides of from the alteration of the minerals of the host rocks - can form various other minerals. Only the most important ones are mentioned, to be able to characterize the mineralogy of the mine waste materials well.

When Ca^{2+} is in dissolved phase from the alteration of Ca-feldspars, clay minerals or some stronger neutralizing mineral such as calcite, in presence of sulphate ion gypsum ($CaSO_4*2H_2O$) or anhydrite ($CaSO_4$) can be formed. It doesn't need low energy and low pH, it can appear in a wide scale of the pH and redox potential scale. The solubility of gypsum is relatively high, thus this mineral has a precipitation-dissolution-transporting cycle. (Jambor et al. 2000/a; Jamieson et al. 1999)

In a simple oxidation process of galena (Eq. 21), the lead sulphate anglesite ($PbSO_4$) can appear which is always free of water, so there is no variety of crystal water content. This simple reaction makes the anglesite so common on the surface of galena. (Jamieson and Przybylowicz 1997)

$$PbS + 2O_2 \rightarrow PbSO_4 \quad (21)$$

The dissolved Zn^{2+} ion - on the model of the formation of melanterite (Eq. 19) - can form zinc sulphate with different amount of crystal water. The most common is the zincmelanterite or goslarite, are characterized with the same chemical components ($ZnSO_4*7H_2O$), but the first is from the melanterite (monoclinic) subgroup, while the second is from the epsomite (orthorhombic) subgroup. Into the zincmelanterite other medium size cations can also built in, like Fe or Cu. (Tiegeng et al. 1995) Although greenockite (CdS) is not common as a separate mineral in the polymetallic ore mineralization, but this sulphide has the solid solution with sphalerite or wurtzite, as the Cd can replace the Zn even up till 5-10%. Unfortunately, the dissolved cadmium ion cannot precipitate in stable form below pH 9-9.5. This can define, that it can just precipitate in form of hydroxide - something like $Cd(OH)_2$ - but it is very uncommon because usually in an oxidizing system the pH is (strongly) below neutral. Although by identification name of “IMA 2002-034” and approximate chemical composition of $CdSO_4*4H_2O$ is known one sulphate form, which belongs to the Starkeyite subgroup. (Jamieson et al. 1999)

If there is no - or not enough - sulphate in the system, but the redox potential is still not high enough for Fe^{2+} - Fe^{3+} alteration, ***Fe^{2+}-hydroxide ($Fe(OH)_2$)*** will be formed, if the pH is higher, as marked by ***zone "b"***. Usually, in a waste dump, where ADR takes place, this type of mineral cannot be precipitated because of the too low pH. (Bigham 1994; Cornell and Schwertmann 1996; Karathanasis et al. 1988)

DOI: 10.14750/ME.2021.004

As the redox potential becomes higher than 0.8V, the Fe^{2+} will have enough energy to be transformed to Fe^{3+}, with help of bacterial activity. The border between Fe^{2+} and Fe^{3+} is not a function of pH, just depending on redox potential, so it is parallel with the pH axis. The Fe^{3+} - solid phase border is independent of the redox potential, but dependent on pH and also on dissolved iron ion concentration.

In presence of dissolved sulphate ion - and potassium - ***jarosite ($KFe_3(SO_4)_2(OH)_6$)*** can be formed, which is the potassium member of the jarosite subgroup, marked as ***zone "c"*** on FIG. 1. For highlighting the most important members of the group, there in the main cation position can be Pb (plumbojarosite), Na (natrojarosite) and H_3O^+ (hydroniumjarosite). (Oliveira et al. 1996; Roca et al. 1999) Although the solubility of the member of the jarosite-group is limited when it starts dissolving it will produce acidity, as the following equation (Eq. 22) shows. This acidic dissolution is very characteristic to this group, thus it could be written to all member of this group. (Chapman et al. 1983; Filipek et al. 1987)

$$KFe_3(SO_4)_2(OH)_6 \rightarrow K^+ + 3FeOOH + 2SO_4^{2-} + 3H^+ \quad (22)$$

The jarosite has a twin, because the alunite ($KAl_3(SO_4)_2(OH)_6$) is just differs it contains Al^{3+} instead of Fe^{3+}. Also, the members of the jarosite group have analogous members from the alunite group. (Jambor 1999; Ripmeester et al. 1986; Scott 2000) The alunites are formed after the weathering of Al-containing silicates, but the acidic producing environment and the high redox potential is the same as in case of jarosite. (Alpers et al. 1992; Long et al. 1992)

If there is no - or not enough - dissolved sulphate in the system, ***Fe^{3+}-hydroxide*** will be formed, marked as ***zone "d"***. During the precipitation of this mineral (Eq. 3), acid is created. A bit higher pH (>4), shown as ***zone "e"*** is necessary for the producing of ***Fe^{3+}-oxyhydroxide***, as ***goethite (FeOOH)***, where extra acid also appears (Eq. 5). As the pH is increasing - ***zone "f"*** - and the redox potential is stable or slightly decreasing, the main iron phase became the ***Fe^{3+}-oxide***, such as ***hematite (Fe_2O_3)***.

This hydroxide - oxyhydroxide - oxide alteration takes place with water loss as well, which is described by equation 6 and 7.

1.3. Reaction influencing critical parameters

In the last 30 years, since the first reaction was described by Nordstrom, the knowledge in ARD effect increased largely. More and more studies and publications proved that from more parameters depend on the sulphide - mainly focusing on pyrite - oxidation. (Dold and Fontboté 2002; Lapakko 2003)

From them, only the most important are described, such as the chemical interactions, the huge impact of the biotic condition, the gas transport in the waste rock or tailing damps. In the followings, these different parameters - which strongly can modify the speeds of the reactions or the reactions themselves - will be discussed.

DOI: 10.14750/ME.2021.004

1.3.1. Mineralogy and mineral chemistry

The primary ore mineralogy defines the suite of heavy metals that may cause potential environmental problems. (Nordstrom et al. 2000) For massive sulphide deposits, there are significant differences among deposit types. Pyrite or pyrrhotite, or both, are the dominant sulphide minerals in most occurrences. Seal and Hammarstorm (2003) stated, that pyrrhotite can be dominant in Besshi-type and some sedimentary-exhalative deposits. Marcasite is commonly present either intergrown with fine-grained pyrite or replacing pyrrhotite. It is generally a minor constituent but locally can constitute a potential source of acidic drainage because it has higher reactivity in weathering processes than pyrite. The rate of weathering depends on the crystallinity of the mineral and chemical stability against the impacts on the mineral surface, as well as from climate conditions. (Dold and Fontboté 2001)

The order in the group of the main sulphides from point of weakness against weathering is already known from earlier studies. The pyrrhotite ($Fe_{(1-x)}S$; x=0-0.17) is the most reactive. It is followed by chalcocite (Cu_2S), galena (PbS), sphalerite (ZnS) and pyrite (FeS_2), finally enargite (Cu_3AsS_4), marcasite (FeS_2), chalcopyrite ($CuFeS_2$) and molybdenite (MoS_2) closing the line. (Nordstrom and Alpers 1999; Seal and Hammarstrom 2003)

Important to mention, that the pyrite can show difference in resistance because cubic crystal forms are more stable than massive pyrite. (Boon et al. 1999; Hammack et al. 1988; McGuire et al. 2001; Rimstidt and Vaughan 2003) From point of dissolved heavy metal load, all of these sulphides are important, but from point of ARD effect and acid production, only those ones, which contains Fe in their structure.

Ritchie (2003) has suggested that in waste-rock dumps that the oxidation rate can vary substantially from one part of a dump to the other. It is convenient to consider the following three classes:

a, the material of the pile oxidizes at substantially the same rate everywhere in the dump and the rate is high;

b, the material of the pile oxidizes at substantially the same rate everywhere in the dump and the rate is low;

c, there are pods of material of high oxidation rate imbedded in the material with a very low oxidation rate.

In practice, the difference between the classes are not clear-cut, and the allocation into a particular class has an element of subjectivity; nevertheless, the most common is the last version.

The most obvious effects of sulphide oxidation impoundments are the digestion of sulphide minerals, the precipitation of secondary minerals and the release of the dissolved products of sulphide oxidation. As the tailing weathers, its colour changes to reddish-brown as the primary sulphide minerals are gradually replaced by Fe-rich oxides and hydroxides. (Blowes et al. 2003/b; Dold and Fontboté 2002)

DOI: 10.14750/ME.2021.004

1.3.2. Microbial activity

The oxidation of sulphide minerals, dissolved sulphur species and Fe^{2+} in mine wastes and mine drainage can be catalysed by bacteria. (Kuenen et al. 1992; Mill 1999; Moses et al. 1997) Singer and Stumm (1970) have concluded that the rate of oxidation of Fe^{2+} to Fe^{3+} is increased by orders of magnitude in the presence of bacteria. The sulphate release, thus the sulphide oxidation (FIG. 2), was much higher in case of biotic, than in abiotic condition. (Scharer et al. 1991; Schippers et al. 2010)

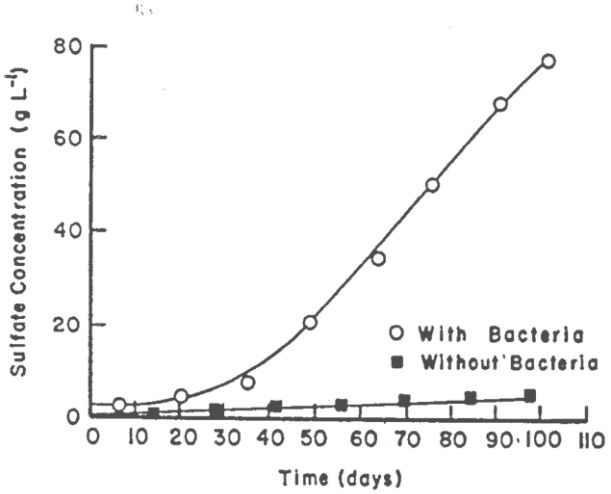

FIG. 2: Comparison of the abiotic and biotic system (after Scharer et al. 1991)

Hundreds of bacterial species can take part in the oxidation process, but in the case of mine wastes the most studied are the Acidithiobacilli and Thiobacilli. (Olson 1991; Tuovinen and Kelly 1972)

The sulphur can be subsequently oxidized to sulphuric acid by either Acidithiobacillus ferrooxidans or other acidophiles. Acidithiobacillus ferrooxidans has a high tolerance for various metal and heavy metal ions and also to some toxic anions such as arsenate ion. Acidithiobacillus ferrooxidans (formerly known as Thiobacillus ferrooxidans), the most well-characterized of the acidophil thiobacilli (i.e., those that will grow only at low pH) was firstly isolated from coal AMD by Colmer and Hinkle (1947).

This thiobacillus is acidophile, so it lives in pH range from 1.0 to 3.5, with an optimum pH around 2.0. Scharer et al. (1991) detected a different species, which prefers a slightly different environment (FIG. 3), pH range from 1.5 to 5.0, with an ideal pH of 3.0-3.5. Moreover he also published a temperature graph showing the ideal temperature for this bacteria species is between 25 and 35°C (FIG. 3).

Tuovinen and Kelly (1972) also proved the efficient catalytic effect of the microbas, so Acidithiobacillus ferrooxidans is a mesophile variant with a temperature optimum near 35°C. The Acidithiobacillus ferrooxidans is autotroph, it obtains all of its C by fixation of CO_2 (Hallbeck and Pedersen 1991) and only low concentration of inorganic N and P compounds, as well as trace amounts of Mg, are required for its growth. (Banfield and Welch 2000) Acidithiobacillus ferrooxidans is capable of obtaining energy from the oxidation of metal-bearing sulphides as well as reduced sulphur

DOI: 10.14750/ME.2021.004

compounds, such as thiosulphate, sulphide and elemental sulphur. Acidithiobacillus ferrooxidans is also able to obtain energy via the oxidation of ferrous iron to ferric iron. (Gould and Kapoor 2003)

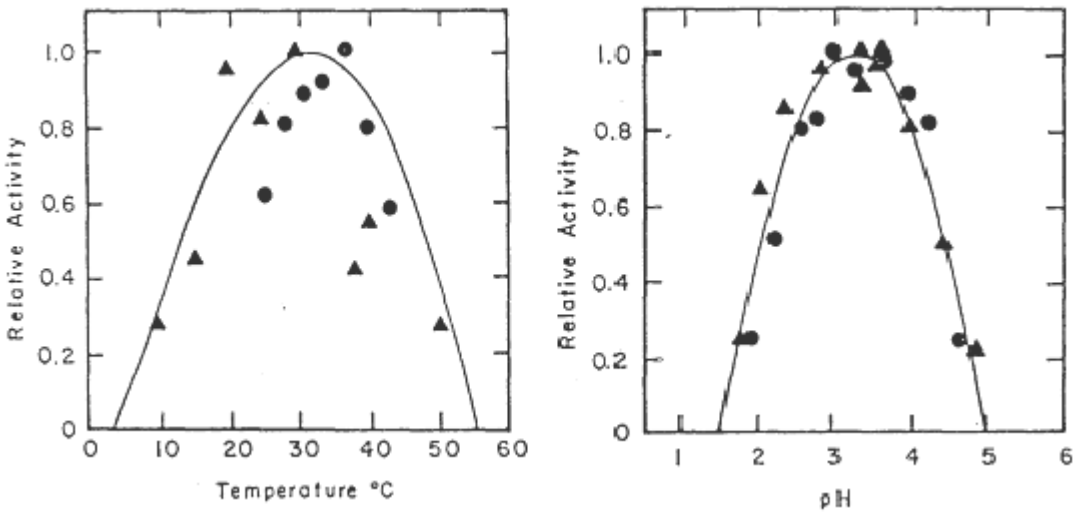

FIG. 3: Optimal living conditions for bacteria species (after Scharer et al. 1991)

At low pH values, the ferric sulphate produced by bacterial oxidation of sulphide minerals can also oxidize (Eq. 23) other metal sulphides (MS) and solubilise additional metal ions:

$$2Fe^{3+} + MS \rightarrow 2Fe^{2+} + M^{2+} + S^{o} \qquad (23)$$

Under low pH conditions, oxidation of Fe^{2+} to Fe^{3+} is catalysed by bacterial species, including Acidithiobacillus ferrooxidans. (Gould and Kapoor 2003) As the pH rises, the role of Fe^{3+} in the oxidation of pyrite becomes less significant, because of the decline in the solubility of Fe^{3+} (Evangelou and Zhang 1995; Jambor et al. 2000/b; Nordstrom and Alpers 1999) and because the rate of pyrite oxidation by O_2 increases as the pH increases. (Nicholson 1994)

1.3.3. Gas transport

Measurements made in several tailing ponds indicated that the concentration of O_2 within the pore spaces of the tailings decrease with increasing depth as O_2 is consumed in sulphide oxidation reactions. (Blowes and Jambor, 1990; Blowes et al., 1991; Smyth, 1981) Measurements of pore-gas O_2 concentration is a sensitive indicator of the location and rate of the sulphide mineral oxidation.

Blowes et al. (2003/b) has shown that the principal mechanism of gas transport in mine wastes is diffusion, in response to concentration gradients and advection in response to pressure gradient. Advective transport may result from pressure gradients due to changes in atmospheric pressure or by changes in density related to consumption of oxygen through sulphide mineral oxidation or by changes in gas temperature due to the exothermic oxidation of sulphide minerals. Because of the fine grain size and low permeability of mill tailings, advective transport of pore gas is unlikely to be significant in most tailings impoundments. (Kuo and Ritchie 1999; Ritchie 2000; Ritchie and Miskelly 2000)

DOI: 10.14750/ME.2021.004

As the impoundment ages, the primary sulphide minerals are depleted at successively greater depths. The most rapid depletion occurs shortly after tailings deposition finished, whereupon O_2-bearing gas diffuses into the tailing and the bacterial population within the tailings created. As oxidation proceeds, the oxidation of sulphide minerals becomes more intensive and oxygen migrates more deeply into the impoundment. (Gunsinger et al. 2006; Vick 2001)

1.3.4. Rain, water and infiltration

Perhaps the greatest source of uncertainty in the prediction of metal loading is the limited insight to the processes controlling water flow through the waste rock. By Smith and Beckie (2003), two factors are predominant in controlling the hydrologic properties of a waste-rock pile:

a, the grain-size distribution of the material and

b, the proportion and spatial arrangement of matrix-supported and matrix-free zones that are created during dump construction.

The lithological properties of the ore deposit and its overburden, the mining method, and the construction technique for the pile largely determine these two factors. (Blowes et al. 1994) For example, end- or push-dumping creates a grain-size variation (FIG. 4), with finer materials near the lip of the lift and with coarser material accumulating at the base of the lift. (McKeown et al. 2000; Wilson et al. 2000)

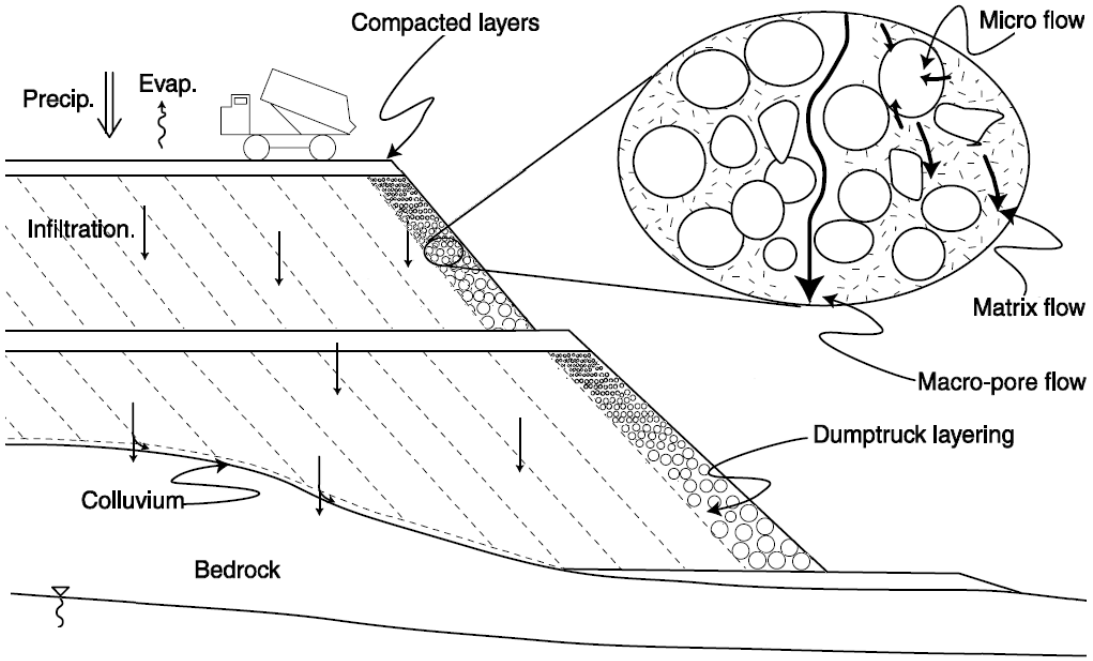

FIG. 4: Dump truck layering effect on mine waste material (after Walder and Stormont 2004)

The layering effect is a normal effect in case of truck-based deposition system, where the gravitation gives the main moving force for the material. Also important to mention that three types of liquid flow types take place (FIG. 4.). The macro-pore flow carries the highest amount of liquid even within the shortest time. This type of flow goes between the grains through cracks and larger pores. The matrix

DOI: 10.14750/ME.2021.004

flow also goes among the grains, but in such places, where finer material fills up the pores among the larger fragments. This type of flow system can also carry significant amount of liquid, but significantly lower volume than the macro-pore flow does. The micro flow uses the cracks and fractures within the grains, or the grain's permeability if it has. This carries the smallest amount and also on the slowest way the liquid, compared the two other methods.

The character of the pile also changes with time as it weathers. The rate at which larger rock fragments break down varies greatly with lithology, depth within the pile, local climate and the amount of reactive material. The magnitude and spatial variation of infiltration at the surface of a pile has the potential to important control on the spatial and temporal variability in metal fluxes at the base of a pile. Smith and Beckie (2003) published, that infiltration of water through the surface of a waste rock pile during a precipitation event will depend upon:

a, rainfall intensity,

b, the infiltration capacity of the surface of the pile,

c, surface texture and topography,

d, antecedent moisture conditions, and

e, the type and amount of vegetation cover.

At least two types of fluid pathways are thought to be present in most waste-rock piles: one is the flow-through finer grained matrix materials and the other is a more rapid flow through so-called macropores.

1.3.5. Solubility

The lower pH values generated by the oxidation of sulphates, dominantly the pyrite and pyrrhotite, enhances the solubility of base metals such as Cu, Zn, Cd, Co, Ni and Pb, and the ability to attack silicate-gangue minerals, thus liberating Al, Mn and other elements. Most metals show greater solubility at lower pH values; however, Al3+ and Fe3+ have solubility minimums at circumneutral pH values, with greater solubility at both lower and higher pH. (Lapakko 2002; Seal and Hammarstrom 2003)

The geochemical impact of mine workings and mine wastes associated with massive sulphide deposits result from an oxidative weathering of sulphide minerals and can produce metal-loaded, acidic sulphate rich waters, which can affect the surface and groundwaters. Within the hydrologic system of mine workings and mine wastes, the minerals and other compounds, such as lime used in flotation circuits, and even monosulphide minerals, such as sphalerite, under anoxic conditions also can neutralize acid, generated by the oxidation of sulphide minerals. (Seal and Hammarstrom 2003)

DOI: 10.14750/ME.2021.004

II. SAMPLES

2.1. Bolivian samples

2.1.1. Origin, mining history, mine site description

The 16 samples were collected from the most famous Bolivian mining districts. Some of them, mainly around Oruro, were already mined under the civilization of the Incas, even before the Spanish conquistadors. (Campbell, 1942; Kozlowski and Jaskolski 1932; Lindgren and Abott 1931)

The tectonic processes created a several hundreds of kilometres extended rich metallogenic zone with dominance of silver and tin. The metallogenic zone forms a NNW oriented line, on the junction of the Central Cordilleras and the Bolivian highland, the Altiplano, called as Bolivian Tin Belt, which zone represents one of the strongly peraluminous igneous provinces of the world. (Chance 1948/a, b) A number of studies of the Bolivian igneous rocks have addressed their relations to tin mineralization, what is typically associated with pervasive alteration of shallow porphyritic plutons or intracaldera volcanic complexes. (Cunningham et al. 1994; Grant et al. 1979, 1980; Schneider and Lehmann 1984) Throughout much of the tin belt, however, magmatism associated with tin mineralization was eventually succeeded by the eruption of unmineralized and largely unaltered volcanic rocks. (Grant et al. 1979)

Till the beginning of the 20th century - in lack of modern mining techniques – only hand small scale mining was done, thus only small amounts of mining waste were produced, because of selective mining methods. This small amount of waste had sufficient time to oxidize naturally, thus ARD effect was negligible. By the exponentially increasing development in the mining techniques in the first half of the 20th century, more and more wastes and tailings were produced. Moreover, the time to produce this increased volume of mine wastes and tailings was much shorter than before. Thus the natural oxidation of the contained sulphide minerals was incomplete or even totally absent. The situation worsened in the second half of the 20th century, as the production rate of the mining waste further increased. The dominant problem is not the acidic environment itself, but the dramatic increase of the heavy metal mobility (such as Pb, As, Cu, Zn, Cd, Sn, Sb, etc....) by the low pH. (Walder 2000, Walder 2009)

The sampling places of the collected mine waste and enrichment process – both as mechanical and flotation – tailings were along the Bolivian Tin Belt, from the most famous mining regions near the city of La Paz and Oruro. The samples contain different types of sulphides in varying amount and also they were in varying stage of oxidation. As the samples contain sulphides which have already started oxidizing, the above detailly described environmental pollution by ARD effect had already taken place.

The aim of the sampling by using kinetic testing was to determine the “worst case scenario”, thus to reach the maximal oxidation speed, that the sample can produce. With this, the maximal heavy metal pollution and mass load can be calculated, so it can let us know, what can be the maximal pollution which will be produced by the mine waste dumps and different types of tailing deposits.

DOI: 10.14750/ME.2021.004

The map below (FIG. 5) shows the 5 different sampling sites, along the feet of the mountains of the Central Cordilleras. 6 samples from Oruro in 2007 (200 km from La Paz in SSE direction), 2 samples from Milluni in 2008 (20 km from La Paz in N direction), 1 sample from "Bolsa Negra" also in 2008 (40 km from La Paz in ESE direction), 5 samples from Morococala in 2009 (40 km from Oruro in SE direction) and 2 samples from Huanuni also in 2009 (50 km from Oruro in SEE direction) were collected.

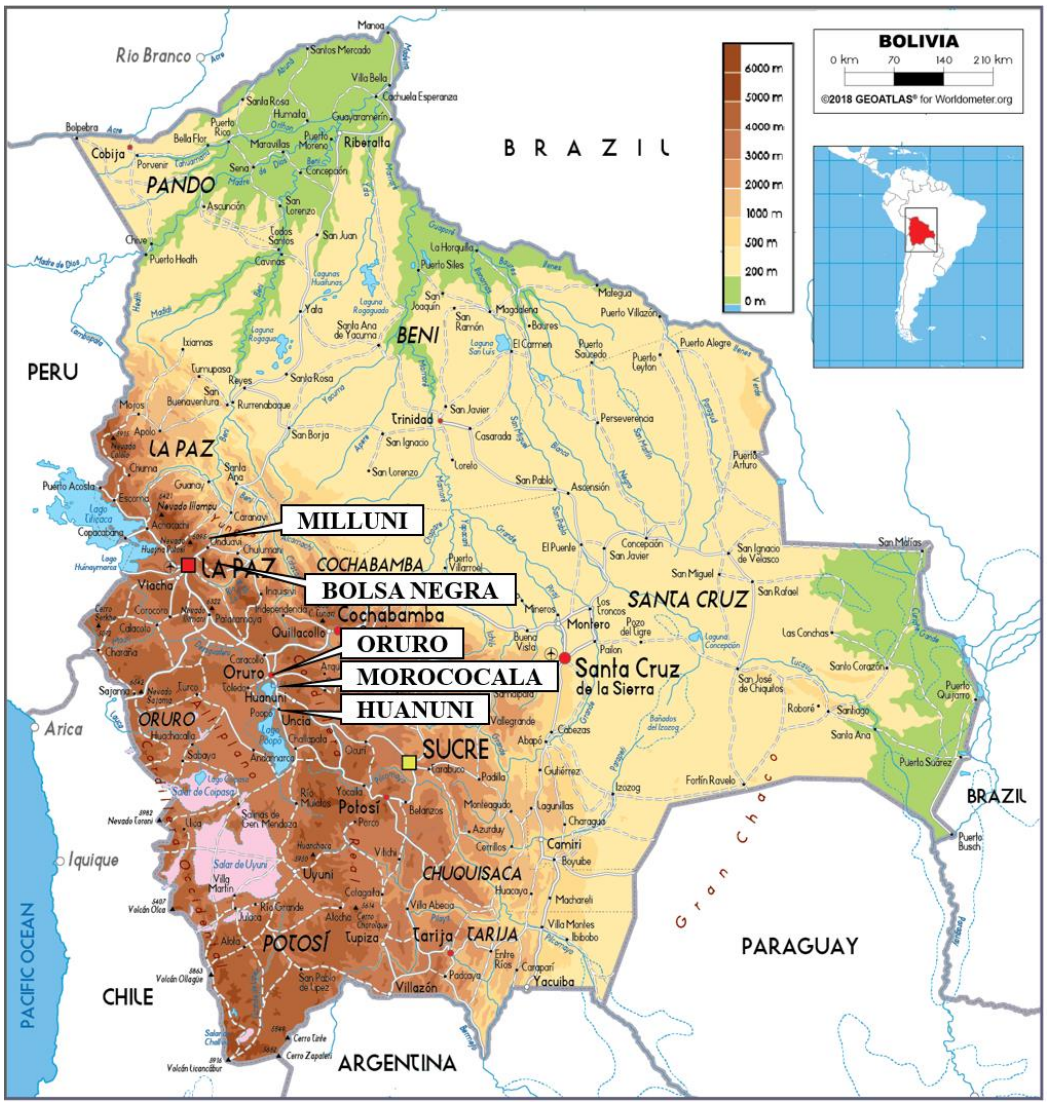

FIG. 5: Locations of the collected samples in Bolivia (Source: after Worldometers 2020/a)

2.1.1.1. Oruro

As we move forward in time, the first sampling was done in autumn of 2007 around Oruro city, Cercado Province, Oruro Department, Bolivia. Oruro is a worldwide well-known mining district of Bolivia. In the first part of the 20th century these mines gave one third of the world's silver production. The mining also resulted in the formation of large, highly sulphidic mine waste piles from waste rock heaps to flotation dumps. Later the economically mineable reserves depleted and the ore production declined. Nowadays only the waste dumps remains, as a legacy of the past mining, and heavy metal polluted water continuously seeps out from these tailing dumps. (Dames and Moore 1999; Walder 2000)

DOI: 10.14750/ME.2021.004

Nowadays the illegal, hand scale mining provides the subsistence level for the local communities. This illegality and the lack of mining databases and maps results in high number and serious mining accidents, year by year. The ore is transported by mules to the smelter, which is only a few kilometres far from the city. (Walder 2000; Walder 2009)

From Oruro and its periphery (FIG. 6) 6 samples were taken: 2 flotation tailings from different places, 2 jig tailings and 2 waste rock material (Table 2.) As the samples are from different categories, such as waste rock, jig or flotation tailing, the "pre lives" of them are also different.

The city of Oruro with approximately a quarter million of citizens is located (about 17˚58' S; 67˚04' W) at about 3700 m high, around a hill (FIG. 6), called Cerros de Oruro, where the mines are also situated. The hill itself is about 200-300 m higher than the Altiplano. The Cerros de Oruro is on the edge of the Bolivian Andes.

FIG. 6: Sampling sites in Oruro, which encompasses both the hill of "Cerros de Oruro" and the mining places

On the sample of ***Jalpha 1-7*** and ***Playa Iroco 1-7*** flotation enrichment process was used. Their grain sizes are small, under 1 mm, but the dominant part of them are in clay size fraction. For their strongly plastic behaviour, they are deposited in mud ponds. ***Jalpha 1-7*** is much less in volume with its storage place size of 50x20 m, in thickness of 4-7 m, compared with ***Playa Iroco 1-7***, which has a reservoir of 650x620 m, with significant thickness of 20-25 m.

The samples called ***Itos Jig 1-7*** and ***Itos Jig 2-7*** were collected from the waste of mechanical separation (Table 2), thus they are jig tailing samples and with average grain size between 2 and 5 mm, but it varies from 0.5 to 25 mm. Both samples are from the same tailing dump with 250x160 m, with thickness of 8-10 m. The endothermic reaction of pyrite oxidation is well characterized by that 55 °C, which was measured at 3 m depth in this waste dump. Important to mention, that the yearly average temperature is about 5-7 °C.

DOI: 10.14750/ME.2021.004

Sample	type	collected	coordinates	altitude	dump size
Jalpha 1-7	FT	2007. autumn	17°57'21.62"S; 67°07'37.97"W	3770 m	50x20 m
Playa Iroco 1-7	FT	2007. autumn	17°58'25.11"S, 67°09'35.94"W	3730 m	650x620 m
Itos Jig 1-7	JT	2007. autumn	17°57'54.30"S; 67°08'17.08"W	3770 m	250x160 m
Itos Jig 2-7	JT	2007. autumn	17°57'54.22"S; 67°08'19.13"W	3770 m	250x160 m
Itos Granza 1-7	WR	2007. autumn	17°58'1.89"S; 67° 08'7.45"W	3760 m	110x120 m
Itos Granza 2-7	WR	2007. autumn	17°58'1.66"S; 67°08'7.15"W	3760 m	110x120 m

Table 2: Samples from Oruro Abbr.: FT: flotation tailing; JT: jig tailing; WR: waste rock

Samples, called ***Itos Granza 1-7*** and ***Itos Granza 2-7*** are waste rocks, with high pyrite content. The dominant particle sizes of the samples are between 4 and 7 mm, but it varies between 0.5 and 40 mm. They were disposed in smaller dumps, with dimension of 110x120 m with several metres in thickness.

2.1.1.2. Milluni

In summer of 2008 a newer sample collecting tour was done by dr. Ingar Walder, the researcher of KREC, from Milluni 2 samples were taken at 29.07.2008. Sample, called as ***BOL 1-8*** is a waste rock and ***BOL 2-8*** is a fine tailing material (FIG. 7 a and b).

Milluni – with about 4000 citizens – is located at elevation of 4500-4600m in the Milluni Valley as part of the Bolivian Tin Belt, in La Paz Department. The Milluni Mine, also known as "La Mina Fabulosa", operated between 1940 and 1990 by the company COMSUR. The most important extracted minerals where the Sn and Zn sulphides. Although the mines are/were dominantly underground, large amount of sulphide-rich mining wastes are on surface and still discharged directly further up in the valley (FIG. 7 a and b). The fine-grained sandstone host rock contains such as sulphide ore minerals like pyrite, marcasite, sphalerite, arsenopyrite and the oxide cassiterite. (Salvarredy-Aranguren, et al., 2008)

Since the beginning of the mining, a number of harmful and toxic elements have been drained into the Laguna Milluni water reservoir. This reservoir used to be one of the principal reservoirs of drinking water for the population of the north part of the city of La Paz between 1940 and 1987. (Rios, 1985)

From pictures and from satellite view (FIG. 7 a and b) clearly visible, that the whole valley is covered by waste or tailing (probably mixture) with 2.5 km length, with width of 250 m upside and 900 m downside in triangular shape in the valley with several ten metres of thickness (Table 3).

Even from this satellite view, it can clearly be defined the different types of mining wastes, their volume, moreover their oxidizing stages (or at least their condition on the surface). Figure 7/a shows the different colour of the two types of material and also the area covered by the produced mining waste.

DOI: 10.14750/ME.2021.004

On top, an oxidized reddish brown coloured older material is found. Lower in the valley, "fresh" unoxidized greyish materials are, probably the high unoxidized pyrite content is visible. The ***BOL 2-8*** fine tailing samples were collected from this material. The dominant grain size is between 0.5 and 1 mm, but it varies in the range of 0.1 and 2 mm. ***BOL 1-8*** was collected from the side of the valley, from a coarser waste rock pile. Its grain size is about 2-15 mm, with 3-5 mm as dominant phase.

FIG. 7 a and b: Sampling place of BOL 1-8 waste rock and BOL 2-8 tailing samples in Milluni

Sample	type	collected	coordinates	altitude	dump size
BOL 1-8	WR	29.07. 2008	16°19'39.15"S; 68° 9'15.45"W	4585 m	900x300 m
BOL 2-8	T	29.07. 2008	16°19'37.60"S; 68° 9'17.27"W	4572 m	650x180 m

Table 3: Samples from Milluni. Abbr.: T: tailing; WR: waste rock

From the processing plants (FIG. 7 a), which are 500 m far from the sampling points in NE direction, the fine material was carried by the processing and machine cooling water downstream in the valley. The water helps to spread the material on floodplains, meanwhile, the water cuts newer and newer shallow channels into the fine material. There is a dam above the Milluni Chico Lake, which was originally built to stop the water, not to infiltrate into the Laguna Milluni. With time, this system seems failed, thus the lake has become contaminated by heavy metals. As freshwater reservoir for the northern side of La Paz could not function furthermore. Because of filling up the valley with tailing, and also the lack of maintenance of the dam, the seepage simply went round and found a pathway into the water reservoir, as it is visible on the middle part of FIG. 8. This seepage and the caused secondary mineralization are clearly visible, together with the feet of the dike at the right bottom.

Even by visual observation of the picture can be told, that the greyish-white surface cover is probably gypsum, the light yellow is jarosite while the reddish or brownish minerals are iron-oxyhydroxides or iron oxides. Important to mention the strange colour of the water of Laguna Milluni, which refers to high dissolved iron concentration.

DOI: 10.14750/ME.2021.004

FIG. 8: Seepage entrance on the northern side of Laguna Milluni, with visible secondary minealization on the shore of the lake in the shallow part (Photo by: Klimmer 2015)

Because of the polymetallic ore mineralization, probably the water is also contaminated with lead, arsenic, zinc, cadmium, and other heavy moreover strongly toxic dissolved metals. The heavy metal water pollution is measured and proved by Kim Driesen (2012), who worked with water pollution by mines of Milluni. He measured in several outflows and springs, but only two sampling points were relevant (Table 4), one water sampling point was the outflow of the Laguna Milluni and the second was a water channel directly from the "La Mina Fabulosa" mine, which is mixing with the outflow water of the lake further down in the valley. From the data, clearly visible the effects of ARD, such as the low pH and the high concentration of sulphate, iron, zinc and arsenic ions.

	pH	TDS	CO_3^{2-}	NO_3^-	SO_4^{2-}	Cu	Fe	Zn	Cd	As
	---	ppm	ppm	ppm	ppm	ppm	ppm	ppm	ppm	ppm
The outflow of Laguna Milluni	2.83	475	0	92.5	500	0.34	58.95	22.58	0.034	4.045
Water from "La Mina Fabulosa"	3.17	1175	0	217.5	2150	2.75	446.4	182.2	0.698	4.619

Table 4.: Chemical parameters of the two relevant sampling points of Laguna Milluni (Driesen 2012)

2.1.1.3. "Bolsa Negra"

In summer of 2008, near the sampling in Milluni further place was sampled in "Bolsa Negra", in Murillo Province, La Paz Department, Bolivia. This mine is still in operation, the main targets are the tungsten in peribatholithic hypothermal veins, as minerals of ferberite ($FeWO_4$), scheelite ($CaWO_4$) and tungstite (WO_3*H_2O). (Werner et al. 1998) As a legacy, this area is also covered by mining wastes from different periods, as it is clearly visible on satellite photo (FIG. 9), as there is high contrast between the green vegetation covered hills and the bare surface of the mining wastes.

The sample, called ***BOL 3-8*** was taken from the coarser material (Table 5). Its average grain size is about 3-5 mm, in range of 2-15 mm with some bigger fragments. The sample is macroscopically similar to the sample BOL 1-8.

DOI: 10.14750/ME.2021.004

FIG. 9: Sampling place of BOL 3-8 waste rock in Bolsa Negra

Sample	type	collected	coordinates	altitude	dump size
BOL 3-8	WR	30.07. 2008	16°33'20.78"S, 67°47'38.75"W	4075 m	200x100 m

Table 5.: Waste rock (WR) sample from "Bolsa Negra"

The mine entrance is located at elevation of 4250 m. The high grade ore is transported down on the serpentine path in the hillside to the 180 m lower located flat area, where the processing plants are. The waste material and the subgrade ore is simply dumped around the mine, producing half-cone shaped waste dumps on the hillside (FIG. 10 a).

After the ore enrichment from the processing plants the produced tailing is simply pumped to the flat area and cause tailing extending downflows (FIG. 10 b) downwards in the valley. The largest one has a size of 400x200 m in deltoid shape, till 3950 m.

FIG. 10 a and b: View of the different mining wastes around "Bolsa Negra" (Photos by: Bolgener, 2015/a and b) a: Standing near the processing plans (4070 m), view of the cones of waste rocks, was poured out from mine entrance (4250 m); b: Standing at the mine entrance of the mine (4250 m), lower the processing plans (4070 m), below it more tailing extending downflows (till 3950 m) downwards in the valley

DOI: 10.14750/ME.2021.004

2.1.1.4. Morococala

In September of 2009 five samples were collected from Morococala (FIG 5), which is 40 km far from Oruro in SE direction, in the Pantaléon Dalence Province, Oruro Department, Bolivia (Table 5). The samples were collected from two different sampling places, the **BOL 1-9, 2-9** and ***3-9*** were from a mining waste dump at northern periphery of the city (FIG. 11) and the rest two (***BOL 4-9*** and ***5-9***) were from 1.8 km further toward southern east (FIG. 12). On both places, it was mined for cassiterite /SnO_2/.

Although the first three samples were collected from the same dump (FIG. 11), the sample ***BOL 1-9*** is categorized as waste rock, while the ***BOL 2-9*** and ***3-9*** are tailing samples. The difference is given by the different deposited material in time and also from the large size (280x190 m) of the dump. BOL 2-9 and 3-9 were collected only a few metres far from each other, so they are listed on the same coordinates (Table 6). Important to mention, that in this mining place there is a dump with significantly darker, greyish colour – at the top of FIG. 11 – which probably came from a more sulphidic section of the mine.

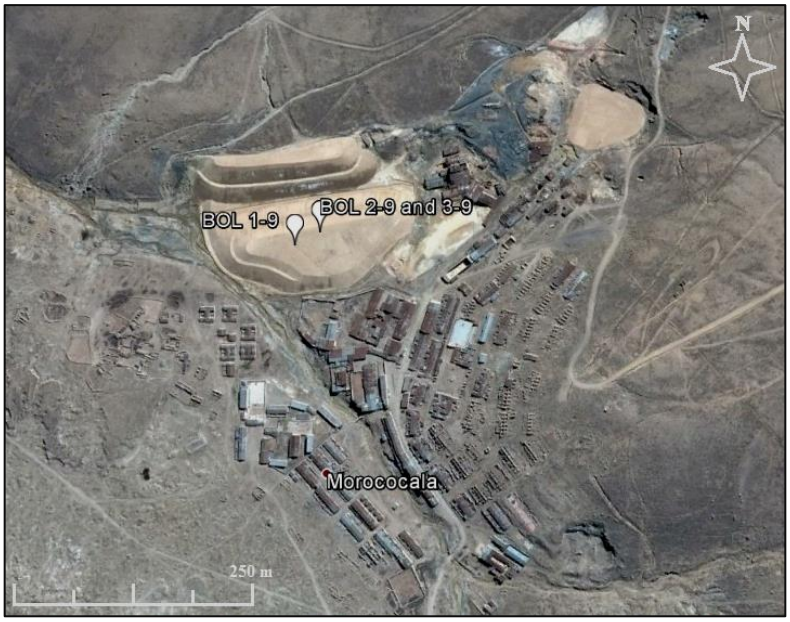

FIG. 11: Sampling points, at the northern periphery of Morococala

Sample	type	collected	coordinates	altitude	dump size
BOL 1-9	WR	Sept. 2009.	18° 8'30.43"S; 66°48'4.86"W	4370 m	280x190 m
BOL 2-9	T	Sept. 2009	18° 8'29.97"S; 66°48'3.80"W	4370 m	280x190 m
BOL 3-9	T	Sept. 2009	18° 8'29.97"S; 66°48'3.80"W	4370 m	280x190 m
BOL 4-9	WR	Sept. 2009	18° 9'20.39"S; 66°47'24.18"W	4520 m	100x100 m
BOL 5-9	FT	Sept. 2009	18° 9'13.80"S; 66°47'16.28"W	4500 m	190x80 m

Table 6: Samples from Morococala. Abbr.: T: tailing; FT: flotation tailing; WR: waste rock

DOI: 10.14750/ME.2021.004

In Morococala – similarly to the previously showed sampling places – the geotechnical rules and waste maintenance are also missing. Huge amount of mining waste with maximal slope angle is located just above the small town. In case of an earthquake, the risk of the slide of the damp's material is high.

The samples ***BOL 4-9*** and ***5-9*** were collected from the other side of Morococala, which is located about 1.8 km further in southern east direction. These two samples are linked to the waste of Santa Fe mine. The ***BOL 4-9*** is a waste rock sample, from a dump which is located under the mine and the processing plants, partly on a flat area, partly on the hillside, while the ***BOL 5-9*** is a flotation tailing sample from the hillside storage. The water demand of the processing plant is covered by the barrage which is located toward southern east further up in the valley (FIG. 12).

The diversity of the mineralization of the Bolivian Tin Belt is well represented by the production of enormous vivianite /$Fe_3(PO_4)_2*8H_2O$/ crystals from the 280 m level of the Santa Fe mine. The vivianite-bearing level has already flooded, although cassiterite /SnO_2/ production continues on higher levels of the mine. (Mindat.org 2015/a)

FIG. 12: Sampling points of BOL 4-9 and 5-9, 1.8km from Morococala in SE direction

2.1.1.5. Huanuni

In Huanuni – which is located 16 km far from Morococala (FIG. 5) in south direction – further two tailing samples (***BOL 6-9*** and ***7-9***) were collected in 2009, from the area of an operating processing plant, located above the city toward the north, at the hillside (FIG. 13). The plant was built on the planned materials of the tailings from the Huanuni mine. As both samples have grain size between 1 and 2 mm, they can be characterized as fine tailings. The dump has about 250x380 m size (Table 7). Around the sampling place, there are several hillside dumps with dimension of approximately 150x250 m. In the western direction, more dumps have greyish colour, which indicates that these have high, unoxidized pyrite content.

DOI: 10.14750/ME.2021.004

The mines in Huanuni city, such as Huanuni, Barreno, Cerro Pozokoni, Pepitos or Porvenir mine are very famous from the high diversity of heavy metal sulphides and oxides. Here tin forms not only oxide as cassiterite, but other Sn-Sb sulphides (franckeite, herzenbergite, stannite and teallite) can be also found. Moreover, the Sb forms sulphosalts, such as jamesonite, bourlangerite or bournonite. The Ag containing pyrargyrite, as the most important and profitable silver ore mineral is also present. (Mindat.org 2015/b)

FIG. 13: Sampling points of BOL 6-9 and 7-9 on the hillside, just above the city of Huanuni

Sample	type	collected	coordinates	altitude	dump size
BOL 6-9	T	Sept. 2009	18°16'53.85"S; 66°50'5.85"W	4065 m	250x380 m
BOL 7-9	T	Sept. 2009	18°16'53.85"S; 66°50'5.85"W	4065 m	250x380 m

Table 7: Tailing samples from Huanuni

The large numbers of the operating mines indicate large mining activity as well as high amounts of mine wastes and tailings. The dams are located only a few metres (FIG. 13) far from the living houses, with maximal slope angle, which creates high risk of slide of the dams' material. Moreover, the seepage with toxic metal content flows through the city.

2.1.2. Macroscopic evaluation

The optical evaluation of the samples was completed by using a Carl-Zeiss stereo microscope, with 8 - 32 times magnification. For those grains which seemed interest for further evaluation, a Carl-Zeiss Discovery V2O stereo microscope with an Axio Cam MRc5 camera was used. Its 150 times maximal magnification was enough to sharply see even the smallest particles. The machine was supported with a Sycop 3 driving panel and Axio Vision SE64 programme. With the auto shifting focus function of it, very sharp pictures are taken even from grains in size of 1–2 mm. This was a helpful tool to define the various secondary minerals, caused by the mineral alteration. Those grains, which were interest or cannot be identified, were separated for further analysis with electron microscope and microprobe.

DOI: 10.14750/ME.2021.004

Each samples were macroscopically evaluated, thus their important characteristic parameters, which can be defined by optical microscope are written down below, with the magnifications, that are noticed.

The sample ***Jalpha 1-7*** has yellowish-ochre colour and fine structure. The amount of clay size and sand-size particles was approximately the same. Only tiny pyrite and quartz crystals were visible, but no other crystalline minerals were recognizable. As a coating on the surface light yellowish secondary mineralization was present, which was jarosite.

The clay type ***Playa Iroco 1-7*** sample contained more clay size than fine sand fraction. Only 0.4-0.6 mm particles of pyrite with shining surface was visible in the material. As a surface coating, uncrystallised jarosite was formed with well developed 2-3 mm in length gypsum needles.

The ***Itos Jig 1-7*** and ***2-7*** samples are discussed together because of their high similarity, as their sampling point is the same dam. The dominant grain size was between 2 and 5 mm, with some fragments of 25 mm. The rate of sand and clay fraction was negligible. The coarser grains of the samples have dark greyish colour with large rate of light yellowish secondary jarosite mineralization on their surface. The 1-3 mm sized reddish-brown irregular shape dots on the surface of rock particles showed the presence of the iron oxy-hydroxides and oxides after the oxidation of pyrite. Using high magnification (150x) became clearly visible (FIG. 14.), that although the surface of the pyrite grains are still shining, the oxidation has already started, as caverns and holes are present on the surface.

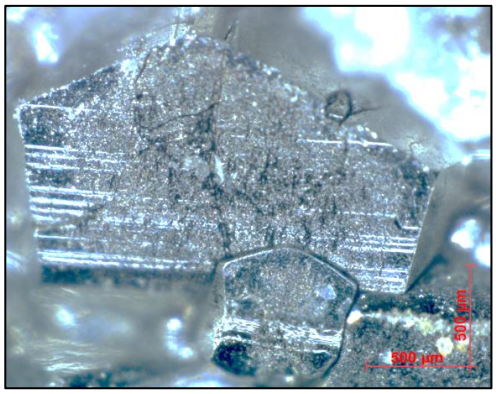

FIG. 14: Oxidation caverns and holes on a well developed pyrite crystal (150X)

Itos Granza 1-7 and ***Itos Granza 2-7*** are evaluated also together. These samples were coarser than the jig tailings were, as their dominant grain sizes were 4-7 mm, with variety between 0.5 and 40 mm. The colour of the rock particles were reddish-brown, which showed the maturity of the oxidation processes by the presence of the iron oxy-hydroxides and oxides. Large amount of massive quartz was visible in association with some elongated prism-shaped dark minerals, probably as iron-containing silicate. The amount of visible pyrite was not significant.

The sample ***BOL 1-8*** had ochre and reddish-brown colour, caused by the presence of iron oxy-hydroxides and oxides, which marked that the oxidation of the material has strongly taken places. It dominantly consists of crushed massive quartz, but several grains were found with well-developed shape. The whole sample was covered by reddish-brown iron oxy-hydroxides or oxides (FIG. 15), but at some places, the original rock was still visible. Pyrite was not found in significant amount.

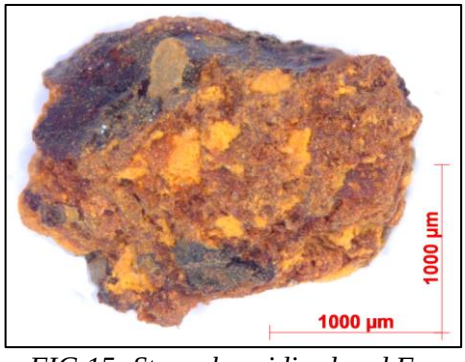

FIG.15: Strongly oxidized and Fe-oxide coated grain of BOL 1-8 (39X)

DOI: 10.14750/ME.2021.004

The sample ***BOL 2-8*** was collected from the same mining place, but from different dump. This sample consists of mainly quartz and dark host rock, with high pyrite content. Under microscope cannot be detected any alteration products. The pyrite grains had dominantly unaltered and shining surfaces. The quartz – similarly to the small number of other rock pieces – looks fresh and uncovered. At higher magnification, oxidation caused holes and caverns became visible (FIG. 16) on the surface of pyrite. 90-95 % of the material had grain size less than 1 mm, with dominant fraction between 0.3 and 0.5 mm.

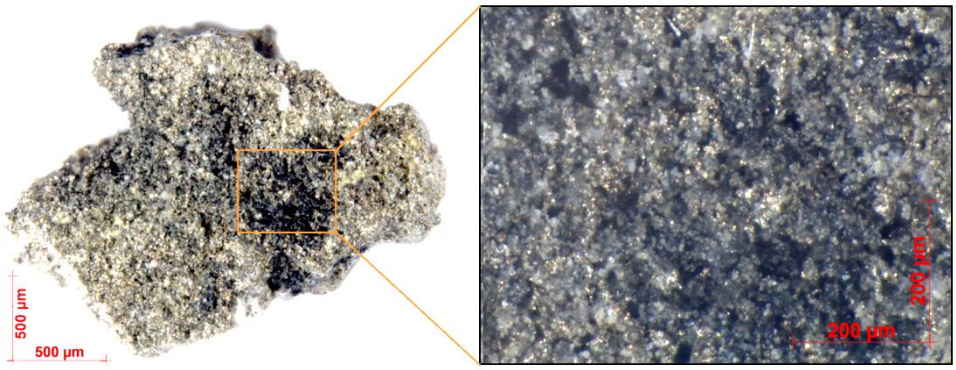

FIG. 16: Oxidization caused holes and caverns in sulphide (pyrite) grain in BOL 2-8 (a:56X; b:150X)

The iron oxy-hydroxides and oxides caused ochre and reddish-brown colour of sample ***BOL 3-8*** indicated the maturity of the oxidation processes. At higher magnification (FIG. 17/a and b) was still visible the shining surface of the pyrite grains under the thin layer of secondary iron minerals. The dominant part of the sample was quartz, with covering of clay and reddish-brown iron oxy-hydroxides or oxides minerals. The grain size was varied, as half amount of the sample was less than 1 mm and a small portion was between 1 and 5 mm, but the rest was over 10 mm.

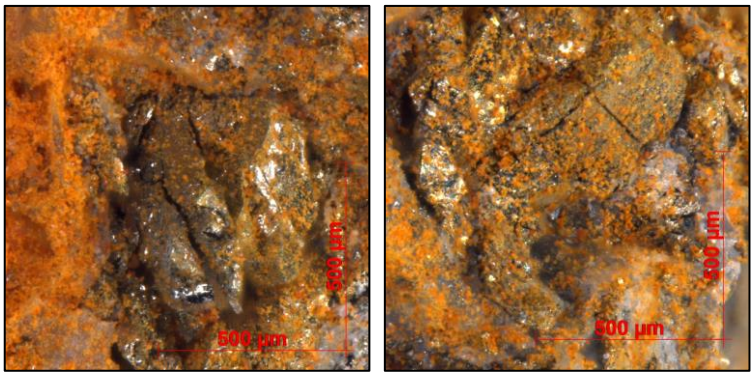

FIG. 17/a and b: Secondary iron mineral on shining pyrite in BOL 3-8 (80X)

Each samples which were collected from Morococala in 2009 (from BOL 1-9 to 5-9) had fine grain size with relatively high rate of the clayish fraction. The sample ***BOL 1-9*** was a light grey coloured fine material, as the dominant part (85-90%) of the sample was in size fraction of 0.2-0.3 mm. Several larger, a few mm size light yellowish aggregates were found. The sample contained approximately 10 % of 2-5 mm fraction. The rate of alteration was so strong, that cannot be detected or recognized any mineral even with the using of high magnification on the microscope. This greyish matrix probably contained sulphides in high rate, as the sulphuric smell felt. The yellowish coloured aggregates were cemented with jarosite, with a few white dots which probably was alunite or gypsum. The probability of alunite

DOI: 10.14750/ME.2021.004

was higher, as the gypsum dominantly appears in more crystallized form. Pyrite – even in strongly altered form – was not detected.

The sample ***BOL 2-9*** looked homogeneous with a fraction of fine sand, as the dominant grain size was between 0.2 and 0.3 mm, with some few mm fragments. Aggregates of iron-oxides, jarosite or alunite were not observed. The sample dominantly consists of crushed quartz without surface covering, but in a few percentages, biotite flakes were visible, with maximal diameter of 1mm. The amount of pyrite grains was negligible. In some of the quartz grain, mineral association was found, which were quartz with cassiterite (FIG. 18) or with pyrite. These minerals are typical for the ore mineralization of the Bolivian Tin Belt.

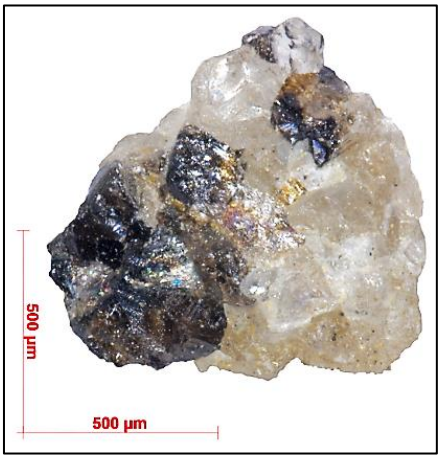

FIG.18: Quartz - cassiterite association in BOL 2-9 (106X)

Sample ***BOL 3-9*** had greyish yellow colour, with average grains size of 0.4-0.7 mm. It mainly consists of quartz, which was finely coated by a small amount of clay minerals. Secondary iron minerals were totally absent, but the light yellow coloured jarosite strongly cemented the sample. With higher magnification (FIG. 19 a and b) even the well developed own shape of the jarosite was clearly visible. Pyrite was found only as several small strongly altered grains.

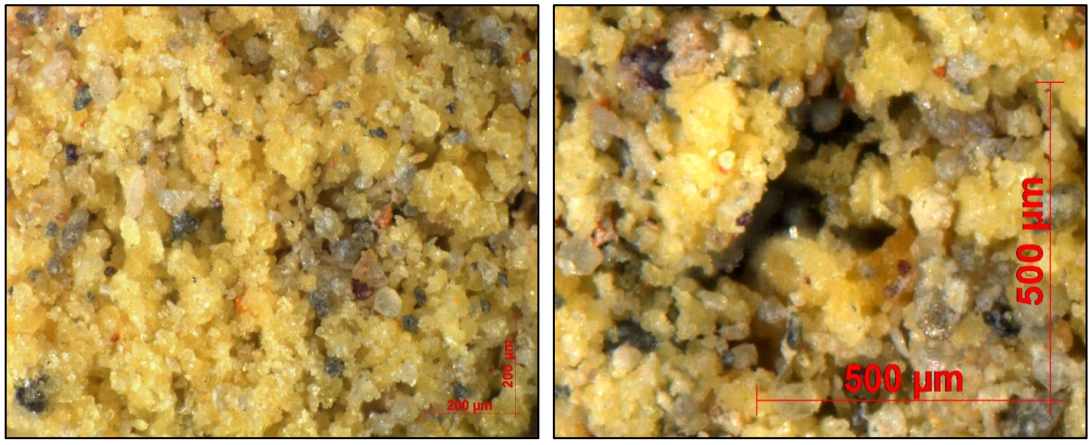

FIG. 19/a and b: Cemented fine grains by jarosite in the sample of BOL 3-9 (a: 53X; b: 72X)

The sample ***BOL 4-9*** was one of the finest one, as its average grain size was under 0.2 mm. Under microscope can be determined that the sample consist of dominantly two phases, which were the quartz and the pyrite in 3:1 ratio, together with 5-10 % of clay minerals. The sample had relatively high cohesion, it was cemented. With high magnification, the material of the cementation can be defined as clay minerals and gypsum. Some larger (5-15 mm) and more solid aggregates were also found. After the breaking of them, became clearly visible the cores of

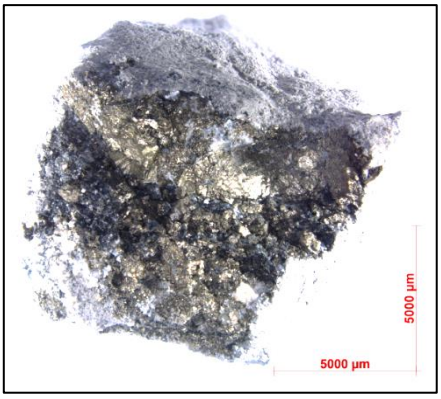

FIG.20: Partly oxidized polymetallic sulphide with clay covering (10X)

DOI: 10.14750/ME.2021.004

them (FIG 20), which were partly or fully oxidized sulphides with covering layer of a mixture of clay and secondary minerals in 1-2 mm thickness.

The ***BOL 5-9*** had a medium grey colour and fine grain size, dominantly between 0.2 and 0.3 mm. The material mainly consists of quartz, but the rate of pyrite is also significant. Well developed gypsum needles were visible. A grain with tiny, but well developed and well crystallized pinkish coloured minerals (FIG. 21) was found in the dimension of 1x2 mm. With higher magnification the welldeveloped crystals could be seen. This high rate of crystallization, presaged it as a secondarily formed mineral. By optically cannot be defined its species, so the grain was prepared for analysis of electron microprobe.

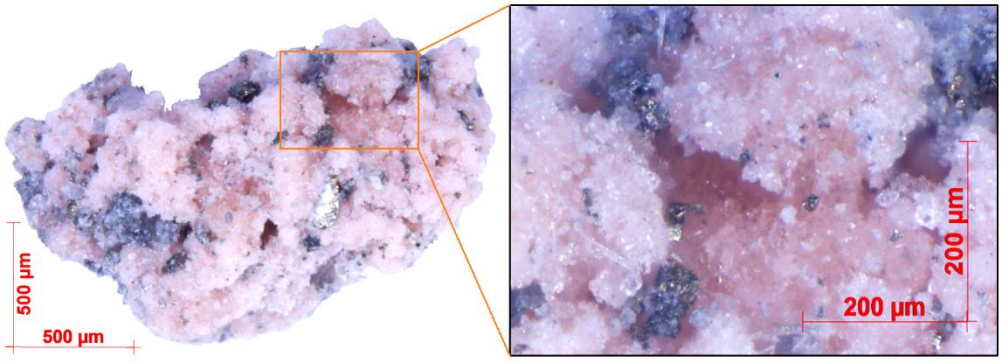

FIG. 21: Unidentified mineral phase with well-developed crystals in the sample BOL 5-9 (25X and 150X)

Still, in 2009, but from another significant mining region – called Huanuni – two samples were collected (FIG 13). Sample ***BOL 6-9*** was a strongly oxidized material in colour from ochre to reddish-brown. The dominant grain size is between 0.5 and 1 mm, but with bigger grains (till 2 mm) in 10 %. The sample consists of mainly quartz, pyrite and other sulphide minerals and some biotite. Each grain was covered by iron oxy-hydroxide or oxide. Clay minerals were not visible under the microscope.

The ***BOL 7-9*** was collected from the same dam, but the colour of it is lighter, probably caused by the smaller amount iron-oxyhydroxide or oxide. This sandy sample had grain size between 0.5 and 1 mm, with some larger fragments (2-3 mm) at a smaller rate (5-10 %). It consist of dominantly quartz, pyrite and other sulphide minerals. Not each grain was coated or cemented by iron minerals. An interest grain in size of 1x2 mm with light yellow coloured, secondarily formed jarosite mineralization was found (FIG. 22). With higher magnification, well-developed jarosite crystals with own shape was found. For further electron microprobe analysis, it was prepared.

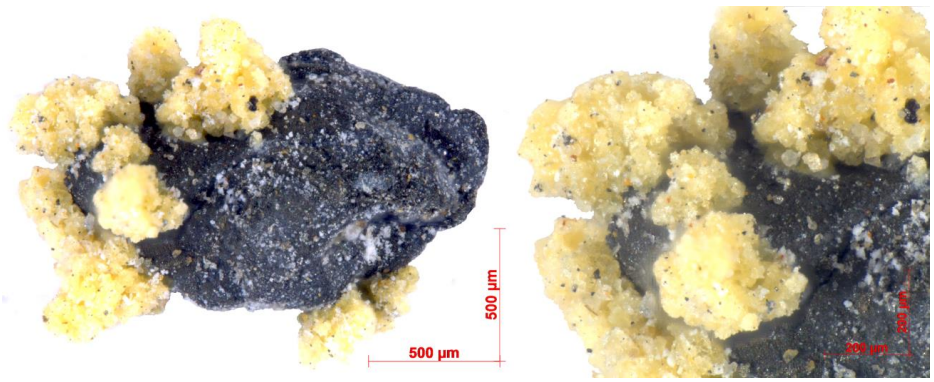

FIG. 22: "Flowering" jarosite crystals on rock fragment in the sample BOL 7-9(a:77X; b:150X)

DOI: 10.14750/ME.2021.004

As a conclusion for the optical evaluation, the samples can be categorized by two different properties. These are the material of the cementation and the surface covering. Table 8 shows the sorting of the samples based on these two parameter. Of course, some sample name is duplicated, as both jarosite and gypsum crystals covered it, like Jalpha 1-7. In the column of cementing mineral, is also written, whether cohesion was observed or not.

		Surface covering		
		none (fresh, shining)	***jarosite*** (yellow)	***Fe-oxide*** (ochre, reddish brown)
Cementing mineral	***none*** (no cohesion)	BOL 2-8;	Itos Jig 1-7 and 2-7; Itos Granza 1-7 and 2-7;	Itos Jig 1-7 and 2-7; Itos Granza 1-7 and 2-7; BOL 1-8 and 3-8;
	gypsum (cohesion, white)		Jalpha 1-7; Playa Ir. 1-7; BOL 1-9; BOL 2-9; BOL 4-9; BOL 5-9;	BOL 2-9;
	jarosite (cohesion, yellow)		Jalpha 1-7; Playa Ir. 1-7; BOL 1-9; BOL 3-9; BOL 4-9;	
	Fe-oxide (cohesion, ochre, reddish brown)			BOL 6-9; BOL 7-9;

Table 8: Classification of the Bolivian samples in the function of cementing and surface covering

2.2. Hungarian (Recsk) samples

2.2.1. Origin and mining history

Sulphidic ore mineralizations can be found also in the Mátra Mountains, in NE Hungary (FIG. 23). In 2011, sulphidic sample was collected from the waste dump of the Recsk -900 deep level. The ore body was a copper porphyry and skarn copper deposit. The sample was taken from the extracted material of the “Western 3” ore exploration adit, which drove the contact of the exoskarn and the carbonates.

FIG. 23: Locality of the sampling point of HU series at Hungary (source: after Worldometers 2020/b)

DOI: 10.14750/ME.2021.004

Near the waste dumps were located, the original Shaft No.1, which served for transportation (FIG. 24)., which was closed down in 1999. The dominant part of the original damp had already been transported or recultivated (Table 9), only a small portion of it remained as an exhibition material. This material – which took approximately 300-350 tonnes altogether – was sampled. In eastern direction 350 m from the collecting place, the closed buildings of the old mine and its servicing places were located.

FIG. 24: Original waste dumps of HU series, with the old mine's buildings at the top on the right side

Sample	type	collected	coordinates	altitude	amount	dump size
HU series	WR	autumn 2011	47°55'41.51"N, 20°04'34.06"E	310 m	total of 20kg	200x100 m

Table 9: Sampling details of the HU waste rock sample series

For the experiments, fragments of 10-20 cm were selected. After the removal of the secondary mineralization (such as iron oxides) from their surface, they were crushed into five different grain sizes: between 1-2; 2-4; 4-8; 8-16 and 16-32 mm, in amount of 3.0 kg in each sections.

The crushing process gave fresh, non-oxidized surface, which is ideal for the kinetic test analysis.

FIG. 25: Microscopical view of the HU series (HU 1-2 member)

2.2.2. Optical evaluation

The crushing process ensured, that all of the grains had fresh surface. Under the microscope, near the quartz and fragments of andesite, different types of sulphide minerals were observed, such as galena, sphalerite, chalcopyrite and high amount of pyrite. The ore had a local nickname, called as "worm ore", which represents well the irregular appearance of the above mentioned heavy metal sulphides. The ratio of carbonates was also significant, which is clearly visible on FIG. 25. Based on observation, it was estimated as about 10-15 %, which consist of mainly calcite. Because of the different fracturing parameters of the rock-forming minerals, the fragments have totally irregular shape.

DOI: 10.14750/ME.2021.004

III. MEASURING METHODS

3.1. Brief introduction into the principles of the humidity cell tests

The humidity cell test is a standardized process which was developed in Canada. It was designed to determine the acid-producing and neutralizing potential and the rate of oxidation. (Grant et al. 1980; Lapakko et al. 2000) Moreover, it does on such a way, that the system can reach the maximal oxidation rate, thus with this method the "worst case scenario" can be mimicked. (Lapakko et al. 1995; Lapakko 2003) This gives us an insight into the oxidizing system, what can be the maximal speed of oxidation and what can be the maximal environmental and heavy metal load. (EIPPCB 2004; Pearce et al. 2015)

Although the humidity cell test is standardized, but it is commonly used with some modifications, which provide, that it was fitted to the properties of the samples, as much as possible. (Lapakko and White 2000) In case of these samples, the system modification also happened, but the frame of the original test was kept, so through the samples, moisture saturated air was pumped. Periodically, on every 7^{th} day (if possible even at the same time, to keep the equal time length among the sampling), the samples are flushed through with distilled water. The leachate was collected and analysed for pH, conductivity, alkalinity and anion concentrations. Unfortunately, the cation analysis was not possible to complete.

The weights of the Bolivian samples were at least 1.5 kg, but dominantly between 1.5 and 2.5. In the Hungarian set, each fraction were 3.00 kg, because the main question was whether the grain size effects on the pyrite oxidation rate or not. During the test, the samples were kept in acryl columns, with diameter of 150 mm and depth of 140 mm, with 2 mm mesh and 5 μm acid-resistant filter at the bottom.

The technical realization of the humidity cell test is shown in a schematic draw (FIG. 26), where the main parts of the system are imaged. The air pump (1) pushes air (light blue arrow) into the water containing tank (2), through a bubbler (3). The air fills up with humidity and via the air pipe (4) and the valve (5) can enter the acrylic sample keeper (6). The humidified air can go through the filter and the mesh (7) and the sample (8) before it exits through the holes (9) on the top of the sample keeper. The humidified air is a perfect tool to give O_2 for the oxidation of the sulphides – to be sure, several magnitude larger amount than it can use up – as well as H_2O for the mineral alteration reactions. As it was already mentioned, the samples were weekly rinsed – along the yellow arrow – with 1000 cm^3 of distilled water. The valve (5) was switched from air flowing mode to rinsing mode, thus the seepages were drainaged through the drainage collecting pipe (10). The collected seepages were measured for the main parameters and filtered with 0.2 μm mesh and stored in plastic bottles on 4 °C for further analysis.

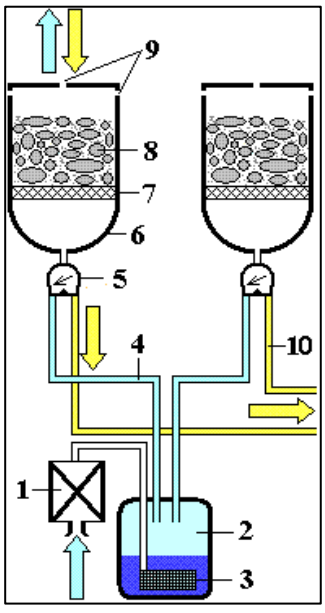

FIG. 26: Outlined setup of the humidity cell test

DOI: 10.14750/ME.2021.004

3.2. Mineralogical and chemical measuring methods

3.2.1. Chemical composition measuring by WDXRF

For measuring the chemical concentrations of both the main and trace elements of the bulk sample was used a Rigaku® Supermini 200 WDXRF (wave-length X-ray fluorescence spectroscope) machine, which has a detection limit of 0.002-0.01 % for main and 5-10 ppm for trace elements.

Rigaku Supermini 200 type (WDXRF) wavelength dispersive X-ray fluorescence spectrometry equipment was used to analyse the samples at the Department of Mineralogy and Petrology, University of Miskolc, Hungary. The machine was provided by a 200 W (50kV and 4.0mA) Pd cathode X-ray tube, with LiF, PET and XR25 analyser crystals, which was driven by ZSX programme.

The qualitative mode can be used, without standardization, to check the chemical spectra, in the range between ^{9}F and ^{92}U. In quantitative mode, the individual elements are measured separately, but much higher accuracy can be reached. To decrease the fluctuation, caused by the measuring mistakes, every element 7-times were measured. The system in the calibration was setup to measure the in advance defined background points before and after the peak for 10 - 10 s, while the peak position was measured for 40 s.

Compared to the XRD method – which determine the mineralogical composition by using phase analysis – the XRF analysis measures the elemental composition of the sample. The disadvantage of both techniques, that their results are referred for the bulk, powderized sample.

3.2.2 Mineral phase determination by XRD

Bruker D8 Advance X-ray Powder Diffractometer (Cu-Kα source, 40kV 40mA, Bragg-Brentano geometry) equipped with secondary graphite monochromator was used to analyse the sample at the Department of Mineralogy and Petrology, University of Miskolc, Hungary. The measurement was run in the $2\Theta = 5 - 65°$ domain, with goniometer speed of $0.04°(2\Theta)$ in 2 seconds.

The evaluation of patterns was performed with EVA module of Bruker DiffracPlus data handling software package and Search/Match was carried out in the ICDD PDF-2(2005) database. Bruker software TOPAS3 was employed for the quantitative analysis and Fundamental Parameters Approach was used for modelling the instrumental profile. Rietveld refinement was performed using Crystallography Open Database structural cards. Background was modelled as 1/x function for air scattering at low angles and as 4th degree Chebyshev polynomial.

The amorphous materials contribution is observed as background elevation termed “amorphous hump” and is quantitatively determined with XRD. The low crystallite size, which in some cases may be considered to be poor crystallinity of e.g. clay minerals, is observed trough peak broadening (increase

DOI: 10.14750/ME.2021.004

of Full Width at Half Maximum, FWHM). This effect is modelled for quantitative determinations by adjusting the mean crystallite size, usually as volume weighted column length.

In case of a fresh sample, the XRD method gives accurate results of the mineralogical composition of the samples, as all of the minerals are well crystallized. The method has already lost its accuracy as oxidizing or already oxidized samples are measured. The secondary minerals dominantly formed quickly, so they are poorly crystallized or even amorphous. This property indicates, that the measuring of these minerals with XRD method is difficult and not accurate enough. If these secondarily formed minerals are amorphous, they cannot be identified with this type of method. Moreover, another maleficent effect has also appeared. In those samples, which have iron content higher than 5 %, during measuring the Cu anode in the X-ray tube has interference, which creates noisy background during the measuring of the samples. The elevated noise creates a lower peak - noise ratio, which pushes up the detection limit from 0.5 % to 1.0 or even 1.5 %.

3.2.3. Electron microscope and microprobe

Quite often, the oxidation and alteration of the mineral phases cannot be determined with the above mentioned methods, so necessary to find a method which can measure the chemical compositions in μm scale. For this purpose, the electron microscope and microprobe is the perfect tool. With the microscope function, high magnification can be reached in black and white colour, where the brightness depends on the average atomic weights. By this the μm scale tiny grains with alteration products became visible. With the microprobe function, the chemical measuring can be done in pots of diameter from 5 to 100 μm. As the system works with energy dispersive system (EDS), the detection limit is as high as about 0.5 – 1 %.

All of the samples were analysed by electron microscope, which can give high-resolution images and by microprobe, which can measure the chemical composition of the tiny grains. Both measuring methods were completed in the Institute of Mineralogy and Geology of the University of Miskolc with JEOL JXA-8600 Superprobe EMPA. The measurements were made with an upgraded SAMX software, with 15-20 kV acceleration voltage and 20 nA beam current. PAP correction was used during the measurement.

DOI: 10.14750/ME.2021.004

IV. HUMIDITY CELL TEST METHOD AND ITS RESULTS

Important to highlight, that in this dissertation the results of the humidity cell test are only used as a useful tool for the confirmation of the thesis points in the different topics. The purpose of the PhD dissertation does not directly show the results of the humidity cell test, as a reached and final target, but this information is only a kit of tools.

In 4 consecutive years on the 16 Bolivian and the 5 Hungarian samples humidity cell test was completed. The place for the testing and the laboratory was assured by KREC (Kjeøy Research and Education Centre) in Northern-Norway, at Kjeøy Island. Because of the different sampling time, not each sample was analysed in each year. The earliest collected ones were analysed for 4 years – like the samples from Oruro – while the Hungarian samples only for 1 year (Table 10). The samples were analysed for 3-4 months, then a break was kept for the rest of the year, so the samples were left without rinsing and ait pumping, but with opened up sample keeper. On the other hand, human capacity was also a limitation in the number of samples. The humidity cell test is a time consuming geochemical method.

Sample	***2008 summer***	***2009 summer***	***2010 autumn - 2011 spring***	***2011 autumn - 2012 spring***
Year code	1st year	2nd year	3rd year	4th year
Jalpha 1-7, Playa Iroco 1-7	0 - 101 days	0 - 42 days	0 - 115 days	---
Itos Jig 1-7; Itos Jig 2-7	0 - 101 days	0 - 42 days	0 - 121 days	0 - 119 days
Itos Granza 1-7, Itos Granza 2-7	0 - 101 days	0 - 35 days	0 - 121 days	0 - 119 days
BOL 1-8; BOL 2-8; BOL 3-8	---	0 - 42 days	0 - 121 days	0 - 119 days
BOL 1-9; BOL 2-9; BOL 3-9; BOL 4-9; BOL 5-9	---	---	---	0 - 112 days
BOL 6-9; BOL 7-9	---	---	0 - 115 days	0 - 119 days
HU 1-2; HU 2-4; HU 4-8; HU 8-16; HU 16-32	---	---	---	0 - 119 days

Table 10: Length of the humidity cell test periods in the four consecutive years of the humidity cell test analysis

During the 4 consecutive years of analysis, huge amount of data were produced, from measuring, observations and sampling. All of the measured data from the humidity cell test, the results of the sequential chemical extraction with additional information are detailly listed in the Appendix.

To take an overview of the geochemical behaviour of the samples during the humidity cell test period, the most important parameters of the seepage are plotted on the diagrams below. The pH (FIG. 27), the redox potential (FIG. 28) as well as the sulphate content (FIG. 29) represent well the oxidizing system itself. Difficult to visualize clearly on graphs such amount of data, which was produced. To make it as clear as possible, doubled plotting was used. This means, that in each sample, in case of each parameter in each year, two figures are plotted. The circle represents the data, which was measured in the effect of "first flush", while the rectangular represents the stabilized parameter during the test period.

DOI: 10.14750/ME.2021.004

The pH content (FIG 27.) of the seepages vary between wide range. This doubled plotting method helps to filter out the effect of the "first flush", which can be very significant in case of some samples. Generally, the first rinsing resulted in a unit lower pH – which means ten times higher H^+ concentration – than it was later in the stabilized phase of the samples, where the H^+ was given by the oxidation of the pyrite. In the first rinsing, the dissolution of secondary sulphides – such as jarosite – cause the elevated concentration of H^+. This dissolution reaction was described in equation 22.

Although dominantly the "first flush" effect causes one unit lower pH in the first rinsing, than later, but in some case, the samples – like Playa Irroco 1-7 in the 1st or BOL 2-8 in the 2nd year – started with pH 1, but later stabilized between pH 2.5 – 2.8. The opposite also happened, when the first flush effect didn't cause a significant difference in acidity, like in case of the BOL 1-8 in the 2nd and BOL 1-9 in the 4th year. These samples produced seepage with pH 2.6 and 2.4 both in the first rinsing and both in the stabilized phase. In these case, the absent of jarosite mineral caused, that the pH decreased not at all.

In case of the Hungarian samples, the first three set, so the HU 1-2, HU 2-4 and HU 4-8, cause typical aspect in the first rinsing, as the pH was decreased, but in case of the two coarser fraction – so HU 8-16 and HU 16-32 – the firstly measured pH is within the stabilized ranges. Although necessary to mention, that the Hungarian samples produced acidity is significantly – at least 2-3 unit – lower than the pH were produced by the Bolivian samples. The reason is mainly that the Hungarian ones are fresh samples, while the Bolivian ones were in the stage of oxidation. Moreover, the Hungarian sample set contained neutralizing minerals, such as calcite and dolomite.

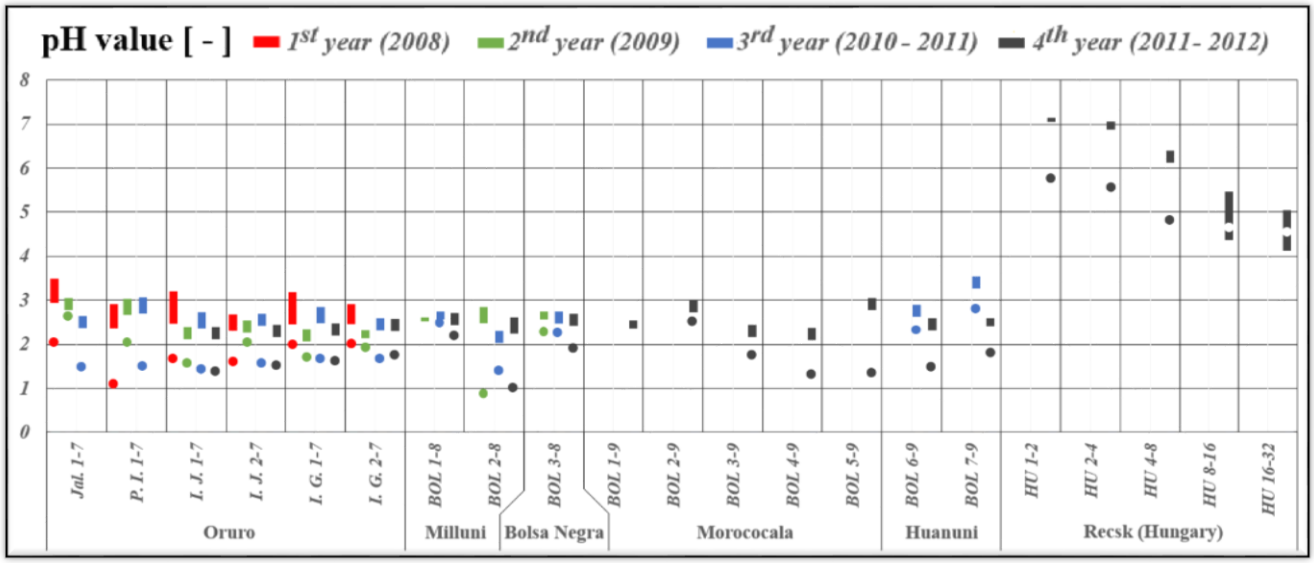

FIG. 27: Changes of the pH values of the seepage during the humidity cell test analysis

In case of the redox potential (FIG. 28) the results were not as standard, as in case of the pH were. Three trends can be observed, such as the Eh was the lowest in time of the first rinsing, then it also can be somewhere within the whole range, that the sample produced during the humidity cell test, or finally, it can be the highest in case of the first rinsing, then later in the test period. For each attitude, the mineralogy and its changing gives the answer.

DOI: 10.14750/ME.2021.004

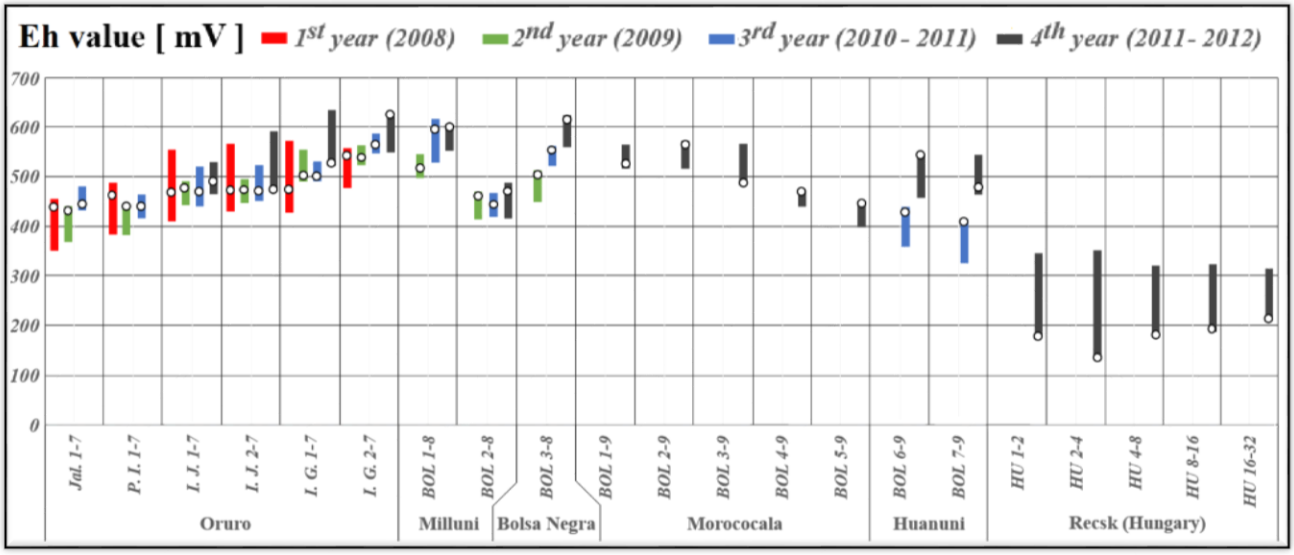

FIG. 28: Changes of the redox potential (Eh) values of the seepage during the humidity cell test analysis

Those samples, which had the lowest Eh results in case of the first rinsing – such as Itos Granza 1-7 from Oruro – had increasing oxidation during the test. For them, was necessary the rinsing water to clean down the secondarily formed minerals from the pyrite surface, to give fresh surface for the reaction. Based on this, as much sampling was done, as much energy thy sample had from the oxidation process. In the breaks between the sampling periods such secondary minerals were formed, which decreased the energy of the oxidizing system, thus as the active rinsing and air pumping stopped, the oxidizing system slowly lost its redox potential, as the alteration reactions slowed down or even stopped.

Although the Hungarian sample set behaved in the same way, but the reason was different. It was caused because the samples had fresh surface, no pyrite oxidation reaction had started before the first rinsing. This means, that the oxidation process just started with the humidity cell test. All of the five samples had low redox potential in the beginning, which continuously increased during the test period, as the oxidation reaction takes place on the pyrite surface in the samples. The fresh surface pyrite needed time to start and also to speeded up the reactions, created higher redox potential for the system.

In case of that samples – such as Itos Jig 1-7, where the first rinsing's redox potential were within the range of the data set, the pauses caused such mineralogical changes, which partly used up the energy of the oxidizing system. The again started rinsing and sampling period helped to get rid of the secondary alteration products during a few weeks and the system after a redox potential decreasing during this transition period reached an increasing, as on the cleaned pyrite surface the oxidation rate speeded up.

Some samples – such as BOL 3-8, BOL 5-9 and BOL 6-9 in all years – started the humidity cell test period with the highest redox potential which decreased later. In these samples, active part of the test period cleaned the surface of the grains down and during the 8-9 months break between the active test periods such kind of mineral alteration was formed, which indicated the elevated level of Eh for the first rinsing. Important to mention, that these samples produced 50-60 $^{g}/_{l}$ dissolved sulphate for the first rinsing, which confirmed the high rate of mineral alteration during the half year long break.

DOI: 10.14750/ME.2021.004

The sulphate content (FIG. 29) behaved more simply than the redox potential did. In case of all samples in all years the first rinsing caused significantly higher concentrations than later the system had stabilized. In general, the starting concentration was – at least – one magnitude, thus 10-times higher than later, when thy system became stable. But in some cases, the starting values were several magnitudes higher. For example, the sample Itos Jig 1-7 produced this, when the concentration after a 20 740 starting stabilized during a month at around 100 $^{mg}/_{l}$, or in case of BOL 3-9 the starting 64 790 concentration felt down to 856 already for the second rinsing time. The sample BOL 5-9 and BOL 6-9 had similar extremities, as they started with 55 500 and 70 640 and stabilized around 150 and 300 $^{mg}/_{l}$ concentrations. The reason for these extreme decreasing during so short time, the high rate of easily dissolvable secondary sulphate minerals – such as gypsum and jarosite – which were build up and accumulated during the 8-9 months length pauses between the 3-4 months of active test periods. These samples – which produced these extreme changes in dissolved sulphate content in the seepage –were exactly the sample, which were produced the highest jumping of pH during the first flush effect.

Unfortunately the SO_4^{2-} contents of the seepage were not measured in the 2nd year, so in summer of 2009 by personal and technical problems, when the humidity cell test period took 35 and 42 days.

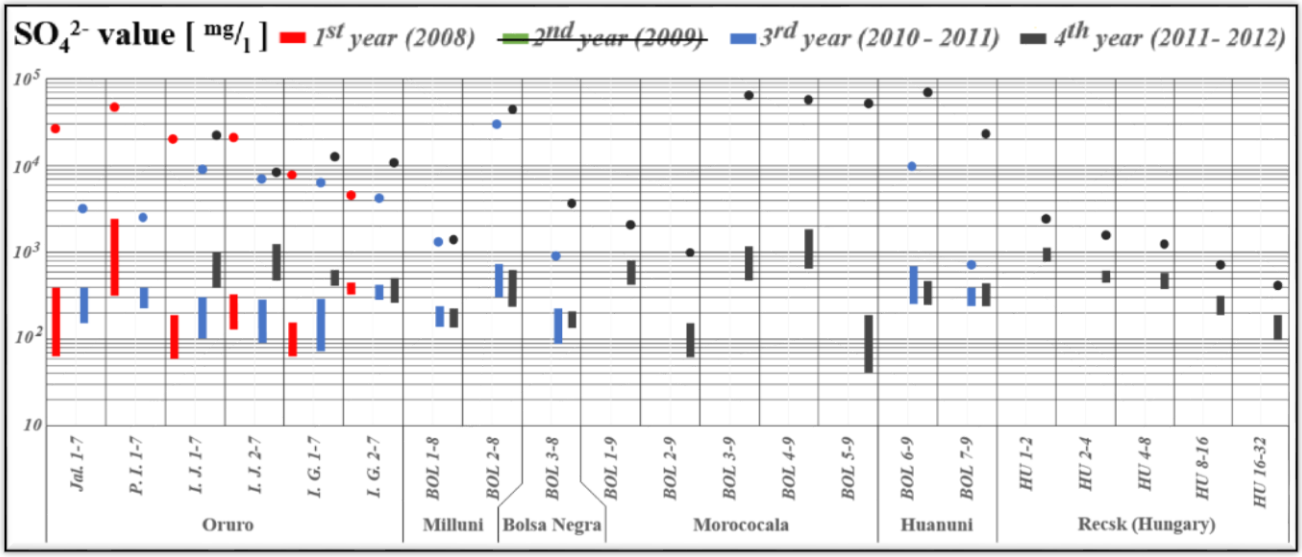

FIG. 29: Changes of the sulphate concentrations of the seepage during the humidity cell test analysis

The original aim with the Hungarian sample set was to determine how the different grain size can modify the pyrite oxidation rate. During the 119 days of analysis of the 4th year, this effect was not determined yet, as there were no significant changes in that time period. 17 weeks (119 days) were analysed by me and further 66 weeks were analysed by Rodrigo Embile, who continued the test, which was designed, setup and started only by me. A common article (Embile et al. 2016) was published in the Mine Water and the environment Journal, with title of: "*Grain Size Effects on Mine Water Quality and Acid/Neutral Rock Drainage Production in Kinetic Testing Using Recsk Porphyry Skarn Cu–Zn Deposit Rocks.*" As the result is not only my own property, I will not use in this dissertation. Based on this, the topic of the grain size effects on the oxidation will be not discussed.

DOI: 10.14750/ME.2021.004

V. MINERALOGICAL AND SOLID PHASE CHEMICAL MEASUREMENTS

The humidity cell test alone – does not matter how accurately it was done – is not enough to be able to characterize an oxidizing system. The determination of the mineralogical composition, done by X-ray powder diffraction (XRD) method is also necessary. Also important to see the chemical composition of the samples, especially in those cases, where questions are raised during the analysis. In these cases, complementary measuring techniques – such as WDXRF or electron microscope and microprobe – need to be called for help. Although, these other methods can also be used in such cases when extra information is necessary from the bulk or from any separate part(s) of the samples.

5.1. Mineral phase determination by XRD

Similarly to the result of the humidity cell test, the result of the mineralogical analysis is also only a useful tool for the proving of my theories and not the final aim of this PhD thesis.

Two sets of samples will be shown, for different purpose. Firstly I would like to show the high differences among the samples, although they were collected from the same mining district. For this purpose the samples from Oruro – where 6 samples were collected – are ideal. Furthermore, 4 from the 6 ones were collected from the same ore mineralization, which was linked to the Itos mine. Table 11 shows the high similarity of the four samples from the Itos mine.

Mineral	***Formula***	Jalp.	P. I.	I.J. 1	I.J. 2	I.G. 1	I.G. 2
		$^{m}/_{m}\%$		$^{m}/_{m}\%$	$^{m}/_{m}\%$	$^{m}/_{m}\%$	$^{m}/_{m}\%$
Quartz	SiO_2	59.0	33.2	44.1	39.9	53.3	54.1
Pyrite	FeS_2	5.0	5.3	6.8	3.6	2.4	1.7
Illite	$(K;H_3O)Al_2Si_3AlO_{10}(OH)_2$	12.8	17.2	19.2	24.3	16.1	13.1
Biotite	$K(Mg,Fe)_3[AlSi_3O10(OH)_2$			0.9	0.9	0.5	0.5
Titanomagnetite	$(Fe,Ti)_3O_4$			0.5	0.5	0.7	0.7
Dravite (schorl)	$Na(Mg_3)Al_6(Si_6O_{18})(BO_3)_3(OH)_3(OH)$		20.7	14.5	15.8	14.8	12.9
Rutile	TiO_2					0.2	0.3
Cassiterite	SnO_2						0.4
Jarosite	$KFe_3(SO_4)_2(OH)_6$						1.3
Hydronium jarosite	$(H_3O)Fe_3(SO_4)_2(OH)_6$	0.1					
Plumbojarosite	$PbFe_6(SO_4)_4(OH)_{12}$	3.6					
Anglesite	$PbSO_4$	0.8	1.4				
Gypsum	$CaSO_4*2H_2O$	0.7	3.0				
Coquimbite	$AlFe_3(SO_4)_6(H_2O)_{12}*6H_2O$		2.2				
Rozenite	$FeSO_4*4H_2O$		1.6				
Voltaite	$K_2Fe_8Al(SO_4)_{12}*18H_2O$		1.9				
Kaolinite	$Al_2(Si_2O_5)(OH)_4$	ind.					
Chalcopyrite	$CuFeS_2$	ind.					
Amorphous components		18	13.5	14	15	12	15

Table 11: Quantitative mineralogical composition of the samples from Oruro (Abbr.: Jalp.: Jalpha 1-7; P.I.: Playa Iroco 1-7; I.J. 1: Itos Jig 1-7; I.J. 2: Itos Jig 2-7; I.G. 1: Itos Granza 1-7; I.G. 2: Itos Granza 2-7)

DOI: 10.14750/ME.2021.004

Furthermore, they can be split into two groups, as between the two jig tailings and waste rock samples have some slight differences. The waste rocks have higher quartz and titanomagnetite, but lower pyrite, illite and biotite content. From another point of view, the two fine-grained, flotation tailing samples, the Jalpha 1-7 and Playa Iroco 1-7 are slightly similar in their mineralogical composition, but they are totally different than the Itos samples. Furthermore in the two fine samples several secondary minerals appeared after the alteration and the oxidation. These minerals are sulphate minerals, like gypsum, anglesite, and two versions of jarosite: the hydronium and the plumbo types.

With the X-ray powder diffractometry measuring the other aim was to prove the mineralogical homogeneity of the sample set of the ***Hungarian samples***. The qualitative results (Table 12) for each grain size fraction shows, that the mineralogical composition is roughly the same. In all samples magnesium and calcium-containing siderite and tetrahedrite were present, but in such low concentration, that it can be listed only as an indication.

Mineral	***Formula***	***HU 1-2***	***HU 2-4***	***HU 4-8***	***HU 8-16***	***HU 16-32***
Pyrite	FeS_2	35.4	34.2	33.5	30.0	39.1
Quartz	SiO_2	44.7	42.1	42.3	42.4	39.2
Dolomite	$CaMg(CO_3)_2$	2.7	0.9	2.7	6.7	9.7
Ankerite ($Fe_{0.55}$)	$Ca(Fe,Mg)(CO_3)_2$	4.1	4.2	7.0	8.0	5.9
Calcite (magnesian)	$Mg_{0.1}Ca_{0.9}CO_3$	1.7	2.1	1.4	0.4	0.4
Calcite	$CaCO_3$	5.8	8.1	6.9	4.8	1.5
Chalcopyrite	$CuFeS_2$	1.6	1.9	1.9	1.2	1.0
Sphalerite iron	ZnS	3.3	5.5	3.9	6.3	2.2
Titanomagnetite	$Fe(Fe_{1.17}Ti_{0.54})O_4$	0.7	0.6	0.3	0.1	0.3
Hercynite	$FeAl_2O_4$	0.1	0.5	0.1	0.1	0.7
Siderite (Mg, Ca)	$Ca_{0.1}Mg_{0.33}Fe_{0.57}(CO_3)$	ind.	ind.	ind.	ind.	ind.
Tetrahedrite	$Cu_{12}Sb_4S_{13}$	ind.	ind.	ind.	ind.	ind.

Table 12: Qualitative mineralogical composition (in unit of $^m/_m$%) of the HU sample set, measured by XRD

The diffractograms of the different grain size samples were plotted on a common x-axis chart (FIG. 30), to be able to see visually the homogeneity or the differences among the rain sizes. As it is determined from the height of the peaks, the mineralogical composition is almost the same for each size fraction. The only difference, that there are changes at the height of the peaks between 29.5 and 31°.

In the finer fractions, there are more calcite and less dolomite, in the 4-8 mm grain size is approximately equal and at larger grain size, the amount of the dolomite and ankerite are a bit more than the calcite itfelf. These changes are possibly caused by milling the original material because different stress resistance has the different carbonates, thus they will brake on different ways, shapes and sizes. However all of them neutralizers, so these mineralogical changes cannot cause any difference in the neutralizing capacity. The hercynite belongs to the spinel structure, thus it is an inert mineral from point of ARD, similarly to quartz.

DOI: 10.14750/ME.2021.004

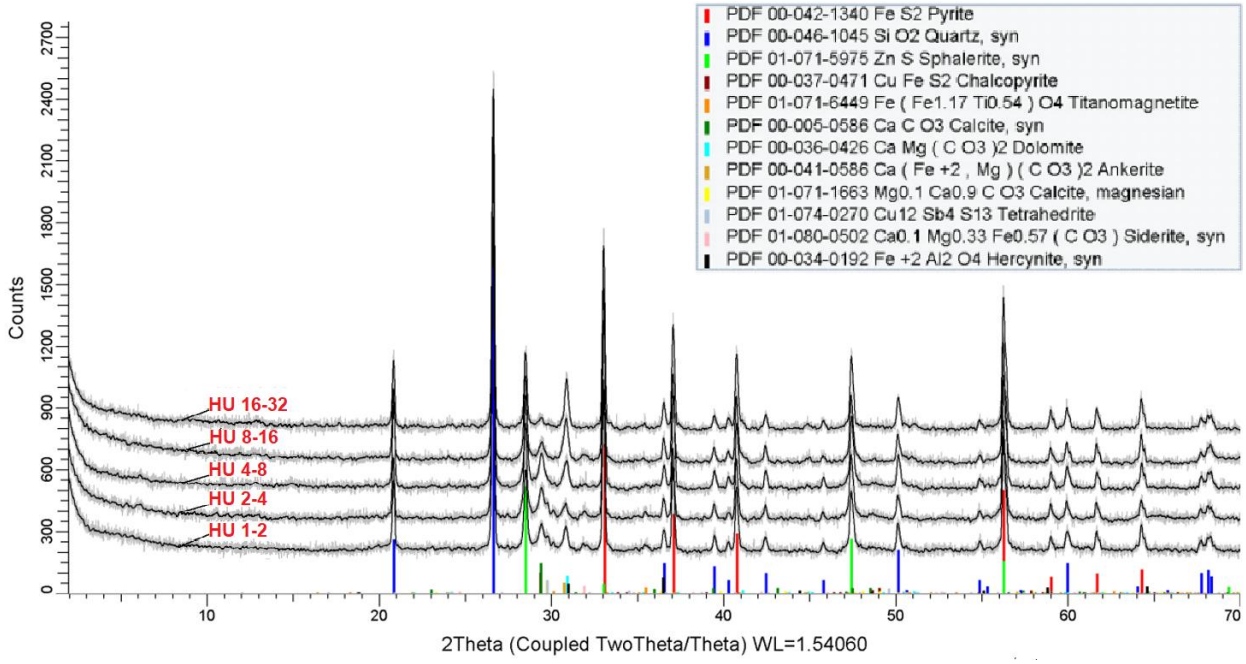

FIG. 30: XRD diffractograms of the five different size fractions of the HU series, plotted on a common x-axis

5.2. Solid phase chemical analysis - Bulk element analysis by WDXRF

All the samples were measured for their chemical composition – both for main (Table 13/a) and trace (Table 13/b) elements – by the Rigaku® Supermini200 WDXRF machine. The measurements were supplemented by the determination of LOI. The results of the main elements represent well, that the samples – except the Itos series – have significantly different chemical composition.

Sample	***SiO_2***	***Al_2O_3***	***MgO***	***CaO***	***Na_2O***	***K_2O***	***Fe_2O_3***	***MnO***	***TiO_2***	***P_2O_5***	***S***	***F***	***LOI***
Det. limit	***0.1***	***0.1***	***0.01***	***0.01***	***0.01***	***0.01***	***0.01***	***0.005***	***0.005***	***0.005***	***0.005***	***0.3***	***-***
Unit	$^m/_m\%$	$^m/_m\%$	$^m/_m\%$	$^m/_m\%$	$^m/_m\%$	$^m/_m\%$	$^m/_m\%$	$^m/_m\%$	$^m/_m\%$	$^m/_m\%$	$^m/_m\%$	$^m/_m\%$	$^m/_m\%$
Jal. 1-7	49.1	12.9	0.52	0.10	0.36	2.57	8.43	0.025	0.438	0.127	7.59	<0.3	15.8
P. I. 1-7	47.2	14.8	0.62	1.43	0.30	2.08	11.7	0.006	0.521	0.109	9.57	<0.3	13.9
I. J. 1-7	59.7	17.4	0.64	0.04	0.21	2.42	9.92	0.006	0.094	0.139	5.04	<0.3	9.9
I. J. 2-7	58.1	18.0	0.70	0.03	0.23	2.72	8.68	0.007	0.730	0.089	3.82	<0.3	8.4
I. G. 1-7	64.7	17.9	0.65	0.06	0.27	2.29	6.31	0.008	0.579	0.105	2.19	<0.3	7.6
I. G. 2-7	66.6	15.9	0.57	0.14	0.32	2.21	6.16	0.010	0.573	0.129	1.91	<0.3	5.0
BOL 1-8	78.1	9.7	0.41	0.64	0.13	1.82	4.67	0.022	0.340	0.463	0.70	<0.3	3.1
BOL 2-8	56.1	7.4	0.40	0.11	0.14	1.01	21.1	0.009	0.323	0.017	15.1	<0.3	16.0
BOL 3-8	76.1	10.2	0.82	0.13	0.25	2.04	6.69	0.026	0.451	0.078	1.08	<0.3	3.3
BOL 1-9	63.8	14.7	0.48	0.32	0.39	3.06	4.34	0.007	0.719	0.145	2.17	<0.3	7.2
BOL 2-9	68.3	11.7	0.63	0.82	1.39	2.60	5.84	0.023	0.531	0.134	0.98	<0.3	5.1
BOL 3-9	66.7	8.8	0.39	0.11	0.18	1.43	8.78	0.006	0.533	0.090	5.19	<0.3	10.4
BOL 4-9	49.9	10.6	0.28	0.19	0.11	1.53	16.9	0.005	0.586	0.065	13.1	<0.3	21.7
BOL 5-9	52.7	5.72	0.23	0.07	0.06	0.98	21.6	0.007	0.275	0.103	16.1	<0.3	21.6
BOL 6-9	76.6	8.8	0.78	0.13	0.28	0.76	5.88	0.024	0.490	0.064	2.86	<0.3	3.6
BOL 7-9	78.9	9.0	0.86	0.15	0.32	0.67	6.33	0.038	0.482	0.067	2.01	<0.3	3.0

Table 13/a: Main elements composition of the Bolivian samples (Abbr.: Jal 1-7.: Jalpha 1-7; P.I. 1-7: Playa Iroco 1-7; I.J. 1-7: Itos Jig 1-7; I.J. 2-7: Itos Jig 2-7; I.G. 1-7: Itos Granza 1-7; I.G. 2-7: Itos Granza 2-7)

DOI: 10.14750/ME.2021.004

These significant differences can be found also in the trace element composition of the samples. Especially the heavy metal concentrations show high deviation, especially in case of zinc, lead and arsenic. The metal concentration shows the fingerprint of the polymetallic ore mineralization, along the sampling places.

Sample	***Cu***	***Zn***	***Pb***	***Rb***	***Sr***	***Ba***	***As***	***Cr***	***Co***	***Ni***	***Zr***
Det. limit	***5***	***5***	***5***	***5***	***5***	***15***	***5***	***5***	***5***	***5***	***5***
Unit	***ppm***	***ppm***	***ppm***	***ppm***	***ppm***	***ppm***	***ppm***	***ppm***	***ppm***	***ppm***	***ppm***
Jal. 1-7	115	18800	8657	23	382	157	180	31	<5	<5	64
P. I. 1-7	346	102	5796	50	87	210	3257	61	<5	11	53
I. J. 1-7	25	35	1944	82	175	315	912	54	21	10	95
I. J. 2-7	17	31	1656	116	119	252	1077	66	20	9	112
I. G. 1-7	19	28	909	100	119	330	371	49	31	6	126
I. G. 2-7	14	28	935	96	141	357	390	40	39	6	151
BOL 1-8	63	111	661	118	25	144	728	76	<5	7	200
BOL 2-8	149	410	2020	30	7	110	1881	71	<5	8	87
BOL 3-8	294	20	525	105	26	350	612	71	14	11	179
BOL 1-9	35	168	1408	150	295	1107	70	49	<5	10	321
BOL 2-9	32	228	637	127	290	639	634	41	<5	9	299
BOL 3-9	48	1112	849	59	87	259	509	46	<5	9	258
BOL 4-9	15	285	1152	50	47	399	849	47	<5	11	140
BOL 5-9	7	130	1647	21	29	206	1250	34	<5	6	81
BOL 6-9	327	404	305	48	38	18	327	53	<5	14	197
BOL 7-9	408	804	382	44	39	424	727	100	5	15	213

Table 13/b: Trace elements composition of the Bolivian samples (Abbr.: Jal 1-7.: Jalpha 1-7; P.I. 1-7: Playa Iroco 1-7; I.J. 1-7: Itos Jig 1-7; I.J. 2-7: Itos Jig 2-7; I.G. 1-7: Itos Granza 1-7; I.G. 2-7: Itos Granza 2-7)

The same analysis was completed both for main (Table 14/a) and trace elements (Table 14/b) on the Hungarian sample set to prove – parallel with the XRD analysis – that the 5 different grain size fractions have the same composition, or at least so low, that can be negligible. The results of the WDXRF measuring show clearly, that the differences among the samples are negligible, thus practically each member of the sample set have the same mineralogical and chemical composition.

Sample	***SiO_2***	***Al_2O_3***	***MgO***	***CaO***	***Na_2O***	***K_2O***	***Fe_2O_3***	***MnO***	***TiO_2***	***P_2O_5***	***S***	***F***
Det. limit	***0.1***	***0.1***	***0.01***	***0.01***	***0.01***	***0.01***	***0.01***	***0.005***	***0.005***	***0.005***	***0.005***	***0.3***
Unit	***$m/_m$%***	***$m/_m$%***	***$m/_m$%***	***$m/_m$%***	***$m/_m$%***	***$m/_m$%***	***$m/_m$%***	***$m/_m$%***	***$m/_m$%***	***$m/_m$%***	***$m/_m$%***	***$m/_m$%***
HU 1-2	34.4	2.42	4.13	8.34	0.10	0.07	29.41	0.347	0.091	0.064	24.2	<0.3
HU 2-4	33.3	2.36	4.17	8.21	0.12	0.08	29.50	0.389	0.090	0.063	22.7	<0.3
HU 4-8	36.9	2.10	2.93	8.08	0.11	0.14	27.02	0.302	0.074	0.062	24.6	<0.3
HU 8-16	33.1	2.89	4.51	7.86	0.10	0.28	28.32	0.320	0.081	0.062	23.5	<0.3
HU 16-32	34.6	3.37	3.94	5.48	0.11	0.19	30.13	0.123	0.120	0.067	26.3	<0.3

Table 14/a: Main elements composition of the Hungarian sample set

DOI: 10.14750/ME.2021.004

Sample	*Cu*	*Zn*	*Pb*	*Rb*	*Sr*	*Ba*	*As*	*Cr*	*Co*	*Ni*	*Zr*
Det. limit	***0.001***	***0.001***	***5***	***5***	***5***	***15***	***5***	***5***	***5***	***5***	***5***
Unit	***m/m%***	***m/m%***	***ppm***	***ppm***	***ppm***	***ppm***	***ppm***	***ppm***	***ppm***	***ppm***	***ppm***
HU 1-2	0.380	1.037	31	< 5	21	< 5	27	35	37	10	11
HU 2-4	0.363	1.237	25	< 5	21	< 5	8	37	7	9	11
HU 4-8	0.376	1.255	28	< 5	18	< 5	11	31	26	14	10
HU 8-16	0.141	1.009	36	< 5	15	< 5	24	38	9	9	8
HU 16-32	0.356	0.709	26	< 5	22	< 5	21	48	33	12	11

Table 14/b: Trace elements composition of the Hungarian sample set

Necessary to mentione, that the relevance of the results of this method is not high. Dominantly the element concentrations in the individual grains – measured by electron microscope and microprobe – gives much more information and characterize better the system, than the bulk chemical analysis by WDXRF method. Nevertheless in some cases, like the original sample BOL 6-9 with its 7 derivative samples in Chapter 10.2.2., where the WDXRF results help to characterize and understand the special processes inside the column. Thus in such cases, the importance cannot be queried.

5.3. Solid phase chemical analysis - Electron microscope and microprobe

The different grain sizes samples indicated different preparation for the measuring. On the clayish samples, such as Jalpha 1-7 three types of sample preparation were done, the first was that the original clayish sample was glued to a flat surface, the second one was a washed and heavy mineral separated sample and finally a glued into acrylate resin and polished.

On coarser samples, two types of preparation were done, firstly the selected grains were measured without any washing, and secondly, polished sections were made from them with help of acryl resin.

Not each sample will be discussed in this chapter. Only an overview will be done, as the most relevant, important and interest results will be shown of the 16 samples. In some cases in other chapters will be interpreted the results of the measuring, if that sample is more relevant in the given chapter, such as Jalpha 1-7 and Itos Jig 2-7 in Chapter 7., where the accuracy and the applicability of the combined method will be proved on them. Some of the separated grains were already shown in the chapter of the optical evaluation (Chapter 2.1.2.).

The ***Playa Iroco 1-7*** sample was so clayish, that it was necessary to wash down some sample, to get rid of the secondary and fine, “clayish” fraction, to be able to see at all any crystal. A well-developed crystal group of pyrite (FIG. 31) was found which was a bit surprising, because in such an acidic condition (pH≈1.5-2) usually it starts oxidizing and secondary minerals should be on its surface. But these crystals were free of them, although, small darker pots were visible, which are probably places of

DOI: 10.14750/ME.2021.004

oxidation. From the same sample, another interest grain caused high brightness contrast on the BSE image, as galena with well-developed quartz crystals in accretion (FIG. 32/a) become visible. By higher magnification (FIG. 32/b) the own shapes of the quartz crystals are presented. On the galena, the fingerprint of the oxidation was visible, as in some place partly have already altered to anglesite.

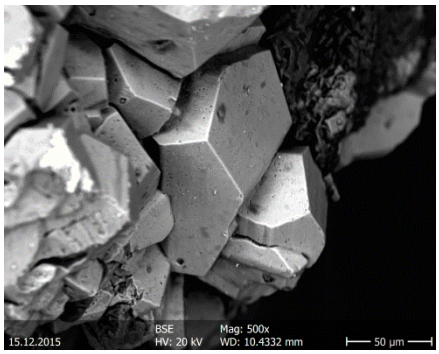

FIG. 31: Own shaped pyrite (500X)

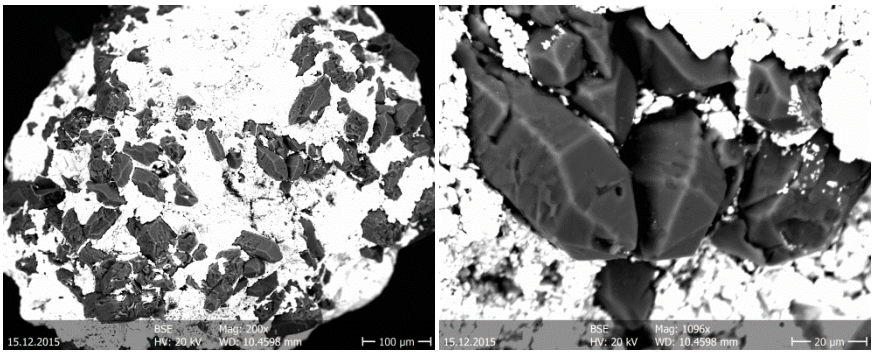

FIG. 32/a and b: Well-developed quartz and galena accretion (200X; 1096X)

As on the surface of the sample set of Itos mine was no clay fraction, no washing was necessary, so the totally or partly soluble secondary minerals could stay present. In sample ***Itos Jig 1-7*** on a jarosite crystals covered surface, pyrite crystals were visible (FIG. 33/a). Although sometimes they were well developed, the strong alteration has already smoothed the surface of the pyrite cubes (FIG. 33/b). Some of them felt out from their original place and become visible, that the structure under the pyrite grains has also totally altered to secondary minerals. As the electron beam was moved to small grain from ***Itos Granza 2-7***, much more altered minerals took place. The oxidation product of galena, the anglesite in association with strongly oxidized pyrite crystals (FIG. 34) were found. The real shape was not visible, which could remind for pyrite, only form microprobe measuring was determined.

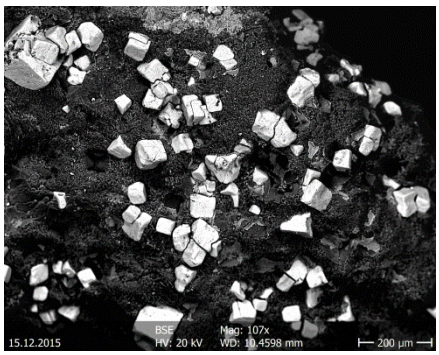

FIG. 33/a and b: Secondary jarosite with smoothed surface pyrite cubes

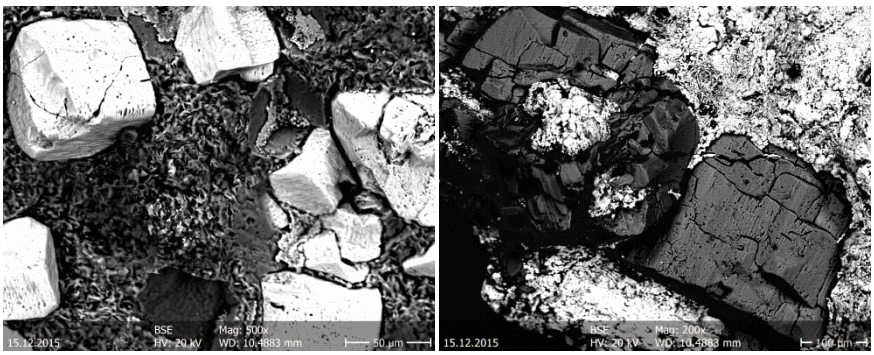

FIG. 34: Altered pyrite and anglesite

On the grain of the second sample from Milluni, the ***BOL 2-8***, which was shown (FIG. 16/a and b) in the optical evaluation chapter microprobe measuring were completed and also BSE images were taken. The grain itself is a strongly altered sulphide (FIG. 35) in composition of pyrite and arsenopyrite with hundreds of oxidation caverns. In the sponge-style structure, tiny crystals were formed (FIG 36/a), which consisted of oxygen, iron, and arsenic with a tiny amount of sulphur (<1 %). By the ratio of the elements (FIG. 36/b), it was identified as an iron arsenate, as scorodite /$FeAsO_4$*$2H_2O$/, which can be formed in the oxidation zone on sulphidic materials after the alteration of arsenopyrite.

DOI: 10.14750/ME.2021.004

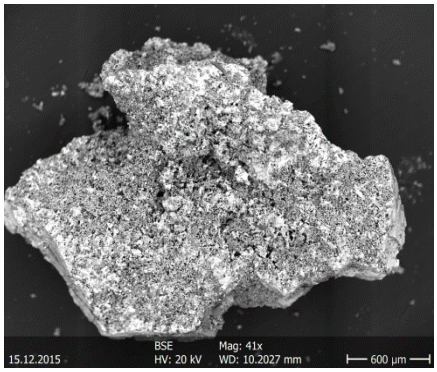

FIG. 35: Altered sulphides

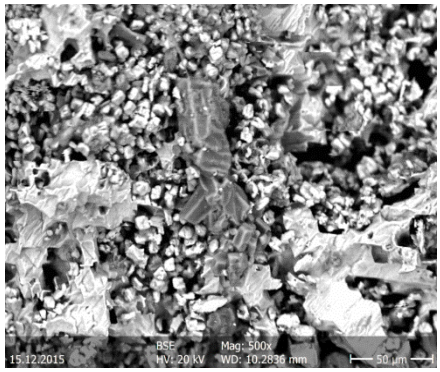

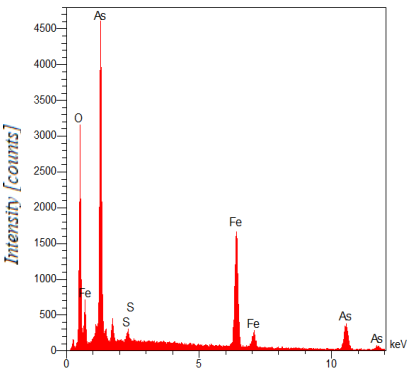

FIG. 36/a and b: BSE image and spectrum of the found Fe-arsenate phase

The sample ***BOL 2-9*** from Morococala contained lots of broken biotite flakes, which has been mentioned during the optical evaluation part. Although the neutralizing capacity of this silicate mineral is totally negligible, the acidic environment corrodes its structure as well. On the edge of the crystal the marks of the degradation, caused by the acidity, have already formed (FIG. 37/a). There were brightness contrasts on the upper flake of the biotite grain, so on such two places, where clay minerals were not present, microprobe measurements were completed. The analysis proved the slightly different colours, because the iron concentration is almost double in the lighter zones, than in the darker one. The spectrums of the two measures are plotted on the same chart (FIG. 37/b), but with a bit shifted x-axis.

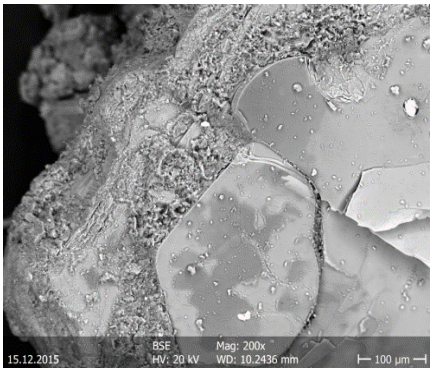

FIG. 37/a: Degradation of biotite

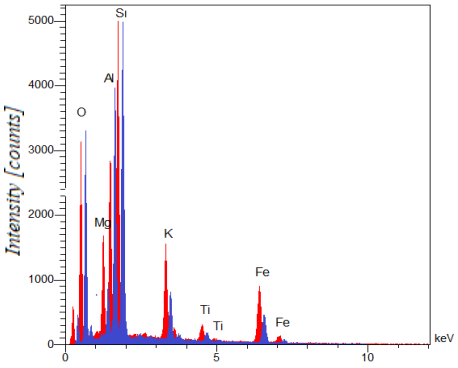

FIG. 37/b: Chemical spectrum

Still stayed at sample from Morococala, the ***BOL 3-9*** has shown high rate of possibly jarosite minerals under the optical microscope (FIG. 19/a and b). The BSE images (FIG. 38/a and b) proved the well-developed shape of the crystals and the microprobe analysis proved that it is effectively jarosite mineral. From a different mining place, but still form Morococala, in sample ***BOL 4-9*** on a pyrite fragment the BSE image (FIG. 39) shown tiny strongly bright minerals in a dark massy aggregation. The chemical composition analysis defined the dark zone as potassium-containing clay minerals, probably as illite, while the brightest dots were small cassiterite grains.

DOI: 10.14750/ME.2021.004

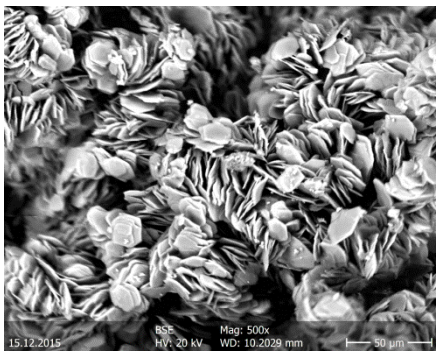

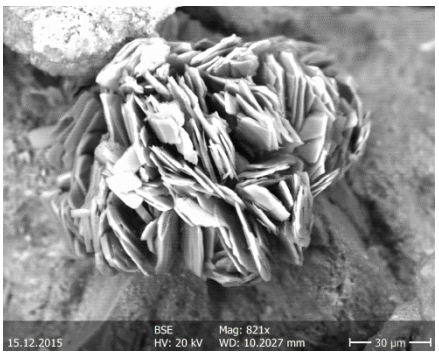

FIG. 38/a and b: Secondarily formed well-developed jarosite crystals

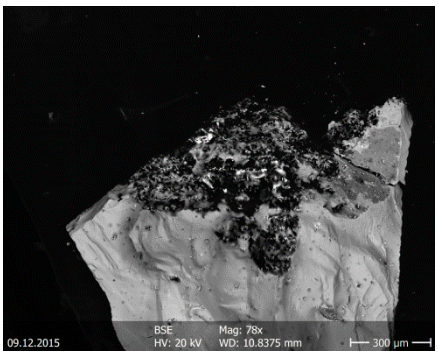

FIG. 39: Pyrite, clay and cassiterite

From the last sample of the Morococala set, from the ***BOL 5-9*** a well developed pinkish crystal formation (FIG. 21) was picked out. Although it was well crystallized, by optical microscope it was not possible to identify what mineral it is, but even not which mineral group it belonged to. It had to be something secondary formation, as it totally encompassed a grain. When the electron beam gave the first BSE image from it, it started to disappear, as the well-developed crystals firstly changed only to smoothed surface, but a few seconds later, the smoothed crystals have already formed a common, amorphous, and shapeless material, with only a few still detectable crystals (FIG. 40/a). The chemical measuring identified this mineral as an iron sulphate, but the oxygen content was so high, that high amount of crystal water also had to be involved. The effect of the "visible melting" confirmed this theory because the high vacuum of the sample chamber of the electron microscope creates such a process with the high water containing minerals. The partial pressure became so low, that the water simply started boiling and evaporated immediately.

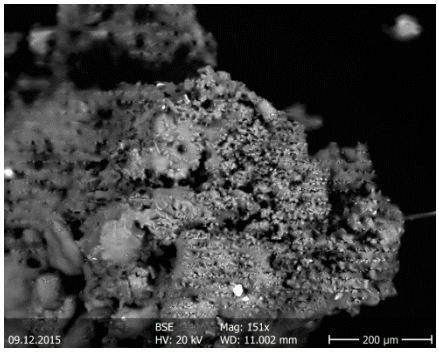

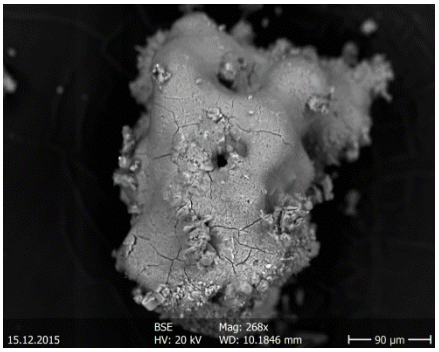

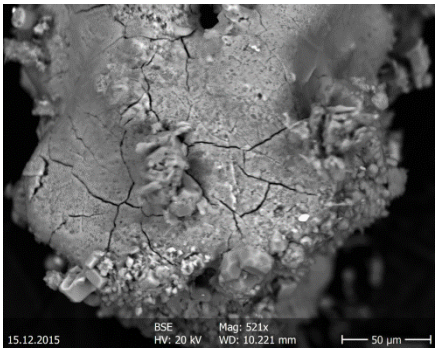

FIG. 40/a, b and c: Morphological changes of the separated mineral by water loss, caused by high vacuum

This effect is even stronger when the electron beam hits the mineral and starts "burning" it. A week later the same grain was analyzed again, so it was exposed to vacuum for almost 2.5-3 hours already, but between the analyses, it was stored in normal room condition. This time, the surface was even more smoothed (FIG. 40/b), probably caused by the further vacuum was maintained last time. Even this magnification cracks were visible, but on higher focus (FIG. 40/c) it became clearer. These cracks were caused by further water loss, probably as a collective effect of the 2.5-3 hours of vacuum and the week length storage on open air. Beside the BSE imaging, the sample, which at the end looked like an amorphous noodle, time by time was remeasured by microprobe. The results were very instructive, as the Fe-S ratio stayed constant, but the oxygen continuously decreased. This is visually presented also on

DOI: 10.14750/ME.2021.004

a common (FIG. 40/d) plotted spectrum, wherethe x axis of the individual measurings were shifted always by 0.2 keV. The first three measurings (shown as red, dark blue and green) were done during the first time of analysis, but the last two measurements (colored as light blue and orange) were completed a week after. As during the measuring the y axis is automatically fitted to the highest peak, some type on normalization was needed to do. This was simple, because the Fe-S ratio was fix, the sulphur was chosen as it had higher peak than the iron. In the five measuring the S peaks were shrunk to the same height, but of course, the other two elements was shrunk with the same ratio. On the prepared spectrum is clearly visible, that the Fe peaks have the same high, as the Fe-S ratio was constant in the measurings and the S peaks were normalized to the same height, so the Fe peaks followed them and kept the ratio. This constant behaviour cannot be told from the oxygen contents, which decreased continuously as the sample lost water by dewatering caused by the high vacuum of the sample chamber. From the oxygen content, the amount of crystal water can be calculated. It shows decreasing tendencies, as it was 5.6 moles in the first measuring, then 4.7, 3.0, 1.4 and finally the sample totally lost its water, as the calculation defned it as zero.

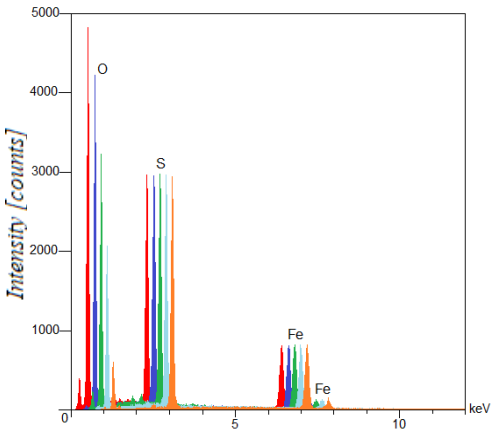

FIG. 40/d: Decreasing O by waterloss

As moved to the last and latest Bolivian sampling place, from the ***BOL 7-9*** a strongly yellowish grain were separated out under the optical evaluation (FIG. 22/a and b). By the typical yellowish colour, it was identified as jarosite. As the magnification of the electron microscope was increased from 72 times, till 1000 times (FIG. 41/a, b, and c), more and more fine details of the individual grains became visible. The BSE images showed very similar crystals like in the case of BOL 3-9 it was. The microprobe measuring proved that these are jarosites also.

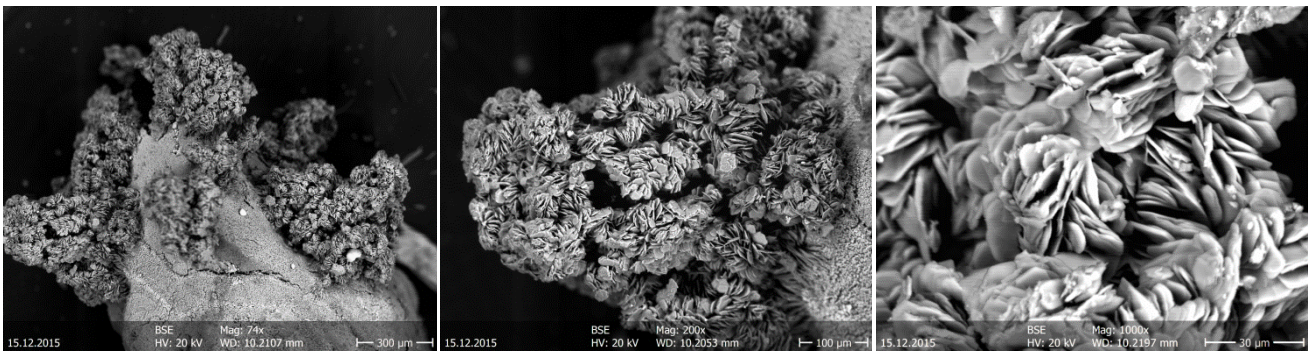

FIG. 41/a, b and c: Well developed, secondarily formed jarosite crystals with own shape (a:72X; b:200X; c:1000X)

DOI: 10.14750/ME.2021.004

VI. PYRITE OXIDATION UNDER CIRCUMNEUTRAL pH CONDITION

6.1. Introduction

In the last four decades in the sulphidic ores mining, the effect of Acid Rock Drainage (ARD) has become the leading environmental problem. In the wastes, the principal weathering process is the sulphide oxidation, resulted in low pH and increased heavy metal mobility (Blowes et al. 2003/a). If neutralizing minerals are available, they can buffer the acid production and reduce the heavy metal mobilization. As the amount of the acid-producing minerals exceeds the neutralizing ones, by time the acid-producing capacity will exceed the neutralizing capacity, thus acidic environment will be formed.

From the mining waste management point of view, a crucial question is whether there are enough available buffering minerals, which can consume acidity. Regulations require that the neutralisation potential should exceed by 3-4 times the acid-producing potential to consider the waste material is safe from ARD effect. However, this does not mean that pyrite oxidation not starts or stops even under these conditions. In the porous waste rock material in presence of water and oxygen, pyrite grain surfaces start oxidizing, thus creating an acidic micro-environment. Calcite, as a quick neutralizing mineral, is able to maintain a pH range. The net chemical reaction does not show acid production, but sulphide oxidation with possible metal leaching is able to take place.

In this chapter, the aim is to show on the Hungarian samples that strong pyrite oxidation can happen, although the pH of the system will be still circumneutral. Moreover, it would be necessary to change the thinking of the waste management, because most commonly only the pH value is monitored. It is an important parameter and easy to build up a system for monitoring it, but the too much focus on it can cover other important parameters, which can show much earlier the presence of the oxidation. The problem of those oxidations where the pH is buffered to circumneutral, that it is not visible – especially if only the pH is monitored –, but near the pyrite, other sulphides (Jambor 1994) will oxidize as well, thus Pb, Zn, Cu, As and Cd will be also loaded into the seepage, groundwater or simply to nature.

This process was detected at some mining waste facilities (e.g. mines in the Kola Peninsula, Russia /high-F/, the Schwaz and Brixlegg Mines, Austria /high-Sb/, the Endako Mine, BC, Canada /high-Mo/), where weathering and consequent metal leaching takes place under circumneutral conditions (Nordstrom 2010), so by just monitoring the acid content of the system, it would seem normal.

6.2. Theory of the oxidation

The theory, if there is strong and quick neutralizer mineral, such as calcite, which is the most effective, the system can keep a stable pH around 7, by consuming the acidity, slowing the oxidation rate and stopping the metal release by precipitation of them in solid form. The reaction is written (Eq. 24), where the dissolution of the calcite is defined. (Cotter-Howells and Patterson 2000; Lapakko et al. 1999)

DOI: 10.14750/ME.2021.004

$$CaCO_3 + 2H^+ \rightarrow Ca^{2+} + H_2O + CO_2 \quad (24)$$

To be able to realize the oxidation itself, necessary to leave the idea on focusing of the pH, and turn to the measuring of the other parameters in the system. The concept is based on the summary of a set of equations, such as Nordstrom's (1982) abiotic oxidation of the pyrite (Eq. 1), the Fe^{2+} - Fe^{3+} alteration (Eq. 3), the iron oxyhydroxide forming (Eq. 5) and the calcite dissolution (Eq. 24) processes. Because of the circumneutral pH of the seepage is not ideal for the iron hydroxide forming (Eq. 3), so iron oxyhydroxide (goethite) or oxide (hematite) will be formed. (Stumm and Morgan, 1981) The relatively quick precipitation reaction pushes the possibility of goethite formation much higher, than the oxide form. By dissolution of calcite, carbon dioxide needs to be produced, while the generated Ca^{2+} will form gypsum with the dissolved sulphate ion. Necessary to mention, that the gypsum is moderately water-soluble, as it can dissolve till the concentration of about 2.0–2.5 g/l at 25 °C. (Bock 1961) This means, that not all of the SO_4^{2-} and Ca^{2+} ions will react with each other to form solid phase (gypsum or anhydrite) but some from them will remain in dissolved form. As a conclusion of these reactions, the following equation (Eq. 25) has to take place. This reaction will not remove all of the dissolved sulphate, iron and calcium from the seepage, so some should remain in it, which can be measured.

$$2FeS_2 + 3CaCO_3 + 3H_2O + 6O_2 \rightarrow 2FeOOH + 3CaSO_4 * 2H_2O + 3CO_2 \quad (25)$$

The key to proving the oxidation process of the pyrite is to find the by-products of the reaction, such as Fe-oxyhydroxide, gypsum and carbon dioxide, moreover to find some remained sulphate and calcium ions in the seepage. The reason that the HU series of the sample was chosen for this test, that the mineral grains have free surface by the fresh crushing, so there are no goethite or gypsum on the surface of pyrite and calcite. Sulphate also cannot form without pyrite (or sulphide) oxidation, because the grains have fresh surface. Although some oxidation could take place during a few weeks even on open air, so without the speeding up of the humidity cell test. Based on this, some "first flush effect" can take place, but it will be not significant. The whole oxidation and neutralizing process (Eq. 25) is shown (FIG. 42) to be able to follow visually the different reactions and by-products.

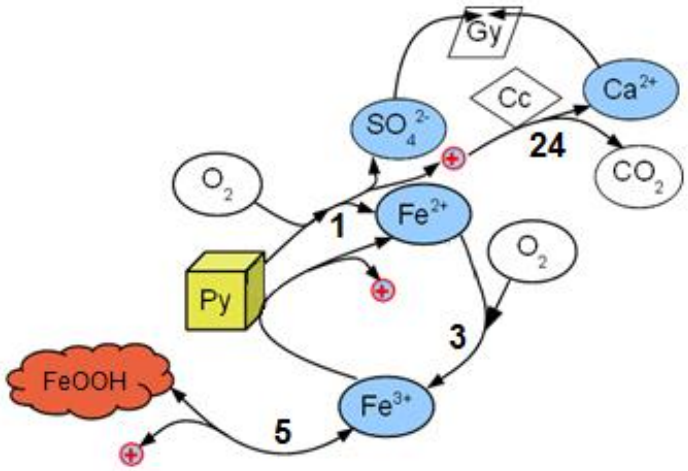

FIG. 42: Schematic representation of equation 24 (mixing of equation 1, 3, 5 and 24) Abbr.: Py: pyrite, Cc: calcite, Gy: gypsum, +: H^+ ion.

DOI: 10.14750/ME.2021.004

6.3. Analysis and results

In the experiment, a kinetic test (humidity cell test) was done on a sulphidic mine waste sample (HU series) from Recsk to speed up the sulphide oxidation and therefore mimic the long-term geochemical behaviour of the sulphidic mining waste material. The major mineral composition of the investigated sample (HU 1-2) is about 45% quartz, 35% pyrite, 15% carbonates (dominantly calcite, but subserviently ankerite and dolomite) and alltogether 5% of sphalerite and chalcopyrite (discussed in details in Chapter 5.1)

6.3.1 Humidity cell test

From the sample, 3.00 kg was investigated by humidity cell test at Kjeøy Research and Education Centre, Norway, to mimic the long-term behaviour of the sulphidic mine wastes. The test was completed for 119 days (17 weeks). Continuously humid air was pumped through to provide the oxygen and humidity for the pyrite oxidation and weekly the sample was rinsed through with 1000 ml distilled water. From the seepage basic chemical parameters (pH, alkalinity), anion and cation content was measured.

The pH graph (FIG. 43; left axis) clearly indicates that after 2 weeks the system has already stabilized. The circumneutral pH (between 7.1 and 7.3) shows that the calcite buffers the acidity perfectly, so the system is in balance. The instability of the first 2 weeks and the initial lower pH was caused by the week effect of the "first flush", which resulted lower pH.

The same effect is visible in the SO_4^2 concentration (FIG. 43; right axis). The gradually decreasing sulphate release after the first 2 weeks shows that there was some available fine-grained – therefore quickly oxidizing – pyrite powder in the sample. As it is consumed, the SO_4^{2-} release gradually stabilizes.

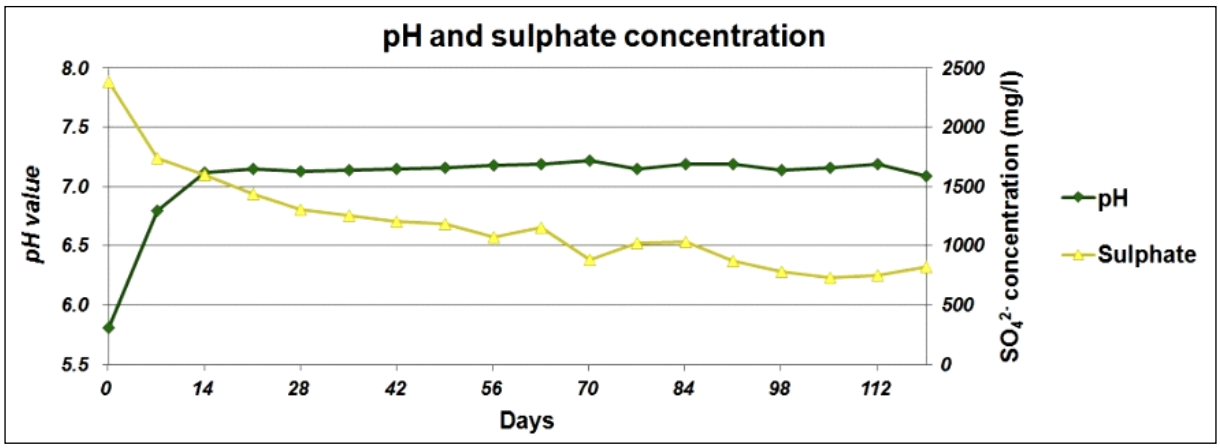

FIG. 43: pH value and sulphate content in the seepage of the HU 1-2 sample during the humidity cell test

At the end of the test period, the column was sealed hermetically for a week to measure the oxygen consumption and carbon dioxide release by the oxidation (Eq. 1 and 3) and neutralizing (Eq. 23) process. FIG. 44 shows clearly that carbon dioxide content increased continuously, which shows the dissolution (Eq. 23) and efficient neutralizing effect of calcite, while the decreasing oxygen content shows the presence of the oxidation process.

DOI: 10.14750/ME.2021.004

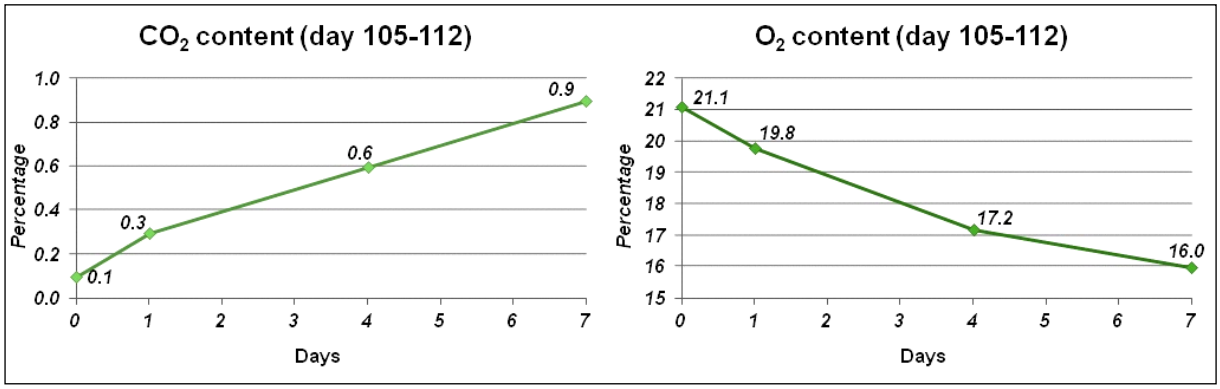

FIG. 44: CO_2 release and O_2 consumption in the hermetically closed sample keeper of the HU 1-2 sample, between the 105th and 112th days of the humidity cell test period

6.3.2 Mineralogical changes

The combined equation (Eq. 24) tells us that if pyrite is oxidizing and calcite is present, a secondary iron mineral and gypsum should be formed. Backscattered SEM images were taken from the samples' surface (FIG. 45) – which was supplemented with microprobe measuring – and clearly can be seen, that on the surface of the pyrite grains secondary iron minerals and a gypsum coating on the calcite's surface were formed. The high magnification shows, that well-developed gypsum needles (darker crystals) have grown on the calcite and the gypsum already has started the encapsulation of the calcite grain. Some pyrite crystals were prepared for the same analysis, which shows (FIG. 46/a) pyrite grains (brighter) are started to be coated with secondary iron oxidation product (darker colour). On higher magnification (FIG. 46/b), become clearly visible, that the pyrite crystal has already partly covered by plates of alteration products.

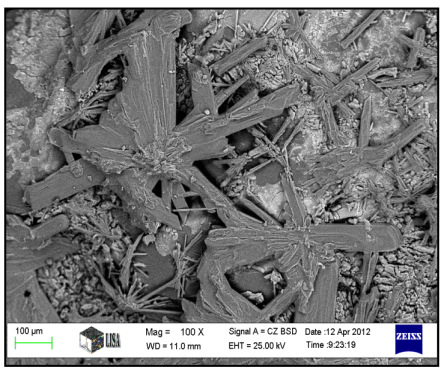

FIG. 45: Secondarily formed gypsum needles on calcite surface (100X)

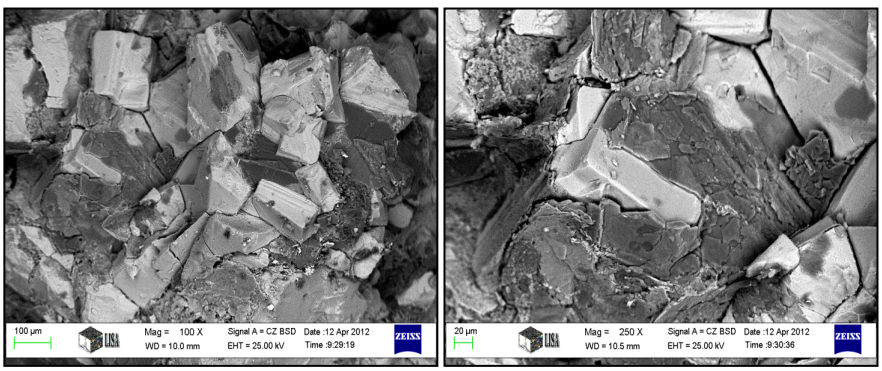

FIG. 46/a and b: Secondary Fe mineral coating on pyrite, with composition dominantly as $Fe(OH)_3$ and FeO(OH) (a:100X;b:250X)

6.4. Conclusion

The pyrite oxidation in the sample was detected and proved by the sulphate concentration (FIG. 43) from the seepage, the appearance of CO_2 and decreasing of O_2 in the hermetically closed sample holder (FIG. 44). By backscattered SEM images gypsum coating on the surface of the calcite (FIG. 45) and secondary iron mineral crust on the surface of the fresh pyrite grains (FIG. 46/a and b) were found. Conversely, no acidity appears, because of efficient neutralization by the calcite (Eq. 25).

DOI: 10.14750/ME.2021.004

The phenomena, that the gypsum has already started to cover and encapsulate the calcite grains. This shows that the still effective neutralizing capacity will decrease in the future, as the free reactive surface of calcite decreasing.

The Eh-pH diagram in FIG. 47 shows that Eh-independent stability zones of calcite + goethite ↔ calcite + gypsum + goethite occur at pH 7.2 – 7.3. The measured and rather constant pH of the seepage was between 7.1 and 7.3 (marked as a vertical blue strip) which indicates that the system is upper-limited at this pH by the calcite dissolution. (Embile et al. 2016) The diagram indicates that in less oxidative microenvironments, dissolved Fe^{2+} can appear within the porous waste rock, which is favourable for pyrite oxidation.

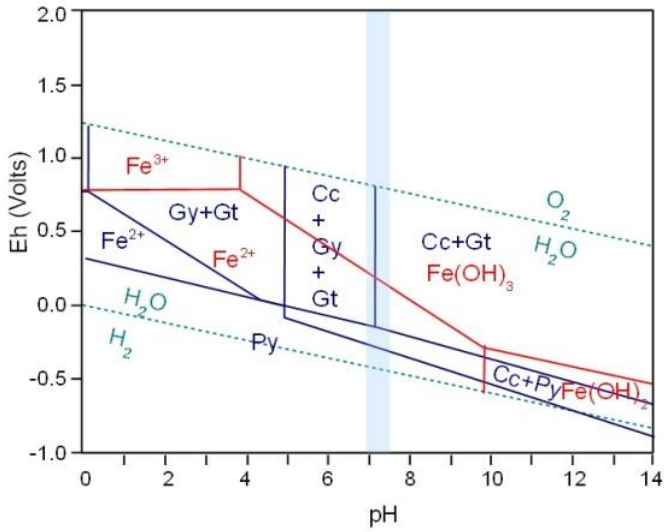

FIG. 47: Eh-pH diagrams of C-Ca-Fe-S-H_2O (blue) and Fe-O_2-H_2O (red) systems at standard conditions (by HSC Chemistry) (Embile et al. 2016)

As the amount of pyrite in the sample is more than double the amount of calcite (carbonates), ARD could take place in the future. Kinetic test results show that the oxidation rate currently is present, continuous and stable.

Although, this can work until the neutralizing capacity is higher or at least equal with the acid production. After that, the oxidation will increase exponentially, because there will be no available minerals which can quickly buffer the oxidation. Moreover, the natural coating of the pyrite by secondary Fe phases will not help in reducing the reactive surface, because when the calcite – as the main neutralizing mineral, which is able to keep the buffered pH – will disappear, the pH will drop down, as all of the secondary Fe alteration products will be dissolved back as the pH decreases under 3.5-4. After Singer and Stumm (1970) firstly a wave of increased dissolved iron content will appear, then as the surface of the pyrites will be free of alteration products, the pH value will drop down, as the oxidation rate will increase.

Without appropriate waste management the increased pyrite oxidation will lead to acidification accompanied by toxic element mobilization from associated sulphides, such as chalcopyrite or galena, although the waste rock heap currently does not show any sign of environmental risk.

DOI: 10.14750/ME.2021.004

VII. X-RAY POWDER DIFFRACTION (XRD) VERSUS SEQUENTIAL CHEMICAL EXTRACTION (SCE) - A NEW COMBINED METHOD FOR EXACTING MINERALOGICAL SPECIATION OF SULPHIDIC MINE WASTES

7.1. Introduction

Determination of the exact mineralogical composition of an unknown rock or a mineral sample has always been a big challenge for scientists. It is the same in the geochemical tests, where the exact mineralogical characterization is essential to understand more precisely those reactions which could take place during weathering. X-ray diffraction (XRD) is an efficient method for this purpose. But, in case of altered and not well-crystallized rocks, the efficiency of this method sometimes dramatically decreases and the detection limit may rise by a few percent, which is already not acceptable. This is a typical problem for oxidized or just oxidizing sulphidic samples, where acid rock drainage (ARD) takes place. The produced secondary minerals are poorly crystallized or even quite often by quick forming become amorphous.

The alteration of sulphide minerals is a natural process. It can be considered as a continuous alteration from hypogene primary to tertiary alteration mineral phases, via the supergene secondary mineral phases. As a result of the alteration, the already oxidized or just oxidizing sulphides, mainly pyrite, produce secondary minerals, such as secondary sulphates (Eq. 19), hydroxides (Eq. 3), oxy-hydroxides (Eq. 5 and 6) or oxides (Eq. 7). These secondary minerals are very diverse both in mineralogical properties and in chemical composition. Moreover, these minerals have weaker crystallinity, loaded with defects or contaminating elements than normal rock-forming minerals. These problems are typical in cases when the XRD analysis technique is not able to give accurate results.

In the late 70's, a sequential chemical extraction (SCE) method was developed to determine heavy metal mobility in soils. This measuring technique was more than a simple bulk chemical elemental analysis of materials, because the leaching happened in several steps. Thus, the composition of the leachate at a certain step can be linked with mineral speciation. The disadvantage of the method is that the varieties of possible dissolving minerals or mineral groups are high. Therefore, the applicability of SCE method was criticized and attacked.

This chapter try to show how the X-ray powder diffraction (XRD) and the sequential chemical extraction (SCE) can complement each other. Both methods have their own limitations, but using them as a combined method, the efficiency of determination of the mineralogical composition can be dramatically increased. A further aim of this study is to show via two case studies the applicability of the combined method for altered sulphidic mine waste materials, where the mineral(s) of the amorphous phases could be figured out, or even the altered sulphides with extremely low concentration could be calculated out.

DOI: 10.14750/ME.2021.004

7.2. Applied methods

7.2.1. Sequential Chemical Extraction (SCE)

Sequential chemical extraction is a geochemical method used to evaluate the mobility of different elements in the samples under different chemical condition. In the consecutive steps, stronger and stronger chemicals are used for degradation of the analysed sample, which can be soil, minerals, rock fragments, waste or tailing material. This dissolution processes start from the phase of water-soluble to the silicates, via several intermediate phases. Nevertheless, there are some significant limitations for the applicability of SCE, such as the limited selectivity of extractants, the redistribution of metals during the extraction process, the deficiency of a reagent dose if metal content is too high (Ramos et al. 1994) and the inability to distinguish between metal associations with organic matter and sulphides. (Adamo et al. 1996; Barona and Etxebarria 1996; Leinz et al. 2000)

These extraction procedures take advantage of the solubility mechanisms in water, ionic exchange, oxidation processes, as well as complexation and digestion of mineral and organic soil components. Separated fractions are defined in a conventional and operational manner, and present a certain approximation in describing different metals species. For the appeasement of the pretence of the mining companies and environmental agencies, several different sequential chemical extraction methods were developed and published, but only three of them became wide prevalent, such as the Tessier 5 steps (Tessier et al. 1979), the BCR 3 steps method (Ure et al. 1993) and the Dold 7 steps method (Dold 2003).

Firstly, the Tessier method was developed in 1979, which was an adaptation of the McLaren and Crawford leaching methods for copper fractionation. It gained the highest acknowledgement and broadest application in soil and geological studies, as well as in environmental protection. The method defines the mineral phases in five steps, such as exchangeable fraction (I.), carbonates (II.), Fe-Mn oxides (III.), organic matters (IV.) and residuals (V).

The Standards, Measurements and Testing Programme (SM&T) established a common procedural scheme consisting of a 3-step extraction method (BCR method), which was published in 1993 (Ure et al. 1993). The BCR sequential procedure determines metal quantities in three extracts, such as exchangeable metals (I.), metals bound to iron and manganese oxides (II.), metals bound to organic matter and sulphides (III.) and finally residuals (IV.). Although the extraction protocol proposes a 3-step procedure, a fourth fraction (residual phase) can be determined as well. This fraction includes the amount of metals bound to the mineral lattice of the soils or in general, the amount of metals not measured in the previous 3 steps and strongly bound to the soil.

One of the latest developed SCE procedure was the Dold type 7-step method (Table 15) established in 2003. This is a slightly modified 6-step sequential extraction method (Sondag 1981), was used for evaluation of primary and secondary minerals from porphyry copper deposits. Each step can be linked to a certain mineral group that is preferentially dissolved. Similarly to the steps in previous methods, the

DOI: 10.14750/ME.2021.004

first step is the degradation of the water soluble minerals and the final is for dissolving the residuals, gradually dissolving the secondary and later the primary minerals. Due to the variety of selected reagents and extraction conditions, the comparison of the obtained results from different methods is not possible. (Gworek et al. 2003)

Step	*Leached fraction and method*	*Preferentially dissolved minerals*
1st	***Water-soluble fraction*** 1.0 g sample, 50 ml dest. water; shake for 1 h	secondary sulphates, such as chalcanthite ($CuSO_4*5H_2O$), gypsum ($CaSO_4*2H_2O$) or melanterite ($CuSO_4*5H_2O$)
2nd	***Exchangeable fraction*** 1 M NH_4 acetate, pH 4.5, shake for 2 h	calcite ($CaCO_3$) and vermiculite-type mixed layer, adsorbed and exchangeable ions
3rd	***Fe^{3+}oxy-hydroxides*** 0.2 M NH_4 oxalate, pH 3.0, shake for 1h in dark	two-line ferrihydrites, secondary jarosite ($KFe_3(SO_4)_2(OH)_6$) or schwertmannite ($Fe_{16}O_{16}(OH)_{12}(SO_4)_2$)
4th	***Fe^{3+}oxides*** 0.2 M NH_4 oxalate, pH 3.0, keep 80 °C for 2 h	goethite (FeOOH), hematite (Fe_2O_3), higher ordered primary jarosite ($KFe^{III}_3(SO_4)_2(OH)_6$) or primary Na-jarosite ($NaFe^{III}_3(SO_4)_2(OH)_6$)
5th	***Organics and secondary Cu sulphides*** 35% H_2O_2 heat in water bath for 1 h	organics, covellite (CuS), chalcocite – digenite series [chalcocite (Cu_2S), djurleite ($Cu_{31}S_{16}$) and digenite (Cu_9S_5)]
6th	***Primary sulphides*** combination of $KClO_3$ and HCl, followed by boiling with 4 M HNO_3	pyrite (FeS_2), chalcopyrite ($CuFeS_2$), sphalerite (ZnS), galena (PbS), tetrahedrite ($(Cu,Fe)_{12}Sb_4S_{13}$), stibnite (Sb_2S_3)
7th	***Residual*** HNO_3, HF, $HClO_4$, HCl boiling	silicates, quartz, zircon, residual

Table 15: Steps and leached out minerals of the 7 steps Dold type sequential extraction (Dold 2003)

The huge advantage of the Dold type 7-step method compared to other methods is that it can differentiate secondary products - such as hydroxides, oxy-hydroxides and oxides - to split them into 3 and also the sulphates into 3 or 4 stages (depending on primary or oxidation products). Moreover, even primary sulphides are split into 2 steps. It is obvious that the higher numbers of steps mean higher cost in analysis, but this disadvantage is not comparable to the surplus of information that the better separation gives.

In this thesis, the Dold type 7-step sequential chemical extraction was used, which is the most applicable – and also the most fitting – method for sulphidic mine waste characterization, because it can differentiate the different primary and secondary minerals of the sulphide - sulphate alteration system. Since very aggressive chemicals were used in the last (two) steps, SCE analysis was performed with an inductively coupled plasma atomic emission spectroscopy (ICP-AES) machine in the SGS lab in Ontario, Canada.

DOI: 10.14750/ME.2021.004

7.2.2. X-ray diffraction (XRD)

For the determination of the solid phases in the sample, the same equipment was used as it was already discussed in details in Chapter 3.2.2. Moreover, the measuring properties and the evaluation of the samples are also in accord to that information, which was described there.

7.2.3. Calculation method

As Table 11 showed, each step in the SCE was specified for the dissolution of a specified group of minerals. The new idea in case of oxidizing sulphidic sample analyses – which can contain amorphous or poorly crystallized minerals in high rate – was to use the XRD patterns, which allowed detecting mineral groups in the sample. For instance, the presence of jarosite was determined with the patterns, but by measuring the crystal structure could hardly distinguish weather which member of the jarosite subgroup, such as potassium, hydronium, lead, ammonium or sodium-containing jarosite, especially if they are poorly crystallized. In addition, XRD analysis is not required in this case because the compounds have hardly any differences and the exact members cannot be determined. On the other hand, because of the poorly crystallized structure, the amount of this mineral will be over or underestimated.

The SCE analysis is used to define the species of mineral groups, by using the measured leached out cation concentration, moreover the exact amount of the mineral species can be calculated out.

On the other hand, the quartz – if it is not an amorphous opal or chalcedony –, together with the clay minerals, where the crystallite size is small is usually well crystallized, so the XRD measuring for these "inert" minerals usually good even in these oxidizing samples. If qualitative analysis is done, so the amorphous content is counted, the exact amount of them can be determined. The situation is the same with the common rock-forming minerals, like silicates, as albite, feldspar, orthoclase, dravite or with the common oxide forms, such as rutile, ilmenite or hematite.

The aim of this chapter and also the method is not to define the rock-forming minerals, which are much more resistant against weathering – compared with sulphates –, so they are measurable with smaller inaccuracy. The aim is to define the strongly altered minerals and the secondary oxidation products, even in that case, when their concentrations are under 0.01 %.

Recalculations require a strong chemical, geochemical and mineralogical background, together with the understanding of the XRD method. The variety of the possible minerals in the sample could be high, but if the origin of the sample is known, it significantly decreases the number of the possible minerals. Nowadays several high quality online databases can help in this, such as www.mindat.org or www.webmineral.com, where even for localities or mines can be searched.

DOI: 10.14750/ME.2021.004

7.3. Results

Two already oxidizing samples – a flotation tailing and a jig tailing – were chosen to complete the recalculation processes. The sample called Jalpha 1-7 is a strongly weathered material of a sulphidic flotation tailing with yellowish-ochre colour, collected from the Oruro Ag-Sn deposit originating from Oruro city, Bolivia. It is important to mention, that a decade after the flotation process was performed, the tailing material went through a weak hydrochloric acidic leaching to dissolve out the residual silver content in complex form.

The other sample was the Itos Jig 2-7, which had no chemical enrichment, only the jig processing, as a gravitation and density differences based enrichment process, from the same Oruro Ag-Sn deposit, from Oruro city. By macroscopic and optical microscopic visualization was clearly visible modified present of pyrite and the high rate of clay minerals, as a result of the intensive weathering. Large areas of the surface of the grains were covered by yellowish secondary poorly crystallized minerals, with reddish-brown, probably iron hydroxides after the oxidation of pyrite.

7.3.1. Sequential chemical extraction (SCE)

The results of the SCE measurements are listed below in Table 16 and 17. From a quick overview of the heavy metal content in case of Jalpha 1-7, the high concentration of lead, zinc and cadmium together with the elevated amount of sulphur indicates the polymetallic origin of the sample. This fact is also proved by historical data. (Chance 1948/a) Necessary to mention, that the amount of leached lead and zinc exceeded the 10000 ppm, which was the upper detection limit of the ICP machine for these two elements. This disappointing information will be important in the step of the calculation, as not the exact amount of the mineral phase can be calculated, but only a minimum amount that can be in the sample.

The elevated levels of heavy metals and sulphur in the first four steps represent well the presence of secondary minerals as a result of the sulphide oxidation process. Unfortunately, the Si content was not measured by ICP-MS. Thus, in the 7^{th} step, which is the stage for dissolution of silicates, the quartz content from SCE results could not be recalculated from ICP-MS data. On the other hand, this element only important in the last fourth of the steps, so from point of such alteration products, as sulphates, jarosites, hydroxides and oxyhydroxides or from point of oxidizing sulphides, it is not relevant. The exception is the clay minerals, as they form as byproducts of the weathering of the rock-forming silicates. Based on this unfortunate fact, for the calculation of the amount of the clay minerals the missing Si content cannot be used, so the only way is the use of the element, which is in the main cation position. For example, in the case of illite, the K content can be the reasonable way.

All the elements, which were used in the recalculation of the mineral composition are listed (Table 16 and 17). In some cases, the amount of elements was lower than the detection limit (marked with

symbol "<"). The elements, which appeared in significant concentration in the leachate, or represented well the distribution in the individual steps, are listed below.

Element	*Det. limit*	*Step 1st*	*Step 2nd*	*Step 3rd*	*Step 4th*	*Step 5 th*	*Step 6 th*	*Step 7 th*
Ca (ppm)	100	500	<100	<100	<100	<100	<100	200
Mg (ppm)	100	<100	<100	<100	<100	<100	<100	2400
Na (ppm)	100	<100	<100	<100	100	<100	100	300
Al (ppm)	100	1200	<100	100	300	<100	700	55100
K (ppm)	100	<100	<100	300	700	<100	<100	23400
Cr (ppm)	1	12	13	13	13	<1	5	37
Fe (ppm)	100	5100	1800	5600	17500	7600	21800	2300
Cu (ppm)	0.5	46.4	<0.5	6.9	11.7	22.6	10.1	0.6
Zn* (ppm)	0.5	>10000	435	144	434	966	1160	28.2
As (ppm)	3	<3	9	40	74	13	92	7
Cd (ppm)	1	358	12	2	1	20	27	<1
Sn (ppm)	10	<10	<10	<10	<10	<10	30	30
Sb (ppm)	5	<5	<5	29	60	<5	55	132
Pb* (ppm)	2	204	>10000	759	290	113	>10000	932
S (ppm)	100	14400	2100	2000	5200	13000	41700	3700

Table 16: Concentrations of the dissolved elements in the different steps of the sample Jalpha 1-7
** The concentration was higher than the upper detection limit (10000 ppm) of the ICP-MS*

Element	*Det. limit*	*Step 1st*	*Step 2nd*	*Step 3rd*	*Step 4th*	*Step 5 th*	*Step 6 th*	*Step 7 th*
Ca (ppm)	100	<100	<100	<100	<100	<100	<100	200
Mg (ppm)	100	<100	<100	<100	<100	<100	<100	3900
Na (ppm)	100	<100	<100	<100	<100	<100	100	1900
Al (ppm)	100	800	<100	300	700	100	1300	87100
K (ppm)	100	300	100	600	500	<100	N.A.	23000
Cr (ppm)	1	14	24	17	17	1	11	108
Fe (ppm)	100	1600	600	4500	2100	15300	2900	16800
Cu (ppm)	0.5	2.5	<0.5	2.3	1.3	5.9	2.2	2
Zn (ppm)	0.5	5.7	<0.5	1.5	1.5	4.9	3.7	13.7
As (ppm)	3	6	22	345	97	143	64	22
Sr (ppm)	0.5	5.1	4.4	<0.5	1.7	<0.5	8	152
Cd (ppm)	1	1	<1	<1	<1	<1	<1	<1
Sn (ppm)	10	<10	<10	50	150	<10	50	70
Sb (ppm)	5	<5	11	88	494	<5	63	207
Pb (ppm)	2	192	434	684	86	<2	46	27
S (ppm)	100	3600	300	1600	800	19500	4000	600

Table 17: Concentrations of the dissolved elements in the different steps of the sample Itos Jig 2-7

7.3.2. X-ray Powder Diffraction (XRD)

In Jalpha 1-7 the presence of a relatively high rate of clay minerals in the sample was already seen under the microscope. The XRD measurements (Table 18) proved the presence of clay minerals in the sample. Besides the relatively high amount of quartz, different members of the jarosite group and pyrite, which is the "fuel" of the ARD process also occurred. Traces of kaolinite and chalcopyrite were visible

DOI: 10.14750/ME.2021.004

on the XRD pattern as well. In addition, “amorphous hump” was detected and quantitatively evaluated. The amount of amorphous material in the sample accounted for almost one-fifth of the total weight.

Mineral	***Formula***	***$^{m}/_{m}$%***
Quartz	SiO_2	*59.0*
Pyrite	FeS_2	*5.0*
Anglesite	$PbSO_4$	*0.8*
Illite	$(K;H_3O)Al_2Si_3AlO_{10}(OH)_2$	*12.8*
Plumbojarosite	$PbFe_6(SO_4)_4(OH)_{12}$	*3.6*
Hydronium jarosite	$(H_3O)Fe_3(SO_4)_2(OH)_6$	*0.1*
Gypsum	$CaSO_4{\cdot}2H_2O$	*0.7*
Kaolinite	$Al_2(Si_2O_5)(OH)_4$	*ind.*
Chalcopyrite	$CuFeS_2$	*ind.*
Amorphous components		*18.0*

Table 18: Quantitative mineralogical composition of the sample Jalpha 1-7, based on XRD

In Itos Jig 2-7 had high amount of illite content - which already exceeds one third of the sample - which proves that this sample has already strongly altered. The XRD result (Table 19) showed more than tenth jarosite in the sample. From the original rock containing minerals, the inert quartz, together dravite and high amount of muscovite was detected, as well as the fuel of the ARD process, the pyrite. Significant "amorphous hump” was detected and calculated as 15%.

Mineral	***Formula***	***$^{m}/_{m}$%***
Quartz	SiO_2	*39.9*
Pyrite	FeS_2	*3.6*
Illite	$(K;H_3O)Al_2Si_3AlO_{10}(OH)_2$	*24.3*
Biotite	$K(Mg,Fe)_3[AlSi_3O_{10}(OH)_2$	*0.9*
Titanomagnetite	$(Fe,Ti)_3O_4$	*0.5*
Dravite	$NaMg_3Al_6(BO_3)_3Si_6O_{18}(OH)_4$	*15.8*
Amorphous components		*15*

Table 19: Quantitative mineralogical composition of the sample Itos Jig 2-7, based on XRD

7.4. Process of the recalculation

The basic concept of this recalculation method is similar to CIPW norm calculation, which is a good method for calculating out the mineralogical composition on an unaltered igneous rock, but it is not applicable or adaptable for other rock types, especially not suitable for such mine wastes, which is just altering or already altered.

The theory of this method was sharpened and focused on sulphides and their alteration products, such as sulphates, hydroxides, oxyhydroxides and oxides. The reason is simple, the determination of these

DOI: 10.14750/ME.2021.004

are the difficult or sometimes impossible by XRD, in contrast with the original minerals of the host rocks, such as quartz, oxides (except alteration products) or silicates, which can be measured well or acceptably with XRD method, even if they have already started to degrade.

Based on this thinking, these minerals will be excluded from the calculation, their amount from XRD result will be accepted. On the other hand, Si analysis is not completed in frame of a normal ICP-MS measuring, because it needs different sample preparation method. The lack of the concentration of this element makes recalculation of the silicate phase not possible, even if all of the other cations are known.

The present study applied a similar, but a more complex calculation than CIPW norm calculation method because of much larger varieties of minerals. This indicates it was not possible to automatized or standardize it, like in case of the CIPW norm made. It is obvious, that mineral groups cannot be linked completely to a specified step, as their crystallization rate was slightly different. This effect is well detectable in Table 20, where not significantly, but the mineral phase can dissolve earlier – in previous step – or if the mineral is in high concentration, a few percentages of it could remain for the next step.

In the calculation only one data set is used at a certain time, so just calculating step by step, started with the water-soluble phase and finishing with the silicates. Knowing which mineral with a selected element was detected in a particular step were of essential importance. In the next step, the molecular weights of both the mineral and the element itself was defined in order to calculate the weight ratio of the mineral compared to the element. Finally, the starting concentrations of those elements were decreased, which were used in the calculated mineral.

The recalculation itself and also the results with the sets of the calculated sulphides and sulphates are shown via two case studies. Both samples were chosen randomly from the Bolivian samples, from the Oruro sample set. Both of them had been discussed and shown in Chapter 2.1.1. and 2.1.2., which deals with the samples. The first one is the clayish type Jalpha 1-7 flotation tailing and the other is the Itos Jig 2-7 jig tailing.

7.4.1. Case study I. - Sample Jalpha 1-7

In the 1st step, which contains the water-soluble fractions and the selected element was Ca, the mineral could be only the gypsum ($CaSO_4*2H_2O$), which is the only water-soluble calcium sulphate, which can appear in an oxidizing and acidic environment. Moreover, the XRD measuring also detected it. A detailed description of the flowchart is given in FIG. 48. The molecular weight gypsum is 172.17 $^{g}/_{mol}$ and the Ca element has 40.08 $^{g}/_{mol}$. Thus, the ratio between them is 4.296. The measured Ca content was 500 ppm, which was 0.05 %. So the gypsum content (0.215 %) was calculated by multiplying the 0.05 % Ca content by the molecular weight ratio of 4.296. An essential step, that as gypsum contained 18.62 % S, the starting S content needs to be decreased with the already used up amount. This amount can be calculated if gypsum content (0.215 %) was multiplied by S content in gypsum (18.62 %), which gives

DOI: 10.14750/ME.2021.004

0.04 % or 400ppm. The next selected element was Fe and mineral was melanterite ($FeSO_4*7H_2O$), because in the oxidizing and acidic environment, this is the dominant water-soluble iron sulphate mineral. Few other minerals also could be, but they have the same chemical composition as melanterite, only the amount of crystal water in them are different. Of course, in case of any hydrated sulphates the different amount of crystal water indices slightly different content of the mineral in the sample, but not significant one. The process of calculation for melanterite is the same as for gypsum was.

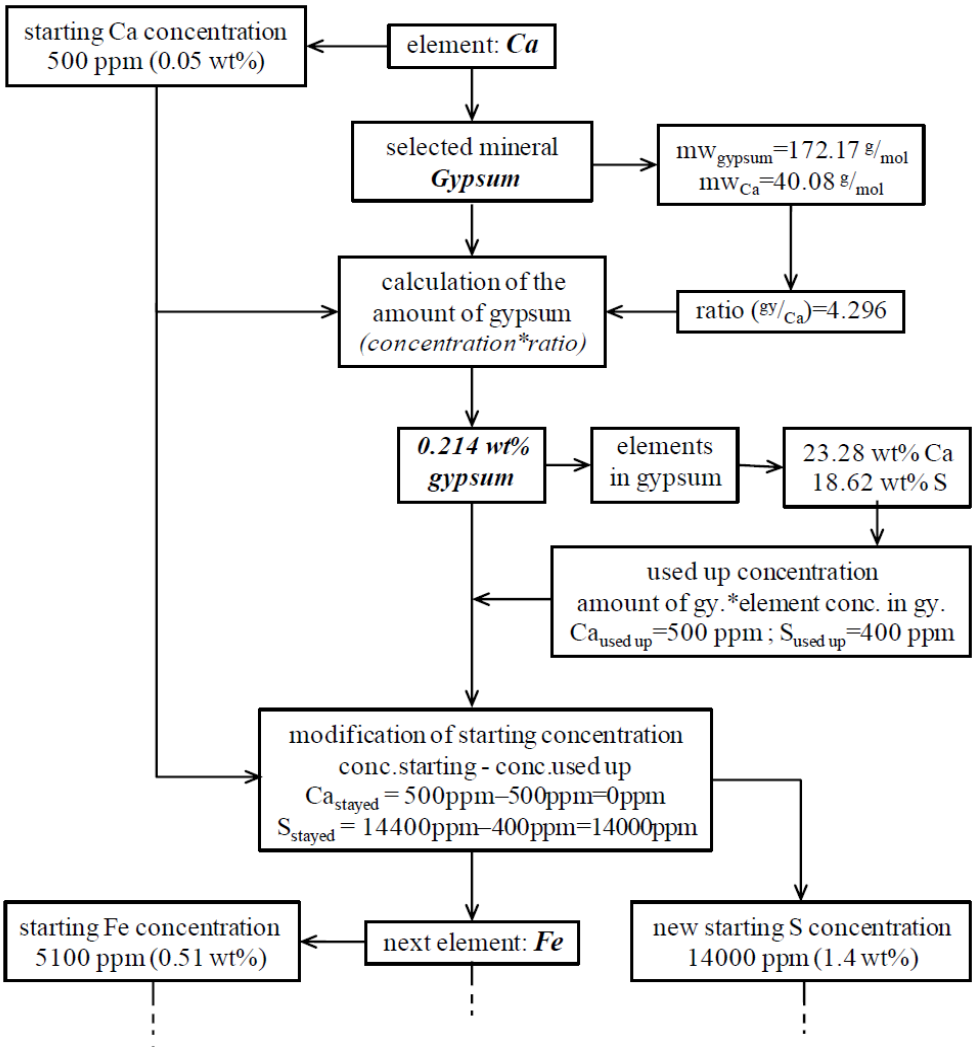

FIG. 48: Recalculation flow sheet for gypsum in the 1st step in the sample Jalpha 1-7

The element of Zn determines whether the mineral is goslarite or zinc-melanterite. They are almost polymorphs, but the last one can contain some Cu as replacing. There can be some small mistakes in the calculation, because similarly to the iron sulphate, the zinc sulphates also have several various with different amount of crystal water content. Moreover, need to take into consideration, that the Zn content in the leachate exceeded the upper detection limit (10 000ppm) of the ICP-MS, thus the calculated amount for this mineral is the minimal one, that the sample can contain. In addition, the relatively high content of this mineral in the sample also indicates that the leaching process of the current step will be not effective enough and some portion of the mineral will be remained for the next step. This effect is visible as 0.19 % remained zinc-sulphate appeared in the 2nd step. Cd likes to move together with Zn, thus it probably functions as replacing element in the zinc-sulphate. This mineral was marked separately

DOI: 10.14750/ME.2021.004

as Cd-sulphate, with the same amount of crystal water as melanterite. The alunogen ($Al_2(SO_4)_3*17H_2O$) is the most common mineral that is formed in an acidic environment, as water-soluble Al-sulphate.

The last selected element, which appeared in a measurable concentration, was the lead. Need to be mentioned, that Pb is a not replacing element for the previous or the other ones, because their oxidation number is 2+, not as the lead. This fact indicates that other mineral combination or replacing is not possible for the lead. Among water-soluble lead minerals, there is no such a lead mineral, which likes the acidic environment, only the anglesite ($PbSO_4$), but it is not water-soluble, but very common minerals in sulphidic mining wastes. This fact proposes to check the amount of Pb in the next step. It is high – even over the detection limit of the ICP-MS – so the low lead concentration in the first step is already the result of the slight dissolution of the anglesite, which is in high content in the 2nd step. This effect is not surprising, because the strongly acidic and oxidizing environment in the sample has already debilitated the crystal structure of the anglesite, or simply it was not crystallized perfectly. The situation for anglesite is the same in case of the Zn-sulphate was, as only the minimal amount of it can be calculated. As it has already been mentioned before, a small amount of melanterite ($FeSO_4*7\ H_2O$) and goslarite or zinkmelanterite ($ZnSO_4*7\ H_2O$) remained from the first step.

In the 3rd and 4th steps, numerous members with different cations of the jarosite group were likely to dissolve. Among the members of this group, there were complete replacing series, thus the possibilities of these minerals by element replacing are also several. This proves why four different jarosite could appear in the same sample. In the mineral composition based on XRD measurements, plumbojarosite and hydronium jarosite were listed with alltogether 3.7 %. The cumulative amount of recalculated jarosite minerals was about 5 %, which was more with $^1/_3$, than it was measured by XRD. By the different cations, it can be separated the different members, and also the individual amounts of them can be defined. Besides these anhydrous sulphates, the pH-sensitive metal-hydroxides also disappeared in the third step, such as ferrihydrite. The 4th step is the dissolution step of the more stable iron minerals, such as secondary goethite.

Similarly to the two previous steps, the 5th and 6th steps can be discussed together, because they strongly overlap each other. The only exception was Zn- and Pb-sulphide, which occurred in 3 consecutive steps. The amount of galena can be calculated for the minimum amount.

The peak of the dissolution appears in the 6th step, the leached out concentration in the previous and the next step is much less, especially in case of galena. This effect strongly depends on the sensitivity of the mineral for that step, or rather for the chemical is used in that step. Moreover, the quality of the crystallization of the mineral is important, because a weaker crystallized mineral will start partly dissolving in the previous, such as pyrite (Table 20), but a stronger one will start to degrade in the ideal step, but some of it can remains for the next step, like in case of anglesite. In those minerals which contain both, such as a zonation, it can start to dissolve in the earlier step, the peak will be in that step,

where it should be, but some concentration can stay for the next step, as in case of galena it happened (Table 20). A further explanation for the 3 steps dissolving of zinc sulphide is that it contains some iron in its structure. The Fe concentration in it is not constant; it is variable by the producing environment, even within an individual crystal, chemical zonality can be found. As more Fe was built in the structure, it becomes more sensitive against weathering. Zinc does not work as a replacing element for the jarosites, so it needs to be an early indication of an oxidizing zinc-sulphide. Two possible Zn-sulphides could be, such as sphalerite and wurtzite – but they are polymorphs –, however, the typical locality for wurtzite in the world is Oruro. The choice between them could not bring any mistake in the calculation. In this step, a smaller amount of antimony and tin leached out in a ratio, which was very specific for a Sb-Sn-Pb-sulphide, called franckeite. This mineral is strongly linked to the region of Oruro and Potosi.

Only a small amount of As could be an indication of arsenopyrite because no other As-containing sulphide mineral is known from that region, moreover arsenopyrite is very common in such an ore mineralization, which is in Oruro. Some Cu and Sb were detected in the 5th and 6th steps. These elements probably came from chalcopyrite and stibnite. Also possible, that it can be other sulphides or sulphosalts, which contain both elements, such as bournonite ($PbCuSbS_3$) or tetrahedrite ($Cu_6(Cu_4(Fe,Zn)_2)Sb_4S_{13}$), but as the XRD indicated the presence of chalcopyrite, so the antimony should appear without it.

The listed greenockite has complete series with the Zn containing wurtzite, so it was not possible to identify, whether it was an individual mineral or a mixture with wurtzite. The alteration of these two sulphides is the source of the goslarite and Cd-sulphate, which was calculated in an earlier step. As the Pb concentration in the solution of the 6th step was over the upper detection limit of the ICP-MS, it has a mark, that the galena content in that step was at least 1.15 %. However, this mineral was not detected with XRD method. The pyrite content (6.25 %) was slightly higher than it was detected (5.0 %) by XRD measurement. It seems that the oxidation of this mineral was strong, because the leaching by chemicals in the test split it in the ratio of 1:3 between the 5th and the 6th steps.

As it was mentioned the recalculation of the silicates are not part of this method, moreover, the missing Si analysis makes it more difficult. But based on the K and Al content in the last leaching step, the calculated illite content (12.82 %) was exactly the same in the calculation than it was measured (12.8 %) by XRD. Unfortunately, for kaolinite and quartz the calculation method cannot give result by the missing Si content. The XRD results of these two minerals are accepted and listed here, as an indication of the kaolinite clay mineral and 59.0 % for SiO_2.

Important to highlight, that this sample is very complex from point of mineralogy, because it contains lots of various sulphides and also their by-products. The high number of original and also the alteration products makes the recalculation method difficult for this sample. As the complexity of this sample is viewed, gently can be declared, that this can be considered as the maximally complex and difficult sample.

DOI: 10.14750/ME.2021.004

For conclusion of this sample can be decelerated, that the amount of the calculated minerals together with those minerals, which were accepted from XRD measuring, like an indication of kaolinite and quartz, give 97.23 % for the total amount. But cannot forget, that for tree mineral phases – such as the Zn-sulphate, the anglesite and the galena – only the minimal amount can be calculated from the ICP-MS data.

Mineral	***$^{m}/_{m}$%***	***Formula***	***Leached out minerals in the different steps***						
			1	***2***	***3***	***4***	***5***	***6***	***7***
Gypum	***0.21***	$CaSO_4*2H_2O$	***0.21***						
Alunogen	***1.44***	$Al_2(SO_4)_3*17\ H_2O$	***1.44***						
Cd-sulphate	***0.11***	$CdSO_4*7H_2O$	***0.11***						
Melanterite	***3.44***	$FeSO_4*7\ H_2O$	***2.54***	***0.90***					
Goslarite or zinkmelanterite	***>4.59***	$ZnSO_4*7\ H_2O$	***>4.40***	***0.19***					
Anglesite	***>1.49***	$PbSO_4$	***0.03***	***>1.46***					
Ferrihydrite	***0.18***	$Fe(OH)_3$			***0.18***				
Alunite	***0.20***	$KAl_3(SO_4)_2(OH)_6$			***0.05***	***0.15***			
Jarosite	***1.03***	$KFe_3(SO_4)_2(OH)_6$			***0.32***	***0.71***			
Plumbojarosite	***0.57***	$PbFe_6(SO_4)_4(OH)_{12}$			***0.41***	***0.16***			
Hydronium jarosite	***3.14***	$H_3OFe_3(SO_4)_2(OH)_6$			***0.61***	***2.53***			
Natrojarosite	***0.21***	$NaFe_3(SO_4)_2(OH)_6$				***0.21***			
Goethite	***0.81***	$FeOOH$				***0.81***			
Wurtzite	***0.42***	$Zn_{0.9}Fe_{0.1}S$				***0.07***	***0.16***	***0.19***	
Pyrite	***6.25***	FeS_2					***1.61***	***4.64***	
Galena	***>1.25***	PbS					***0.01***	***>1.15***	***0.09***
Chalcopyrite	***0.010***	$CuFeS_2$					***0.007***	***0.003***	
Greenockite	***0.006***	CdS					***0.003***	***0.003***	
Arsenopyrite	***0.023***	$FeAsS$					***0.003***	***0.020***	
Franckeite	***0.022***	$Pb_{4.7}Sn_{2.3}FeSb_2S_{14}$						***0.022***	
Stibnite	***0.004***	Sb_2S_3						***0.004***	
Illite	***12.82***	$K_{0.6}(H_3O)_{0.4}Al_{1.3}Mg_{0.3}Fe_{0.1}Si_{3.5}O_{10}(OH)_2*(H_2O)$							***12.82***
Kaolinite (XRD)	***ind.***	$Al_2Si_2O_5(OH)_4$							***ind.***
Quartz (XRD)	***59.0***	SiO_2							***59.0***

Table 20: Recalculated mineralogical composition of the sample Jalpha 1-7 (Abbr.: ind.: indication)

DOI: 10.14750/ME.2021.004

7.4.2. Case study II. - Sample Itos Jig 2-7

The calculated mineralogical composition (Table 21) of Itos Jig 2-7 sample is less variable than the Jalpha-1. Although the ARD takes place here as well, which is proved by the presence of the original ”fuel” minerals such as pyrite and its alteration products, like different types of sulphates. In this sample the Al element appeared in higher rate than in the others, especially, which means that the environment was not as strongly acidic to be able to mobilize the entire Al-containing minerals from the oxidizing system, so the rate of alteration was lower and the pH was higher, compared to Jalpha 1-7.

In the 1st step, 1% of readily water-soluble Al-containing sulphates appeared, in the rate of $^2/_3$ of Al-sulphate and $^1/_3$ of K-Al-sulphate. Furthermore, just the melanterite and the anglesite appeared in this and also in the next step, but the Pb-sulphate has as tiny concentration as 0.09%. Nothing else was leached out in the 2nd step.

In the 3rd and 4th step three type of jarosite (K containing, hydronium- and plumbo-) appeared in all together 1.35%, associated with 0.5% of a member from the other large group of sulphates, the alunite. From point of iron oxides in the 3rd step the ferrihydrite, while in the 4th step the magnetite appear - which was detected also by XRD (Table 19), but much less concentration was calculated (0.17%) than it was measured (0.5%).

The 5th and 6th step is also very similar to each other, in both cases, the pyrite is the dominant sulphides. Beside the pyrite there is no significant amount of other sulphides, in very tiny concentrations, such as arsenopyrite (0.04%), the previously in detail discussed wurtzite (0.002%), galena (0.005%), stibnite (0.009%) and chalcopyrite (0.003%). Tin appeared in the 6th step, it was not significant, but it possible came from the herzenbergite or berndtite minerals, which are present and significant in ore mineralization of the Oruro-Potosi region, especially the herzenbergite, which has a type location in Maria Teresa Mine, near the city of Oruro, not so far from the origin of this sample.

In the 7th steps, high rate of illite content (38.1%) was calculated, which is significantly higher than the XRD method gave for 24.3%. On the other hand, cannot forget, that the amorphous content was as high as 15%. If the clay minerals were formed as alteration products, their crystallite size can be small, thus their rate in the sample will be underestimated by XRD method. By the calculation, the dravite content decreased from 15.8% to 7.91%, which is sharply the half of it. In this step, cassiterite and valentinite were also calculated. Both are common in Oruro.

Beside the silicate minerals, chromium, tin and antimony oxides appeared. The cassiterite and the valentinite need to be mentioned because Oruro was one of the leader tin producers on the world. Near the silver, this was the other aim of the mining activity. The sources of the ore were several meters wide cassiterite rich veins. This sample got its name after this, because it is from the Itos mine and it had gravity a enrichment process, the jig method.

DOI: 10.14750/ME.2021.004

For the conclusion of this sample can be decelerated, that the amount of the calculated minerals together with those minerals, which were accepted from XRD measuring, like dravite, muscovite, illite and quartz, give 95.2 % as the total amount.

Mineral	$^{m}/_{m}$%	Formula	*Leached out minerals in the different steps*						
			1	2	3	4	5	6	7
Alunogen	***0.71***	$Al_2(SO_4)_3*17\ H_2O$	***0.71***						
Alum-(K)	***0.36***	$KAl(SO_4)*12H_2O$	***0.36***						
Melanterite	***1.10***	$FeSO_4*7\ H_2O$	***0.80***	***0.30***					
Anglesite	***0.09***	$PbSO_4$	***0.03***	***0.06***					
Ferrihydrite	***0.14***	$Fe(OH)_3$			***0.14***				
Hydroniumjarosite	***0.14***	$H_3OFe_3(SO_4)_2(OH)_6$			***0.14***				
Jarosite	***0.79***	$KFe_3(SO_4)_2(OH)_6$			***0.58***	***0.21***			
Plumbojarosite	***0.42***	$PbFe_6(SO_4)_4(OH)_{12}$			***0.37***	***0.05***			
Alunite	***0.51***	$KAl_3(SO_4)_2(OH)_6$			***0.15***	***0.36***			
Magnetite	***0.17***	Fe_3O_4				***0.17***			
Pyrite	***3.87***	FeS_2					***3.26***	***0.61***	
Arsenopyrite	***0.04***	$FeAsS$					***0.03***	***0.01***	
Wurtzite	***0.002***	$Zn_{0.9}Fe_{0.1}S$					***0.001***	***0.001***	
Chalcopyrite	***0.003***	$CuFeS_2$					***0.002***	***0.001***	
Galena	***0.005***	PbS						***0.005***	
Stibnite	***0.009***	Sb_2S_3						***0.009***	
Herzenbergite or Berndtite	***0.008***	SnS or SnS_2						***0.008***	
Cassiterite	***0.009***	SnO_2							***0.009***
Valentinite	***0.025***	Sb_2O_3							***0.025***
Dravite	***7.92***	$NaMg_3Al_6(BO_3)_3Si_6O_{18}(OH)_4$							***7.92***
Illite	***38.1***	$K_{0.6}(H_3O)_{0.4}Al_{1.3}Mg_{0.3}Fe_{0.1}\,Si_{3.5}O_{10}(OH)_2*(H_2O)$							***38.1***
Biotite (XRD)	***0.9***	$K(Mg,Fe)_3[AlSi_3O_{10}(OH)_2$							***0.9***
Quartz (XRD)	***39.9***	SiO_2							***39.9***

Table 21: Recalculated mineralogical composition of the sample Itos Jig 2-7

7.5. Verification of the calculated minerals by electron microprobe

Till this point of this chapter, the method was only a theory. It will stay only a theory, until the presence of the calculated minerals, even the lowest concentration phases will be not proved. Although, few of the minerals are in so small concentration in the samples that it can be difficult – or simply not possible – to find them, such as greenockite (0.006 %) in Jalpha 1-7 or anglesite (0.09 %), wurtzite

DOI: 10.14750/ME.2021.004

(0.002 %), galena (0.005 %), stibnite (0.009 %) or cassiterite (0.009 %) in Itos Jig 2-7. To find them, scanning electron microscopy (SEM) coupled with energy dispersive spectrometry (SEM–EDS) was used. SEM and microprobe analysis was performed using a JEOL JXA 8600 Superprobe. Both backscattered (BSE) and secondary electrons (SE) methods were used to image the grains.

On the samples three types of sample preparation was done, the first was, that the original clayish samples were glued to a flat surface, the second one was a washed and heavy mineral separated sample and finally, a glued into acrylate resin, cut and polished. The three different types of sample preparation created three different types of measuring results. The powder glued on a flat surface indicated, that the clay minerals and other alteration products cover the grains, moreover, the low quality coal covering on its surface resulted that BSE image cannot be made by surface charging. Despite of this technical difficulty, the microprobe analyses were completed, so chemical compositions are measured. All of the chemical analyses were done in EDS (energy dispersive) mode, but important to mention that this type of measuring is not accurate enough for the small concentrations, moreover its resolution is weaker than the WDS (wavelength dispersive) mode. Although the EDS analysis is perfect for the quick analysis, especially on flat and polished surfaces. On small grains, even up to 2-3 mm size, also can be measure with it, but the shape and the morphology of the grains strongly decrease the quality and the accuracy of the results of the measuring. In half of the cases even BSE images cannot be done, because the coal layer on the surface of the grains is not continuous, so charging can take place and false brightness can appear at some part of the minerals, which looks like (much) higher average atomic weight concentrations. In that case, when the clayish material was simply glued on a fat aluminium electric driving plate, microprobe analysis could be completed, but BSE images cannot be made by strong charging.

7.5.1. Sample Jalpha 1-7

From this sample there all of the three sample types were done. In case of the grain separation type, from the original sample suspension was done to get rid of the clay minerals, the coarse grains - which still did not reach the 0.5 mm size - were washed down with distilled water and separated the heavy minerals from the quartz (and other light ones) by sodium polytungstate solution (ρ=3.0 $^{g}/_{cm^3}$). Because of the washing or other process during the sample preparation, most of the water-soluble minerals are dissolved, so they cannot be found.

The clay covering of the grains and minerals resulted that in every measuring, the K-Al-Si-O components are included, which is the ***illite*** itself. From measuring two of them are presented. In both cases, the components of the illite are present, but the concentrations of the elements can be decreased with it, so the mineral(s) under the clay mineral can be figured out from stoichiometry, what it is. ***Jarosite*** (FIG. 49/a) were found, with a tiny amount of lead-containing mineral, but without measurable surface it cannot be defined whether it is plumbojarosite, galena or anglesite. Near the illite, ***galena*** (FIG. 49/b)

DOI: 10.14750/ME.2021.004

takes place. But the oxygen concentration is too high to be only in the clay minerals, so ***anglesite*** is also present, which usually appears together, when the galena starts oxidizing (Eq. 21) in an acidic environment. The ***pyrite*** (FIG. 49/c), which causes the ARD effect by weathering, was measurable in many grains, so it is in high rate in the sample. This is further proved by the 5 % of it from the XRD measuring and also from the 6.25 % as calculated pyrite content.

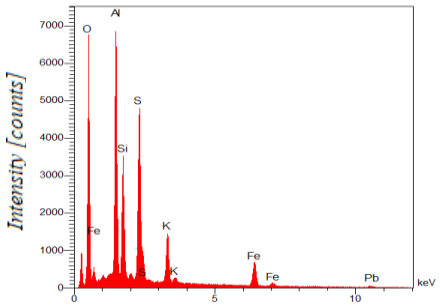

FIG. 49/a: Illite + jarosite phase

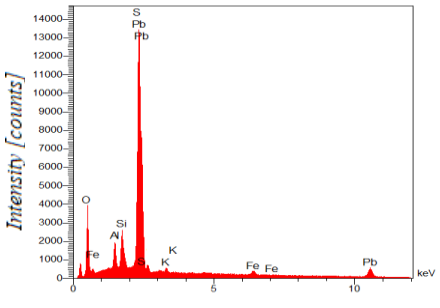

FIG. 49/b: Illite + Pb phase

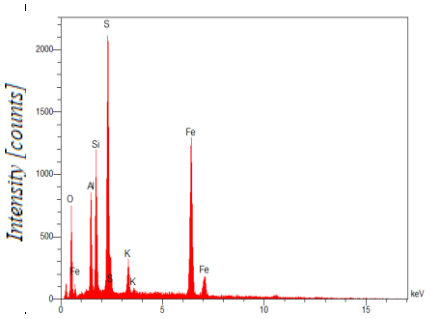

FIG. 49/c: Illite + pyrite phase

From the calculated mineralogy result of Jalpha 1-7 (Table 20), water-soluble sulphates were also measured. On an aggregate, microprobe measuring was done. From the first measuring, it has already seemed that it is a mixture of sulphates, with Fe member as ***melanterite*** /$FeSO_4$*7 H_2O/ and with Al member as ***alunogen*** /$Al_2(SO_4)_3$*17 H_2O/.

To get more chemical information in two further points the microprobe measuring was repeated. In the three different results (FIG. 50) there is deviation, but all of them show the two sulphate, but in slightly different ratio. By stoichiometry the $FeSO_4$ and $Al_2(SO_4)_3$ as main and constant phases of these minerals, were calculated without crystal water content. In the first measuring (red) the ratio is 1:3, in the second (blue) it is 1:4, while in case of the last (green) one it results 2:3. From the three different ratios, it is clearly visible, that these two minerals were formed in the same time and condition, but some quick changes in the fluids, from which they crystallized out, induced such a difference in ratios. As oxygen content was measured also, from the rest of it after the $FeSO_4$ and $Al_2(SO_4)_3$ calculation, the approximately water content can be calculated as an average for the mix of the sulphates. It gives 16 % for the first and 22 % water content for the second measurement, but in the third one the sulphates were calculated for almost water free. As a background information, the water content of melanterite is 45.3 % and 47.2 % for alunogen. The reason for that anomaly, that only one third or half amount of water there is in the structure of the sulphates, is that by time the crystal water content in these high water containing sulphates decreasing by dehydration. Moreover, the used high vacuum in the microprobe analysis dramatically decreases the water content by evaporation, which is caused by the low partial pressure.

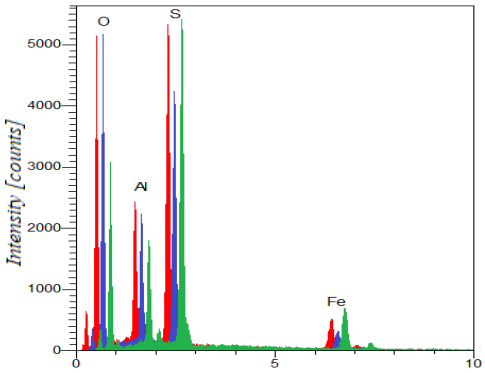

FIG. 50: Mix of Fe and Al sulphates

DOI: 10.14750/ME.2021.004

This water losing effect has already been visible in Chapter 5.3, where the water content loss was proved on hydrated iron sulphate by microprobe measuring and during measuring the BSE images proved that the high water containing sulphides with well-developed crystals lost its structure, then looked like an amorphous gel with perfectly smoothed, but cracked surface. Moreover on the BSE images about a week later, has already cracks were formed, by further dehydration on free air between the two measuring times.

On an other aggregate, which looked microcrystallized, was not possible to differentiate the different grains, there were pour or even no contrast border among the crystals, so probably they crystallized in the same time and quickly, thus not formed separate and individual crystals. Microprobe analysis (FIG. 51) was done in two different points, which show slightly different concentrations, but only the bulk chemical composition could be measured, because of the above mentioned properties. For the Al-Si ratio, the ***kaolinite*** fits perfectly by stoichiometry. The ratios of the rest elements – included the remaining oxygen – is very characteristic for the group of jarosites. Potassium indicates ***jarosite*** */$KFe_3(SO_4)_2(OH)_6$/* while the lead content with the other elements determines the ***plumbojarosite*** */$PbFe_6(SO_4)_4(OH)_{12}$/*. As the kaolinite does not contain sodium, thus this element also belongs to the jarosites, as an indication of ***natrojarosite*** */$NaFe_3(SO_4)_2(OH)_6$/*. This appearance is normal, because the sodium and the potassium-containing jarosite commonly crystallize together, as the element concentration in the fluids modify.

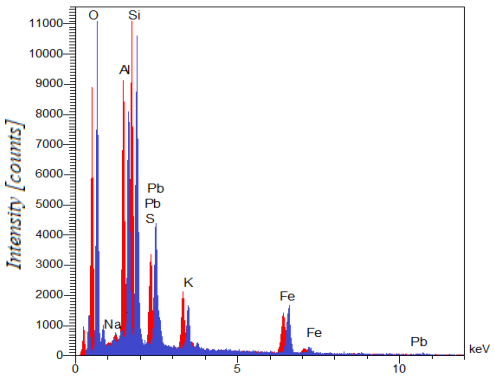

FIG. 51: Kaolinite and jarosites

Within the heavy mineral separation measuring, element mapping was done for Zn, Cd, Cu, As, Fe, Pb, Sn and Sb element. Unfortunately, a larger grain near this preparation makes shadow for the detector, so the left bottom of the picture is black. The BSE image (FIG. 52/a) and the individually coloured and combined element map (FIG. 52/b) well visualize the relatively homogeneous grain size (about 50-70 µm) of the washed and separated heavy mineral grains.

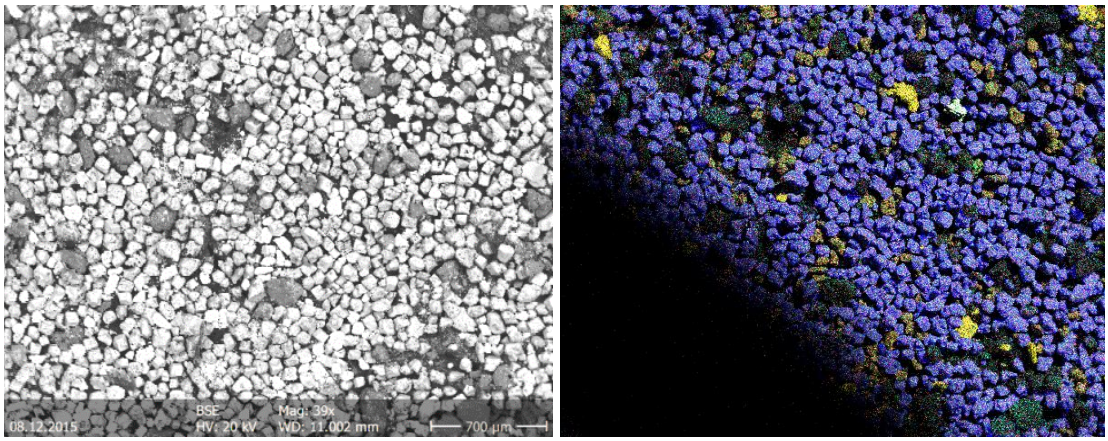

FIG. 52/a: BSE image of the separated grains (destilled water washed) from Jalpha 1-7
FIG. 52/b: Element map of the analysed area (Elements: Zn: yellow; Cd: pink; Cu: orange; As: turquoise; Fe: blue; Pb: ochre; Sn: purple and Sb: light green

DOI: 10.14750/ME.2021.004

Clearly visible, that the dominant sulphide phase is the pyrite, as the iron (blue) phases are at the highest rate, which is absolutely parallel with the result of the XRD (Table 18) and also with the recalculated amount (Table 20) of it. This element mapping helps to realize the different species with different cation content of the minerals. These small grains were not glued and polished, thus the rough surface and the not equal grain size and height indicated that the picture is not so high quality.

Two grains were found, where the element map of Cd showed some enrichment. On the first grain only one measuring (FIG. 53/a), but on the secondly found grain two measurements were done, which is shown on the same graph (FIG. 53/b), but the energy axis is shifted a bit of the second measuring to show the differences of the element ratios.

From the measuring became defined, that the Cd in sulphide form, so as ***greenockite***, built in the structure of ZnS, as ***wurtzite*** or sphalerite. The ZnS grains were not free of iron, it contained 3.5-4.5 %, and also the Cd content was significant, about 3 %. If it is calculated into sulphide form, it takes about 4 % of the ZnS grain.

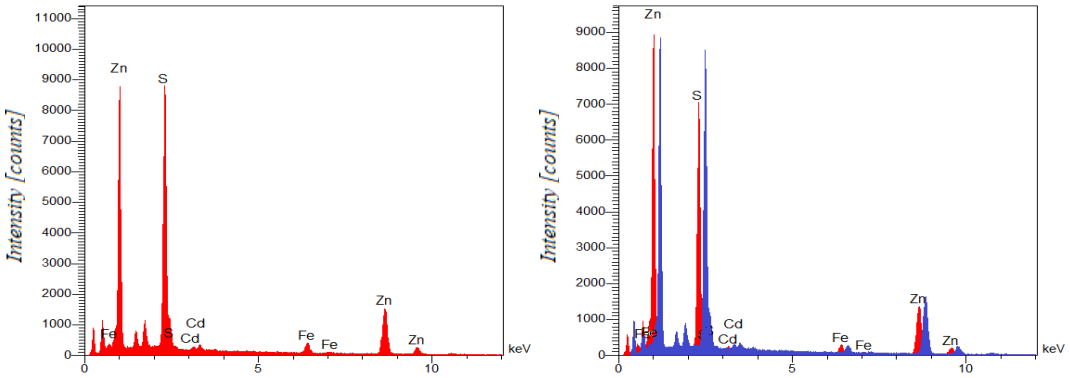

FIG. 53/a and b: Cd element replacing in zinc sulphide grains in three different measurings

7.5.2. Sample Itos Jig 2-7

As the analysis started with the separated grain section, on a pyrite grain's surface at least two types of amorphous looked secondary minerals could be separated. They could not be really separated from each other, probably produced at the same time, or partly the first one has already started to be altered to the second one. The electron beam burned a hole in it, so the water content was high. The microprobe analysis (FIG. 54) showed elements of iron, sulphur and oxygen. The stoichiometric calculation gives as iron sulphate, probably as significantly water lost ***melanterite***, with an iron hydroxide, probably as ***ferrihydrite***. The last mineral can derive either from the pyrite oxidation or from the further oxidation of some iron sulphate mineral.

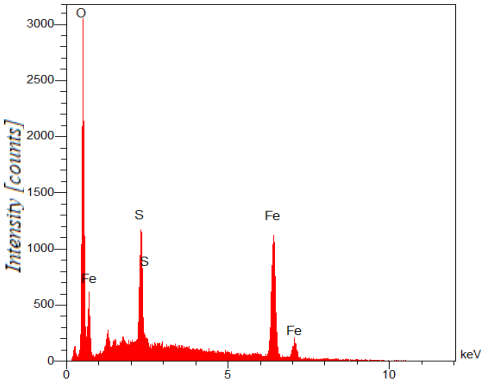

FIG. 54: Alteration products on pyrite

DOI: 10.14750/ME.2021.004

From a few of the grains, where the coal coating the grain was good, BSE image could be done, which showed high zonality (FIG. 55) its right side, which is caused by the changing of the average atomic number. With microprobe measuring it was determined as zinc sulphide, so ***wurtzite*** grain. The zonality was caused by the changing of the Fe content in the structure of the ZnS mineral. It varies between 3.2 and almost 8 %, created high contrast for the zones. At the left side of the grain, the mark of the weathering had been appeared, in forms of holes and caverns. Those zones started to degrade much stronger, where the Fe content was higher, so it was weaker against oxidation than zones with less impurities of iron.

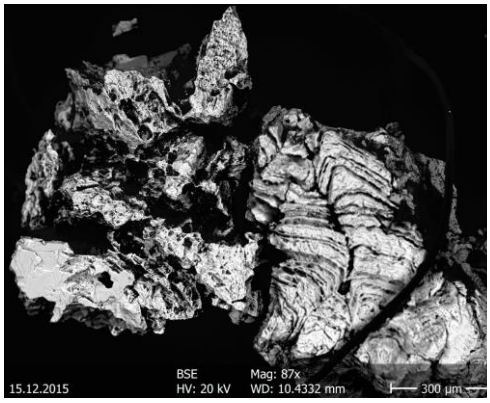

FIG. 55: Weathering caverns in a zonalited wurtzite grain in Itis Jig 1-7

By the analysis of another area of the polished section, very complex mineralization became visibly by BSE image (FIG. 56). The frame of the structure is given by the ***pyrite*** (a) and the ***quartz*** (b) phases. With bright colour, a silver chloride (FIG. 56/a) phase, the ***chlorargyrite*** (AgCl) appeared. The vein in the quartz is filled by ***anglesite*** (d). In a thin zone (e) the minerals were so thin and tiny, that individual measuring of the grains with electron microprobe was not possible, so only the mixture of them (FIG. 56/b). From the result of the element concentration, can be calculated by stoichiometry that it clearly consists of ***cassiterite*** and ***arsenopyrite***. Inside the pyrite grain, a tiny ***galena*** (f) crystal with its usual cubic shape was found with high Ag content (FIG. 56/c), which reached 15%. The grain was too small (<10 µm) to be able to define whether the silver was built in the structure of galena, or it forms a separate mineral. In lack of Cl, the possible form would be the sulphide, as ***acanthite*** (Ag_2S). The frame, created by pyrite and quartz, is filled out with a small crystal sized mixture of undefined ***APS minerals*** (g) with some iron content clay (like nontronite from smectites), but based on electron microprobe, in lack of visible and measurable clear and individual mineral grains, it is not possible to determine the mineralogical composition of the filling.

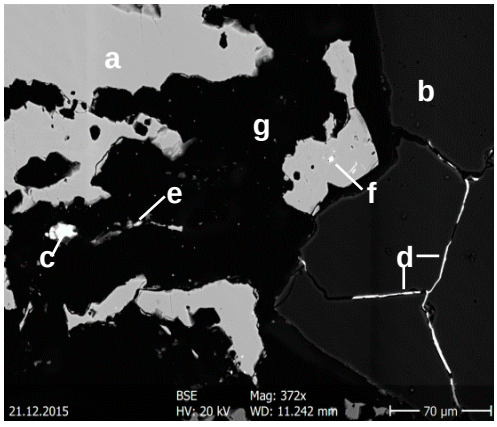

FIG. 56: Complex sulphidic mineralization, with chlorargirite, cassiterite and anglesite

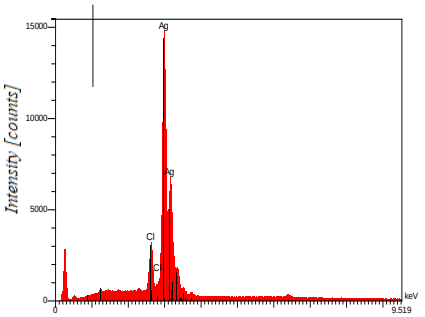

FIG. 56/a: Spectrum of Phase "c"

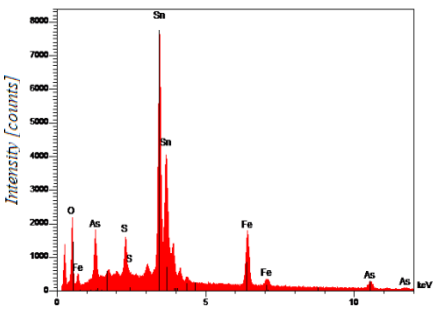

FIG. 56/b: Spectrum of phase "e"

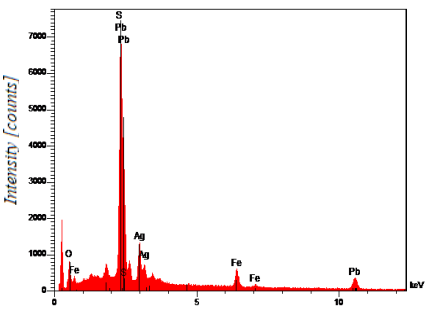

FIG. 56/c: Spectrum of phase "f"

DOI: 10.14750/ME.2021.004

A tiny (15 µm) grain was found with its own shape and zonality. At least 3 zones can be distinguished: the brightest core, a darker inner and a brighter outer mantle (FIG. 57). The circular brightish-darkish shape is not a difference in chemistry, only the electron beam burned the sample because of the high water content. By stoichiometry, the core (FIG. 57/a) consists of a mixture of ***plumbojarosite*** and ***jarosite*** (a), with Al or Al-K sulphate from the background. The high water content inner core, based on the microprobe measuring (FIG. 57/b) consists of ***alum-(K)*** (b). Alone it has no high enough water content for such a burned hole and also from the K-Al ratio, where the Al is much higher than in this mineral can be calculate from stoichiometry that ***alunogen*** (b) also has to be there, as a mixture of the two minerals. The mineral of the outer mantle (FIG. 57/c) consists of K, Fe, S and O, in such ratio, that it can be defined by stoichiometry that it is ***jarosite*** (c).

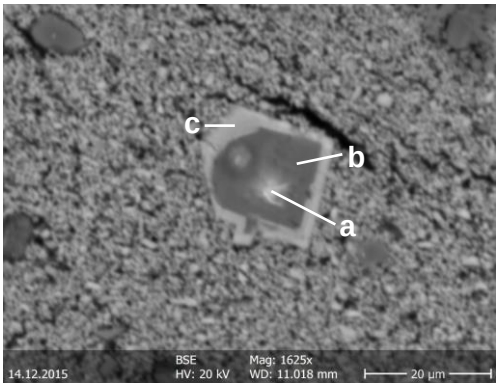

FIG. 57: Zonalited alteration products

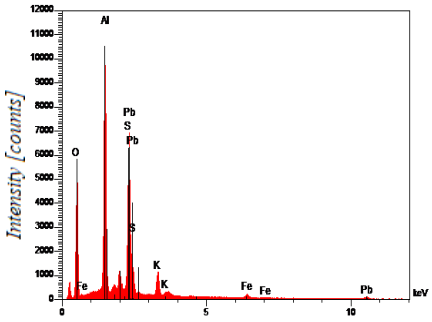

FIG. 57/a: Core (a) of the grain

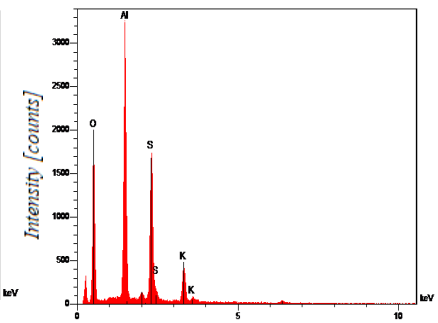

FIG. 57/b: Inner mantle (b)

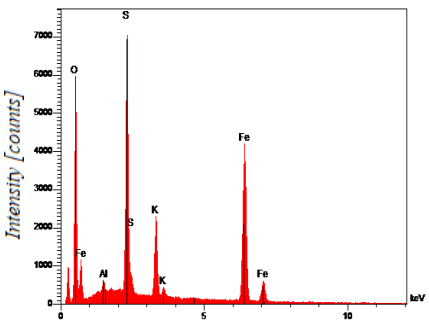

FIG. 57/c: Outer mantle (c)

At some place, Fe-containing by-products (FIG. 58) were found, as the result of the pyrite oxidation. A ***pyrite*** (a) grain (FIG. 58/a) was found among ***quartz*** (b) crystals. The alteration products of the pyrite surround it in form of oxyhydroxide or oxide (c). This phase cannot be measured individually, becasue it was to thin, so with the electron microprobe the pyrite and its alteration product (FIG. 58/b) was measured together. By calculation with stoichiometry, it is given as ***hematite*** (c). Among the grains, the matrix is dominantly ***nontronite*** (d) from smectites with an indication of other types of clay minerals (FIG. 58/c), which contains some element of Na and K.

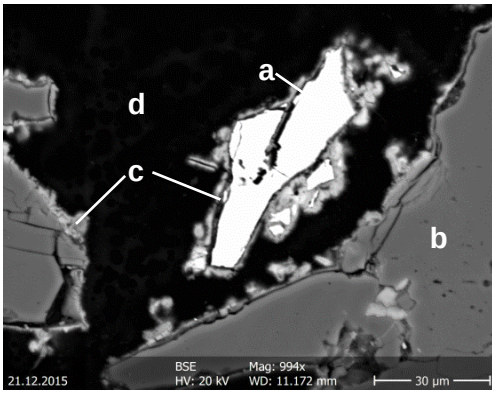

FIG. 58: Pyrite grain with oxidation rim

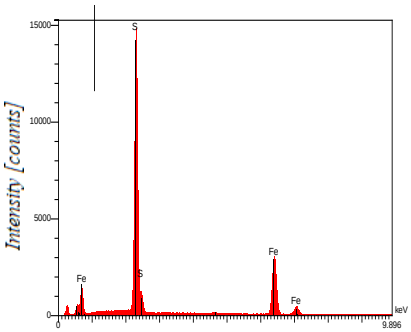

FIG. 58/a: Spectrum of phase "a"

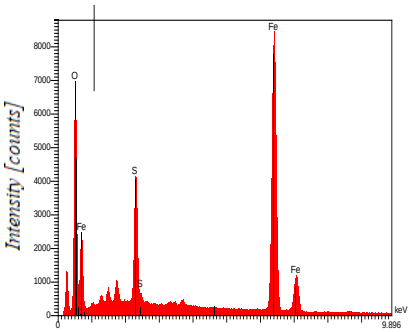

FIG. 58/b: Spectrum of phase "c"

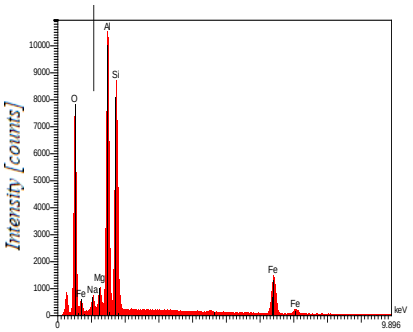

FIG. 58/c: Spectrum of phase "d"

DOI: 10.14750/ME.2021.004

From lead-containing minerals, only a small amount was calculated from the concentration of the leachate. The heavy molecule weight helped to find them, by the bright colour on BSE image. The inner and brightest core is ***galena*** (a), around it – as a coating its alteration products (after Eq. 21) – the ***anglesite*** (b) takes place. This partly altered grain is located in a crack of a ***pyrite*** (c) grain, which has middle grey colour at the corners of the image (FIG. 59). The other part of the crack is filled by acrylate resin, which is represented by dark colour on the BSE image.

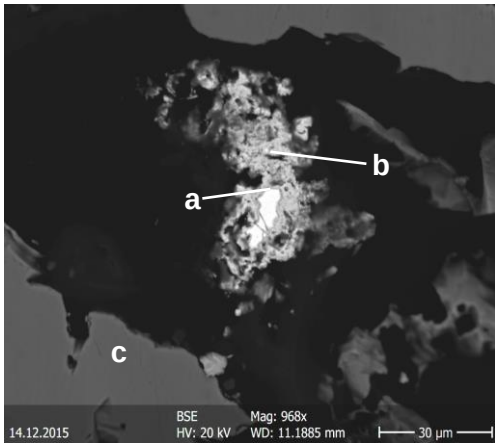

FIG. 59: Alteration of galena to anglesite phase in the crack of a pyrite grain

By BSE image of a polished ***pyrite*** (a) surface (FIG. 60) with several other sulphide minerals appeared. The common appearance is usual, because these sulphides are formed in the same environment, so they can appear together. This is the situation with the elongated crystals of antimony sulphide, the ***stibnite*** (b), because it has well developed and own shape crystals, so it is formed before or together with the pyrite, which simply encompassed the crystals. Tiny and shapeless grains, the ***cassiterite*** (c) and the ***wurtzite*** (d) also appeared. It is not so common for the Zn-sulphide to form in well-developed crystals in such an environment.

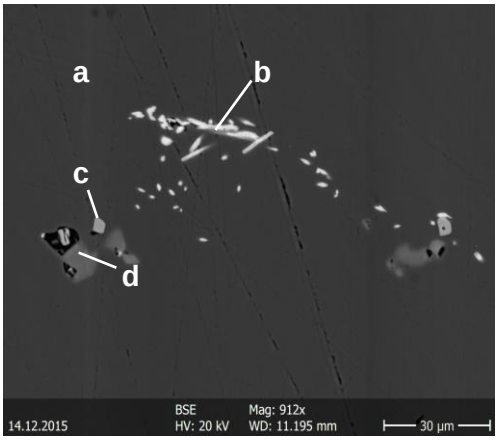

FIG. 60: Different sulphides inside pyrite

In the polished section, among those alteration products, which were stable enough to maintain themselves during the preparation of the polished section, some were measured. The BSE image (FIG. 61) shows zonation in the individual crystals, which is the result of the changes in the chemical composition. In the core of the crystal (a) near the S, O and Al element the dominant cation is K with some Na content, which shows that this is a dominantly K containing ***alunite***, with some moving to the ***natroalunite*** mineral composition. On the peripheries the chemistry changes, as the Na content become half and some Fe and P appears. The chemical composition defines this zone, as some ***APS mineral*** (b). Around the analysed grain, several others are with the same zonation, so an ***alunite*** (a) core with ***APS mineral*** (b) peripheries. This shows, that the condition firstly was ideal for alunite formation, later as the chemistry changed, the secondary mineral formation turned toward the APS mineral. Nevertheless, the chemical composition of the two mineral groups is not so far from each other. Among these crystals ***anglesite*** (c) appeared.

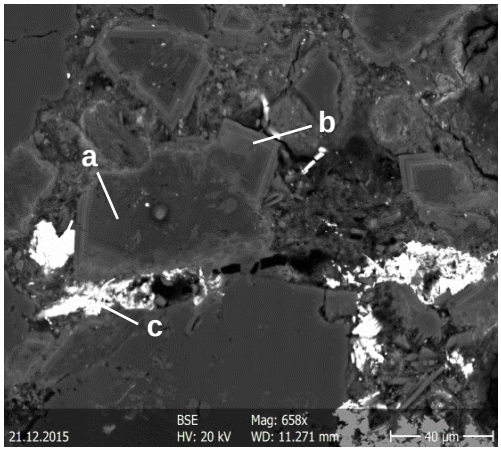

FIG. 61: Zonality in alunite crystals, with different members from alunite subgroup

DOI: 10.14750/ME.2021.004

A rectangular shape crystal with zonality and straight cracks became visible by BSE image (FIG. 62). The contrast shows, that the average molecular weight is slightly different. The electron microprobe measuring gives as the brighter zone is a pure Fe-O phase, by the ratio, it is ***magnetite*** (a). The darker zone is also a dominantly iron ***oxide*** (b), but the near the iron, magnesium and manganese is also present in its structure, in Mg-Mn-Fe ratio of 1:1:4. No oxide mineral is known with such a chemical composition and Mg-Mn-Fe ratio, so element replacing of Mg and Mn for Fe can cause this. The brightest minerals were ***pyrite*** (c). The surface and inner structure of them looked oxidized and altered, especially for the right species.

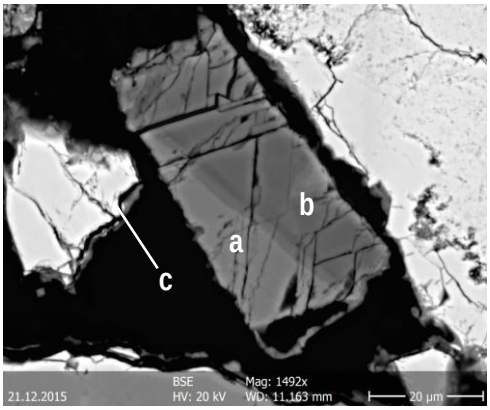

FIG. 62: Zonation in an Fe-oxide crystal, with measured different Mg:Mn:Fe ratio

For curiosity, near the chlorargyrite (FIG. 56/a) and achantite (FIG. 56/c) or high silver containing galena, a shapeless bright grain (FIG. 63/a and b) of ***native gold*** (a) was found between ***pyrite*** (b) grains. This type of appearance of the gold is not unusual in those type of ore mineralization, like in the Potosi-Oruro region has. Moreover, the native gold is resistant against any type of weathering or acidic environment, thus it will not degrade.

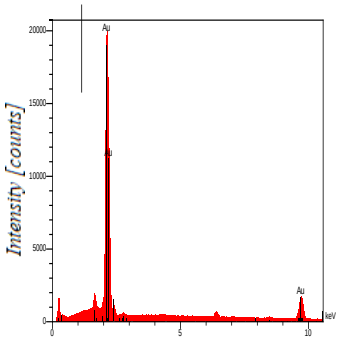

FIG. 63/a: Measured spectrum

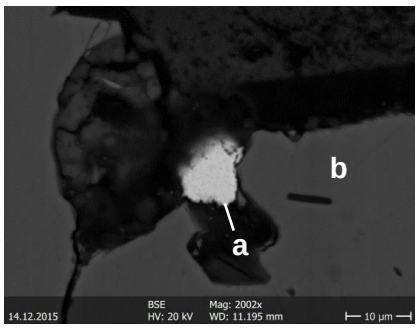

FIG. 63/b: BSE image of the gold

7.6. Conclusions

It can be declared, that the BSE images and the electron microprobe analyses absolutely proved the presence of those minerals, which were calculated from the sequential chemical extraction combined with X-ray diffraction method. Both the sulphides and their alteration products were found, even in such low quantities, as 0.04 % of arsenopyrite, 0.002 % of wurtzite, 0.005 % of galena, 0.009 % of stibnite and also 0.009 % of cassiterite. Near these several high water containing sulphate minerals, as by products were found, like alunogen, melanterite or alum-(K). Furthermore, the calculated different jarosite, such as the potassium and the lead members were determined by-microprobe, even with some indication of the sodium member.

These results confirm the correct working in the calculation, furthermore, it shows this combined method could stand its place among geochemical methods.

But it is important to mention that the calculation method requires a strong chemical, geochemical and mineralogical background, with some additional information from the ore geological origin of the sample. Nevertheless its result can be very valuable.

DOI: 10.14750/ME.2021.004

VIII. CALCULATIONS OF BULK PYRITE OXIDATION RATE FROM HUMIDITY CELL TEST RESULTS

8.1. General background

In the last four decades, the acid rock drainage (ARD) became a world-wide serious phenomenon of sulphidic mining. To avert the ARD caused environmental problems, necessary to know those processes, which can lead to the acidic environment and the heavy metal pollution, produced by the increased metal mobility. In ARD, the key question is the characterization of the problem, included such processes, which were shown in earlier chapters. In long term thinking for the ARD characterization, one of the most important parameter is the oxidation speed of the sulphides, especially the pyrite. Thus the determination of the oxidation speed became one of the most important – as well as the most searchest – parameter in the oxidizing system. Moreover, to create a well-fitting geochemical model of the fresh or already oxidizing sulphidic wastes, the oxidation speed is almost essential information.

To be able to produce those parameters, which are essential for the determination of the oxidation rate, on the samples kinetic test needs to be done. The humidity cell test is designed to optimize oxidation, which will have a significant impact on overall leaching rates. (USEPA 2009)

Lapakko (2003) and Elbering et al. (1994) published that the leaching rates for the standardized tests are 1 to 2 orders of magnitude higher than in nature, which is parallel with the thinking to reach the worst case scenario.

The aim of this chapter is to determine calculations for the oxidation rate, based on the different parameters which are measured during the kinetic tests, either in humidity cell or column one. Further aim is to check the applicability of the calculation methods via case studies and also to specify those parameters in the system which can drive to over or underestimation.

8.2. Earlier applied determinations for sulphide oxidation rate

During the last three decades, several equations were created to determine the oxidation rate. Most of these, are based on laboratory or chemical measuring. Williamson and Rimstidt (1994) developed more equations for pyrite oxidation from experimental data. The first is based on the ratio of dissolved oxygen (DO) and H^+ ion, while the second one compares the amounts of ferrous (Fe^{2+}) and ferric (Fe^{3+}) iron.

The rate (Eq. 26) expression for the reaction between pyrite and DO was determined as:

$$r = 10^{-8.19(\pm 0.10)} \frac{m_{DO}^{0.5(\pm 0.04)}}{m_{H^+}^{0.11(\pm 0.01)}} \quad (26)$$

Where r is expressed in $mol*m^{-2}*s^{-1}$. This reaction rate is applicable for DO concentrations changing over 4 orders of magnitude and a pH range from 2 to 10.

DOI: 10.14750/ME.2021.004

After Williamson and Rimstidt (1994), the rate of pyrite oxidation by Fe^{3+} was observed to vary significantly with the presence or absence of DO. Experiments conducted in solutions with DO concentrations of ambient air and pure O_2, showed no discernible differences. In the presence of DO, the ferrous-ferric alteration takes place, thus the rate (Eq. 27) expression is:

$$r = 10^{-6.07(\pm 0.57)} \frac{m_{Fe^{3+}}^{0.93(\pm 0.07)}}{m_{Fe^{2+}}^{0.40(\pm 0.06)}} \quad (27)$$

Mineral reaction rates are commonly given as the amount of mineral (moles) reacted per time unit and surface area. (Nicholson and Scharer 1994; Rimstidt et al. 1994; Williamson and Rimstidt 1994) The literature is usually referring to pure minerals and not bulks material, such as rock with mixed mineralogy.

The reaction rates established from kinetic tests performed on mine waste materials are commonly given per mass unit unless a relation can be established between grain-size for material and the surface area for the mineral(s) in question (CEN 2012) due to the difficulties in establishing a surface area of a specific mineral within a crushed/milled rock material.

After USEPA (2009) the calculation of the leaching rate (LR) can be performed using calculation (Eq. 28). (Morin and Hutt 1997; Price 2009;)

$$LR = \frac{c_r * V_r}{M_s * t_r} \quad (28)$$

Where *LR* is the leaching rate given as mg constituent leached per time (s) per kg of waste material; c_r is the constituent concentration in the rinse in mg/l; V_r is the volume of the rinse in l; M_s is the mass of the sample in kg, and t_r is the time between each rinse interval in unit of seconds.

In 2012, the CEN/TR 16363 directive was made by the European Committee For Standardization agency, which describes two equations for calculating bulk sulphide oxidation rate. The first equation is based on Caruccio (1975) first order of kinetic equation and sulphide sulphur oxidized to sulphate sulphur (Eq. 29). The kinetic constant can be expressed (Eq. 30) in terms of half-life of sulphide sulphur (t½ days) that reflects both total sulphide sulphur content in waste material.

$$S_t = S_0 e^{(-k*t)} \quad (29)$$

$$k = -ln\frac{S_t}{t} * lnS_0 \quad (30)$$

Where S_t is the residual sulphide sulphur content in the waste rock after a period of time *t* since the beginning of the test in weight percentage, S_o is the sulphide sulphur content at t=0 (at the start of constant sulphate release) also in weight percentage.

The sulphide sulphur content S_0 at *t*=0 is calculated as the initial total sulphur subtracted by the measured sulphate sulphur during a period with the stable release. This with the assumption that all non-sulphide sulphur minerals and/or compounds have been leached out during the lag-time and after the

DOI: 10.14750/ME.2021.004

microbial activity is established. The residual sulphide sulphur content after time *t* is calculated as S_0 subtracted by the measured sulphate sulphur release during the time *t*. (CEN 2012)

The second calculation, which was presented by CEN/TR 16363, determines the pyrite oxidation rate (R_{FeS2}) from the measured O_2 depletion during the kinetic testing (Eq. 31), like the following equation shows:

$$R_{FeS_2} = \frac{P_{I(O_2)} - P_{(FO_2)}}{t * 3.75 * M_{py}} \quad (31)$$

Where R_{FeS2} is the pyrite oxidation rate in the unit of moles*kg^{-1}*day^{-1}; $P_{I(O2)}$ is moles O_2 initially in the confined; $P_{(FO2)}$ is moles O_2 at the end of the measuring period, in a confined reaction space; *t* is the time (in days) M_{Py} is the mass of pyrite in the sample at start of oxygen depletion measurement (in kg); and 3.75 is the ratio of moles of O_2 per mole of pyrite oxidized.

8.3. Reaction rate calculations

Based on the pyrite abiotic oxidation reaction (Eq. 1) of Nordstrom (1982) three products that can be analysed in seepage water. In addition, the reactant – the O_2 gas – can also be measured by consumption of it. Each of these parameters gives the possibility of calculating the pyrite reaction rate.

The pyrite oxidation is at normal pH (circumneutral or only weekly acidic) primarily controlled by abiotic reactions even though there are bacteria that utilize energy from the oxidation of sulphides and ferrous iron. If the system becomes more acidic, as the pH decreases under 3.5-4, the effect of the bacterial processes will increase. The length of time for the shifting from the primarily abiotic to the primarily biotic pyrite oxidation is depending on many factors where mineralogy and climate conditions can be often the main ones.

The properties of the oxidizing system and the mineral alterations products define which method can be applied. To use the data in the reaction rate calculations, the system has to reach a steady-state, where the used parameters show stability or at least the dispersion and the fluctuation of the concentrations in the seepage is minimal in the function of time. It is important to know how the applicability of the various calculations could change. Some of the parameters are sensitive whether the system is abiotic or biotic, such as the O_2 based method, but for some of them, like the sulphate based calculation has no influence of the biochemical type of the oxidation.

Based on the abiotic (Eq. 1) and biotic (Eq. 8) pyrite oxidation the following alteration reactions take place by using a simplification of deleting the water and the oxygen, only used mole ratios between pyrite and its byproducts, both in abiotic (Eq. 1/b) and in biotic (Eq. 8/b) case.

$$1M\ pyrite \rightarrow 2M\ SO_4^{2-} + 1M\ Fe^{2+} + 2M\ H^+ \quad (1/b)$$

$$1M\ pyrite + 14M\ Fe^{3+} \rightarrow 2M\ SO_4^{2-} + 15M\ Fe^{2+} + 16M\ H^+ \quad (8/b)$$

When the ferrous (Fe^{2+}) ion oxidizes to ferric (Fe^{3+}) ion (Eq. 2) it uses H^+ in the ratio of 1:1, thus for production of 14 moles of Fe^{3+} consumes 14 moles of H^+. If this amount is deducted from the amount of H^+ in the end product of the reaction (Eq. 8/b), shows that the pyrite – H^+ ratio is the same in both reactions, as 1:2. Thus there is no impact for the calculation, whether abiotic or biotic reaction or a mixture of them takes place. The reason is that, from the 16 moles of H^+, 14 moles will be turned to produce the 14 moles of Fe^{3+}. Based on this, in both in abiotic and net biotic case the ratio between the starting product – as pyrite – and the by-product, such as dissolved ferrous (Fe^{3+}), sulphate (SO_4^{2-}) ion or acid (H^+), is the same.

8.3.1. Methods based on seepage components

As the pyrite – but it is true for the other iron or iron-containing sulphides – starts oxidizing, both in biotic and abiotic case the byproduct of the reactions (Eq. 1 and 8) are sulphate and iron ion release and acidic environment, so H^+ ion. From the seepage these components and the pH value can be measured, thus they can give information about the size of the oxidation rate, by calculation.

8.3.1.1. pH value based method

The amount of oxidized pyrite in unit of gram, based on pH (py_{ox}^{pH}) can be calculated at each individual rinsing time. To reach this, firstly necessary to calculate (Eq. 32) the concentration (C_{H^+}) of the produced H^+ in the unit of g/dm^3 by inversion of the pH value and multiply with the H^+ molecule weight.

$$C_{H^+} = 10^{-pH} * H^+_{mw} \tag{32}$$

To calculate the amount of the oxidized pyrite (Eq. 33), this result need to multiply with the rate of pyrite and H^+ from the pyrite oxidation reactions, which is 1:2 both in abiotic (Eq. 1 and 1/b) and abiotic case as well (Eq. 8 and 8/b) and further normalize with the volume of the rinsing liquid (V_{rs}). If the leachate is not distilled water, it is necessary to define the pH of the initial rinsing solution (pH_{rs}), not only the seepage's one (pH_{sp}). The result is given in the unit of gram because the pyrite molecular weight (py_{mw}=119.98 g/mol) and H^+ molecular weight (H^+_{mw}=1.01 g/mol) is included in the equation (Eq. 32).

$$py_{ox}^{pH} = (10^{-pH_{sp}} - 10^{-pH_{rs}}) * H^+_{mw} * \frac{py_{mw}}{2 * H^+_{mw}} * V_{rs} \tag{33}$$

The pH result used in this calculation should be taken from a steady-state zone, where the dispersion and the fluctuation of the pH of the seepage is minimal, where the average pH represents well the reaction rate. As the pH value is logarithm, the average pH cannot be calculated as a simple mathematical average. The following formula (Eq. 34) shows how the average pH can be calculated, both for the seepage and the rinsing water.

$$pH^{avg.} = -log_{10}\left(\frac{\sum_{i=1}^{n} 10^{-pH_n}}{n}\right) \tag{34}$$

DOI: 10.14750/ME.2021.004

To be able to determine the pyrite oxidation as a real reaction rate (R^{pH}) in the unit of g pyrite / week / kg of sample, it is necessary to include into the formula (Eq. 35) the calculation of the oxidized pyrite (Eq. 33) during the steady stable state in the sampling period, the total volume of the rinses ($V_{rs}^{tot.}$) in dm^3 from the first to the last used sampling, the time (N_d) in days between first and last rinsing. To reach the state of rate, the already set up equation need to be split with the mass (M_s) the sample in the unit of kg. This indicate that the result will function as a rate, moreover the different samples with various weight can be compared.

$$R^{pH} = \frac{\left(10^{-pH_{sp}^{avg.}} - 10^{-pH_{rs}^{avg.}}\right) * H_{mw}^{+} * \frac{py_{mw}}{2 * H_{mw}^{+}} * V_{rs}^{tot.} * \frac{7}{N_d}}{M_s} \quad (35)$$

8.3.1.2. Sulphate concentration based method

Both abiotic (Eq. 1) and biotic (Eq. 8) pyrite oxidation defines that 1 mole of pyrite produces 2 moles of sulphate, so the amount of altered pyrite can be calculated from it for each individual sampling using Eq. 36. The calculation is similar to the pH based one, only the parameters need to replace, such as the concentration of the sulphate (C_{SO42-}) in the unit of g/dm^3. The amount of the altered pyrite (36) will be in the unit of gram because the pyrite molecular weight (py_{mw}) and sulphate molecular weight ($SO_4^{2-}{}_{mw}$=96.07 g/mol) are included in the equation. It is multiplied with the rate of pyrite and sulphate from the pyrite oxidation reactions and normalized with the volume of leachate (V_{rs}).

$$py_{ox}^{SO_4^{2-}} = C_{SO_4^{2-}} * \frac{py_{mw}}{2 * SO_{4\,mw}^{2-}} * V_{rs} \quad (36)$$

The sulphate concentration used ($C_{SO42-}^{avg.}$) for calculating the pyrite oxidation rate (R^{SO42-}) by formula (Eq. 37), which will be determined in the unit of g pyrite / week / kg of sample also from a period of the stable release. Firstly needs to calculate the amount of oxidized pyrite, which is multiplied with the volume of the rinses ($V_{rs}^{tot.}$) in dm^3 from the first to the last used rinsing time used for the sulphate release and the time (N_d) in days between first and last rinsing. This needs to be divided by the mass (M_s) in kg of the sample, to be a rate and become comparable.

$$R^{SO_4^{2-}} = \frac{C_{SO_4^{2-}}^{avg.} * \frac{py_{mw}}{2 * SO_{4\,mw}^{2-}} * V_{rs}^{tot.} * \frac{7}{N_d}}{M_s} \quad (37)$$

8.3.1.3. Iron concentration based method

The dissolved iron based oxidation rate determination is similar to the previous two methods. This calculation is also applicable either for abiotic (Eq. 1) and biotic (Eq. 8) system, or for a mixture of them. Calculation of the reaction rate based on iron is given in equation 38, which includes the multiplication of the concentration of the iron in the seepage (during a steady-state release period), the ratio of the pyrite and iron (55.85 g/mol) molecular weight and the quantity of the volume leachate. Normalization

DOI: 10.14750/ME.2021.004

is not necessary, because in the oxidation reactions (Eq. 3 and 4) instead of pyrite-H^+ or pyrite-sulphate ratio, which is 1:2, the relation between pyrite and iron is 1:1, so the factor is 1.

$$py_{ox}^{Fe} = C_{Fe} * \frac{py_{mw}}{Fe_{mw}} * V_{rs} \quad (38)$$

To form real rate – the dissolved iron based reaction rate – the amount of the oxidized pyrite need to be normalized by the mathematical average of the stable iron value of the seepage ($Fe^{avg.}$) from the steady stable state period, the total volume of the rinses ($V_{rs}^{tot.}$) in dm^3 from the first to the last used sampling, the time (N_d) in days between the first and last rinsing and the mass (M_s) in kg of is the sample. The reaction rate (Eq. 39) will be in the unit of g pyrite / week / kg of sample.

$$R^{Fe} = \frac{C_{Fe}^{avg.} * \frac{py_{mw}}{Fe_{mw}} * V_{rs}^{tot.} * \frac{7}{N_d}}{M_s} \quad (39)$$

8.3.2. Method based on oxygen consumption

The CEN/TR 16363-2012 directive has given a formula (Eq. 30) for calculating the bulk sulphide oxidation rate based on oxygen consumption. The bulk oxidation rate can be calculated both from laboratory and field investigations.

According to the abiotic pyrite oxidation of Nordstrom (Eq. 1), $^7/_2$ moles of O_2 is necessary as the oxidizing agent to the oxidation of 1 mole of pyrite. Nordstrom and Southam (1997) defined the pyrite oxidation reaction based on ferric iron (Fe^{3+}) as the oxidizing agent (Eq. 8) without the direct need for oxygen. Moreover, the ferric iron is a magnitude stronger oxidizer agent than the O_2. However, to maintain this reaction, there is a need for a high supply of ferric iron, which requires oxygen (Eq. 2), but this can be dissolved one also. One mole of ferrous iron (Fe^{2+}) requires $^1/_4$ moles of O_2 for oxidation to ferric iron (Fe^{3+}). If this ratio is put into Equation 2 ($^1/_4$*14 = $^7/_2$), the result for the pyrite-oxygen ratio is the same as in case of pyrite oxidation with oxygen, thus also 3.5 moles of O_2 will be used up in oxidation of 1 mole of pyrite.

Similarly to the previous oxidation rate determination, the first step defines the amount of oxygen consumption. It is necessary to include the universal gas law (Eq. 40), which can define the amount of the gas (n) in the unit of mol, as a function of absolute temperature (T) and pressure (P).

$$n = \frac{P*V}{R*T} \quad (40)$$

The equation above can be reformed (Eq. 41) for the oxidizing system to define the consumed oxygen (m_{O_2}) in the unit of gram.

$$m_{O_2} = \frac{V_{free} * \left(O_{2\,conc.}^{t_o} - O_{2\,conc.}^{t_x}\right) * P_{t_x}}{R * T_{t_x}} * O_{2_{mw}} \quad (41)$$

Where V_{free} is the volume of free pore space in m^3; $O_2^{to}{}_{conc}$ and $O_2^{tx}{}_{conc}$ is oxygen concentration at the start (to) and at the end of measurement in percentage; t_x is length of the measurement period in days;

P_{tx} is pore gas at the closing time in Pa; R is Universal gas constant; T_{tx} is temperature of the gas and O_{2mw} is the molecular weight of O_2 (32.00 g/mol).

The Eq. 41 can be transformed further (Eq. 42) to define the amount of oxidized pyrite ($py_{ox}^{O_2}$) in gram, by multiplying with the rate of the pyrite-oxygen from the pyrite oxidation reactions.

$$py_{ox}^{O_2} = \frac{V_{free} * \left(O_{2\,conc.}^{t_o} - O_{2\,conc.}^{t_x}\right) * P_{t_x}}{R * T_{t_x}} * O_{2_{mw}} * \frac{py_{mw}}{3.5 O_{2\,mw}} \quad (42)$$

It is necessary to include the time (N_d) in days between the starting and the finishing of the test of O_2 measuring period and the mass (M_s) in kg of the sample. The reaction rate (Eq. 43) will be in unit of g pyrite / week / kg of sample.

$$R^{O_2} = \frac{\frac{V_{free} * \left(O_{2\,conc.}^{t_o} - O_{2\,conc.}^{t_x}\right) * P_{t_x}}{R * T_{t_x}} * O_{2mw} * \frac{py_{mw}}{3.5 O_{2\,mw}} * \frac{7}{N_d}}{M_s} \quad (43)$$

For the first view, the starting O_2 concentration would not be necessary to include into the equation, because it makes the calculation more complex. The situation is the same with the pressure, for the first look, it seems unimportant. We are used to that, the oxygen content is 21% and the pressure is 101kPa. But the situation can be different, as it is in Bolivia. Commonly the ore mineralizations as well as the mining waste and tailing materials are at high altitude. Each collecting points of the Bolivian samples were higher than 3760 m, but $^2/_3$ of them exceed the 4400-4500 m. At this altitude, the O_2 concentration as well as the pressure of the open air is significantly lower, than we are used to it.

8.4. Calculated result effecting parameters

The four pyrite reaction rate calculations, based on the parameter of pH, dissolved SO_4^{2-} and Fe, or the O_2 consumption have limitations. In the case of pH (Eq. 35), the reactions that are consuming or releasing H^+ during precipitation or H^+ released/consumed by the dissolution of the solid phase are important for the reaction rate calculation based on pH measurement.

One of the most characteristic reaction is the precipitation of secondary ferric (Fe^{3+}) ion hydroxide minerals. These minerals are primarily goethite (Eq. 5 and 6) or ferrihydrite (Eq. 3), which can form as solid phases. (Greffié et al. 2001; Jambor 1994; Jambor and Dutriaz 1998) These reactions increasing the acidity, so the amount of H^+ in the seepage will increases.

Although, these reactions have enough importance to significantly modify the pH of the leachate, these iron minerals will not precipitate in pH less than apx. 3.5, unless there is a very high iron concentration. Below this value, the Fe^{3+} stays in solution - as dissolved ion. The reactions are reversible, thus under pH 4 dissolution of iron hydroxides may consume hydrogen ions and therefore, act as a buffering mineral until consumed. (Stumm and Morgan 1981)

DOI: 10.14750/ME.2021.004

The water-soluble secondary iron sulphate minerals – such as melanterite – produces H^+ by dissolution (Eq. 20), thus the acidity and the sulphate concentration in the leachate increases. Most of these acid-producing secondary minerals dissolve easily and they will do it, therefore, if they were present in the original sample, be leached out in the early rinsing cycles of the kinetic tests. For this reason, kinetic tests on already weathered materials also need a start-up period (lag-time) before leaching rate has stabilized.

All four components used for reaction rate calculations are included in the products of jarosite dissolution. Jarosite minerals, which formed in the waste material are highly soluble, so the calculations based on using sulphate, ferric iron or hydrogen ion concentrations are overestimated, as long as jarosite minerals are present, which were formed before the test period. Generally, the first flush effect dissolves the jarosite already in the beginning period of the test. Neutralizing reactions including calcium-containing minerals (e.g. calcite, anorthite) may result in gypsum precipitation, which will affect the calculation of the pyrite oxidation rate using sulphate release.

If the prepared waste material for the kinetic test is fresh, unweathered material there is also going to be a lag-time. At the beginning of the kinetic test, the pyrite oxidation will start slowly. If neutralizing reactions does not control the sulphide oxidation, the release rate of products from the oxidation rate is continuously increasing until the system reaches the steady-state condition, as the worst case scenario. However, pH can become lower, if the oxidation is controlled by ferric iron, because the oxidizing system can reach higher oxidation speed.

The precipitation / hydration of ferric iron will give false calculated pyrite oxidation rate when using iron concentration for the calculation (Eq. 35) because the iron hydroxide minerals will not easily dissolve in the next rinse cycle. Altogether, the calculation works well, if the iron stays in dissolved form, thus when the pH is lower than 3.5-4. On the other hand, if it is significantly lower, the earlier formed secondary iron hydroxides, oxyhydroxides and oxides can be dissolved, which results in elevated level of iron in the seepage.

The calculation of pyrite oxidation rate based on O_2 consumption (Eq. 43) is independent of pH, iron precipitation or sulphate release, however, it requires hermetically closed reacting system and measurements of temperature, pressure and concentration of the O_2. Bacterial activity and oxidation of ferrous (Fe^{2+}) to ferric (Fe^{3+}) iron will affect the oxygen consumption as well.

For the calculation that time period of the kinetic test is necessary to use in each calculation method, when the parameters show stability week by week. The oxygen consumption also need to measure in that period of the test, when the other parameters show stability, so the release rate of the products of the sulphide oxidation is constant or close to it.

DOI: 10.14750/ME.2021.004

8.5. Case studies

The applicability as well as the limitations of the four different calculation are demonstrated using five different sulphidic mine waste material. The first sample is the HU 16-32 from Hungary, which contains neutralizing minerals in high rate, the BOL 6-9 and 7-9 tailing, which were strongly oxidizing from Huanuni, and also the BOL 3-9 tailing and BOL 4-9 waste rock from Morococala, where macroscopically visible secondary alteration products, such as gypsum and jarosite were visible. The oxidation rate was calculated for the last year because only in that one was O_2 measuring. The gas concentration measuring was done for a week, at the last week of the year 4th period of the humidity cell test series. In the case of sulphate and pH value based calculation, the same period was used from the humidity cell test results, to create comparable results. Unfortunately, there was no possibility for iron concentration measuring.

The sample ***HU 16-32*** is a sulphidic waste from the copper porphyry and skarn copper deposit, from Recsk, Hungary. Table 22 shows those results from humidity cell test, such as pH value, concentrations of the sulphate during the last test period (119 days) and the oxygen concentration measuring between the 105th and 112th days, which was used in the pyrite oxidation rate.

pH based:	pH_{sp}^{avg}=4.46; pH_{rs}^{avg}=7.00; V_{rs}^{tot}=6 dm^3; N_d=42days; M_s = 3.000 kg
SO_4^{2-} based:	C_{SO4}^{avg}=0.119 $^g/_L$; V_{rs}^{tot}=8 dm^3; N_d=56 days; M_s = 3.000 kg
O_2 consumption:	V_{free}=0.002686m^3; $O_2^{to}{}_{conc}$=21.1%; $O_2^{tx}{}_{conc}$=19.0%; P_{tx}=101300Pa; T_{tx}=290°K; N_d=7days; M_s = 3.000 kg

Table 22: Input data set of the four different oxidation rate calculations for the sample HU 16-32

For sample HU 16-32 sample by the source of the previous data, the following results are calculated (Table 23) for the oxidation rate:

Method	***Oxidation rate*** mg pyrite/week/kg sample
pH value based	R^{pH}=0.7
SO_4^{2-} release based	R^{SO4}=24.8
O_2 consumption based	R^{O2}=27.1

Table 23: Results of the oxidation rate calculations of the sample HU 16-32

From these result is visible, that the pH based method gives such a low result, which shows practically there is no pyrite oxidation, which can be interpreted by the high amount of calcite in the sample, thus the high neutralizing capacity which neutralized the H^+ from the seepage. The sulphate based gives similar, but slightly lower rate, than the oxygen consumption one. The reason for the poorly decreased sulphate result is that, as around pH 4.5 there is a border on the Eh-pH diagram (FIG. 47), where above gypsum can be produced, so tiny part of the sulphate ion can stay in the system as solid phase of gypsum. In the case of this sample, where there were no dissolvable sulphate minerals, which could increase the sulphate release in the seepage, but many acid consuming minerals were present,

DOI: 10.14750/ME.2021.004

which neutralized the acid from the pyrite oxidation. The highest result, so the oxygen consumption based calculation can be the closest to the real oxidation rate, so it is chosen.

The samples from Huanuni (BOL 6-9 and 7-9) are strongly oxidizing sulphidic tailings. Table 24 and 25 shows the applied data set of the humidity cell test for the calculation.

pH based:	pH_{sp}^{avg}=2.64; pH_{rs}^{avg}=7.00; V_{rs}^{tot}=5 dm^3; N_d=35 days; M_s = 2.148 kg
SO_4^{2-} based:	C_{SO4}^{avg}=0.267 $^g/_L$; V_{rs}^{tot}=5 dm^3; N_d=35 days; M_s = 2.148 kg
O_2 consumption:	V_{free}=0.002200 m^3; $O_2^{to}{}_{conc}$=21.1 %; $O_2^{tx}{}_{conc}$=17.3 %; P_{tx}=101300 Pa; T_{tx}=290 °K; N_d=7 days; M_s = 2.148 kg

Table 24: Input data set of the four different oxidation rate calculations for the sample BOL 6-9

pH based:	pH_{sp}^{avg}=2.51; pH_{rs}^{avg}=7.00; V_{rs}^{tot}=12 dm^3; N_d=84 days; M_s = 2.022 kg
SO_4^{2-} based:	C_{SO4}^{avg}=0.414 $^g/_L$; V_{rs}^{tot}=12 dm^3; N_d=84 days; M_s = 2.022 kg
O_2 consumption:	V_{free}=0.002210 m^3; $O_2^{to}{}_{conc}$=21.1 %; $O_2^{tx}{}_{conc}$=17.3 %; P_{tx}=101300 Pa; T_{tx}=290 °K; N_d=7 days; M_s = 2.022 kg

Table 25: Input data set of the four different oxidation rate calculations for the sample BOL 7-9

From these results, the oxidation rate calculation on different methods for BOL 6-9 (Table 26) and BOL 7-9 (Table 27) are calculated, thus the following results are presented:

Method	***Oxidation rate*** mg pyrite/week/kg sample
pH value based	R^{pH}=63.5
SO_4^{2-} release based	R^{SO4}=77.6
O_2 consumption based	R^{O2}=55.9

Table 26: Results of the oxidation rate calculations of the sample BOL 6-9

Method	***Oxidation rate*** mg pyrite/week/kg sample
pH value based	R^{pH}=91.0
SO_4^{2-} release based	R^{SO4}=127.9
O_2 consumption based	R^{O2}=107.2

Table 27: Results of the oxidation rate calculations of the sample BOL 7-9

The results show, that in the case of sample BOL 6-9, the oxidation rate, the different parameters based are roughly similar, with an average of 65. Although the sulphate concentration was higher because of the slowly, but continuous dissolution of secondary sulphates which were already in the sample and also the oxidation of other sulphide minerals, such as galena, wurtzite, chalcopyrite, etc.., can increase its level. Some of sulphides, like arsenopyrite (Eq. 10) or chalcopyrite (Eq. 12) produce acid in oxidation process and some of the secondary minerals produce acid by dissolution, moreover if iron-hydroxide (Eq. 3) or goethite (Eq. 5) is formed, also can add some acid into the system, so the calculation based on the modified pH, can results higher oxidation rate. The same processes are true for the results of BOL 7-9, although in this case, the sulphate is even more increased compared to the others.

DOI: 10.14750/ME.2021.004

Two more Bolivian samples were chosen, the BOL 3-9 and BOL 4-9, which seemed for good examples, because even macroscopically secondary alteration products, such as gypsum and jarosite crystals are visible. From this observation, strongly increased sulphate based oxidation rates can be expected. Both samples have relatively similar input data (Table 28 and 29).

pH based:	pH_{sp}^{avg}=2.22; pH_{rs}^{avg}=7.00; V_{rs}^{tot}=16 dm^3; N_d=112 days; M_s = 1.600 kg
SO_4^{2-} based:	C_{SO4}^{avg}=0.834 $^g/_L$; V_{rs}^{tot}=16 dm^3; N_d=112 days; M_s = 1.600 kg
O_2 consumption:	V_{free}=0.002062 m^3; $O_2^{to}{}_{conc}$=21.1 %; $O_2^{tx}{}_{conc}$=17.4 %; P_{tx}=101300 Pa; T_{tx}=290°K; N_d=7 days; M_s = 1.600 kg

Table 28: Input data set of the four different oxidation rate calculations for the sample BOL 3-9

pH based:	pH_{sp}^{avg}=2.22; pH_{rs}^{avg}=7.00; V_{rs}^{tot}=12 dm^3; N_d=84 days; M_s = 1.700 kg
SO_4^{2-} based:	C_{SO4}^{avg}=1.518 $^g/_L$; V_{rs}^{tot}=12 dm^3; N_d=84 days; M_s = 1.700 kg
O_2 consumption:	V_{free}=0.002408 m^3; $O_2^{to}{}_{conc}$=21.1 %; $O_2^{tx}{}_{conc}$=16.7 %; P_{tx}=101300 Pa; T_{tx}=290°K; N_d=7 days; M_s = 1.700 kg

Table 29: Input data set of the four different oxidation rate calculations for the sampleBOL 4-9

From these results, the oxidation rate calculation on different methods for BOL 3-9 (Table 30) and BOL 4-9 (Table 31) are calculated, thus the following results are presented:

Method	***Oxidation rate*** mg pyrite/week/kg sample
pH value based	R^{pH}=224.1
SO_4^{2-} release based	R^{SO4}=325.5
O_2 consumption based	R^{O2}=126.4

Table 30: Results of the oxidation rate calculations of the sample BOL 3-9

Method	***Oxidation rate*** mg pyrite/week/kg sample
pH value based	R^{pH}=210.9
SO_4^{2-} release based	R^{SO4}=557.6
O_2 consumption based	R^{O2}=87.3

Table 31: Results of the oxidation rate calculations of the sample BOL 4-9

The results confirmed the observation of the secondary sulphate minerals and the idea of increased sulphate content in the seepage by the dissolution of them. In some case, such as BOL 4-9, the sulphate content based calculation resulted more than six-times higher oxidation rate, than the oxygen consumption based. For the twice higher pH based results are also the above discussed processes are responsible. The dissolution of gypsum gives higher sulphate release, while the dissolution of jarosite, near the increase of the sulphate concentration, H^+ is also formed. The acidity will increase in case of jarosite, while the sulphate content will be increased by both minerals' dissolution. For such samples, where these sulphate minerals are present in high rate, thus the sulphate content will be increased and the pH decreased by dissolution, the oxygen consumption based calculation could give the realistic result for the oxidation rate, because this parameter is the less disturbed by (geo)chemical processes.

DOI: 10.14750/ME.2021.004

8.6. Conclusion

Through the two most important pyrite oxidation reaction, such as the abiotic (Eq. 1) and the biotic (Eq. 8), new ways of oxidation rate determination were showed. In these, the aim was to determine the reaction rate used by the pH (Eq. 35), the SO_4^{2-} (Eq. 37) or the Fe (Eq. 39) concentration of the seepage, furthermore the O_2 consumption (Eq. 43) of the oxidizing system. Naturally in the seepage – as in all auriferous solution – different chemical reactions take place. The most important, especially those which can change the concentrations in the seepage, need to be taken into consideration and chose that calculation, which fits the best on the given oxidizing system and mineralogy.

Carefully need to characterize the whole system before the methods will be set up. As much variety as possible should be closed out, to be able to get the best result, which will be equal or at least could be close enough to the real one, that the oxidation system presents.

The independence of the calculation formulas from the biochemical properties were proved, thus the four new equations can be used either for abiotic or biotic condition, or for a mixture of them with an unknown ratio between them. Practically this means, that not necessary to determine the system from point of the bacterial activity or to analyse weather ferrous-ferric alteration takes place or not.

Via case study, which consists of totally differently behaviour sulphidic mine wastes, was shown the different methods and its applicability. Also, it contained an explanation of the possibly best one, moreover, the chosen one was explained why it can be chosen as the most realistic one.

DOI: 10.14750/ME.2021.004

IX. TEMPORAL CHANGES OF PYRITE OXIDATION RATE IN SULPHIDIC MINING WASTES

9.1. Introduction

The determination of the sulphide / pyrite oxidation rate (Chapter 8.) is a useful tool to characterize the changes of the mining material, especially thinking on the possibility of "the worst case scenario". On the other hand, if on the same material several times the humidity cell test was completed, the results of the changes of the rate show much forward than in the individual years it does. The comparison of changes in the rates can give a real long term behaviour for the sample, because on the changes of the calculated rate from the several "worst case scenario" can be seen, as they are decreasing, increasing or become stable. Thus the results give much more information than the oxidation rate for an individual test periods, showing the changes for the long time future.

In 4 consecutive years humidity test was investigated on the same 7 samples. 5-7 months pauses were left between the test periods, which allow mimicking the alternation of wet and dry periods, which is typical of the climate of Bolivia.

The result of the humidity cell test shows that samples can be split by the changes of the pyrite oxidation rate into three different stages: where the oxidation rate shows increasing (marked type “A”) or decreasing tendencies (marked type “C”) or where the oxidation is maximal, so stable in the different years (marked type “B”).

9.2. Analysed samples

Among the 7 samples, 4 were collected in 2007 in Oruro, from tailing (Itos Jig 1-7 and 2-7) and waste rock (Itos Granza 1-7 and 2-7) material. The rest samples, so the BOL 1-8 waste rock and the BOL 2-8 tailing samples were from the "La Mina Fabulosa” mine in Milluni and the BOL 3-8 waste rock were collected from "Bolsa Negra" in 2008.

The maturation stage of the sample, the residence time under field conditions will affect on the time that is required to reach the steady-state oxidation during the humidity cell test. Fresh sample needs more time to start oxidizing as well as longer test investigation to reach a steady-state pyrite oxidation rate compared to the already oxidized samples.

In Oruro there were no strict mining regulations, thus the composition and the size of the waste dumps and tailing heaps were not known. The time of deposition was also uncertain, so there was no exact information about the residence time of these samples, except BOL 2-8, which is relatively fresh sample, as it stayed only 1-2 years as tailing (Table 32).

DOI: 10.14750/ME.2021.004

From macroscopic and stereo microscopic observation seems that the other samples were stored for a much longer time, because their rate of alteration were already high, so the time could be somewhere around 15-25 years (Table 32), but this is only a rough estimation assumption.

In the four-year test period, the length of the tests were different for the individual years (Table 9/b). The four Itos samples underwent 4 years of analysis, whereas the three BOL samples had no humidity cell test analysis in the 1st year, so they were analysed from the 2nd to the 4th year.

Sample	***2008 summer***	***2009 summer***	***2010 autumn - 2011 spring***	***2011 autumn - 2012 spring***
Year code	1st year	2nd year	3rd year	4th year
Itos Jig 1-7; Itos Jig 2-7 Itos Granza 1-7; Itos Granza 2-7	0 - 101 days	0 - 42 days	0 - 121 days	0 - 119 days
BOL 1-8; BOL 2-8; BOL 3-8	---	0 - 42 days	0 - 121 days	0 - 119 days

Table 10/b: Length of the humidity cell test period of the selected samples in the four consecutive years

The 7 samples have different physical parameters (Table 32). The grain sizes were very similar, only the sample BOL 2-8 was the exception, which had much smaller fractions, furthermore indices much higher reactive surface compared to the others.

Sample	***Estimated resid. time***	***Character***	***Grain size / main fraction***
Itos Jig 1-7	15–25 years	jig tailing	0.5-25 / 2-5 mm
Itos Jig 2-7	15–25 years	jig tailing	0.5-25 / 2-5 mm
Itos Granza 1-7	15–25 years	waste rock	0.5-40 / 4-7 mm
Itos Granza 2-7	15–25 years	waste rock	0.5-40 / 4-7 mm
BOL 1-8	15–25 years	waste rock	2-15 / 3-5 mm
BOL 2-8	1–2 years	tailing	0.1-2 / 0.5-1 mm
BOL 3-8	15–25 years	waste rock	2-15 / 3-5 mm

Table 32: Estimated residence time with the grain size parameters of the 7 chosen samples

9.3. Results in oxidation rates

Among the possibilities of the oxidation rate determination only the pH and the sulphate based method can be taken into consideration because these parameters were measured in all of the years of analysis. The oxygen consumption was checked only in the last (4th) year, while the Fe concentration in the seepage was measured none at all.

In the question of choosing between the two possibilities, the key answer is the mineralogy. As significant amount of secondary sulphates can be into the system, so the sulphate content in the seepage can be increased by the slow dissolution of these minerals, thus the pH based method was chosen. From

DOI: 10.14750/ME.2021.004

the result of the pH changes can be seen that after the first flush effect in the first weeks, the pH value become stable, so oxidation rate calculation can be done on them. To show the stabilization and the selected data, the Itos Jig 2-7 sample is chosen for visual demonstration (FIG. 64). The jumping in pH in year 1st at day 42 and 101 and in year 3rd at day 70 and 77 were only a technical mistake in sampling, so these data will be excluded from the calculation.

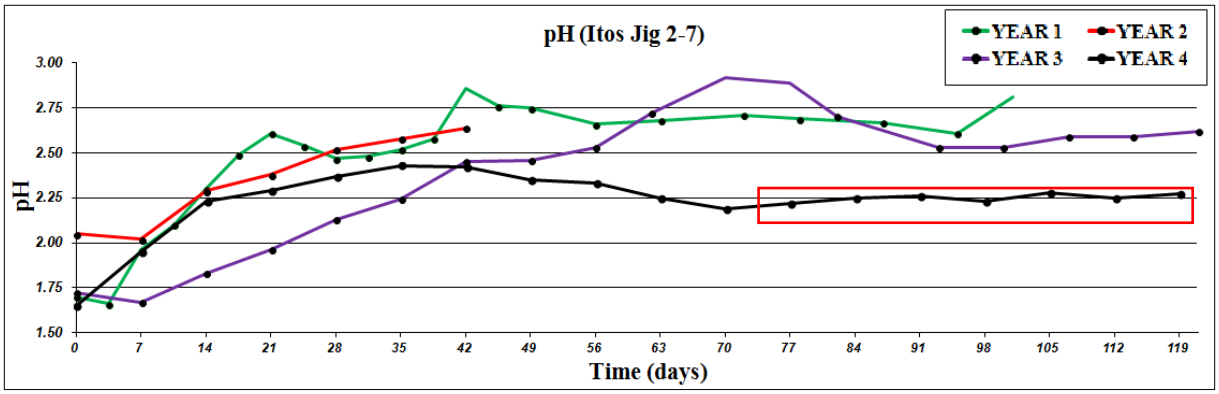

FIG. 64: Changes of the pH in the consecutive years of analyses, with the mark of the stable period

Each year of the humidity cell test started with an up-running part, caused by the effect of the first flushes, where the secondary minerals, accumulated during the dry period were dissolved and washed out. After this quickly changing period, the pH has been stabilized and the stable pH refers to the pyrite oxidation. The stable zones can be marked in each year (only shown on year 4th with red rectangular) and after the average calculation of the pH, the pyrite oxidation rate can be determined (Eq. 35). In year 2nd, when only 42 days (6 weeks) were available for running the tests, but even during this short time, the pH started to stabilize, so for the pyrite oxidation rate calculation, the pH values from the last week(s) were used.

From point of the changes in the oxidation rate, three groups can be defined: the first is when the oxidation rate is ***increasing (type "A")***, which is typical for the fresh samples, where the surface of the grains are free of secondary minerals, so quick and acute oxidation takes place. By moving forward in time, the oxidation rate becomes ***maximal and stable (type "B")***, so it is not changing (significantly) in time, while the last class, when the oxidation rate starts ***decreasing (type "C")*** in time, as the pyrite starts to be consumed and also its surface started to be covered by relatively chemically resistant iron oxides.

In the seven samples, all type of changes appears, in both Itos Jig tailing sample (FIG. 65) are increasing: gently in 1-7 and significantly in 2-7. It looks, although in the Itos Jig 1-7 sample the oxidation rate is increasing by time, but it has no enough energy to be able to significantly increase the oxidation, like a chain reaction, as usually happens in case of fresh or relatively fresh sulphidic / pyritic samples. This chain reaction with exponentially increasing oxidation rate is clearly visible in Itos Jig 2-7, where more acute reactions took place in the last year, which more than doubled the rate itself.

DOI: 10.14750/ME.2021.004

The waste rock set from the Itos series, so the two Itos Granza sample was stable, so no significant changes is visible. In the graph of 1-7 in the 3rd year happened a dropping in oxidation rate. It looks huge, but the pH just increased from 2.47 to 2.67. The reason can be mineralogical, as more stable secondary alteration products encapsulated the pyrite grains, thus the effective reaction surface decreased. The theory is that, after the 3rd year of the test period, probably jarosites were formed in such an acidic environment, which are acidic enough to be able to dissolve the iron oxyhydroxide or oxide phases. The other waste rock sample shows stable oxidation rates in the different years. This means, that the oxidation is stable and maximal, it is on its peak.

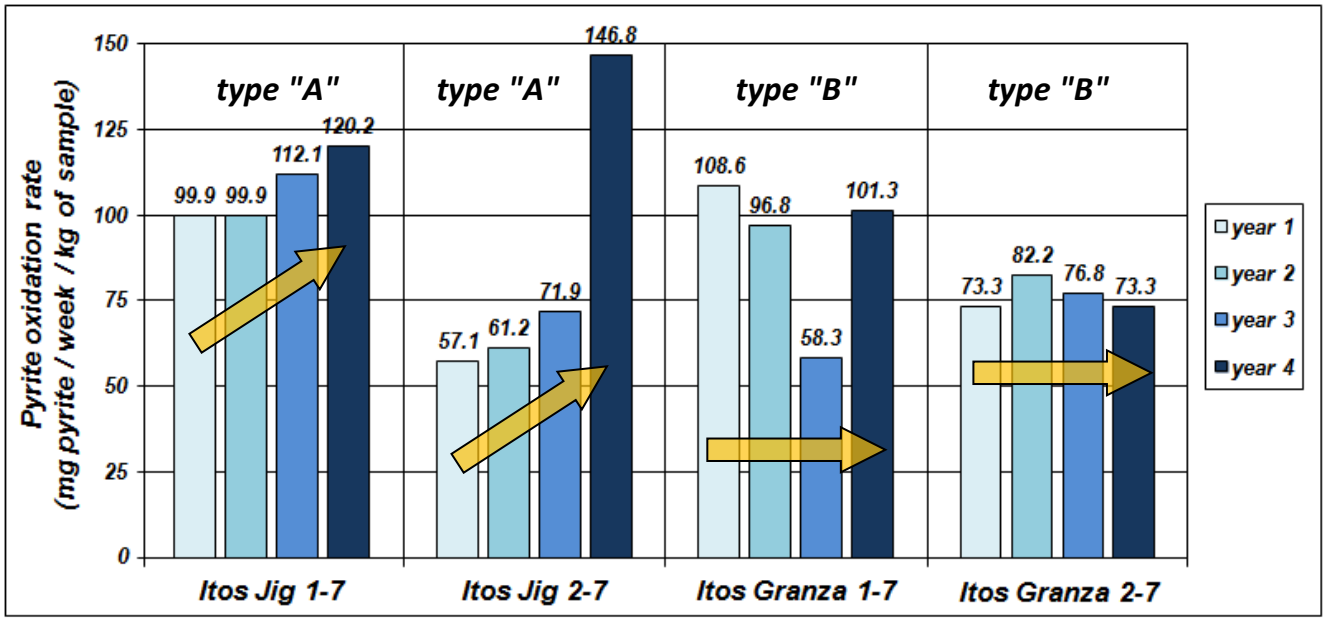

FIG. 65: Changes in the pyrite oxidation rates in Itos sample series during the four consecutive years of the humidity cell test

From the Milluni samples, the waste rock (BOL 1-8) has a distinct decreasing in the oxidation rate (FIG. 66), it has already started to burn out and the pyrite amount was decreased as it was replaced by alteration products. This effect looked macroscopically on the sample, because it had reddish-brown colour, so more stable iron oxyhydroxides and oxides were present, not just the sulphates, as jarosite. The BOL 2-8 sample was a relatively fresh tailing sample, which looks from the changes in the oxidation rates, as after a relatively calm year, the rate increased to the five times. This blasting-like increasing is typical for fresh samples with fine grain size and high pyrite content, which indicates high effective reaction surface. The sample from the "Bolsa Negra" mine (BOL 3-8) shows stable geochemical behaviour, as the oxidation rate is not changing by time.

As it was discussed in details previously (Chapter 5.3.), scanning electron microscope analyses were completed on samples before the humidity cell test to investigate the mineral alteration and pyrite oxidation. The SEM analysis also proved that the samples have already been strongly corroded. In addition to the primary minerals – such as quartz, pyrite, galena and cassiterite –, secondary sulphates (various members from the jarosite subgroup and gypsum), different iron oxyhydroxides and oxides were found.

DOI: 10.14750/ME.2021.004

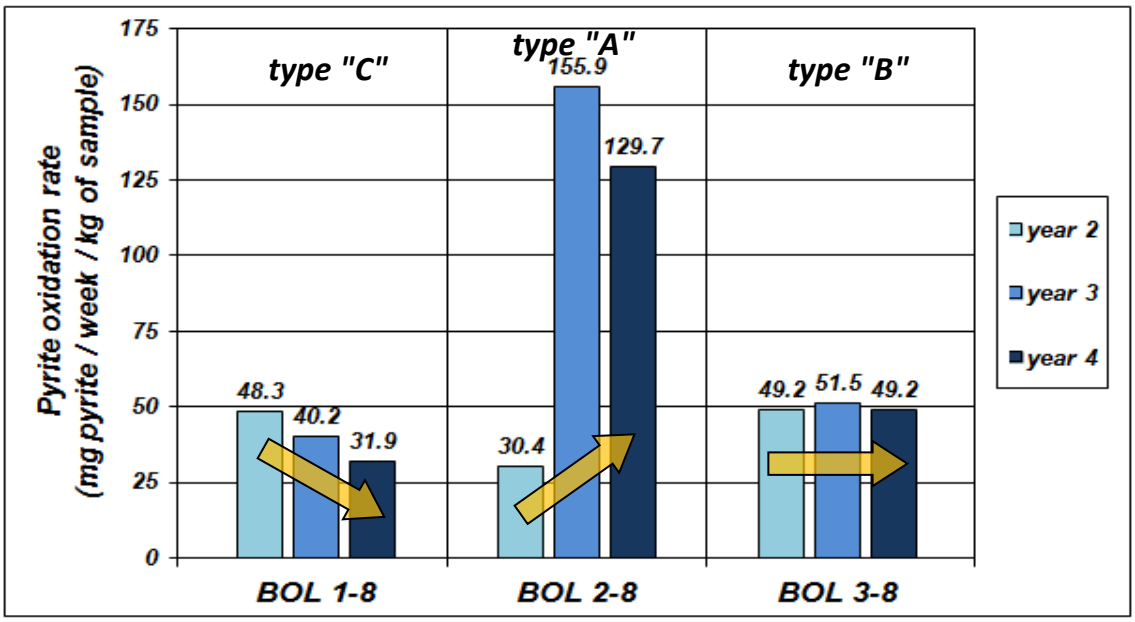

FIG. 66: Changes in the pyrite oxidation rates in BOL sample series during the three consecutive years of the humidity cell test

Intensive pyrite corrosion was detected both in tailings (Itos Jig 1-7 and 2-7) and waste rock samples (Itos Granza 1-7 and 2-7) where the pyrite oxidation was usually complemented by formation of secondary iron sulphates. In FIG. 67/a, a corroded pyrite (Py) crystal with cassiterite grains is shown from the sample Itos Granza 2-7. Strongly corroded pyrite (Py) particles with secondary iron sulphates are in FIG. 67/b from sample Itos Granza 1-7. The image of FIG. 67/c shows, that secondary gypsum with well-developed twin crystal was formed on galena and pyrite crystals in samples Itos Jig 1-7.

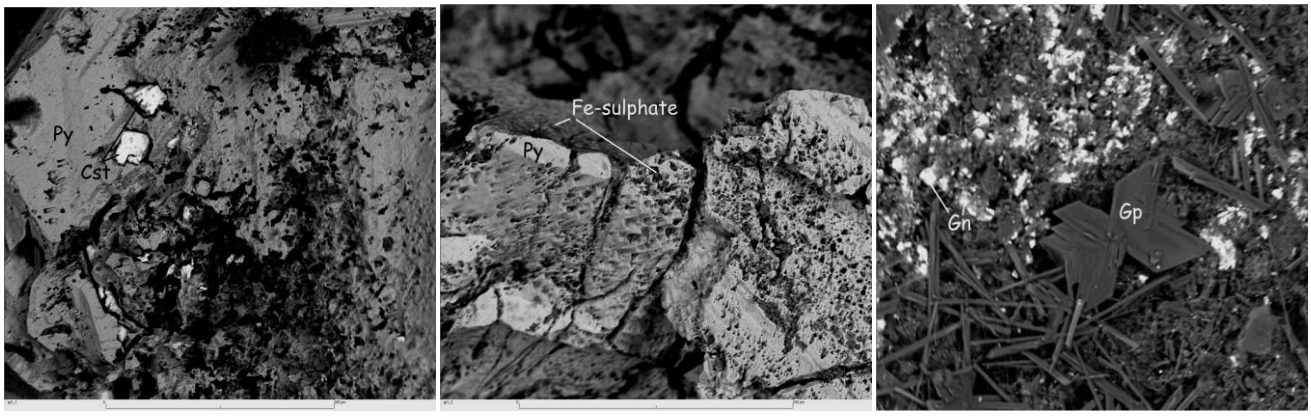

FIG. 67/a: "Sponge-structured" corroded surface of a pyrite grain with cassiterite in the sample Itos Granza 2-7
FIG. 67/b: Altered pyrite surface with secondarily formed iron-sulphates and oxyhydroxides in the sample Itos Granza 1-7
FIG. 67/c: Well-developed twin gypsum crystal with gypsum needles around it, with galena in the sample Itos Jig 1-7

9.4. Discussion

Compared the stabilized pH values, thus the pyrite oxidation rates for the consecutive test periods, the maturity of the samples could be assessed. The samples can be split into three different stages: fresh / weakly oxidized, premature / partly oxidized and mature / strongly oxidized. Other important indicators are the corrosion textures of pyrite and the appearing different secondary mineral groups. The following stages are determined:

DOI: 10.14750/ME.2021.004

In the ***weakly oxidized stage*** (marked type "A") the pyrite oxidation rate is increasing in the consecutive years. Samples Itos Jig 1-7, Itos Jig 2-7 (FIG. 65) and BOL 2-8 (FIG. 66), are good representations of this type of behaviour. In the beginning, oxyhydroxide minerals appear as alteration products after the sulphides. Then the pH goes below 2-2.5, so the oxyhydroxide minerals dissolve back and under such a low pH only sulphate minerals are formed, such as jarosite, melanterite or gypsum. The increase in pyrite oxidation rate means that in the future the reactions will become faster. Because of the low pH and speeding up of the reactions, the heavy metal mobility increases.

Partly oxidized stage (marked type "B") covers the samples Itos Granza 1-7, Itos Granza 2-7 (FIG. 65) and BOL 3-8 (FIG. 66), where the pyrite oxidation is maximal, thus stable – changes only within a few percentages – in the different years. The maximal pyrite oxidation rate also means that this stage has the lowest pH, which keeps for a longer time. In the beginning of this stage still the sulphate minerals will be the dominant secondary phases, but in the end of the stage as the pyrite oxidation rate starts decreasing and the pH increasing, besides the sulphates some oxyhydroxide minerals can already appear.

Strongly oxidized stage (marked type "C") includes only the sample BOL 1-8 (FIG. 66), where the pyrite oxidation rate is decreasing in consecutive years. The reaction rate slows down, thus the pH continuously increasing, but not as steep as the decreasing was in the first stage. The slow increase of pH in this phase is due to pyrite being excused. Bulk oxidation rate becomes lower due to less pyrite available. In this stage, the formed iron minerals dominantly will be already the hydroxide, oxyhydroxide and oxide phases.

9.5. Conclusion

The three stages shown above are members of a natural progression for weathering of iron sulphide containing tailings and waste rocks. The fresh material starts oxidizing with increasing rate, then with time the reaction rate becomes stable, and finally decreases. The complete process looks like a bell-shaped curve as it is shown on FIG. 68, where a theoretical pyrite oxidation curve is present. The graph is illustrating waste rocks were there are no or little neutralising / buffering reactions, such as massive sulphide deposits and polymetallic veins like the Itos deposit.

Of course, between the maturity stages, there are no well determinable border, moreover the trend line of the changes can be flatter or more steeper. The slope of the increasing or decreasing can be modified by the mineralogical composition of the sample, as well as the oxidation, dissolution or precipitation reactions, which take place in the material of the sample. As time moves forward, the slopes of the graph continuously changing, which is well visible in FIG. 68.

DOI: 10.14750/ME.2021.004

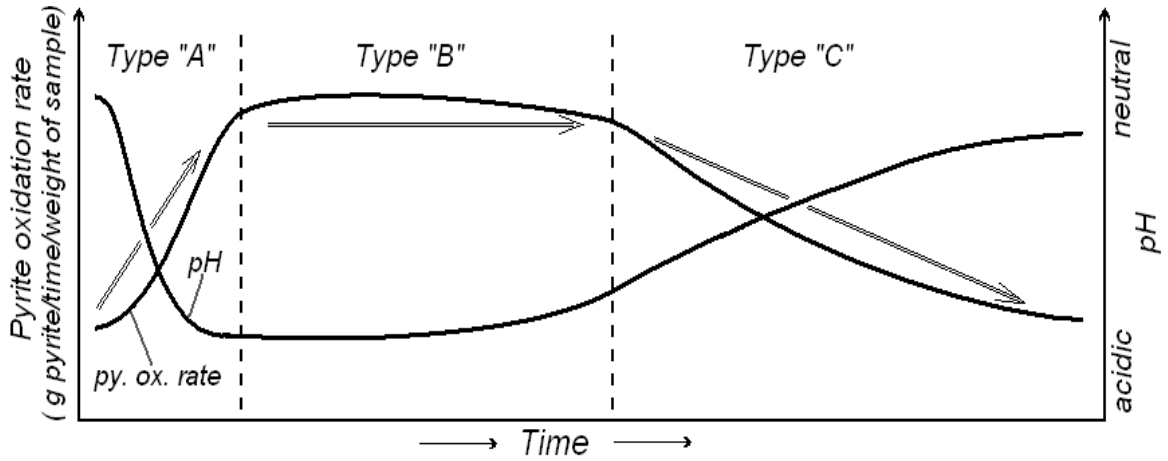

FIG. 68: Pyrite oxidation rate and pH value changes in the function of a long term process, with the marks of the different geochemical stages during the maturity process (after Ritchie 1994)

This three or four-year-long investigation indicated the maturity of the tailings and waste materials. Table 33 gives an overview of the different oxidation rate stages of the samples. The three stages define also the rates of the emitted pollution and heavy metal mobility.

In the first stage – type "A" – the oxidation rate, parallel with the pollution and the heavy metal content will increase with time. The material in this stage needs correct waste management and appropriate handling. For the material in this stage, the monitoring system is essential. If the material is in the premature stage (type "B"), the oxidation and the heavy metal mobility are at the maximum, the peak of the pollution is present, as the pH is the lowest that the material can produce. In this stage at least controlling and monitoring is required. The third, the strongly oxidized (type "C") stage means that the tailing or waste rocks are already after the peak pollution. The material in this stage is stable enough not to be able to cause further increasing environmental problem. The slowing down reactions ensure that heavy metal mobility decreases as the pH increases. The normalizing pH controls mineral alteration, as iron hydroxide, oxy-hydroxide and oxides are produced. Finally, a gossan type mineralization could be formed as a cover, close to the top of waste.

Sample	***Maturity***	***Behaviour in the future***
Itos Jig 1-7	weakly	increasing in pollution and heavy metal mobility, decreasing pH; pollution peak in the future, further problems; the situation calls for management, monitoring is essential
Itos Jig 2-7		
BOL 2-8		
Itos Granza 1-7	partly	stable low pH, maximal pollution and heavy metal mobility; pollution peak at present, problems will not increase, but stays for an uncertain time; monitoring is strongly required
Itos Granza 2-7		
BOL 3-8		
BOL 1-8	strongly	decreasing pollution and heavy metal mobility, increasing pH; pollution peak already in the past, no further increasing problems; monitoring is not required

Table 33: Overview for the future, from point of the behaviour of the pyrite oxidation changes, with recommendations and the characterization of the main geochemical and chemical properties of the system

DOI: 10.14750/ME.2021.004

X. CHEMICAL AND MINERALOGICAL ANALYSIS OF "NON HOMOGENEOUS" MINERAL ALTERATION IN THE MATERIAL OF THE COLUMN FILLING DURING THE HUMIDITY TEST

10.1. Introduction

There is a hypothesis, that the material which is put into the keeper (column) for analysis by humidity cell or column test (in range of 1-4 kg) is relatively homogeneous, so there are no layers with different mineralogy or physical parameters. This hypothetical idea can be true if the grain size is decreased down till such a grain size, if a tiny amount of the material is taken out from any point of the material inside the column, with it, the material of the whole filling can be characterized perfectly.

The hypothesis above works in the rarest case, because those finer materials, which could match into the criteria of homogeneous filling have very small grain size, so significantly decreased porosity and permeability, compared with the coarser materials. These decays in the hydraulic and air ventilation parameters result, that the system of the column or humidity cell will not work properly, so it will not able to reach that aims, such as the worst case scenario and the proving of the maximal oxidation by air pumping and rinsing.

10.2. Discussion about inhomogeneity and its causing processes

As the hydraulic and air ventilation parameters are not appropriate, the circle of oxidation – secondary mineral formation – leaching, brake and inhomogeneities take place. The simplest example, if the porosity and permeability is too low, the rinsing liquid cannot go through with its full volume, thus some slack water remains back at the lower part of the filling. From this remained seepage secondary minerals can form, so already some difference can be detected between the upper and lower part of the filling material. Moreover – what is more critical – this water saturated zone will not let the air through on the samples. The increasing of the pressure is not a solution for the problem, because following the weakest resistant, the higher pressure will create an airflow in the filling material, but only like a chimney, where all of the volume of the air goes through with significantly higher speed. In the rest of the pores will be air ventilation and oxygen supply not at all, which would be necessary for the possibility to reach the maximal oxidation rate. This effect alone – without the remaining water – has already been able to tumble the sensitive stability of such a system, so the oxidation and mineral alterations will be not homogeneous in the column, lateral zones and dikes would be created.

The remained seepage, which partly or fully can block the air ventilation, will cause such an anomaly, where in the bottom or lower part of the sample keeper in lack of gas phase or dissolved oxygen, secondary sulphates can precipitate, like gypsum or melanterit. At the upper part of the column, until that zone, where the remained seepage can lift up by capillary forces, but there is some oxygen, in

DOI: 10.14750/ME.2021.004

presence of sulphate and potassium ion jarosite, while in lack of these, iron hydroxide (Eq. 3) and oxyhydroxide (Eq. 5 and 6) can precipitate or iron oxide can form directly or by dehydratation (Eq. 7).

Unfortunately this heterogeneity takes place not at the beginning of the geochemical tests, so when these mineralogical changes become visible, it is already too late to stop it or redesign the system to avert the formation of further inhomogeneity in the column material.

Among the 16 Bolivian and the 5 Hungarian samples, which were taken part in the humidity cell tests serious, for a few of them the outcome for a successful test were questionable. These samples were on the border of applicability of humidity cell test, such as the clayish samples of Jalpha 1-7 and Playa Iroco 1-7, which have such a fine fraction, that the periodical (weekly) rinsing water hardly could go through on them. In the first two years, the analysis were completed in the regular, circular shape sample keeper (Chapter 3.1.), but for the third year the material was taken into a new type of a flat sample keeper (details are discussed later in this chapter), where the air was not pumped through on the sample, but above the sample, horizontal air ventilation was used in the sample keeper. However inhomogeneity in the mineralogy of the samples did not happen, the low porosity and permeability made more difficult the completion of the weekly sampling, because the rinsing water hardly went through on the sample. This also means, that the air ventilation, so the oxygen supply was very poor. In the second and third year, the rinsing water was collected from the surface of them, because only 50-100 ml of rinsing water went through on them from the 1000 ml and even during 2-3 hours. Moreover, the chemistry of the seepage was extreme, usually, the pH was under 1 and the sulphate concentration exceeds the 4-5 $^{g}/_{l}$.

10.2.1. Sample Jalpha 1-7 analysed with new investigated sample keeper

From the above described two clayish samples the Jalpha 1-7 will be discussed in details, as the main parameters of the seepage will be compared in case of the "regular" and the newly investigated flat sample keeper. The difference between the setup of the two sample keeper types are huge. Necessary to mention, that the flat one (FIG. 69) is the author's innovation, both the design and the investigation.

It is made from acryl in square shape with inside diameter of 250x250 mm and height of 50 mm, with a well-sealed cap, to be able to complete the oxygen consumption test. The two pipe also made from acryl are on its side, as air inlet (blue arrow) and outlet (orange arrow). As the picture shows, in case of this sample keeper, horizontal air ventilation is used, so air is not pumped through the sample, only the surface of it is touched with air, in contrast with the "regular" round cross sectioned sample keeper with air through ventilation. In pursuance of the weekly rinsing, the

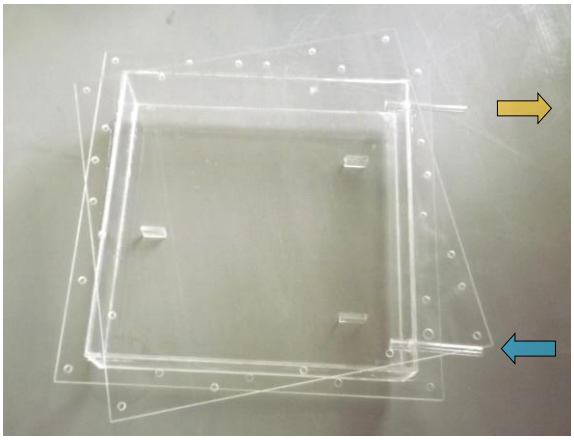

FIG. 69: Newly developed flat sample keeper

DOI: 10.14750/ME.2021.004

seepage was collected from the surface of the sample because there is no water outlet at the bottom of the sample keeper, as it is designed for clayish samples with low permeability and porosity. Although the success and also the applicability of the newly designed sample keeper was strongly questionable in the beginning, but the main parameters of the seepage, such as pH and redox potential gave the answer.

From the results of the kinetic test (FIG. 70) in the 1st (orange line) and 2nd year (shorter red line), relative high volatility can be read down. Both parameters changed significantly among the sampling, sometimes even between the following sampling, which cannot be indicated by chemical or geochemical changes. These huge changes, such as pH value of 2.36, 2.79, 3.38 and 3.07 in four consecutive samplings or redox potential of 452, 401, 359 and 448 mV in the same four sampling time merely was created by the sensitivity of the sampling procedure of rounded column with through flowing seepage for the manual rinsing and sampling. In contrast with this high volatility, the results in the 3rd year show continuity and trustiness (excluded the day 63rd and 70th, when technical problems in the rinsing took place). The pH value has already stabilized after a month, as it stays between 2.34 and 2.55, and also the redox potential was also stable between 450 and 483 mV.

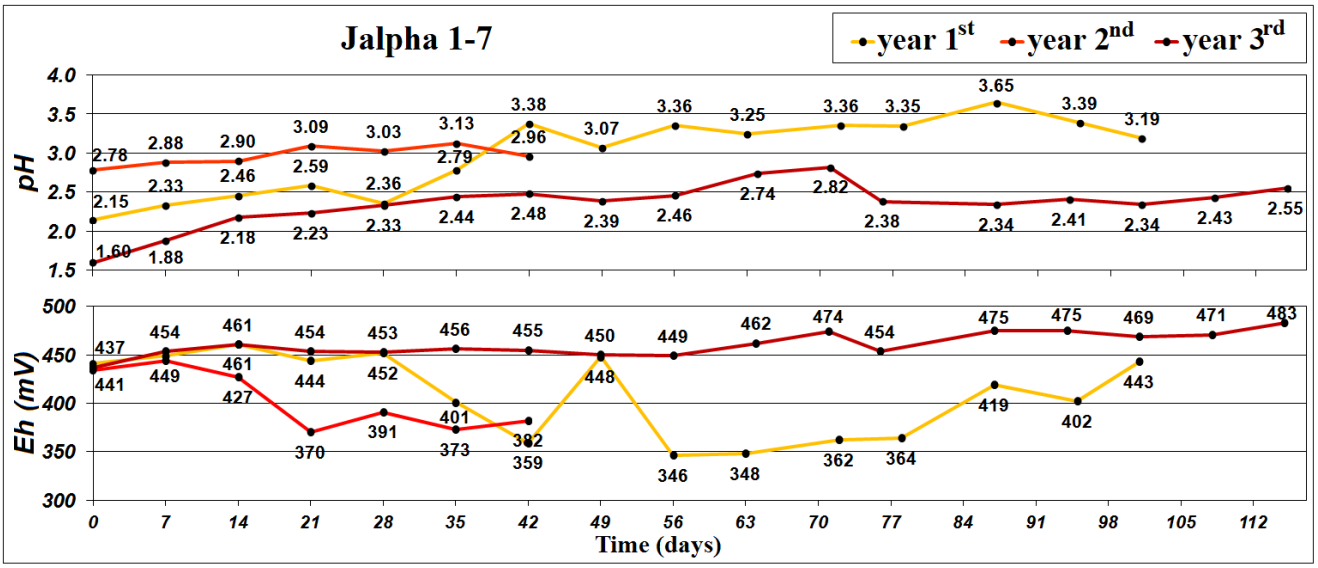

FIG. 70: pH and Eh changes in sample Jalpha 1-7 during the 1st, 2nd and 3rd year of the humidity cell test period

These measured stable values – where the volatility is very low – prove, that the flat keeper is a much better setup for this type of geochemical test in case the of a clayish sample. More stable results give more possibility to characterize well the oxidizing system, because the calculated and derivated results, such as the oxidation rate calculation also become stable. Because of the transcription, a small change in the basic parameter means huge changes in the calculated results.

The chemical result of the seepage, which was created with this newly investigated flat sample keeper is also good for the calculation of the oxidation rate, based on the same formulas were shown in Chapter 8., but the final result of the oxidation rate needs to include, that it is referred to an area of $^1/_{16}$ m^2 (0.0625 m^2), that the sample keeper has.

DOI: 10.14750/ME.2021.004

10.2.2. Sample BOL 6-9 and its lateral mineralogical changes

In case of BOL 6-9 and BOL 7-9 tailings from Huanuni, significant and even visible mineralogical changes happened in the column. Both samples have small grain size (Chapter 2.1.2.), as average is dominantly between 1 and 2 mm with some (max 5-10 %) larger fragments, up till 2 mm. The relatively small grain size did not indicate the necessity of using any special column setup, so regular rounded roll column was used from upward air ventilation. From these two samples, where visible mineralogical changes happened, the BOL 6-9 will be discussed below in details.

The sample BOL 6-9 was analysed in the 3rd and 4th year, for 115 and 121 days. In both years, it reached a stable and continuous system very quickly, as the FIG. 71 shows it. The original material was fine, but when the column was filled, it seemed homogeneous, both from point of mineralogy and grain size distribution. It was reddish-brown, as secondary Fe oxyhydroxide (e.g. goethite) or oxide minerals covered the surface of each grain. These secondary minerals were dissolved slowly during the humidity cell test and the colour of the sample slowly become dominantly grey, with some shade of light brown.

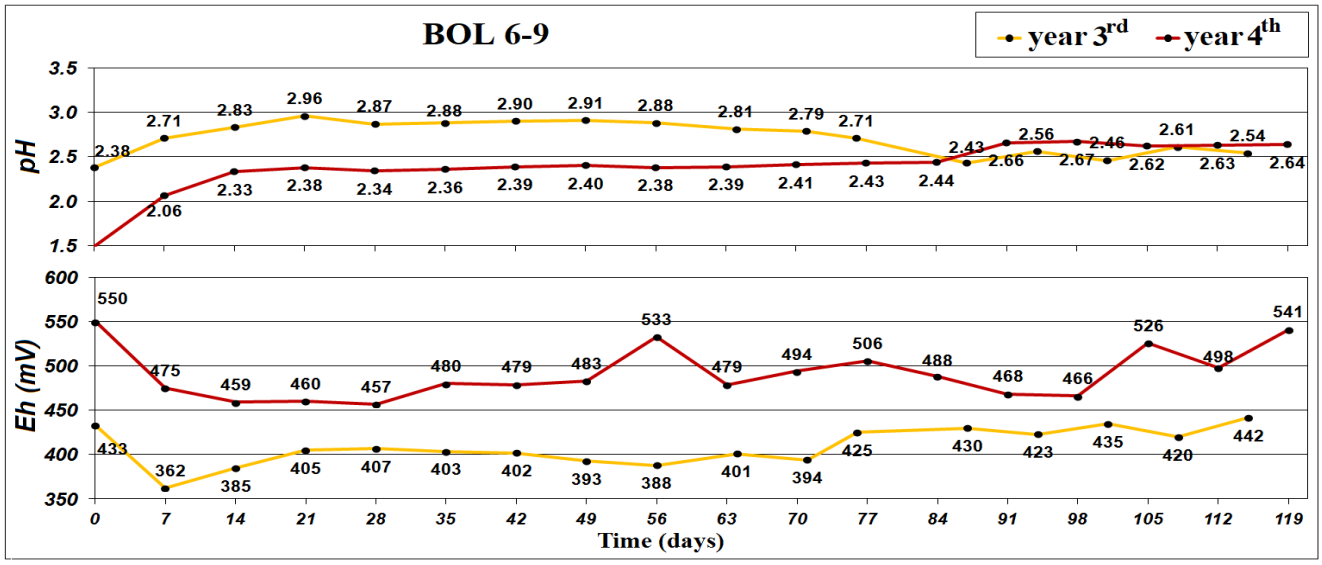

FIG. 71: pH value and Eh changes in sample BOL 6-9 during the 3rd and 4th year of the humidity cell test period

At the last 5 weeks of the 4th year, the pH increased from stable 2.4 to 2.6, which does not seems so much, but it means that the concentration of H^+ in the seepage decreased from 4.0 to 2.5 $^{mmol}/_{l}$, which is almost 40 % dropping (FIG 71). Near the pH change, the redox potential becomes more volatile and starting to increase a bit. Besides changes in the parameters of the seepage, visible mineral alterations (FIG. 72) took place, as a hard reddish lateral layer appeared approximately 3 cm below the top in the thickness of 2-3 mm. Moreover, the sample above this layer becomes reddish-brown again, as same as the original sample colour had before the test.

FIG. 72: The three well separateable zones

DOI: 10.14750/ME.2021.004

As the test period finished, samples were taken from different places of the approximately 11-12 cm thick sample filling: from the bottom, the middle and the top and also the hard layer was sampled. Before the 4th year test, the top, the middle and the bottom of the filling in the column were sampled, on such a way, that the acryl wall of the keeper was drilled through and taken the 6-7 g of samples from these two holes, not to disturb the whole material.

The marking of the "original" and the "after the 4th year" is obvious, but the sign of "before the 4th year" means that the sampling happened just before the 4th year humidity cell test started.

These three samples, together with the original and those samples, were taken at the end of the 4th year, give a good set to be able to characterize the possible mineral alteration of the sample in the column. XRD and XRF analysis were done on these samples, to know the mineral and chemical compositions, moreover, BSE images were taken with electron microprobe analysis. The bulk chemical composition helps to understand the mineral changes in the column, because several very important oxidation by-products are amorphous, such as goethite or some iron sulphates, so it is not possible to assign them by solid phases determination. The XRF results (FIG. 73) for silicon shows, its enrichment slightly in the 3rd year (labelled as "before 4th year"), but much more to the end of the 4th year. This is a normal process, because the silicon is dominantly only in the phase of quartz, which is totally inert in the ARD system, so as the amount of the other minerals decrease by oxidation, the ratio of Si content will increase. For the aluminium, this allegation is just true at the end of the 4th, while in the 3rd year it decreased compare to the original sample. This decreasing is caused that the coating on the grains of the original sample contained clay minerals together with cementing material as the secondary iron minerals, which were dissolved during the 3rd year, so the clay fraction become free and it is transported downwards by the seepage. On the other hand that 0.5-0.6 % difference is not so high. During the 3rd year, the Fe and the S content decrease parallel, this together with their ratio determines pyrite. At the end of the 4th year, the Fe and S parallel continued the decreasing, as the pyrite oxidized out. Only in point of 3cm below the surface, their ratio changes significantly, as more iron stays in place. About 0.4-0.5 % more Fe stays, than it should be, based on the changing of S, which is shown with orange intermitted line and spot. This "extra" iron is cannot be linked to S phase, so it has to be in oxyhydroxide or oxide form. The reddish-brown colour of this 2-3 mm thick hard layer also confirms this theory.

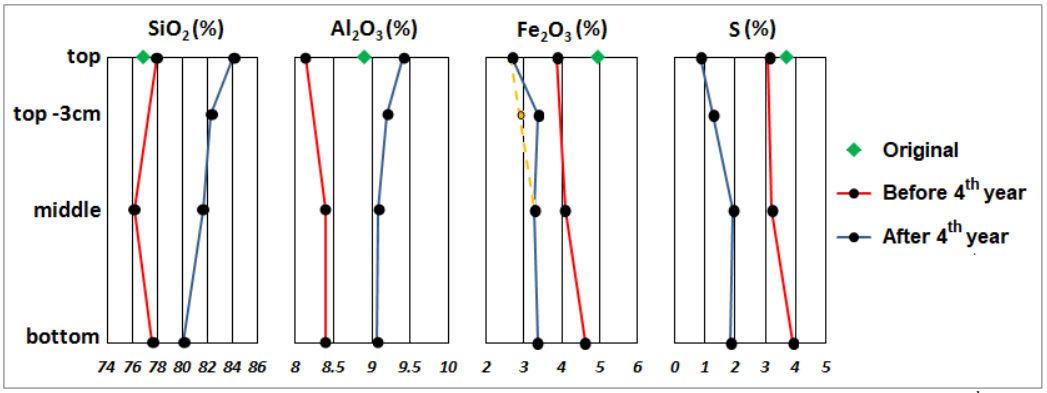

FIG. 73: Si, Al, Fe and S content of the original sample and before and after the 4th year

DOI: 10.14750/ME.2021.004

On the other hand, the XRD analysis (Table 34) of this solid, "gossan type" layer didn't detect any Fe-hydroxide, oxyhydroxide or oxide phase.

Mineral	***Formula***	$^{m}/_{m}\%$
Quartz	SiO_2	73.9
Dravite	$Na(Mg_3)Al_6(Si_6O_{18})(BO_3)_3(OH)_3(OH)$	15.3
Topaz	$Al_2(SiO_4)(F,OH)_2$	1.9
Zircon	$ZrSiO_4$	0.2
Rutile	TiO_2	0.3
Biotite	$K(Mg,Fe)_3[AlSi_3O10(OH)_2$	1.4
Amorphous components		7.0

Table 34: Quantitative mineralogical composition – measured by XRD - of the solid layer, which was formed 3cm under the surface of the sample BOL 6-9 just before the end of the test

Based on the result of the XRF and XRD measuring, can be declared, that the solid layer, which was formed 3 cm below the surface of the sample, was a hard and well cemented layer of secondary iron hydroxide, oxyhydroxide, oxide or a mixture of them. Moreover, that XRD clearly proved, that it had to be in amorphous form, because secondary Fe phases were measured not at all, but the quantitative evaluation of the measuring showed 7.0% of non or nanocrystallized phase.

In the further result of the XRF measuring, the titanium concentration does not show any changes (FIG. 74) during the analysis of the 3rd and 4th year compare to the original sample, which confirms that the original material, which was filled into the column can be considered as homogeneous. The cupper shows continuous decreasing through the tests, although after the 3rd year its concentration almost doubled as moving from the top toward the bottom. During the 2 years of analysis, its concentration decreased almost to one third. In the 3rd year (marked as "before 4th year") there is a significant trend, that its concentration is increasing downwards to the lower zone. This indicates, that the cupper containing minerals are also oxidizing, so they were probably in form of Cu- or Cu-Fe-sulphides. The originally 355 ppm Zn decreased under 50 ppm to the end of the test series, which determines quick oxidizing, that probably it is in highly Fe replaced Zn-sulphide, where the instability in the crystal structure can strongly increase the sensitivity against weathering and oxidation. The lead results are a bit different from the previous two heavy elements, because before the 4th year, its concentration in the whole column was as same as the original sample had, but after the 4th year, at the top of the column, it decreased to half, while in the zone 3cm below the surface a bit enriched.

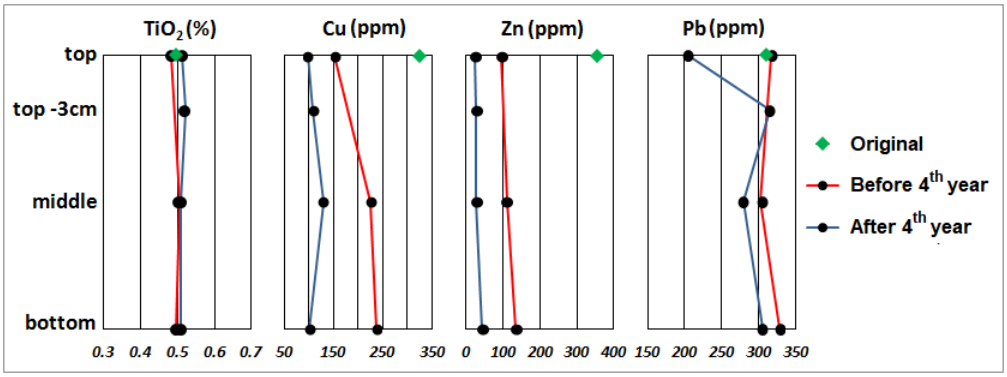

FIG. 74: Ti, Cu, Zn and Pb content of the original sample and before and after the 4th year

DOI: 10.14750/ME.2021.004

From the solid layer, which was located 3 cm below the surface, polished section was made. The high brightness contrast on the BSE image (FIG. 75) shows significantly higher average atomic weight. The microprobe analysis shows a strongly altered pyrite (a) grain in quartz (c) matrix. The darker zones are iron oxyhydroxides or oxides (b), as the alteration products of pyrite. The elevated Pb level is resulted by the brightest zones and vein fillings, which is anglesite (d). This and the other BSE (FIG. 76) images represent well the strongly oxidizing pyrite (a), which is covered or even encapsulated into secondary iron oxyhydroxides– like goethite – or oxides (b) in the solid lateral layer in sample BOL 6-9.

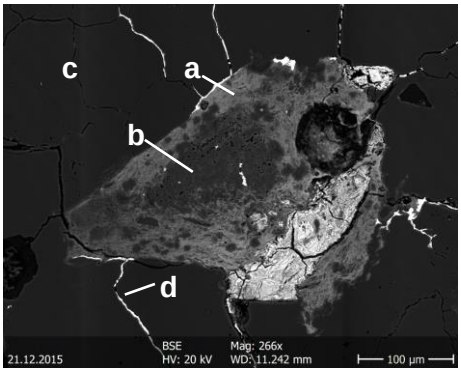

FIG. 75: Altered pyrite grain in cracked quartz matrix with anglesite vein-filling

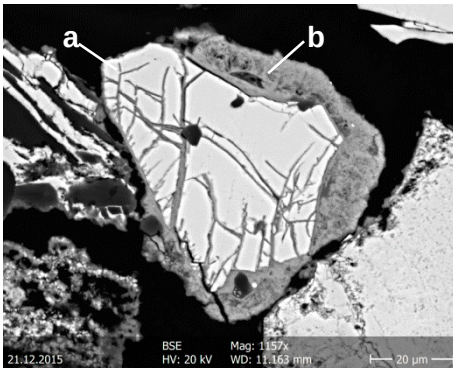

FIG. 76: Oxidation rim around a pyrite grain in sample BOL 6-9

10.3. Conclusion

The difficulties with sample Jalpha 1-7 and Playa Iroco 1-7 reflected that the regular round roll sample keeper with air ventilation through the sample was not the proper setup for the humidity cell test for strongly clayish samples. The low permeability and porosity cause volatility in the basic chemical parameters of the seepage during the test, so makes the further proper geochemical characterization more difficult. The results from the humidity cell test become much more stable, as flat sample keeper started to be used during the 3rd year of the annual test series. This innovation and new design use horizontal air ventilation, which did not go through the sample. This setup is much closer to that oxidizing system that can be formed in nature and able to produce the "worst case scenario".

Although the BOL 6-9 and 7-9 had not as fine grain size as the previous ones, but after 2 years of humidity cell test the average grain size of 1-2 mm generated mineralogical changes in the material of the sample. The reason is that there was too much remaining water between the grains, moreover, the small porosity caused high capillary forces. In case of the sample BOL 6-9 a solid, secondary iron mineral-rich lateral layer was formed 3 cm above the surface. The more solid phase is precipitated out, the more air ventilation became deficient, so this was a self-excitation.

As a conclusion for both cases, the proper and well designed setup is necessary to be able to produce good or even high quality results during the test series, which can be the base for further geochemical characterization. With a well working system, the natural volatility can be decreased down dramatically and also the maximum can be reached out from the test.

DOI: 10.14750/ME.2021.004

XI. THESIS POINTS

1st thesis: By using the results from the humidity cell test of the Hungarian sample HU 1-2 sulphidic mine waste material, can be declared, that **significant pyrite oxidation can take place, even if the pH of the seepage stays circumneutral**. This means, that even if the pyrite oxidation produces acidity, it will not necessarily appear if neutralizing minerals are present. Nevertheless, the oxidation process of pyrite will happen. This was proved by the sulphate release, the O_2 consumption and CO_2 production and also the secondary mineral coatings, such as gypsum on calcite and iron oxyhydroxide on pyrite grains. (Chapter VI.)

2nd thesis: With the using of the combined method of the X-ray powder diffraction (XRD) and the sequential chemical extraction (SCE), exact mineral phases with sharp amounts can be calculated. Moreover, the calculation method perfectly works on such strongly altered sulphidic materials, where the byproducts are amorphous, so the XRD method is not able to determine them. With an electron microscope and microprobe, the presence of such minerals were proved in the samples, which were calculated even as low amount as 0.002 or 0.005 %. (Chapter VII.)

3rd thesis: Four different new formulas were established for the determination of the bulk pyrite oxidation rate, which are applicable both for abiotic or biotic oxidation systems, or even for the mixture of them. The using of these formulas is not limited for laboratory experiments, they can be used in larger scale also, even in field tests. The formulas for the oxidation rate determination are based on the four main parameters of the oxidation process, such as:

3rd/a. pH value of the seepage

3 rd/b. sulphate concentration in the seepage

3 rd/c. iron concentration in the seepage

3 rd/d. O_2 consumption of the oxidizing system

4th thesis: A classification system was defined for the state of maturity of the sulphidic samples, which were analyzed in humidity cell test for consecutive years. The classification shows much forward than the results of the humidity cell test in the individual years in themselves. It can mimick the long-term geochemical behaviour of the analyzed material. (Chapter IX.)

5th thesis: A new, flat sample keeper was designed and developed for the fine or even clayish structured sample. This new innovation proved with humidity cell test, that it can work perfectly, as the chemical properties of the seepage became much less variable, so the evaluation of the humidity cell test can be more accurate and easier. (1st part of Chapter X.)

6th thesis: By analysis of lateral mineralogical changes of the column filling of fine-grained samples, it can be stated that **there is a lower limit for the particle size below which the applicability and result of the humidity cell test in the regular sample keeper becomes strongly questionable**. (2nd part of Chapter X.)

DOI: 10.14750/ME.2021.004

ÖSSZEFOGLALÁS

Annak ellenére, hogy a bányászati tevékenység már a Kőkorszak óta létezik, az általa okozott nagyobb mértékű környezeti szennyezés modern jelenség. A kézi bányászat csak kis mennyiségű meddőt termelt és azt is időben elhúzódóan, viszont a modern – főként felszíni – ércbányászat rövid idő alatt nagy mennyiségű meddőanyagot hoz létre. Ez generálta azt, hogy jelenleg a kőzetsavasodás jelensége (ARD) a színesfém ércbányászat első számú és egyben legnagyobb környezeti károkat okozó problémája a világon.

A vas-tartalmú szulfid ásványok a felszíni körülmények között, víz és oxigén jelenlétében oxidálódnak, savas környezetet teremtve, mely a nehézfémek elemmobilitását drasztikusan megnöveli. Ennek eredményeképpen nem csak az alacsony pH érték, de a megemelkedett nehézfém szennyezés is jelentősen terhelni fogja a környezetet.

PhD disszertációmban ezekre az ásványi átalakulási jelenségekre alapozva elemzem a szulfidos mintákat, mind geokémiai, mind ásványtani tekintetben. Számos új modellezési és számolási folyamatot alkottam, melyek segítségével az oxidációs folyamatok mértéke a jövőre előre vetíthető.

Bemutattam, hogy ARD folyamat és erős szulfid oxidáció lehet jelen, még akkor is, ha a környezet nem mutat savasodást. Bizonyítottam, hogy a semlegesítő ásványok – mint például kalcit – jelenlétében is elindul a szulfid ásványok oxidációja, sőt jelentős mértékűvé válik. Mindez a folyamat addig nem lesz szembetűnő, amíg a semlegesítési reakciók egyensúlyt tudnak tartani a sav termelési reakciókkal.

A doktori disszertációmban bemutattam egy új kombinált számítási folyamatot, melyben a röntgen pordiffrakciós (XRD) adatokat kombináltam a szekvenciális kioldási (SCE) teszt eredményeivel. A számítási folyamat során olyan ásványi fázisokat kalkuláltam ki, melyek koncentrációja jelentősen 1% alatti, és így az XRD méréssel pontatlanul vagy egyáltalán nem detektálhatók, a már bontódott szulfidos mintákban. Elektron mikroszkóp és mikroszonda segítségével olyan ásványi fázisok jelenlétét is sikerült bizonyítanom a mintákban, melyeknek a számított koncentrációja 0.002% vagy 0.005% volt.

Négy számítási módszert állítottam fel a pirit oxidáció mértékének a meghatározására, mely mind a biotikus, mind az abiotikus környezetre, illetve ezek keverékére is alkalmazható. A metódusok a pH értéken, az oldott szulfát és vas tartalom, illetve az oxidáció során felhasznált oxigén mennyiségén alapulnak. Az eljárás mind laboratóriumi, mind terepi körülmények között alkalmazhatók.

Bemutattam, hogy a több éven át, megszakításokkal végzett kioldási tesztek eredményei időben sokkal előremutatóbbak, mint az egyes éveké önmagukban. Továbbá, az összehasonlításukkal három kategóriát hoztam létre, mely segítségével osztályozható a meddőanyag. Ezek az osztályok meghatározzák az anyag jövőbeni geokémiai viselkedését, és egyben iránymutatást adnak a jövőben geokémiai viselkedésükre, továbbá a felmerülő problémákra és azok mértékére.

Terveztem egy olyan mintatartót, mely a kinetikus tesztek során a nagyon kis szemcseméretű, vagy már agyag frakciójú minták geokémiai elemzésére is alkalmas. Használata során sokkal stabilabb oxidációs folyamatok voltak elérhetők.

Kísérleteim alapján kijelentettem és bemutattam, hogy létezik egy olyan szemcseméret határ, mely alatti mintát hagyományos mintatartóban a kinetikus teszttel már nem lehet elemezni, anélkül, hogy jelentős ásványtani inhomogenitás ne alakuljon ki.

DOI: 10.14750/ME.2021.004

REFERENCES

ADAMO, P., DUPKA, S., WILSON, M. J., MCHARDY, W. J. (1996): *Chemical and mineralogical forms of Cu and Ni in contaminated soil from the Sudbury mining and smelting region, Canada*. Environmental Pollution, Vol. 91, pp. 11-19.

AL, T. A., MARTIN, C. J., BLOWES, D. A. (2000): Carbonate mineral/water interactions in sulfide-rich mine tailings. Geochem. Cosmochim. Acta, Vol. 64, pp. 3933-3948.

ALPERS, C. N., RYE, R. O., NORDSTROM, D. K., WHITE, L. D., KING, B. S. (1992): *Chemical, crystallographic, and isotopic properties of alunite and jarosite from hypersaline Australian lakes.* Chem. Geol., Vol. 96, pp. 203-226.

BALAREW, C., KARAIVANOVA, V., ASLANIAN, S. (1973): *Isomorphic relations among the heptahydrate sulfates of single divalent metals (Mg^{2+}, Zn^{2+}, Ni^{2+}, Fe^{2+}, Co^{2+}).* Kristall Technik, Vol. 8, pp. 115-125, (in German).

BANFIELD, J. F., WELCH, S. A. (2000): *Microbial controls on the mineralogy of the environment.* In: Vaughan, D. J. and Wogelius R. A. (Eds.) Environmental Mineralogy. European Mineralogical Union – Notes in Mineralogy, Budapest, Eötvös Univ. Press, Vol. 2, pp. 173-196.

BARONA, A., ETXEBARRIA, B. (1996): *Distribution and extraction of Pb and Zn with chelating agents in soil with varying pollution level.* American Institute On Chemical Engineers, 5th Congress, Chemical Engineering Vol. 3, pp. 576-581.

BAYLESS, E., OLYPHANT, G. A. (1993): *Acid generating stalts and their relationship to the chemistry of groundwater and storm runoff at an abandoned mine site in southwestern Indiana, U.S.A.* J. Contam. Hydrol. Vol. 12, pp. 313-328.

BECKER, U., MUNZ, A. W., LENNIE, A. R., THORNTON, G., VAUGHAN, D. J. (1997): *The atomic and electronic structure of the (001) surface of monoclinic pyrrhotite (Fe_7S_8) as studied using STM, LEED and quantum mechanical calculations.* Surf. Sci., Vol. 398, pp. 66-87.

BIGHAM, J. M. (1994): *Mineralogy of ochre deposits formed by sulfide oxidation.* In: Jambor, J. L., Blowes, D. W. (Eds.) The environmental Geochemistry Of Sulfide Mine-Wastes. Mineral Assoc. Canada Short Course Vol. 22, pp. 103-132.

BLOWES, A. K., JAMBOR, J. L. (1990): *The pore-water geochemistry and the mineralogy of the wadose zone of sulphide tailings, Waite Amulet, Quebec, Canada*. Applied Geochemistry, Vol. 5, pp. 327-346.

BLOWES, D. W., PTACEK, C. J., FRIND, E. O. ROBERTSON, W. D., MOLSON, J. W. (1994): *Acid-neutralization reactions in inactive mine tailings impoundments and their effect on the transport of dissolved metals.* Proceedings of the 3rd International Conference on the Abatement of Acidic Drainage, Pittsburgh, April 24-29, Vol. 1, pp. 429-438.

BLOWES, D. W., PTACEK, C. J., JURJOVEC, J. (2003/a): Mill tailings: hydrogeology and geochemistry. In: Blowes, D. W., Jambor, J. L., Ritchie, A. I. M. (Eds.) The Environmental Geochemistry of Sulfide Mine-Wastes. Short Course Handbook, 2003, Vol. 31, pp. 95-116.

BLOWES, D. W., PTACEK, C. J., WEISENER, C., JAMBOR, J. L. (2003/b): *Geochemistry of acid mine drainage*. Treatise of Geochemistry, Vol. 9, Elsevier Science.

BLOWES, D. W., REARDON, E. J., CHERRY, J. A., JAMBOR, J. L. (1991): *The formation and potential importance of cemented layers in inactive mine tailings.* Geocim. Cosmocim. Acta, Vol. 55, pp. 965-978.

BOCK, E. (1961): *On the solubility of anhydrous calcium sulphate and of gypsum in concentrated solutions of sodium chloride at 25 °C, 30 °C, 40 °C, and 50 °C*. Canadian Journal of Chemistry, Vol. 39, pp. 1746–1751. [DOI:10.1139/v61-228]

BONNISSEL-GISSINGER, P., ALNOT, M., EHRHARDT, J. J., BEHRA, P. (1998): *Surface oxidation of pyrite as a function of pH*. Environ. Sci. Technol., Vol. 32, pp. 2839-2845.

BOON, M., BRASSER, H. J., HANSFORD, G. S., HEIJNEN, J. J. (1999): *Comparison of the oxidation kinetics of different pyrites in the presence of Thiobacillus ferrooxidans or Leptospirillum ferrooxidans*. Hydrometall, Vol. 53, pp. 57-72.

CAMPBELL, D. F. (1942): *The Oruro silver-tin districts, Bolivia*. Economic Geology, Vol. 37, pp. 87-115.

CARUCCIO, F. T. (1975): *Estimating the acid potential of coal mine refuse.* In: Ecology of resource degradation and Renewal. The 15th Symposium of the British Ecological Society. 10-12 July 1973, Bleackwell Scientific Publications, Oxford.

CEN/TC 292: *Directive of "Characterization of waste - Kinetic testing for assessing acid generation potential of sulphidic waste from extractive industries" Characterization of waste.* European Committee For Standardization.

CHANCE, F. M. (1948/a): *Tin-silver veins of Oruro, Bolivia /Part1/.* Economic Geology, Vol. 43, No.5, pp. 333-383.

CHANCE, F. M. (1948/b): *Tin-silver veins of Oruro, Bolivia /Part2/.* Economic Geology, Vol. 43, No.6, pp. 435-470.

CHAPMAN, B. M., JONES, D. R., JUNG, R. F. (1983): *Processes controlling metal iron attenuation in acid mine drainage streams.* Geochim. Cosmochim. Acta, Vol. 47, pp. 1957-1973.

COLMER, A. R., HINKLE, M. E. (1947): *The role of microorganisms in acid mine drainage: A prelimitary report*. Science, Vol. 106, pp. 253-256.

CORNELL, R., SCHWERTMANN, U. (1996): *The Iron Oxides*. VCH Publishers, Weinheim.

COTTER-HOWELLS, D. J., PATERSON, E. (2000): *Minerals and soil development*. In: Vaughan, D. J., Wogelius, R. A. (Eds.) Environmental Mineralogy. European Mineralogical Union – Notes in Mineralogy, Budapest, Eötvös Univ. Press, Vol. 2, pp. 91-120.

DOLD, B. (2003): *Dissolution kinetics of schwertmannite and ferrihydrite in oxidized mine samples and their detection by differential X-ray diffraction (DXRD).* Applied Geochemistry, Vol. 18, pp. 1531-1540.

DOLD, B., FONTBOTÉ, L. (2001): *Element cycling and secondary mineralogy in porphyry copper tailings as a function of climate, mineralogy, and mineral processing*. J. Geochem. Explor., Vol. 74, pp. 3-55.

DOLD, B., FONTBOTÉ, L. (2002): *A mineralogical and geochemical study of element mobility in sulfide mine tailings of Fe oxide Cu–Au deposits from the Punta del Cobre belt, northern Chile*. Chemical Geology, Vol. 189, pp. 135– 163.

EDVARDS, K. J., GIHRING, T. M., BANFIELD, J. F. (1999): *Seasonal varations in microbial populations and environmental conditions in an extreme acid mine drainage environment*. Appl. Environ. Microbiol., Vol. 65, pp. 3627-3632.

EDVARDS, K. J., BOND, P. L., GIHRING, T. M., BANFIELD, J. F. (2000): *An archaeal iron-oxidizing extreme acidophile important in acid mine drainage.* Science, Vol. 287, pp. 1796-1799.

EMBILE R., WALDER I. F,. MADAI F., MORICZ F., RZEPKA P., WALDER P. (2016): *Grain Size Effects on Mine Water Quality and Acid/Neutral Rock Drainage Production in Kinetic Testing Using Recsk Porphyry Skarn Cu–Zn Deposit Rocks.* Mine Water and the Environment, Vol. 35., Issue 4, pp. 421-434. [ISSN 1025-9112] [ISSN 1616-1068 Online]

ELBERLING, B., NICHOLSON, R. V., REARDON, E. J., TIBBLE, P. (1994): *Evaluation of sulphide oxidation rates: a laboratory study comparing oxygen fluxes and rates of oxidation product release*. Can. Geochem. J., Vol. 31, pp. 375-383.

EVANGELOU, V. P., ZHANG, Y. L. (1995): *A review: pyrite oxidation mechanisms and acid mine drainage prevention.* Critical Rev. Environ. Sci. Technol., Vol. 25, pp. 141-199.

FERGUSON, K. D., ROBERTSON, J. D. (1994): *Assessing the risk of ARD.* In: International Land Reclamation and Mine Drainage Conference on the Abatement of Acid Drainage. U.S. Bureau Mines Special Pub. SP 06A-94, pp. 2-11.

FILIPEK, L. H., NORDSTROM, D. K., FICKLIN, W. H. (1987): *Interaction of acid mine drainage with waters and sediments of the West Squad Creek in the West Shasta Mining District, California*. Environ.Sci. Technol., Vol. 21, pp. 388-396.

FRAU, F. (2000): *The formation – dissolution – precipitation circle of melanterite at the abandoned pyrite mine of Genna Luas is Sardinia, Italy: environmental implications*. Mineral. Mag., Vol. 64, pp. 995-1006.

GOLDEN, D. C., MING, D. W., BOWEN, L. H., MORRIS, R. V., LAUER, H. V. JR. (1994): *Acidified oxalate and dithionite solubility and color of synthetic, partially oxidized Al-magnetites and their thermal oxidation products.* Clays Clay Minerals, Vol. 42, pp. 53-62.

GOLDHABER, M. B. (1983): *Experimental study of metastable sulfur oxyanion formation during pyrite oxidation at pH 6-9 and 30°C*. Am. J. Sci., Vol. 282, pp. 193-217.

GOULD, W. D., KAPOOR, A. (2003): *The Microbiology of Acid Mine Drainage.* In: Jambor, J. L., Blowes, D.W., Ritchie, A.I.M. (Eds.) Environmental Aspects of Mine Wastes, Short Course Series, Vol. 31, Mineralogical Association of Canada, pp. 203-226.

GRANT J. N., HALLS C., AVILA W., SNELLING, N. J. (1979): *K–Ar ages of igneous rocks and mineralization in part of the Bolivian tin belt*. Economic Geology, Vol. 74, pp.838-851.

GRANT, J. N., HALLS, C., SHEPPARD, S. M. F., AVILA, W. (1980): *Evolution of porphyry tin deposits of Bolivia.* In: Ishihara, S., and Takenouchi, S. (Eds.) Granitic magmatism and related mineralization. Mining Geology Special Issue, Vol. 8, pp 247.

GREFFIÉ, C., AMOURIC, M., PARRON, C. (2001): *HRTEM study of freeze-dried and untreated synthetic ferrihydrites: consequence of sample processing*. Clay Minerals, Vol. 36, pp. 381-387.

GUNSINGER, M. R., PTACEK, C. J., BLOWES, D.W., JAMBOR, J. L. (2006): *Applied mineralogy to tailings and waste rock piles-sulfide oxidation reactions and remediation of acidic water drainage.* In: William, P. (Eds.) Journal of Contaminant Hydrology, Vol. 83, Issues 3-4. pp. 149-170

GWOREK B., MOCEK A. (2003): *Comparison of sequential extraction methods with reference to zinc fractions in contaminated soils.* Polish Journal of Environmental Studies, Vol. 12, pp. 41-48.

HALLBECK, L., PEDERSEN, K. (1991): *Autotrophic and mixotrophic growth of Gallionella ferruginea*. J. Gen. Microboil. Vol. 137, pp. 2657-2661.

HAMMACK, R. W., LAU, R. W., DIEHL, J. R. (1988): *Methods for determining fundamental chemical differences between iron disulfides from different geological provenances.* US Bur Mines Inf. Circ. IC-9183, pp. 136-146.

JAMBOR, J. L. (1994): *Mineralogy of sulfide-rich tailings and their oxidation products. In Environmental Geochemistry of Sulfide Mine-Wastes*. Mineralogical Association of Canada, Short Course Handbook, Vol. 22, pp. 59-102.

JAMBOR, J. L. (1999): *Nomenclature of the alunite supergroup*. Can. Mineral, Vol. 37, pp. 1323-1341.

JAMBOR, J. L. (2000): *The relationship of mineralogy to acid- and neutralization potential values in ARD.* In: Cotter-Howells, J. D., Campbell, L. S., Valsami-Jones, E., Batchelder, M. (Eds.) Environmental Mineralogy: Microbial Interactions, Anthropogenic Influences, Contaminated Land and waste management. Mineral. Soc. Ser., Vol. 9, pp. 141-159.

JAMBOR, J. L. (2003): *Mine-waste mineralogy and mineralogical perspectives of acid–base accounting.* In: Jambor, J.L., Blowes, D.W., Ritchie, A.I.M. (Eds.) Environmental Aspects of Mine Wastes, Mineral. Assoc. Can. Short Course, Vol. 31, pp. 117-145.

JAMBOR, J. L., TRAILL, R. J. (1963): *On rozenite and siderotil*. Can. Mineral, Vol. 7, pp. 751-763.

JAMBOR, J. L., BLOWES, D. K. (1998): *Theory and applications of mineralogy in environmental studies of sulfide-bearing mine wastes.* In: Cabri, L. J., Vaughan, D. J. (Eds.) Modern approches to ore and environnmental mineralogy. Mineral. Assoc. Canada, Short Course Series, Vol. 27, pp. 367-401.

JAMBOR, J. L., DUTRIAZ, J. E. (1998): *Occurance and constitution of natural and synthetic ferrihydrite, a widespread iron oxyhydroxide.* Chem. Rev. Vol. 98, pp.2549-2585.

JAMBOR, J. L., NORDSTROM, D. K., ALPERS, C. N. (2000/a): *Metal-sulphate salts from sulfide mineral oxidation.* In: Sulphate Minerals - Crystallography, Geochemistry, and Environmental Significance. Rev. Mineral. Geochem., Vol. 40, pp. 305-350.

JAMBOR, J. L., BLOWES, D. W., PATACEK, C. J. (2000/b): *Mineralogy of mine wastes and strategies for remediation.* In: Vaughan, D. J., Wogelius R. A. (Eds.) Environmental Mineralogy. European Mineralogical Union – Notes in Mineralogy, Budapest, Eötvös Univ. Press, Vol. 2, pp. 255-290.

JAMBOR, J. L., DUTRIZAC, J. E., RAUDSEPP, M., GROAT, L. A. (2003): *Neutralization potentials of siderite and other carbonate minerals as determined by Sobek and peroxide test.* J. Environ. Qual.

JAMIESON, H. E., PRZYBYLOWICZ, W. J. (1997): *The incorporation of toxic elements in iron sulfates precipitated from acid mine drainage.* Geol. Assoc. Can. – Mineral Assoc. Can., Program Abstr. 22:A73.

JAMIESON, H. E., ALPERS, C. N., NORDSTROM, D. K., PETERSON R. C. (1999): *Substitution of zinc and other metals in iron-sulfate minerals at Iron Mountanin, California.* In: Goldsack, D., Belzile, N., Yearwood, P., Hall, G. (Eds.) Conference Proc, Sudbury ’99: Mining and the Environment II., Sudbury, Ontario, Canada, Vol. 1, pp. 231-241.

JANZEN, M. P., NICHOLSON, R. V., SCHARER, J. M. (2000): *Pyrrhotite reaction kinetic: Reaction rates for oxidation by oxygen, ferric iron, and for nanooxidative dissolution*. Geochim. Cosmochim. Acta, Vol. 64, pp. 1511-1522.

JENNINGS, S. R., DOLLHOPH, D. J. (1995): *Acid-base account effectiveness for determination of mine waste potential acidity*. J. Hazard. Mater., Vol. 41, pp. 161-175.

JENNINGS, S. R., DOLLHOPH, D. J., INSKEEP, W. P. (2000): *Acid production form sulfide minerals using hydrogen peroxide weathering.* Appl. Geochem., Vol. 15, pp. 235-243.

JURJOVEC, J., PTACEK, C. J., BLOWES, D. W. (2002): *Acid neutralization mechanisms and metal release in mine tailings. A laboratory column experiment.* Geochim. Cosmochim. Acta, Vol. 66, pp. 1511-1523.

KARATHANASIS, A. D., EVANGELOU, V. P., THOMSON, Y. L. (1988): *Aluminium and iron equilibria in soil solutions and surface waters of acid mine watersheds.* J. Environ. Qual., Vol. 17, pp. 534-543.

KOZLOWSKI R., JASKOLSKI S. (1932): *LES GISEMENTS ARGENTO-STANNIFÉRES D'ORURO AN BOLIVIE*. Archieve de Minérelogie de la Société des Sciences de Varsovie, Vol. 8, pp. 1-100.

KUENEN, J. G., ROBERTSON, L. A., TUOVINEN, O. H. (1992): *The genus Thiobacillus, Thiomicrospira, and Thiosphaera.* In: Balows, A., Truper, H. G., Dworkin, M., Harder, W., Schleifer, K. H. (Eds.) The Procaryotes, 2nd ed., Vol. 3, Springer-Verlag, New York, pp. 2638-2657.

KUO, E. Y., RITCHIE, A. I. M. (1999): *The inpact of convection on the overall oxidation rate in sulfidic waste rock dumps.* In: Goldsack, D., Belzile, N., Yearwood, P., Hall, G. (Eds.) Sudburry '99: Mining and the Environment II, Vol. 1, Laurentian University, Sudburry, Ontario, pp. 211-220.

LAPAKKO, K. (2003): *Developments in humidity-cell tests and their application*. In: Jambor, J.L., Blowes, D.W., Ritchie, A.I.M. (Eds.) Environmental Aspects of Mine Wastes, Mineral. Assoc. Can. Short Course, Vol. 31, pp. 147- 164.

LAPAKKO, K. A., WHITE, W. (2000): *Modification of ASTM 5744-96 kinetic test.* In: International Land Reclamation and Mine Drainage Conference and Proceedings of the Third International Conference on Acid Rock Drainage 1. Society for Mining, Metallurgy, and Exploration, Littleton, Colorado, pp. 631-649.

LAPAKKO, K. A., WESSELS, J. N., ANTONSON, D. A. (1995): *Long term dissolution testing of mine waste. Report to the United States Environmental Protection Agency*. Grant No. X-8200322-01-0. Minnesota Department of Natural Resources, Division of Minerals, St. Paul, Minnesota.

LAPAKKO, K, WHITE, W. III., COX, R. L (1999): *Static-test methods most commonly used to predict acid mine drainage.* In: Plumlee, G. S., Logsdon, M. (Eds.) The Environmental Geochemistry of Mineral Deposits, Part A: Theory and background. Society of Economic Geologists Reviews in Economic Geology, Vol. 7A, pp. 325-338

LAPAKKO, K. A., ANTONSON, D. A., WAGNER, J. R. (2000): *Mixing of rotary kiln fines with fine grained acid producing rock.* In: Proceedings for the Fifth International Conference on Acid Rock Drainage 2. Society for Mining, Metallurgy, and Exploration, Littleton, Colorado, pp. 901-910.

LEINZ, R. W., SUTLEY, S. J., DESBOROUGH, G. A., BRIGGS, P. H. (2000): *An investigation of the partitioning of metals in mine waste using sequential extraction.* In: Proceedings for the Fifth International Conference on Acid Rock Drainage 2. Society for Mining, Metallurgy, and Exploration, Littleton, Colorado, pp. 1489-1500.

LINDGREN, W., ABOTT A. C. (1931): *The silver-tin deposits of Oruro, Bolivia*. Economic Geology, Vol. 26, No.5, pp. 453-479.

LONG, D. T., FEGAN, N. E., MCKEE, J. D., LYONS, W. B., HINES, M. E., MACUMBER, P. G. (1992): *Formation of alunite, jarosite and hydrous iron oxides in a hypersaline lake system: Lake Tyrell, Victoria, Australia.* Chem. Geol.,Vol. 96, pp. 183-202.

MCGUIRE, M. M., EDWARDS, K. J., BANFIELD, J. F., HAMERS, R. J. (2001): *Kinetics, surface chemistry, and structural evolution of microbiallymediated sulfide mineral dissolution.* Geochim. Cosmochim. Acta, Vol. 65, pp. 1243-1258.

MCKEOWN, R., BARBOUR, L., ROWLET, D., HERASYMUIK, G. (2000): *Characterization of the grain site distribution for wate rock from metal mine – a review of existing data and an evaluation of the implications for hydrogeologic behavior.* In: Proceedings of the Canadian Society of Civil Engineers, Annual Conference, London, Ontario. Canadian Society for Civil Engineers, Montreal, Quebec, pp. 203-209.

MIKHLIN, YU. L., KUKLINSKIY, A. V., PAVLENKO, N. I., VARNER, V. A., ASANOV, I. P., OKOTRUB, A. V., SELYUTIN, G. E., SOLOVYEV, L. A. (2002): *Spectroscopic and XRD studies of the air degradation of acid-related pyrrhotites*. Geochim. Cosmochim. Acta, Vol. 66, pp. 4057-4067.

MILLS, A. A. (1999): *The role of bacteria in Environmental geochemistry*. In: Plumlee, G. S., Logsdon, M. J. (Eds.) The Environmental Geochemistry of Mineral Deposites. Part A: Processes, Techniques, and Health Issues, Rev. Econ. Geol. Vol. 6A, pp. 125-132.

MORIN, K. A., HUTT, N. M. (1997): *Environmental geochemistry of mine site drainage, practical therory and case studies*. MDAG Publishing, Canada. pp. 330.

MOSES, C. O., NORDSTROM, D. K., HERMAN, J. S., MILLS, A. A. (1997): *Aqueous pyrite oxidation by dissolved oxygen and ferric iron*. Geochim. Cosmochim. Acta, Vol. 51, pp. 1561-1571.

NESBIT, H. W., MUIR, I. J. (1994): *X-ray photoelectron spectroscopy of a pristine pyrite surface reacted with water wapour and air.* Geochim. Cosmochim. Acta, Vol. 58, pp. 4667-4679.

NICHOLSON, R. V. (1994): *Iron-sulfide oxidation mechanisms: laboratory studies*. In: The Environmental Geochemistry of Sulfide Mine-Wastes. Mineral. Assoc. Can., Short Course Series, Vol. 22, pp. 164-183.

NICHOLSON, R. V., SCHARER, J. M. (1994): *Laboratory studies of pyrrhotite oxidation kinetics*. In Alpers, C. N., Blowes, D. W., Environmental geochemistry of sulfide oxidation. Am. Chem. Soc. Symp., Ser. 555, pp 14-30.

NORDSTROM, D. K. (1982): *Aqueous pyrite oxidation and the consequent formation of secondary iron minerals*. In: Kittrick, J.A., Fanning, D.S., Hossner, L.R. (Eds.) Acid Sulfate Weathering. Soil Sci. Soc. Am., pp. 37-56.

NORDSTROM, D. K. (2010): *Various origins of circumneutral mine drainage problems with classification.* U.S. Geological Survey, 2010, GSA Denver Annual Meeting

NORDSTROM, D. K., SOUTHAM, G. (1997): *Geomicrobiology of sulfide mineral oxidation*. In: Banfield, J. F., Nealson, K. H. (Eds.) Geomicrobiology: Interactions between microbes and minerals. Rev. Mineral, Vol. 35, pp. 361-390.

NORDSTROM, D. K., ALPERS, C. N. (1999): *Geochemistry of acid mine waters*. In: The Environmental Geochemistry of Mineral Deposits. Rev. Econ. Geol., Vol. 6A, pp. 133-160.

NORDSTROM, D. K., ALPERS, C. N., PTACEK, C. J., BLOWES, D. K. (2000): *Negative pH and extremly acidic mine waters from the Iron Mountain, California.* Environ. Sci. Technol., Vol. 34, pp. 254-258.

OLIVEIRA, S. M. B. DE, BLOT, A., IMBERNON, R. A. L., MAGAT, P. (1996): *Jarosite and plumbojarosite in gossans of the Canoas District, Parana State*. Rev. Bras. Geocienc., Vol. 26, pp. 3-12.

OLSON, G. J. (1991): *Rate of pyrite bioleachingby Thibacillus ferrooxidans: Result of an interlaboratory comparison.* Appl. Environ. Microbiol., Vol. 57, pp. 642-644.

PEARCE S., SCOTT P., WEBER P. (2015): *Waste rock dump geochemical evolution: matching lab data, models and predictions with reality*. In: Proceedings of the 10th ICARD

PLUMLEE, G. S. (1999): *The environmental geology of mineral deposits*. In: Plumlee, G. S., Logsdon, M. J. (Eds.) The environmental Geochemistry of Mineral Deposits. Rev. Econ. Geol., Vol. 6A, pp. 71-116.

PRATT, A. R., MUIR, I. J., NESBITT, H. W. (1994): *X-ray photoelectron and Auger electron spectroscopic studies of pyrrhitite and mechanism of air oxidation*. Geochim. Cosmochim. Acta, Vol. 58, pp. 827-841.

PRICE, W. A. (2000): *An overview of new developments in ML/ARD at mine sites in British Columbia.* 7th Annual BC MEM - MEND Metal leaching and ARD Workshop. British Columbia Ministry of Energy and Mines, British Columbia.

PRICE, W. A. (2003): *Challanges posed by metal leaching and acid rock drainage, and approaches used to address them.* In: Jambor, J. L., Blowes, D. W., Ritchie, A. I. M. (Eds.) Environmental Aspects of Mine Wastes, Mineral. Assoc. Can. Short Course, Vol. 31, pp. 1-10.

RAMOS, L., HERNANDEZ, L. M., GONZALES, M. J. (1994): *Sequential fractionation of copper, lead, cadmium and zinc in soils from or near Donana National Park*. Journal of Environmental Quality, Vol. 23, pp. 50-57.

RHOTON, F. E., BIGHAM, J. M., NORTON, L. D., SMECK, N. E. (1981): *Contribution of magnetite to oxalate extractable iron in soil and sediments from the Maumee River Basin of Ohio*. Soil Sci. Soc. Am. J., Vol. 45, pp. 645-649.

RIMSTIDT, J. D., VAUGHAN, D. J. (2003): *Pyrite oxidation: A state-of-the-art assessment of the reaction mechanism.* Geochim. Cosmochim. Acta, Vol. 67, pp. 873-880.

RIMSTIDT, J. D., CHERMAK, J. A., GAGEN, P. M., (1994): *Rates of reaction of galena, sphalerite, chalcopyrite and arsenopyrite with $Fe^{(III)}$ and acidic solutions.* In: Alpers, C. N., Blowes, D. W. (Eds.) Environmental geochemistry of sulfide oxidation. Am. Chem. Soc. Symp., Ser. 550. pp. 2-13.

RIOS, C. (1985): *Estudio de la Contaminación Ambiental por las Descargas Mineras de Comsur en la Represa Milluni*. [masterproef] Universidad Mayor de San Andres, Facultad de Ingenieria, Carrera Ingenieria Civil.

RIPMEESTER, J. A., RATCLIFFE, C. I., DUTRIZAC, J. E., JAMBOR, J. L. (1986): *Hydronium ion in the alunite-jarosite group.* Can. Mineral., Vol. 24, pp. 435-447.

RITCHIE A. I. M. (1994): *The waste-rock environment*. In: Jambor, J. L., Blowes, D. W. (Eds.) Environmental Geochemistry of Sulfide Mine-Waste, Mineralogical Association of Canada. Vol. 22, pp. 201-244.

RITCHIE, A. I. M. (2000): *Interpretation of temperature and oxygen profile measurements in piles of sulfidic wastes.* In: Grundon, N. J., Bell, L. C. (Eds.) Proceedings of the 4th Australian Workshop on Acid Mine Drainage. Australian Centre for Mining Environmental Research, Brisbane, Australia, pp. 189-201.

RITCHIE, A. I. M. (2003): *Oxidation and gas transport in piles of sulfidic material*. In: Jambor, J. L., Blowes, D. W., Ritchie, A. I. M. (Eds.) Environmental Aspects of Mine Wastes, Mineral. Assoc. Can. Short Course, Vol. 31, pp. 73-94.

RITCHIE, A. I. M., MISKELLY, P. (2000): *Geometric and phisico-chemical properties determining sulfide oxidation rates in waste rock dumps.* In: Proceedings from the Fifth International Conference on Acid Rock Drainage, 1. Society of Mining, Metallurgy, and Exploration, Littleton, Colorado, pp. 277-288.

ROCA, A., VINALS, J, ARRANZ, M., CALERO, J. (1999): *Characterization and alcaline decomposition/ cyanidation of beudantite-jarosite materials from Rio Tinto gossan ores.* Can. Metall. Quart., Vol. 38, pp. 93-103.

SALVARREDY-ARANGUREN, M., PROBST, A., ROULET, M., ISAURE, M. (2008). *Contamination of surface waters by mining wastes in the Milluni Valley (Cordillera Real, Bolivia): Mineralogical and hydrological influences.* [masterproef] Université Paul Sabatier.

SCHARER, J. M., GARGA, V., SMITH, R., HALBERT, B. E. (1991): *Use of Steady State Models for Assessing Acid Generation in Pyritic Mine Tailings.* In: Proceedings Second International Conference on the Abatement of Acidic Drainage, September 16-18, 1991, Montreal, Canada, Vol. 2, pp. 211-230.

SCHIPPERS A., BREUKER A., BLAZEJAK A., BOSECKER K., KOCK D., WRIGHT T. L. (2010): *The biogeochemistry and microbiology of sulfidic mine waste and bioleaching dumps and heaps, and ovel Fe(II)-oxidizing bacteria*. Hydrometallurgy, Vol. 104, pp. 342-350.

SCHLEPER, C., PÜHLER, G., KLENK, H. P., ZILLIG, W. (1996): *Picrophilus oshimae and Picrophilus Torridus fam. nov., gen. nov., sp. nov., two species of hiperacidophophilic, thermophilic, heterotropic, aerobic archaea.* Int. J. Syst. Bacteriol., Vol. 46, pp. 814-816.

SCHNEIDER, H. J., LEHMANN, R. (1874): *Contribution to a new genetical concept on the Bolivian tin province*. In: Klemm, D., Schneider, H. J. (Eds.) Time- and Strata-Bound Ore Deposits. Berlin, Springer-Verlag, pp. 153-168.

SCHOTT, K. M. (2000): *Nomenclature of the alunite supergroup: a discussion*. Can. Mineral, Vol. 38.

SCHWERTMANN, U., SCHULZE, D. G., MURAD, E. (1982): *Identification of ferrihydrite in soils by dissolution kinetics, differential X-ray diffraction, and Mössbauer spectrometry*. Soil Sci. Soc. Am., Vol. 46, pp. 869-875.

SEAL, R. R., HAMMARSTROM, J. M. (2003): *Geoenvironmental models of mineral deposits: examples from massive sulfide and gold deposits.* In: Jambor, J. L., Blowes, D. W., Ritchie, A. I. M. (Eds.) Environmental aspects of mine wastes. Short course series, Vol. 31, Mineralogical Association of Canada, pp. 11-50.

SEAL, R. R. II., HAMMARSTROM, J. M., FOLEY, N. K., ALPERS, C. N. (2000): *Geoenvironmental models for seafloor base- and precious-metal massive sulfide deposits.* In: Proceedings from the Fifth International Conference on Acid Rock Drainage, 1. Society of Mining, Metallurgy, and Exploration, Littleton, Colorado, pp. 151-160.

SHAW, S. C., GROAT, L. A., JAMBOR, J. L., BLOWES, D. W., HANTON-FONG, C. J., STUPARYK, R. A. (1998): *Mineralogical study of base metal tailings with various sulfide contents, oxidized in laboratory columns and field lysimeters.* Environ. Geol., Vol. 33, pp. 209-217.

SIEBKE, W., SPIERING, H., MEISSNER, E. (1983): *Cooperative pseudo-Jahn-Teller effect of the* $Fe(H_2O)_6^{2+}$ *complexes in the sulfate heptahydrates.* Phys. Rev. B., Vol. 27, pp. 2730-2739.

SINGER, P. C., STUMM, W. (1970): *Acid mine drainage: The rate determining step*. Science, Vol. 167, pp. 1121-1123.

SMITH, L., BECKIE, R. D. (2003): *Hydrologic and geochemical transport processes in mine waste rock.* In: Jambor, J. L., Blowes, D. W., Ritchie, A. I. M. (Eds.) Environmental aspects of mine wastes. Short course series, Vol. 31, Mineralogical Association of Canada, pp. 51-72.

SMYTH, D. J. A. (1981): *Hydrogeological and geochemical studies above the water table in an inactive uranium tailing impoundment near Elliot lake, Ontario.* M.Sc. thesis, University of Waterloo, Waterloo, Ontario.

SONDAG, F. (1981): *Selective extraction procedures applied to geochemical prospecting in an area contaminated by old mine workings*. Journal of Geochemical Exploration, Vol. 15, pp. 645– 652.

STUMM, W., MORGAN, J. J. (1981): *Aquatic chemistry - An introduction emphasizing chemical equilibria in natural waters*. New York, John Wiley & Sons Inc, pp. 470.

TESSIER, A., CAMPBELL, P. G. C., BISSON, M. (1979): *Sequential extraction procedure for the speciation of particular trace metals.* Anal. Chemistry, Vol. 51, pp. 844-851.

TIEGENG, L., GOULONG, G., LIN, Y. (1995): *Discovery and investigation of zinc-melanterite in nature*. Acta Mineral Sinica, Vol. 15, pp. 286-289, (in Chinese).

THOMAS, J. E., SKINNER, W. M., SMART, R. ST. C. (2003): *A comparison of the dissolution behavior of troilite with other iron(II) sulfides; implications of structure*. Geochim. Cosmochim. Acta, Vol. 67, pp. 831-843.

TUOVINEN, E. H., KELLY, D. P. (1972): *Studies on the growth of Thiobacillus ferrooxidans I. Use of membrane filters and ferrous iron agar to determine viable numbers, and comparison with $^{14}CO_2$-fixation and iron oxidation as measures of growth.* Arch. Microbiol., Vol. 17, pp. 297-302.

URE, A. M., QUEVAUVILLER, P. H., MUNTAU, H., GRIEPICK, B. (1993): *Speciation of heavy metals in soils and sediments. An Account of the Improvement and Harmonization of Extraction Techniques undertaken under the Auspices of Commission of the European Communities*. International Journal of Environmental Analytic Chemistry, Vol. 51, pp. 35-151.

USEPA (1994): *EPA 530-R-94-036 Technical Document – Acid mine drainage prediction*. U.S. Environmental Protection Agency, Office of Solid Waste, Special Waste Branch.

USEPA (2009): *EPA-821-R-09-002:2009: Method 1627 - Kinetic Test Method for the Prediction of Mine Drainage Quality*. U.S. Environmental Protection Agency, Washington, DC, USA.

VICK, S. G. (2001). *Stability aspects of long-term closure for sulfide tailings.* Seminar on safe tailings dam constructions. Gallivare, Swedish Mining Association, European Commission. pp. 68-79

WALDER, I. F. (2000): *Mine waste characterisation and evaluation – Oruro mining district, San José mine project.* SARB Consulting project report for COMIBOL, Bolivia

WALDER, I.F. (2009): *Characterization and mitigation of the Ag-Sn San Jose Mining District, Bolivia*. 8th ICARD Proceedings.

WALDER, I. F., STORMONT, J. (2004): *Through characterization of the hydrogeological and geochemical processes in waste rocks are essential for effective reclamation*. Proceedings of the VI International Conference on Clean Technology for the Mining Industry, University of Concepción, Chile.

WERNER, A. B. T., SINCLAIR, W. D., AMEY, E. B. (1998): *International Strategic Mineral Issues Summary Report - Tungsten.* US Geological Survey, Circular 930.

WILLIAMSON, M. A., RIMSTIDT, J. D. (1994): *The kinetics and electrochemical rate-determining step of aqueous pyrite oxidation.* Geochim. Cosmochim. Acta, Vol. 58, pp. 5443-5454.

WILSON, J. A., WILSON, G. W., FREDLUND, D. G. (2000): *Numerical modeling of vertical and inclined waste rock layers.* In: Proceedings from the Fifth International Conference on Acid Rock Drainage, 1. Society of Mining, Metallurgy, and Exploration, Littleton, Colorado, pp. 257-266.

Internet based and other cited references

ATLAS OF EH-PH DIAGRAMS (2005): *Intercomparison of thermodynamic databases*. Geological Survey of Japan, Open File Report No.419 http://www.gsj.jp/GDB/openfile/files/no0419/ openfile419e.pdf

BOLGENER (2015/a): *Compamento Mina Bolsa Negra al fondo la Localidad de Tres Rios*. URL: http://www.panoramio.com/user/4030110; Downloaded: 15.10.2015.

BOLGENER (2015/b): *Desmonte de "Cajas" mina "Bolsa Negra"*. URL: http://www.panoramio.com/ user/ 4030110; Downloaded: 15.10.2015.

CEN (2012): *CEN/TR 16376:2012 Characterization of waste - Overall guidance document for characterization of waste from the extractive industries.* European Comittee for Standardization, Techincal Report.

DAMES & MOORE NORGE (1999): *Hydrogeological study of San José mine aquifer and water supplying aquifers to the city of Oruro.* (Eds.) Aabel, J. P., Progress report.

EIPPCB (2004): *Reference document on best available techniques for management of tailings and waste-rock in mining activitie*. http://eippcb.jrc.es

INAP (2009): *International Network for Acid Prevention – Global Acid Rock Drainage (GARD) Guide*. http://guardguide.com

DRIESEN, K. (2012): *Contamination of surface waters by the former mining industry in the Milluni Valley (Cordillera Real, Bolivia) and the application of the water planning model WEAP*. URL: http://www.weap21.org/Downloads/Milluni.pdf; Downloaded: 01.11.2015.

KLIMMER, H. (2015): *Lake Milluni*. URL:http://www.panoramio.com/user/6056921; Downloaded: 15.10.2015.

LAPAKKO, K. (2002). *Metal mine rock and waste characterization tools: an overview*. Mining, Minerals and Sustainable Development, MMSD; Document. http://www.iied.org/mmsd/

MINDAT.ORG (2015/a): *Detailed data sheet of Morococala Mine, Santa Fé Mining District, Dalence Province, Oruro Department, Bolivia.* URL:http://www.mindat.org/loc-339.html; Downloaded: 17.10.2015.

MINDAT.ORG (2015/b): *Detailed data sheet of Huanuni, Dalence Province, Oruro Department, Bolivia.* URL:http://www.mindat.org/locdetailed-14512.html; Downloaded: 17.10.2015.

WORLDOMETERS (2020/a): *Map of Bolivia (Physical)* URL: https://www.worldometers.info/maps/ bolivia-map/, Downloaded: 02.12.2020

WORLDOMETERS (2020/b): *Map of Hungary (Physical)* URL: https://www.worldometers.info/maps/ hungary-map/, Downloaded: 02.12.2020

DOI: 10.14750/ME.2021.004

ACKNOWLEDGEMENT

I would like to thank my consultants: Dr. Ferenc Mádai (University of Miskolc) and Dr. Ingar F. Walder for their helpfulness and further thank Dr. Walder for providing the technical and analytical background at KREC (Kjeøy Research and Education Centre) in Northern Norway.

Further thanks for Dr. Ferenc Kristály, Dr. Norbert Zajzon, Máté Leskó and Richárd Papp for their instrumental help, for Dr. János Földessy, Dr. Sándor Szakáll, Délia Debus and Andrea Varga for their technical help.

Last, but not least I would like to also thank my family, mainly my wife Zsuzsanna and my two sons, Ákos and Máté, who provided the stable family background during the completion of this PhD dissertation.

DOI: 10.14750/ME.2021.004

APPENDICES

DOI: 10.14750/ME.2021.004

LIST OF THE PHD DISSERTATION RELATED PUBLICATIONS

Articles in journals and books

MÓRICZ, F. (2000): *Calculation of the bulk pyrite oxidation rate from the results of humidity cell test.* In: Kovács, F., Rácz, Á. (Eds.) Műszaki Földtudományi Közlemények, Vol. 89, No. 1, pp. 325-333. [ISSN 2063-5508]

MÓRICZ, F., MÁDAI, F. (2019): *Temporal changes of pyrite oxidation rate in bolivian sulphidic mining wastes.* International Journal of Engineering and Management Sciences (IJEMS) Vol. 4, No. 4, pp. 194-202. [DOI: 10.21791/IJEMS.2019.4.22]

EMBILE, R., WALDER, I. F,. MADAI, F., MORICZ, F., RZEPKA, P., WALDER, P. (2016): *Grain Size Effects on Mine Water Quality and Acid/Neutral Rock Drainage Production in Kinetic Testing Using Recsk Porphyry Skarn Cu–Zn Deposit Rocks.* Mine Water and the Environment, Vol. 35., Issue 4, pp. 421-434. [ISSN 1025-9112] [ISSN 1616-1068 Online]

MÓRICZ, F., MÁDAI, F., WALDER, I. F. (2014): *Temporal changes of pyrite oxidation insulphidic mine wastes.* In: Fehér, B. (Eds.) Az ásványok vonzásában: Tanulmányok a 60 éves Szakáll Sándor tiszteletére. Miskolc-Egyetemváros: Herman Ottó Múzeum, 2014. pp. 179-190. [ISBN 978-963-9271-96-8]

MÁDAI, F., MÓRICZ, F., WALDER, I. F., EMBILE, R., PRAVICZKI, T. (2013): *Ércbányászati meddőhányók vizsgálata: szulfid oxidáció neutrális körülmények között*. Műszaki Földtudományi Közlemények 84. kötet 2. szám, pp. 53-72. [ISSN 2063-5508]

TÓTH, M., MÓRICZ, F., KOVÁCS, B. (2013): *Investigation of heavy metals extraction from surface samples of a waste dump of Rudabánya*. Geosciences and Engineering 2. kötet 3. szám, pp. 45-50. [ISSN 2063-6997]

MÓRICZ, F., MÁDAI, F., WALDER, I. F. (2012): *Pyrite oxidation under circumneutral pH conditions*. Geosciences and Engineering 1. kötet 2. szám, pp. 111-116. [ISSN 2063-6997]

MÓRICZ, F., MÁDAI, F., WALDER, I. F. (2011): *Pyrite oxidation changes in Sulphidic mine Wastes from the Itos Sn-Ag Deposit, Bolivia*. In: Rüde, R. T., Freund, A., Wolkersdorfer, C. (Eds.) 11th International Mine Water Association Congress – Mine Water – Managing the Challenges, pp. 683-688. [ISBN:978-1-897009-47-5]

Conference series

MÓRICZ, F., MÁDAI, F., WALDER, F. (2019): *Erős kőzetsavasodás jelensége semleges pH értéken?!* In: Borzás, S., Antal, T. (Eds) Műszaki tudomány az Észak-kelet Magyarországi régióban 2019. Konferencia kiadvány, pp. 261-264.

MÓRICZ, F., MÁDAI, F. (2018): *Szulfidos meddőhányók anyagának kinetikus teszttel történő geokémiai vizsgálata.* In: Török, Á., Görög, P., Vásárhelyi, B. (Eds.) Mérnökgeológia - Kőzetmechanika 2018. Budapest, Magyarország : BME Geotechnika és Mérnökgeológia Tanszék. Konferencia kiadvány. pp. 303-314. [ISBN: 978-963-313-283-8]

MÓRICZ, F., WALDER, I. F., MÁDAI, F. (2009): *Geochemical and Mineralogical Characterization of Waste Material from the Itos Sn-Ag Deposit, Bolivia.* In: Securing the future : Mining, metals and the environment in a sustainable society and 8thICARD : International Conference on Acid Rock Drainage, Skellefteå, Svédország, Conference series. pp. 525-535. [ISBN: 978-1-61567-816-7]

Posters

MÓRICZ, F., MÁDAI, F., KRISTÁLY, F. (2014): *X-ray powder diffraction versus sequential chemical extraction – a new combined method for exacting mineralogical speciation of sulphidic mining wastes*. Poszter. 92nd Annual Meeting of the German Mineralogical Society (DMG), Jena, Németország.

EMBILE, R., WALDER, I. F., MÁDAI, F., MÓRICZ, F., WALDER, P., RZEPKA, P. (2013): *Characterization of the effects of grain size to mine water quality and Acid Rock Drainage (ARD) production in Kinetic Testing*. Poster. Goldschmidt Conference 2013, Florence, Italy.

EMBILE, R., WALDER, I. F., MÁDAI, F., MÓRICZ, F., RZEPKA, P., WALDER, P. (2013): *Characterization of the effects of grain size to mine water quality and acid rock drainage (ARD) producing in kinetic testing.* Poster. "Advanced Environmental Geology 2: The impact of mining activities on the environment" Conference. 2013, Spisska Nove Ves, Slovakia.

Abstract book of conferences

MÓRICZ, F., WALDER, I. F., MÁDAI, F. (2019): Calculation of the bulk pyrite oxidation rate from the results of humidity cell test. Abstrakt series. AIMS – Aachen Intermational Mining Symposia. 2019, Aachen, Germany, pp. 31. [ISBN 978-3-95886-283-8]

WALDER, I. F., EMBILE, R., TINSLEY, M., STOPA, F., MÓRICZ, F. (2018): *Can we use data from kinetic testing to predict future water quality seeping from mine waste?* In: New Mexico Geological Society Annual Spring Meeting 2018, New Mexico Geological Society, Socorro, New Mexico, pp. 78.

EMBILE, R., WALDER, I. F., MÁDAI, F., MÓRICZ, F., WALDER, P., RZEPKA, P. (2013): *Characterization of the effects of grain size to mine water quality and Acid Rock Drainage (ARD) production in Kinetic Testing.* Abstract series. Goldschmidt Conference 2013, Italy, pp. 1040.

MÓRICZ, F., WALDER, I. F., MÁDAI, F. (2013): *Pyrite oxidation changes in Bolivian sulphidic mine wastes.* Abstract series. Vinterkonferansen 2013, Oslo, Norway, pp. 90. [ISBN 978-82-92-39478-6]

EMBILE, R., WALDER, I. F., MÓRICZ, F., MÁDAI, F. (2013): *Characterization of the effects of grain size to mine water quality and ARD production in Kinetic Testing using Recsk Deep deposit waste rocks.* Abstract series. Vinterkonferansen 2013, Oslo, Norway, pp. 32. [ISBN 978-82-92-39478-6]

MÓRICZ, F., WALDER, I. F., MÁDAI, F. (2012): *Possible acid rock drainage effect on neutral pH, example of mine waste from Recsk*. Abstract series. 5th Mineral Sciences in the Carpathians Conference (MSCC) and the 3rd Central-European Mineralogical Conference (CEMC), Acta Mineralogica-Petrographica, Szeged, Vol. 7, pp. 91. [ISSN 1589-4835] [ISSN 0324-6523]

MÓRICZ, F., WALDER, I. F., MÁDAI, F. (2012): *Possible acid rock drainage effect on neutral pH.* Absztrakt kötet. Földtudományi és Környezetvédelmi Vándorgyűlés és Kiállítás, Miskolc.

MÓRICZ, F. (2012): *Difficulties in the accurate determination of pyrite oxidation*. Absztrakt kötet. Ifjú Szakemberek Ankétja (ISZA) 2012, Tatabánya, pp. 30.

MÓRICZ, F., MÁDAI, F., WALDER, I. F. (2011): *Pyrite oxidation changes in sulphidic mine wastes from the Itos Sn-Ag deposit, Bolivia*. Abstract series. 11th IMWA 2011 Congress, Aachen, Germany, pp. 86.

MÓRICZ, F. (2011): *Mineralogical and geochemical characterization of sulphidic mine waste from the Itos Sn-Ag deposit, Oruro*. Konferencia kiadvány. XXV. MicroCAD, Miskolc.

MÓRICZ, F. (2011): *Changes of the pyrite oxidation rate by time*. Absztrakt kötet. Ifjú Szakemberek Ankétja (ISZA) 2011, Győr.

MÓRICZ, F., MÁDAI, F., WALDER, I.F. (2010): *Kinetic testing and mineralogical characterization of sulphide mine wastes from the Oruro deposit (Bolivia)*. Proceedings of IMA 2010. In: Acta Mineralogica-Petrograhica Vol. 6, Szeged, pp. 374. [ISSN 0324-6523] [ISSN 1589-4835]

MÓRICZ, F. (2010): *Kinetic testing and mineralogical characterization of sulphide mine wastes from the Oruro deposit (Bolivia)*. Abstract series. 1st Students' International Geological Conference, Krakow, Poland, pp. 32-33.

DOI: 10.14750/ME.2021.004

LIST OF FIGURES

DOI: 10.14750/ME.2021.004

DOI: 10.14750/ME.2021.004

LIST OF TABLES

DOI: 10.14750/ME.2021.004

LIST OF EQUATIONS

$$FeS_2 + \frac{7}{2}O_2 + H_2O \rightarrow Fe^{2+} + 2SO_4^{2-} + 2H^+ \quad (1)$$

$$Fe^{2+} + \frac{1}{4}O_2 + H^+ \rightarrow Fe^{3+} + \frac{1}{2}H_2O \quad (2)$$

$$Fe^{3+} + 3H_2O \rightarrow Fe(OH)_3 + 3H^+ \quad (3)$$

$$FeS_2 + \frac{7}{2}O_2 + H_2O \rightarrow Fe(OH)_3 + 2SO_4^{2-} + 2H^+ \quad (4)$$

$$Fe^{3+} + 2H_2O \rightarrow FeOOH + 3H^+ \quad (5)$$

$$Fe(OH)_3 \rightarrow FeOOH + H_2O \quad (6)$$

$$2FeOOH \rightarrow Fe_2O_3 + H_2O \quad (7)$$

$$FeS_2 + 14Fe^{3+} + 8H_2O \rightarrow 15Fe^{2+} + 2SO_4^{2-} + 16H^+ \quad (8)$$

$$Fe_{1-x}S + \frac{2-x}{2}O_2 + xH_2O \rightarrow (1-x)Fe^{2+} + SO_4^{2-} + 2xH^+ \quad (9)$$

$$4FeAsS + 13O_2 + 6H_2O \rightarrow 4H_2AsO_4 + 4H^+ + 4SO_4^{2-} + 4Fe^{3+} \quad (10)$$

$$Fe_{1-x}S + (8-2x)Fe^{3+} + 4H_2O \rightarrow (9-3x)Fe^{2+} + SO_4^{2-} + 8H^+ \quad (11)$$

$$CuFeS_2 + 16Fe^{3+} + 8H_2O \rightarrow Cu^{2+} + 17Fe^{2+} + 2SO_4^{2-} + 16H^+ \quad (12)$$

$$PbS + 8Fe^{3+} + 4H_2O \rightarrow Pb^{2+} + 8Fe^{2+} + SO_4^{2-} + 8H^+ \quad (13)$$

$$ZnS + 8Fe^{3+} + 4H_2O \rightarrow Zn^{2+} + 8Fe^{2+} + SO_4^{2-} + 8H^+ \quad (14)$$

$$2Fe_{1-x}S + \frac{1}{2-x}O_2 + (2-4x)H^+ \rightarrow FeS_2 + (1-2x)Fe^{2+} + (1-2x)H_2O \quad (15)$$

$$PbS + 2H^+ \rightarrow Pb^{2+} + H_2S \quad (16)$$

$$ZnS + 2H^+ \rightarrow Zn^{2+} + H_2S \quad (17)$$

$$Fe_{1-x}S + (2-2x)H^+ + xH_2O \rightarrow (1-x)Fe^{2+} + H_2S \quad (18)$$

$$FeSO_4 * 7H_2O + \frac{1}{4}O_2 \rightarrow Fe(OH)_3 + SO_4^{2-} + \frac{9}{2}H_2O + 2H^+ \quad (20)$$

$$PbS + 2O_2 \rightarrow PbSO_4 \quad (21)$$

$$KFe_3(SO_4)_2(OH)_6 \rightarrow K^+ + 3FeOOH + 2SO_4^{2-} + 3H^+ \quad (22)$$

$$2Fe^{3+} + MS \rightarrow 2Fe^{2+} + M^{2+} + S^o \quad (23)$$

$$CaCO_3 + 2H^+ \rightarrow Ca^{2+} + H_2O + CO_2 \quad (24)$$

$$2FeS_2 + 3CaCO_3 + 3H_2O + 6O_2 \rightarrow 2FeOOH + 3CaSO_4 * 2H_2O + 3CO_2 \quad (25)$$

$$r = 10^{-8.19(\pm 0.10)} \frac{m_{DO}^{0.5(\pm 0.04)}}{m_{H^+}^{0.11(\pm 0.01)}} \quad (26)$$

$$r = 10^{-6.07(\pm 0.57)} \frac{m_{Fe^{3+}}^{0.93(\pm 0.07)}}{m_{Fe^{2+}}^{0.40(\pm 0.06)}} \quad (27)$$

$$LR = \frac{c_r * V_r}{M_s * t_r} \quad (28)$$

$$S_t = S_0 e^{(-k*t)} \quad (29)$$

DOI: 10.14750/ME.2021.004

$$k = -ln\frac{S_t}{t} * lnS_0 \tag{30}$$

$$R_{FeS_2} = \frac{P_{I(O_2)} - P_{(FO_2)}}{t*3.75*M_{py}} \tag{31}$$

$$1M\ pyrite \rightarrow 2M\ SO_4^{2-} + 1M\ Fe^{2+} + 2M\ H^+ \tag{1/b}$$

$$1M\ pyrite + 14M\ Fe^{3+} \rightarrow 2M\ SO_4^{2-} + 15M\ Fe^{2+} + 16M\ H^+ \tag{8/b}$$

$$C_{H^+} = 10^{-pH} * H^+_{mw} \tag{32}$$

$$py_{ox}^{pH} = (10^{-pH_{sp}} - 10^{-pH_{rs}}) * H^+_{mw} * \frac{py_{mw}}{2*H^+_{mw}} * V_{rs} \tag{33}$$

$$pH^{avg.} = -log_{10}\left(\frac{\sum_{i=1}^{n} 10^{-pH_n}}{n}\right) \tag{34}$$

$$R^{pH} = \frac{\left(10^{-pH_{sp}^{avg.}} - 10^{-pH_{rs}^{avg.}}\right) * H^+_{mw} * \frac{py_{mw}}{2*H^+_{mw}} * V_{rs}^{tot.} * \frac{7}{N_d}}{M_s} \tag{35}$$

$$py_{ox}^{SO_4^{2-}} = C_{SO_4^{2-}} * \frac{py_{mw}}{2*SO_4^{2-}{}_{mw}} * V_{rs} \tag{36}$$

$$R^{SO_4^{2-}} = \frac{C_{SO_4^{2-}}^{avg.} * \frac{py_{mw}}{2*SO_4^{2-}{}_{mw}} * V_{rs}^{tot.} * \frac{7}{N_d}}{M_s} \tag{37}$$

$$py_{ox}^{Fe} = C_{Fe} * \frac{py_{mw}}{Fe_{mw}} * V_{rs} \tag{38}$$

$$R^{Fe} = \frac{C_{Fe}^{avg.} * \frac{py_{mw}}{Fe_{mw}} * V_{rs}^{tot.} * \frac{7}{N_d}}{M_s} \tag{39}$$

$$n = \frac{P*V}{R*T} \tag{40}$$

$$m_{O_2} = \frac{V_{free} * \left(O_{2\,conc.}^{to} - O_{2\,conc.}^{tx}\right) * P_{t_x}}{R*T_{t_x}} * O_{2_{mw}} \tag{41}$$

$$py_{ox}^{O_2} = \frac{V_{free} * \left(O_{2\,conc.}^{to} - O_{2\,conc.}^{tx}\right) * P_{t_x}}{R*T_{t_x}} * O_{2_{mw}} * \frac{py_{mw}}{3.5O_{2\,mw}} \tag{42}$$

$$R^{O_2} = \frac{\frac{V_{free} * \left(O_{2\,conc.}^{to} - O_{2\,conc.}^{tx}\right) * P_{t_x}}{R*T_{t_x}} * O_{2_{mw}} * \frac{py_{mw}}{3.5O_{2\,mw}} * \frac{7}{N_d}}{M_s} \tag{43}$$

DOI: 10.14750/ME.2021.004

MINERALOGICAL DATA SHEETS

DOI: 10.14750/ME.2021.004

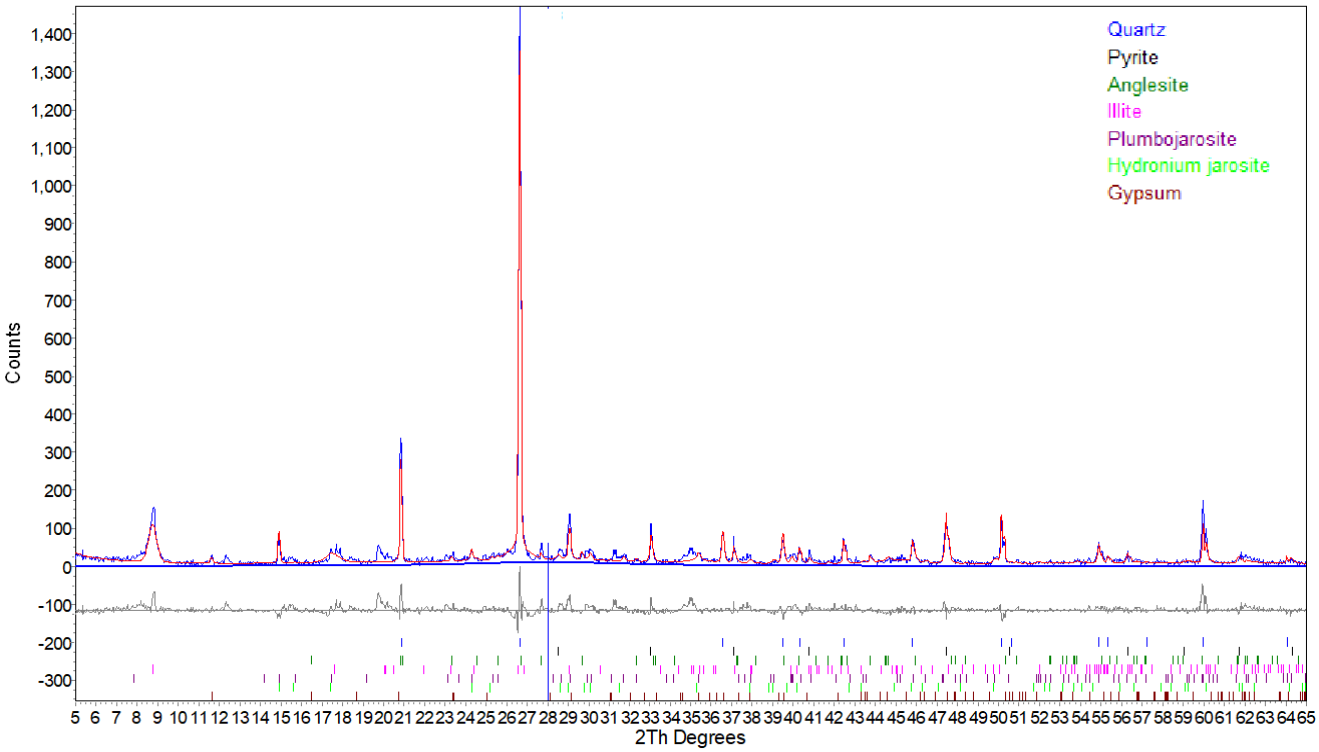

X-ray diffractogram evaluation with Rietveld refinement of the sample Jalpha 1-7

Mineral	***Formula***	$^{m}/_{m}\%$
Quartz	SiO_2	59.0
Pyrite	FeS_2	5.0
Illite	$(K;H_3O)Al_2Si_3AlO_{10}(OH)_2$	12.8
Hydronium jarosite	$(H_3O)Fe_3(SO_4)_2(OH)_6$	0.1
Plumbojarosite	$PbFe_6(SO_4)_4(OH)_{12}$	3.6
Anglesite	$PbSO_4$	0.8
Gypsum	$CaSO_4*2H_2O$	0.7
Kaolinite	$Al_2(Si_2O_5)(OH)_4$	ind.
Chalcopyrite	$CuFeS_2$	ind.
Amorphous components		18.0

Quantitative mineralogical composition of the sample Jalpha-01

DOI: 10.14750/ME.2021.004

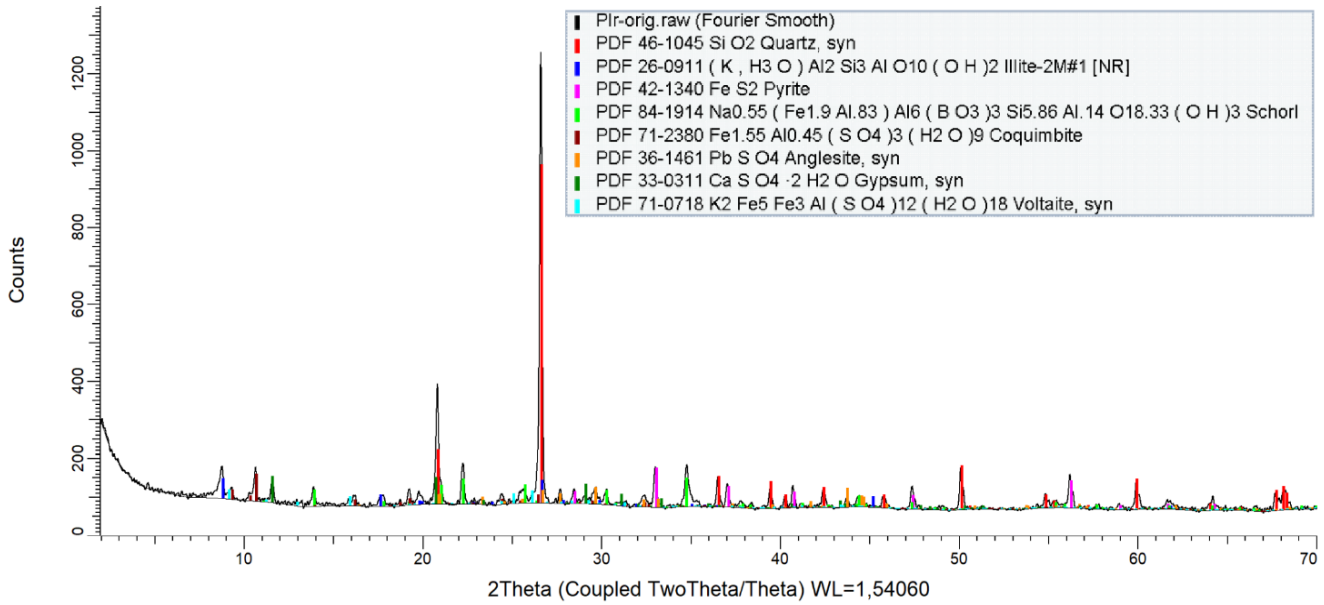

X-ray diffractogram with the identified phases of the sample Playa Iroco 1-7

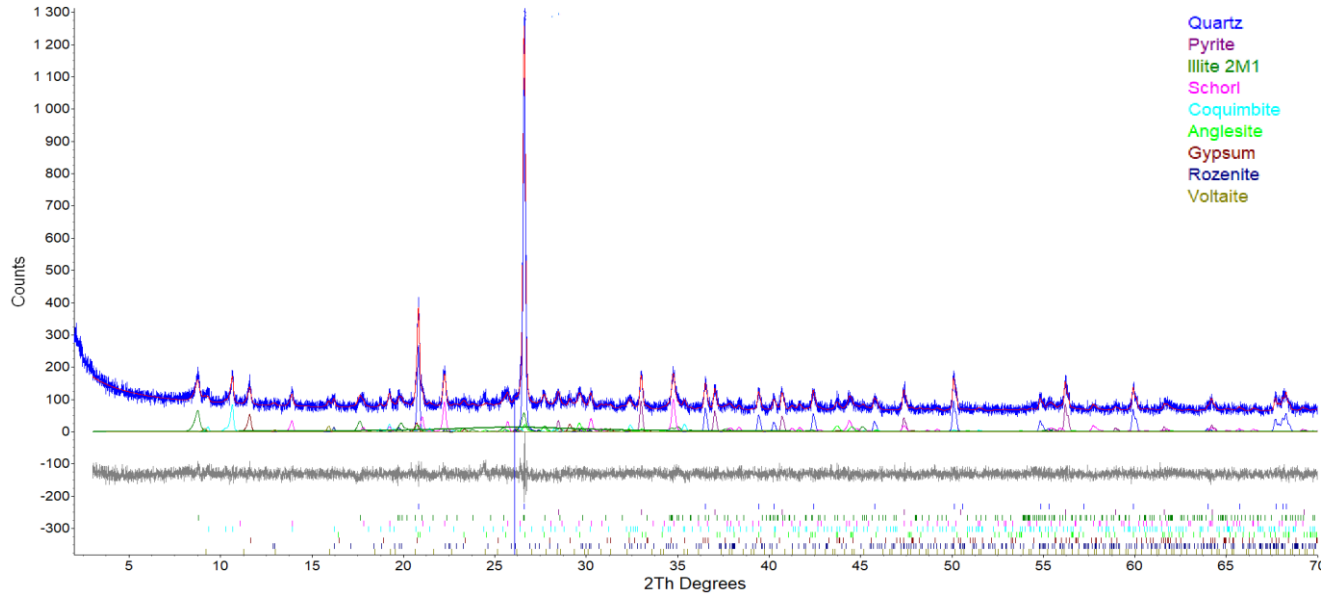

X-ray diffractogram evaluation with Rietveld refinement of the sample Playa Iroco 1-7

Mineral	***Formula***	$^{m}/_{m}\%$
Quartz	SiO_2	33.2
Pyrite	FeS_2	5.3
Illite	$(K;H_3O)Al_2Si_3AlO_{10}(OH)_2$	17.2
Dravite (schorl)	$Na(Mg_3)Al_6(Si_6O_{18})(BO_3)_3(OH)_4$	20.7
Anglesite	$PbSO_4$	1.4
Gypsum	$CaSO_4*2H_2O$	3.0
Coquimbite	$AlFe_3(SO_4)_6(H_2O)_{12}*6H_2O$	2.2
Rozenite	$FeSO_4*4H_2O$	1.6
Voltaite	$K_2Fe_8Al(SO_4)_{12}*18H_2O$	1.9
Amorphous components		13.5

Quantitative mineralogical composition of the sample Playa Iroco 1-7

DOI: 10.14750/ME.2021.004

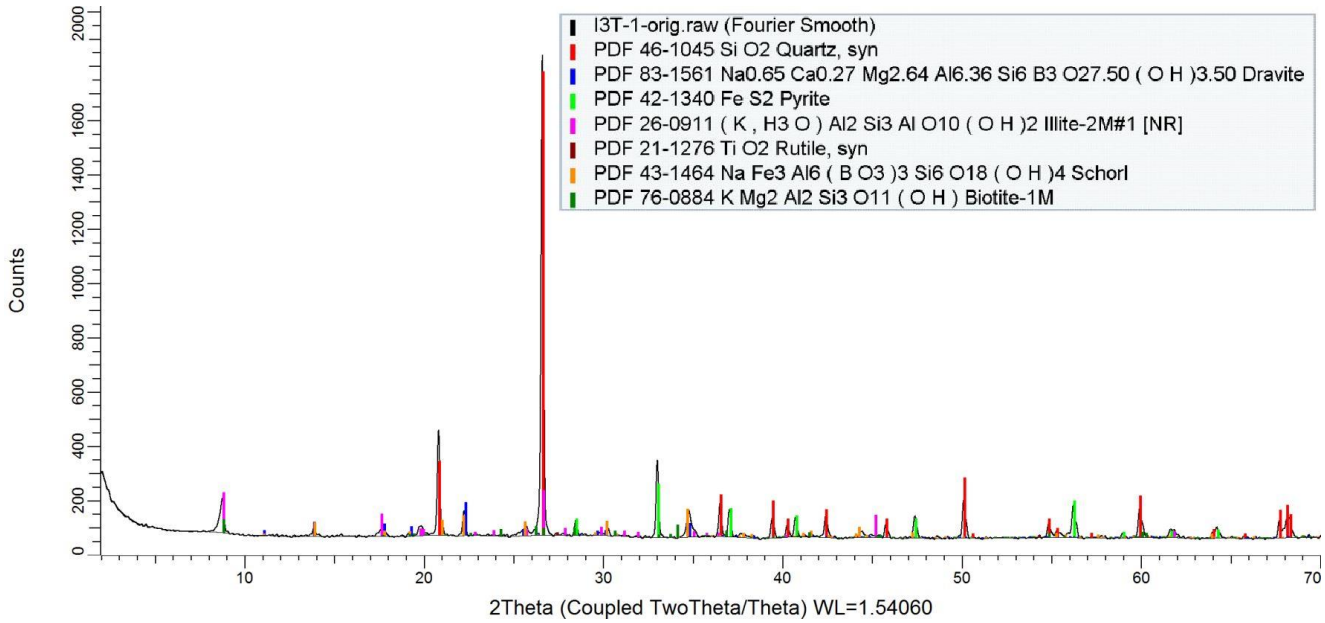

X-ray diffractogram with the identified phases of the sample Itos Jig 1-7

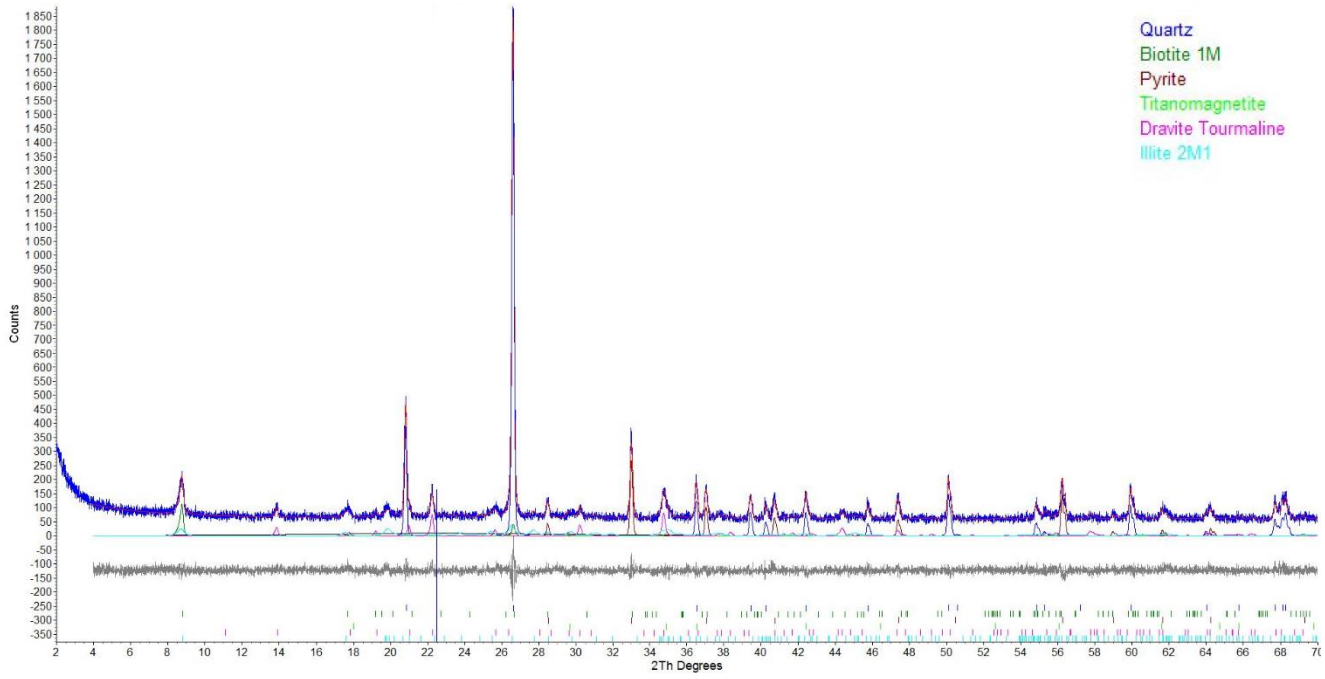

X-ray diffractogram evaluation with Rietveld refinement of the sample Itos Jig 1-7

Mineral	***Formula***	$^{m}/_{m}\%$
Quartz	SiO_2	44.1
Pyrite	FeS_2	6.8
Illite	$(K;H_3O)Al_2Si_3AlO_{10}(OH)_2$	19.2
Biotite	$K(Mg,Fe)_3AlSi_3O_{10}(OH)_2$	0.9
Titanomagnetite	$(Fe,Ti)_3O_4$	0.5
Dravite (schorl)	$Na(Mg_3)Al_6(Si_6O_{18})(BO_3)_3(OH)_4$	14.5
Amorphous components		14.0

Quantitative mineralogical composition of the sample Jig 1-7

DOI: 10.14750/ME.2021.004

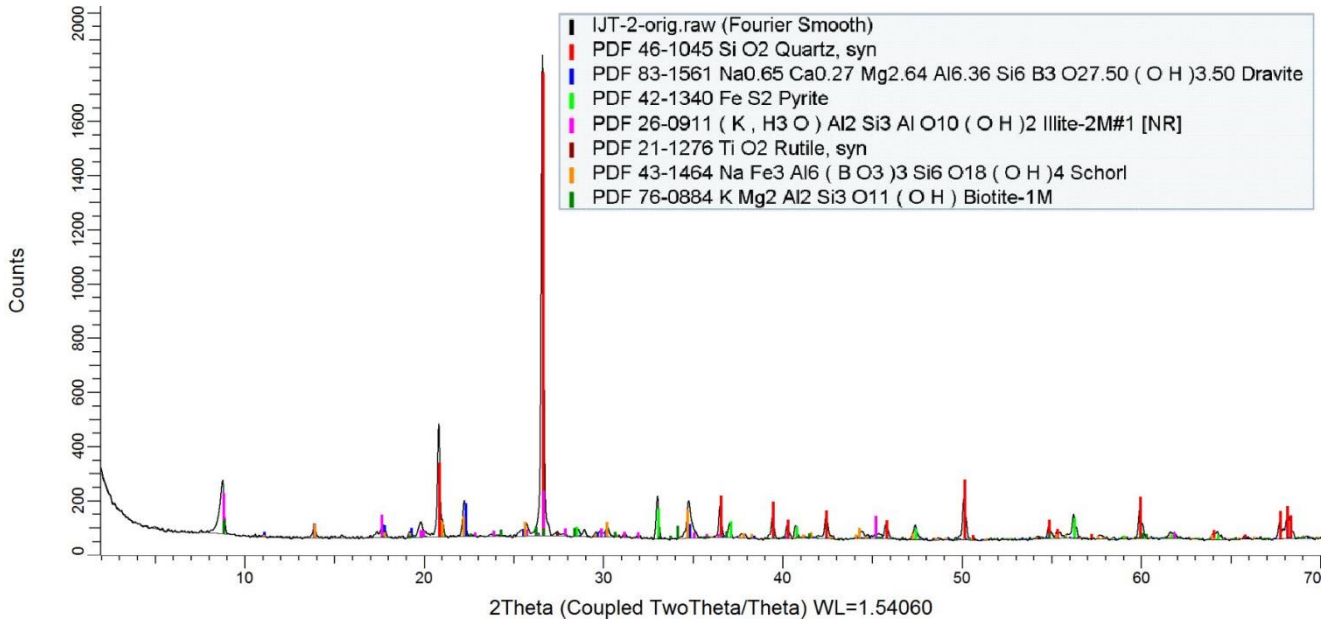

X-ray diffractogram with the identified phases of the sample Itos Jig 2-7

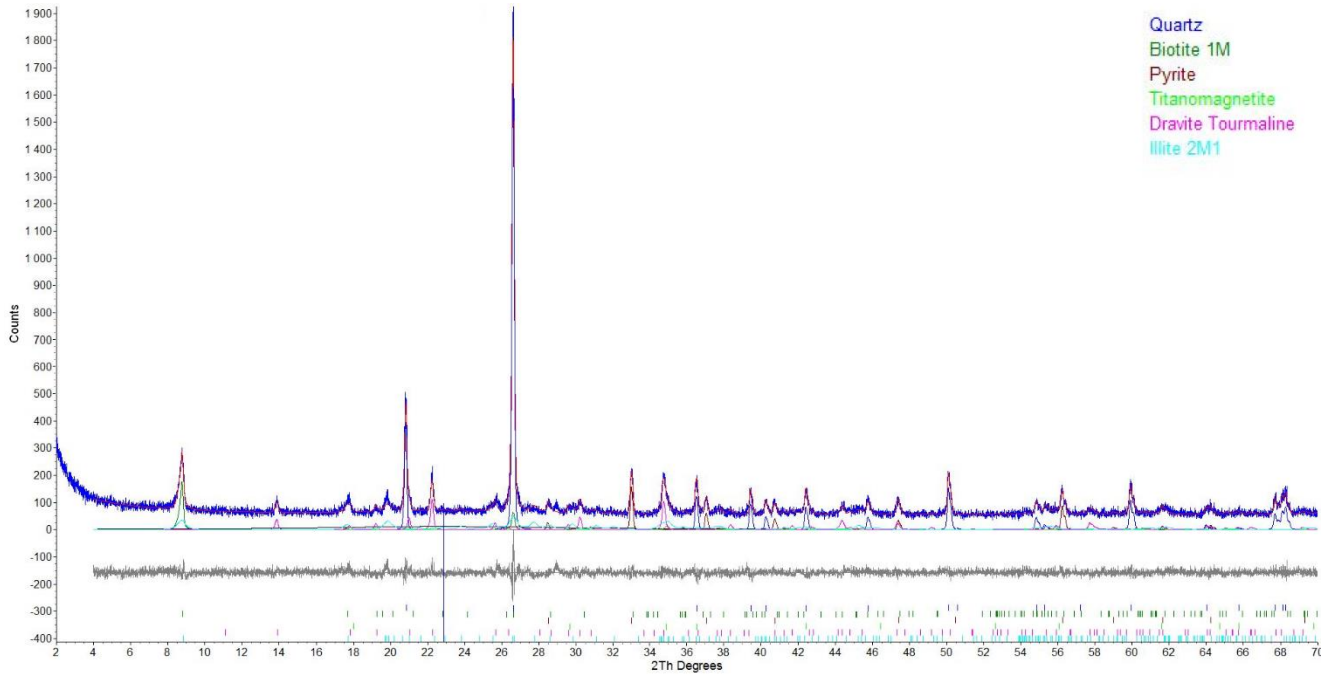

X-ray diffractogram evaluation with Rietveld refinement of the sample Itos Jig 2-7

Mineral	***Formula***	$^{m}/_{m}\%$
Quartz	SiO_2	39.9
Pyrite	FeS_2	3.6
Illite	$(K;H_3O)Al_2Si_3AlO_{10}(OH)_2$	24.3
Biotite	$K(Mg,Fe)_3AlSi_3O_{10}(OH)_2$	0.9
Titanomagnetite	$(Fe,Ti)_3O_4$	0.5
Dravite (schorl)	$Na(Mg_3)Al_6(Si_6O_{18})(BO_3)_3(OH)_4$	15.8
Amorphous components		15.0

Quantitative mineralogical composition of the sample Itos Jig 2-7

DOI: 10.14750/ME.2021.004

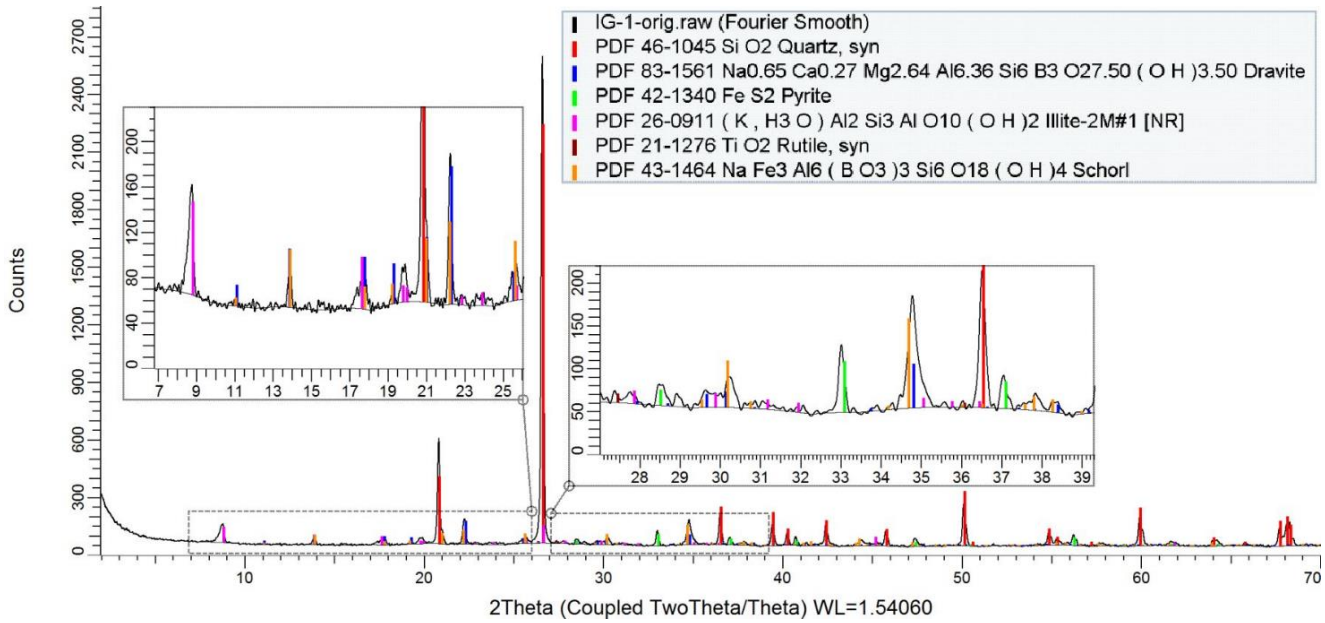

X-ray diffractogram with the identified phases of the sample Itos Granza 1-7

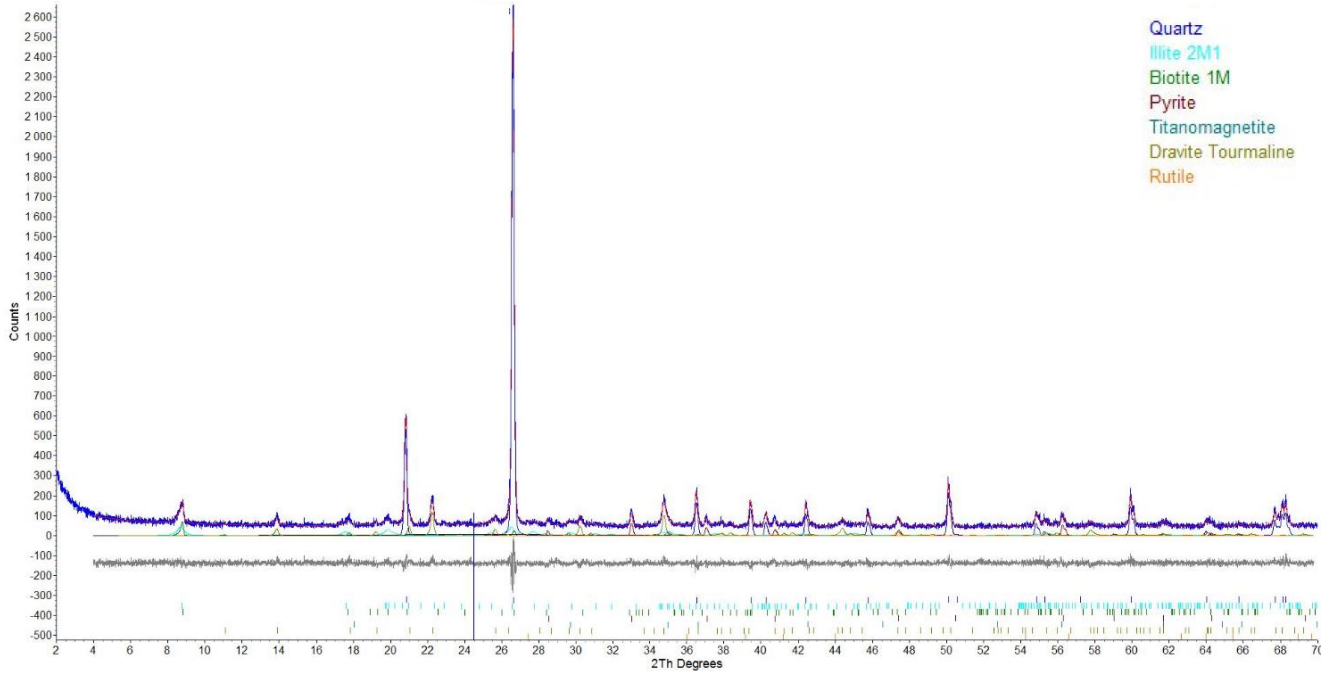

X-ray diffractogram evaluation with Rietveld refinement of the sample Itos Granza 1-7

Mineral	***Formula***	$^{m}/_{m}\%$
Quartz	SiO_2	53.3
Pyrite	FeS_2	2.4
Illite	$(K;H_3O)Al_2Si_3AlO_{10}(OH)_2$	16.1
Biotite	$K(Mg,Fe)_3AlSi_3O_{10}(OH)_2$	0.5
Titanomagnetite	$(Fe,Ti)_3O_4$	0.7
Dravite (schorl)	$Na(Mg_3)Al_6(Si_6O_{18})(BO_3)_3(OH)_4$	14.8
Rutile	TiO_2	0.2
Amorphous components		12.0

Quantitative mineralogical composition of the sample Itos Granza 1-7

DOI: 10.14750/ME.2021.004

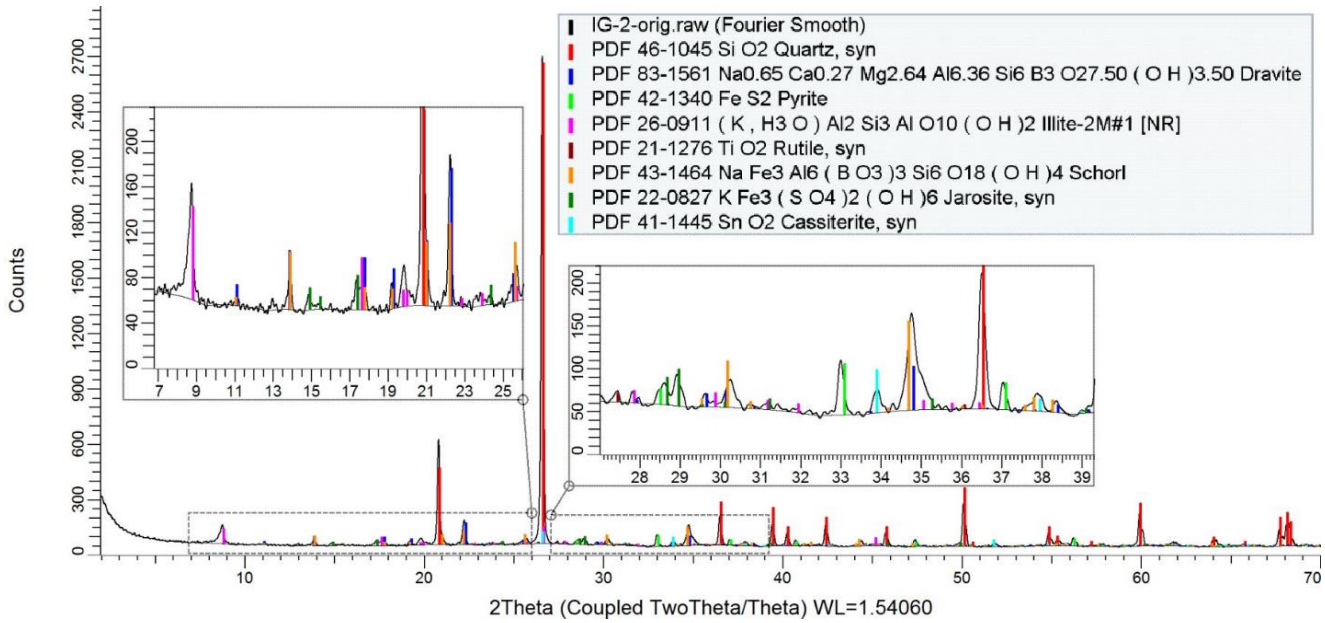

X-ray diffractogram with the identified phases of the sample Itos Granza 2-7

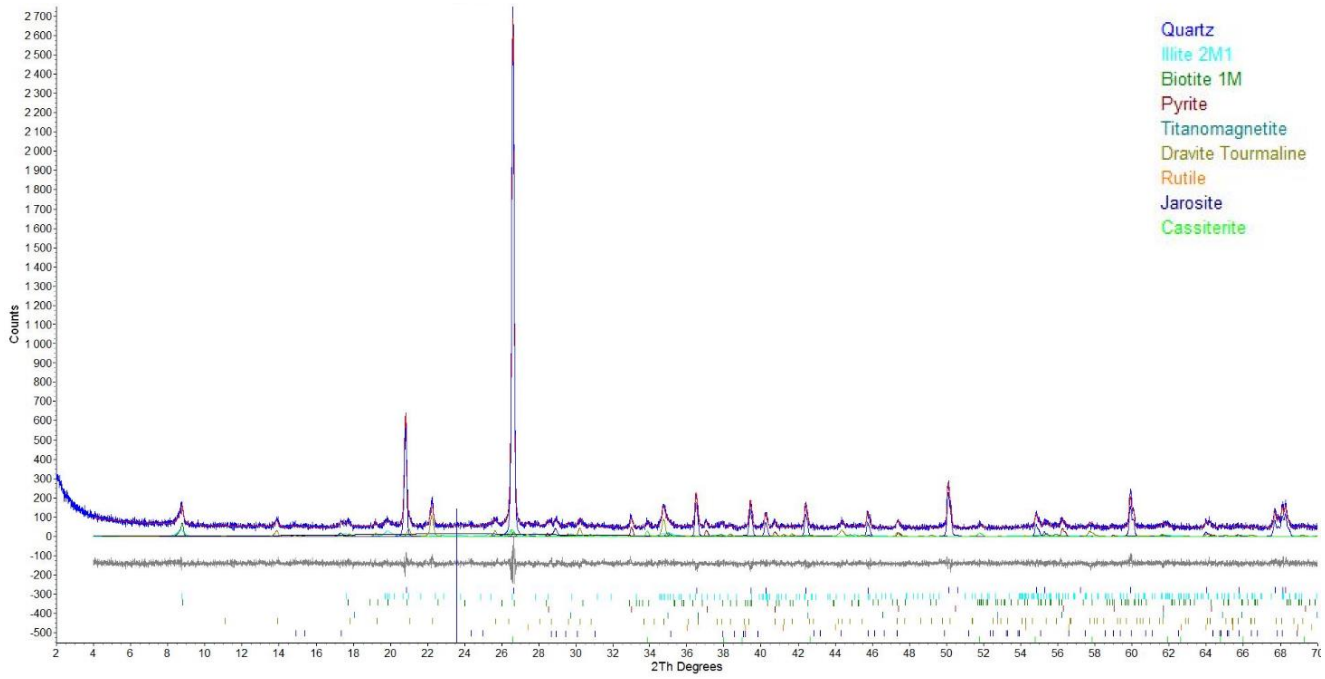

X-ray diffractogram evaluation with Rietveld refinement of the sample Itos Granza 2-7

Mineral	***Formula***	$^{m}/_{m}\%$
Quartz	SiO_2	54.1
Pyrite	FeS_2	1.7
Illite	$(K;H_3O)Al_2Si_3AlO_{10}(OH)_2$	13.1
Biotite	$K(Mg,Fe)_3AlSi_3O_{10}(OH)_2$	0.5
Titanomagnetite	$(Fe,Ti)_3O_4$	0.7
Dravite (schorl)	$Na(Mg_3)Al_6(Si_6O_{18})(BO_3)_3(OH)_4$	12.9
Rutile	TiO_2	0.3
Cassiterite	SnO_2	0.4
Jarosite	$KFe_3(SO_4)_2(OH)_6$	1.3
Amorphous components		15.0

Quantitative mineralogical composition of the sample Itos Granza 2-7

DOI: 10.14750/ME.2021.004

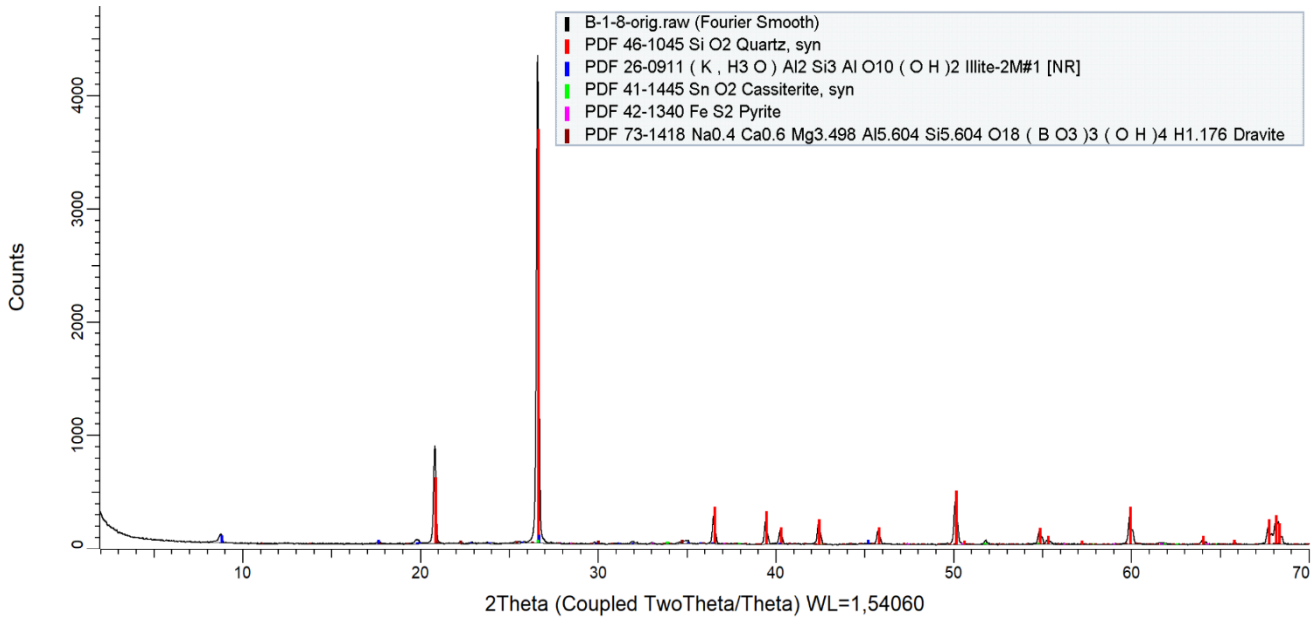

X-ray diffractogram with the identified phases of the sample BOL 1-8

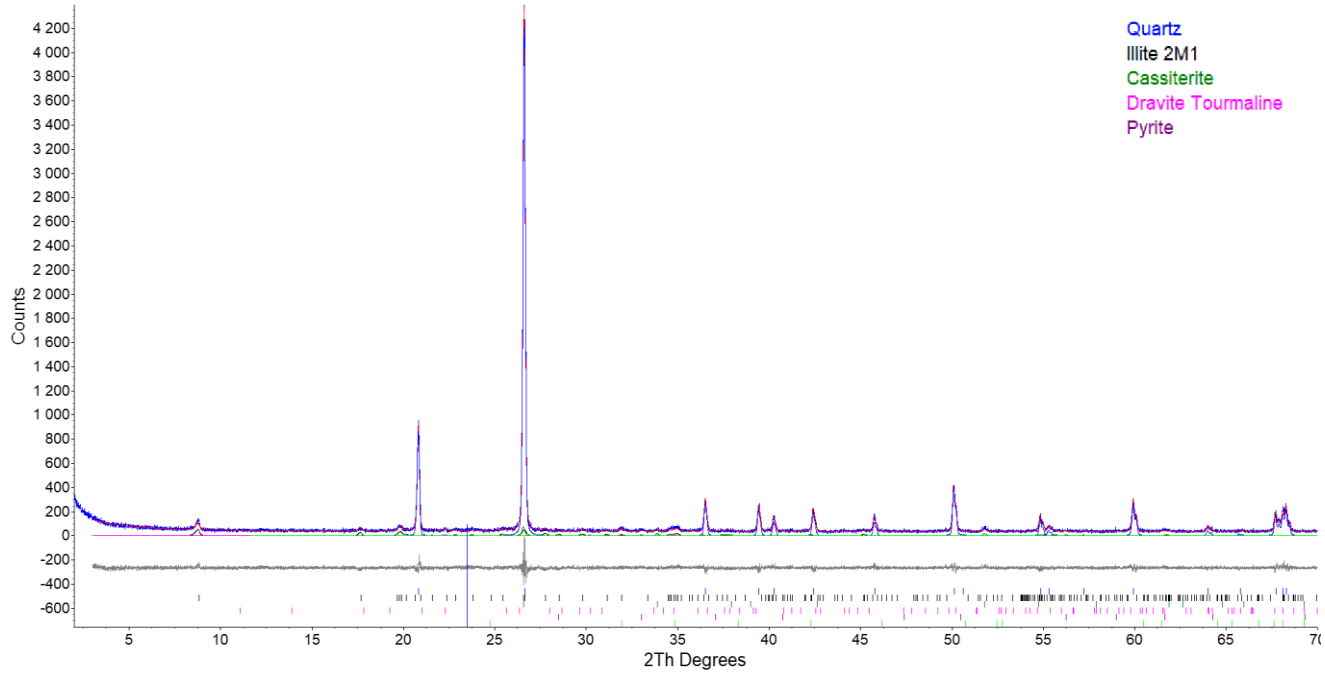

X-ray diffractogram evaluation with Rietveld refinement of the sample BOL 1-8

Mineral	***Formula***	$^{m}/_{m}\%$
Quartz	SiO_2	82.7
Illite	$(K;H_3O)Al_2Si_3AlO_{10}(OH)_2$	10.8
Cassiterite	SnO_2	0.4
Dravite (schorl)	$Na(Mg_3)Al_6(Si_6O_{18})(BO_3)_3(OH)_4$	2.7
Pyrite	FeS_2	0.4
Amorphous components		3

Quantitative mineralogical composition of the sample BOL 1-8

DOI: 10.14750/ME.2021.004

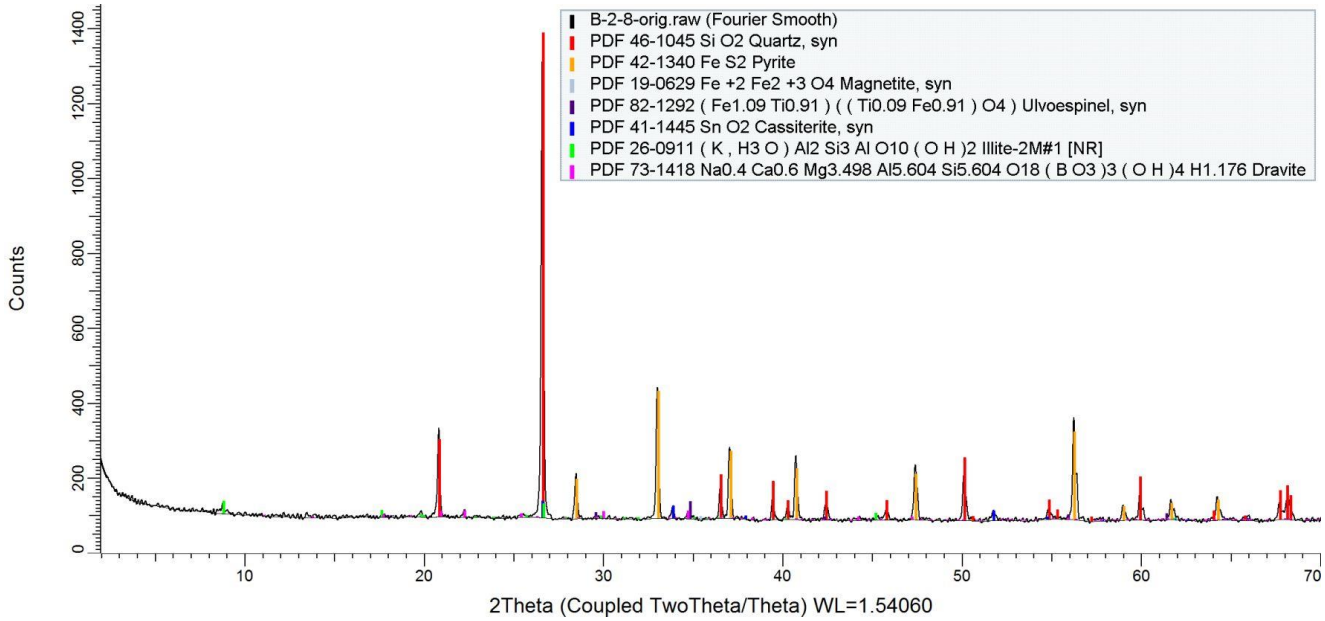

X-ray diffractogram with the identified phases of the sample BOL 2-8

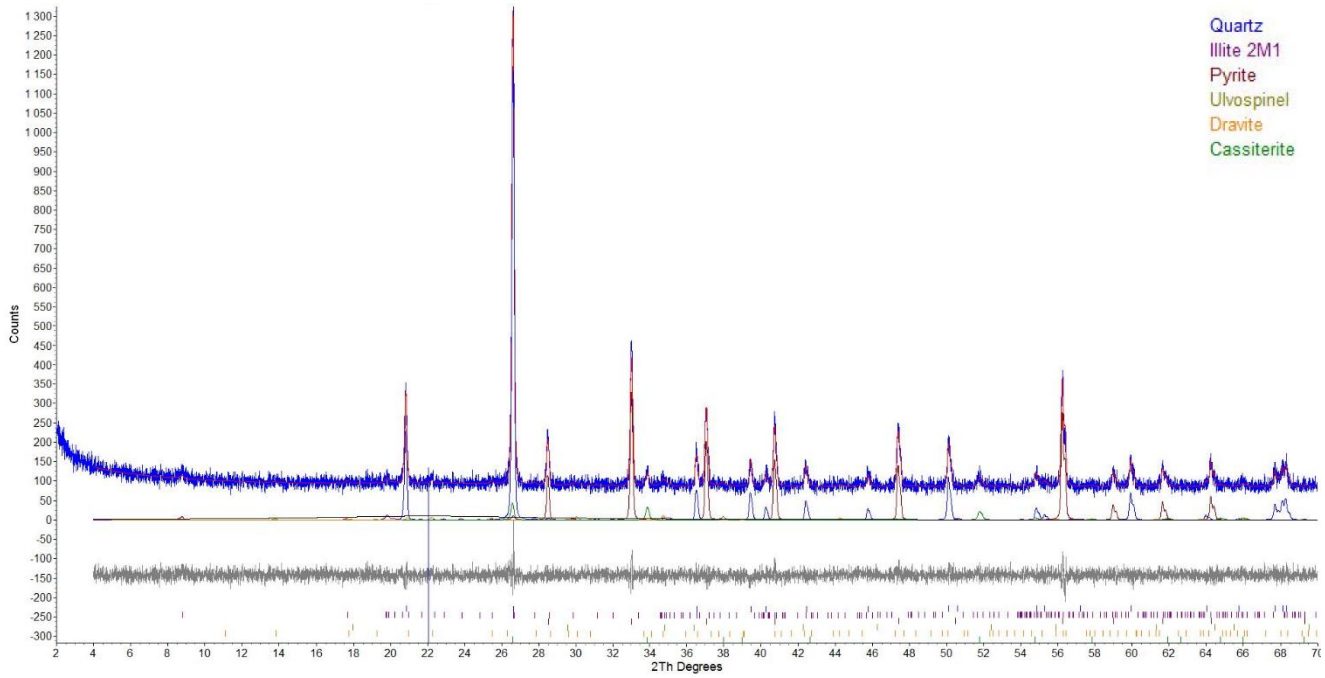

X-ray diffractogram evaluation with Rietveld refinement of the sample BOL 2-8

Mineral	***Formula***	$^{m}/_{m}\%$
Quartz	SiO_2	48.8
Illite	$(K;H_3O)Al_2Si_3AlO_{10}(OH)_2$	5.3
Pyrite	FeS_2	21.0
Ulvospinel	$TiFe_2O_4$	0.3
Dravite (schorl)	$Na(Mg_3)Al_6(Si_6O_{18})(BO_3)_3(OH)_4$	3.6
Cassiterite	SnO_2	1.1
Amorphous components		19.9

Quantitative mineralogical composition of the sample BOL 2-8

DOI: 10.14750/ME.2021.004

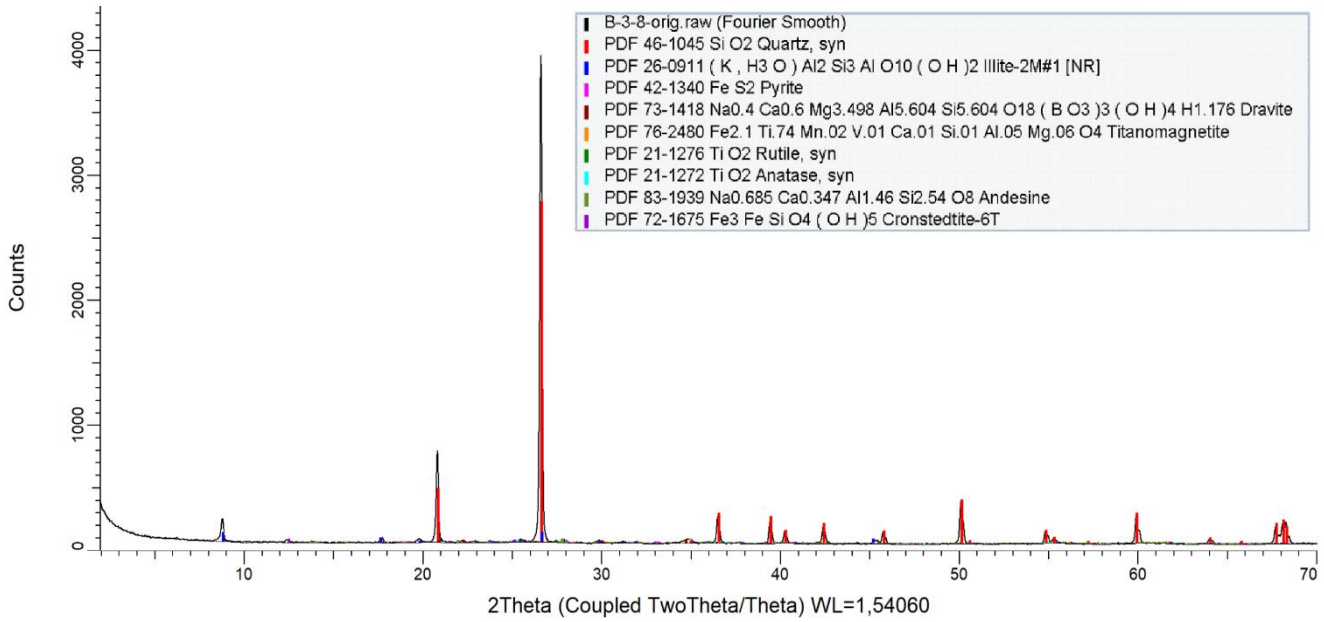

X-ray diffractogram with the identified phases of the sample BOL 3-8

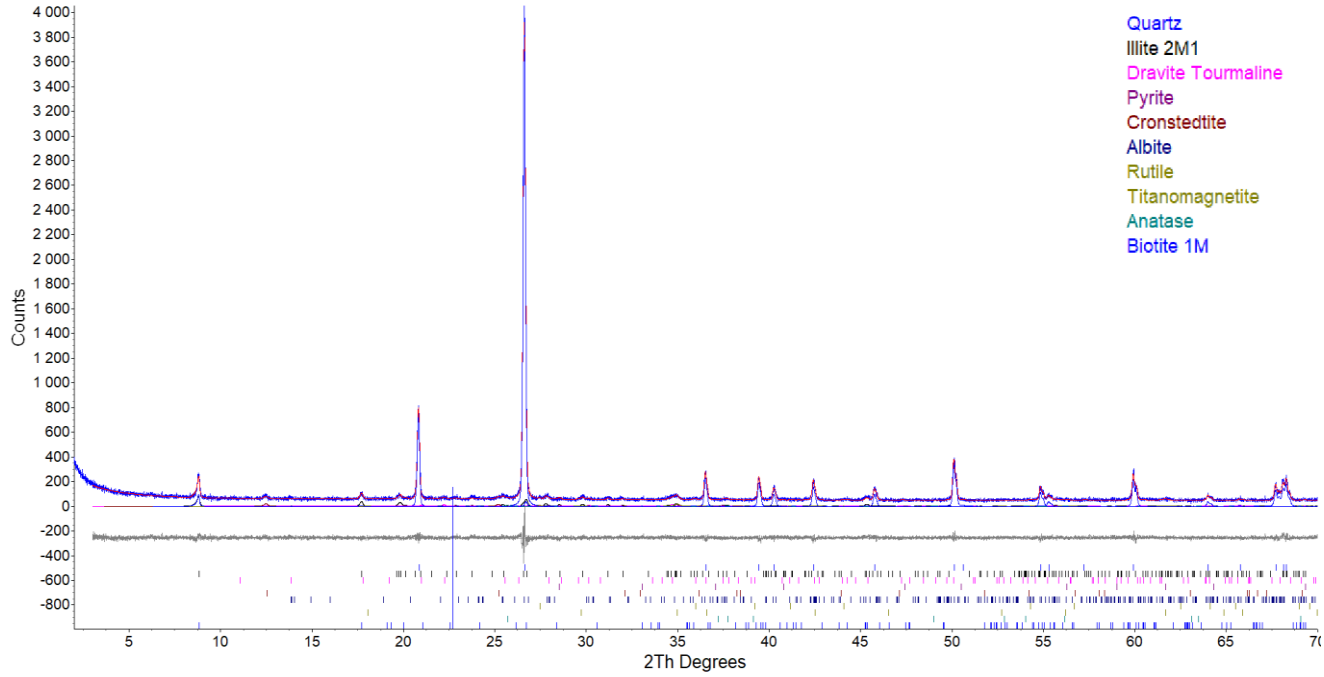

X-ray diffractogram evaluation with Rietveld refinement of the sample BOL 3-8

Mineral	***Formula***	$^{m}/_{m}\%$
Quartz	SiO_2	79.7
Illite	$(K;H_3O)Al_2Si_3AlO_{10}(OH)_2$	10.1
Dravite (schorl)	$Na(Mg_3)Al_6(Si_6O_{18})(BO_3)_3(OH)_4$	3.0
Pyrite	FeS_2	0.1
Cronstedtite	$Fe_4SiO_5(OH)_4$	0.2
Albite	$NaAlSi_3O_8$	0.6
Rutile	TiO_2	0.3
Titanomagnetite	$(Fe,Ti)_3O_4$	0.9
Anatase	TiO_2	0.2
Biotite	$K(Mg,Fe)_3AlSi_3O_{10}(OH)_2$	0.5
Amorphous components		4.4

Quantitative mineralogical composition of the sample BOL 3-8

DOI: 10.14750/ME.2021.004

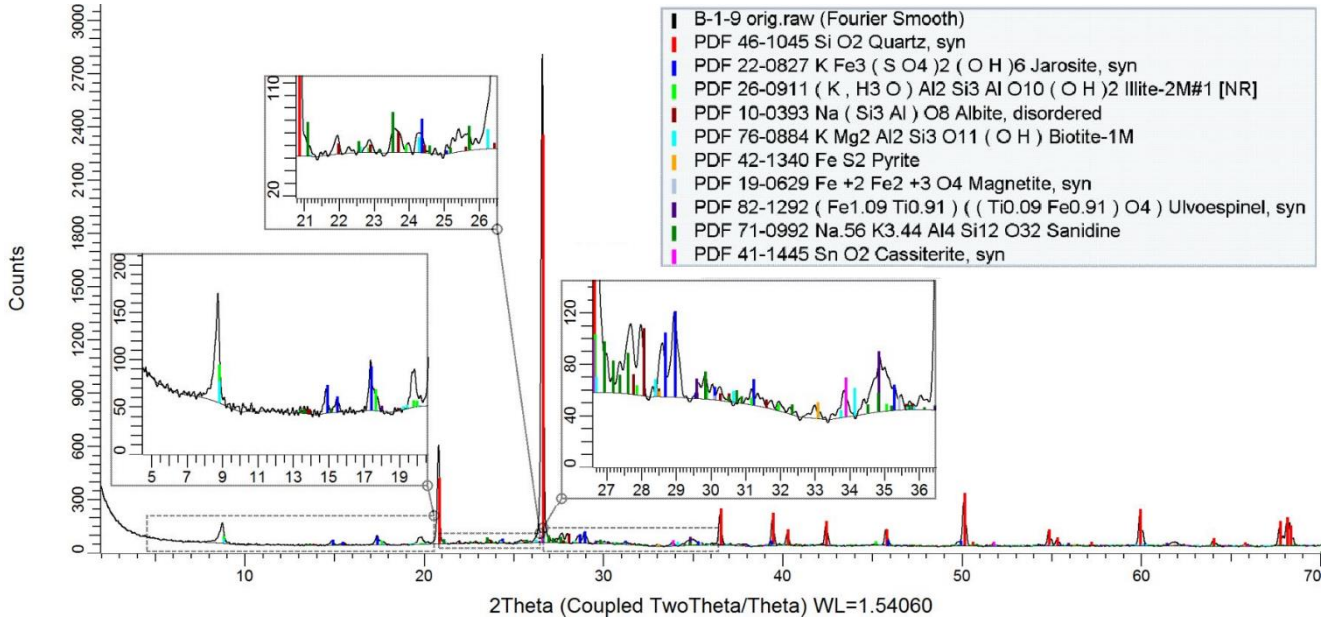

X-ray diffractogram with the identified phases of the sample BOL 1-9

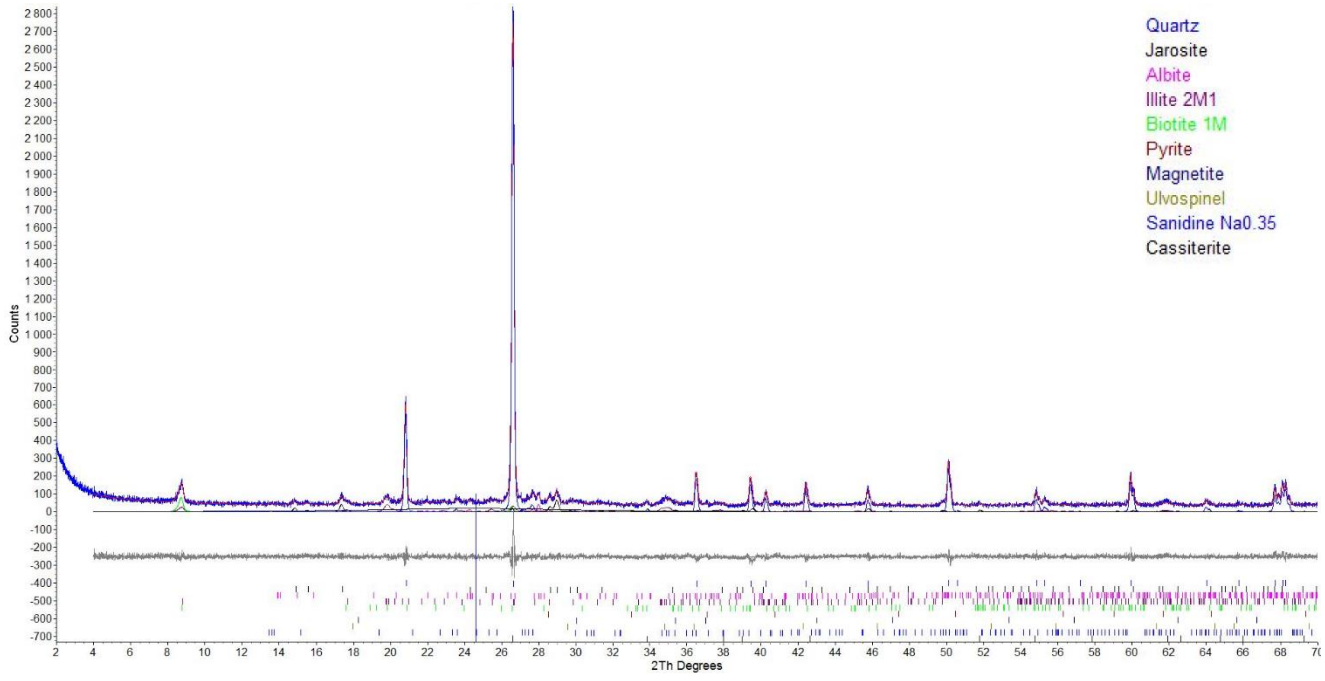

X-ray diffractogram evaluation with Rietveld refinement of the sample BOL 1-9

Mineral	***Formula***	$^{m}/_{m}\%$
Quartz	SiO_2	56.7
Jarosite	$KFe_3(SO_4)_2(OH)_6$	3.1
Albite	$NaAlSi_3O_8$	1.9
Illite	$(K;H_3O)Al_2Si_3AlO_{10}(OH)_2$	13.5
Biotite	$K(Mg,Fe)_3AlSi_3O_{10}(OH)_2$	1.1
Pyrite	FeS_2	0.2
Magnetite	Fe_3O_4	0.5
Ulvospinel	$TiFe_2O_4$	0.5
Grossularia	$Ca_3Al_2(SiO_4)_3$	2.3
Sanidine (Na0.35)	$K_{0.65}Na_{0.35}AlSi_3O_8$	0.2
Amorphous components		20.0

Quantitative mineralogical composition of the sample BOL 1-9

DOI: 10.14750/ME.2021.004

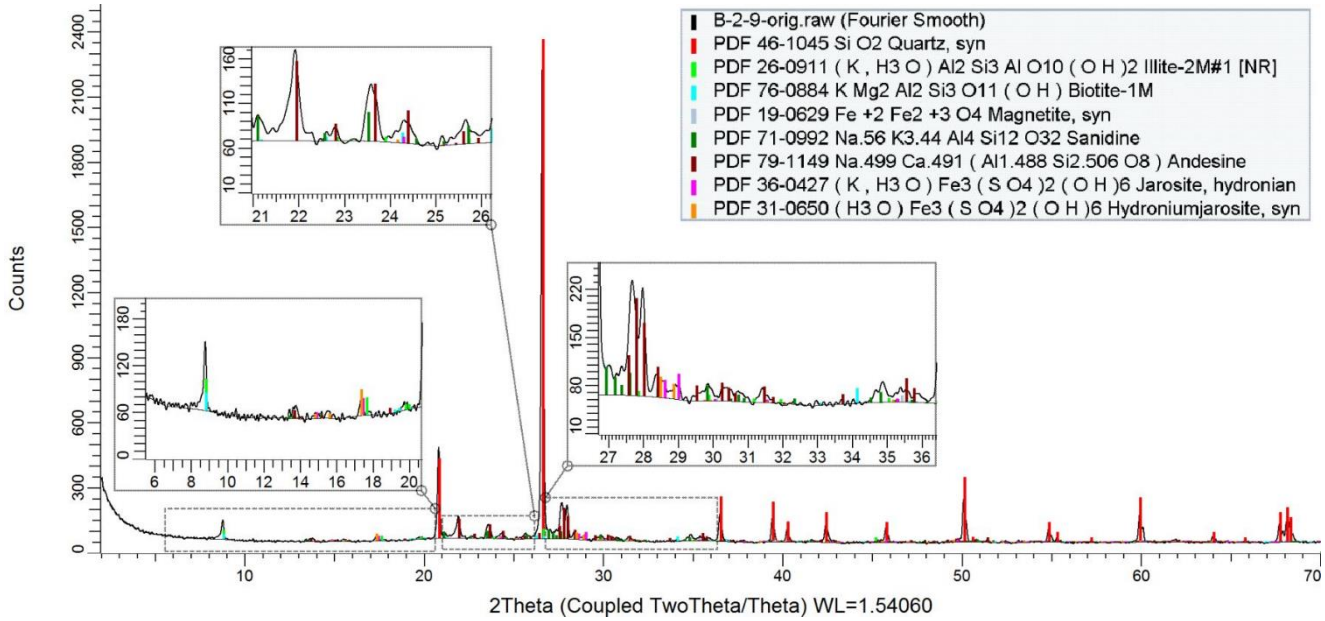

X-ray diffractogram with the identified phases of the sample BOL 2-9

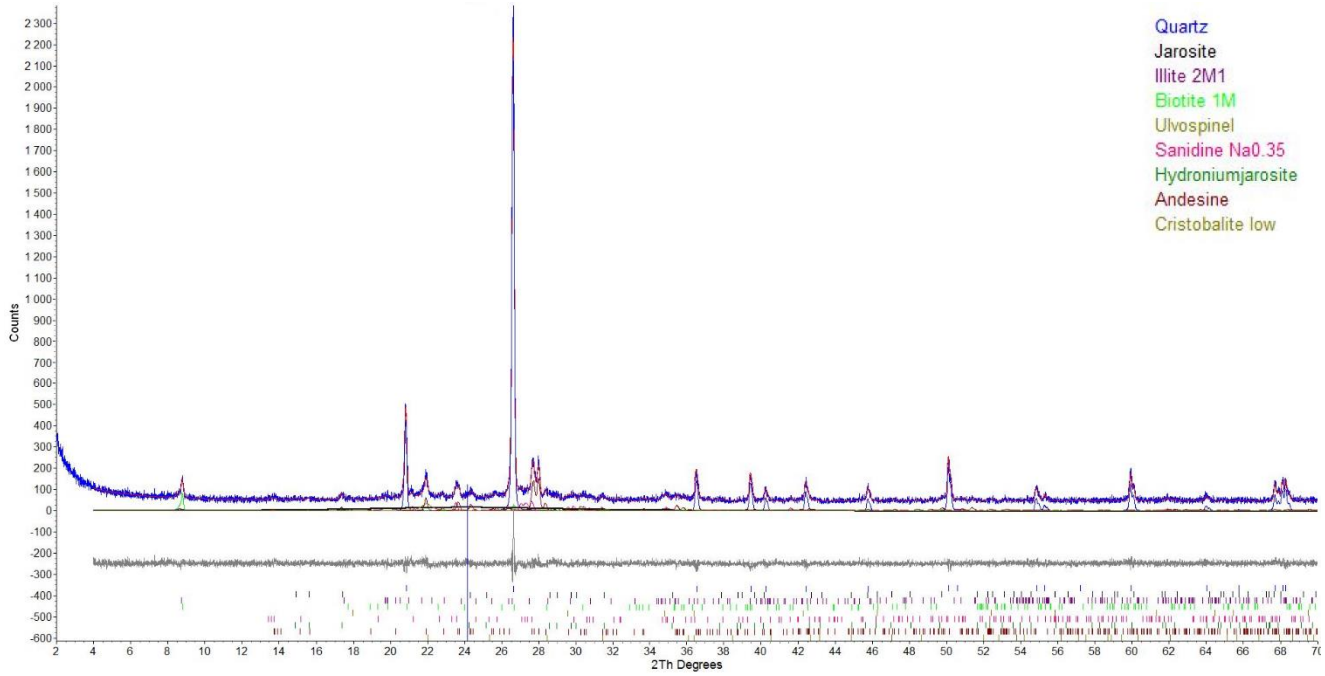

X-ray diffractogram evaluation with Rietveld refinement of the sample BOL 2-9

Mineral	***Formula***	$^{m}/_{m}\%$
Quartz	SiO_2	46.2
Jarosite	$KFe_3(SO_4)_2(OH)_6$	1.0
Illite	$(K;H_3O)Al_2Si_3AlO_{10}(OH)_2$	7.1
Biotite	$K(Mg,Fe)_3AlSi_3O_{10}(OH)_2$	0.7
Ulvospinel	$TiFe_2O_4$	0.5
Sanidine Na0.35	$K_{0.65}Na_{0.35}AlSi_3O_8$	6.6
Hydroniumjarosite	$(H_3O)Fe_3(SO_4)_2(OH)_6$	0.2
Andesine	$Na_{0.6}Ca_{0.4}(Al,Si)_4O_8$	14.3
Cristobalite	SiO_2	3.4
Amorphous components		20.0

Quantitative mineralogical composition of the sample BOL 2-9

DOI: 10.14750/ME.2021.004

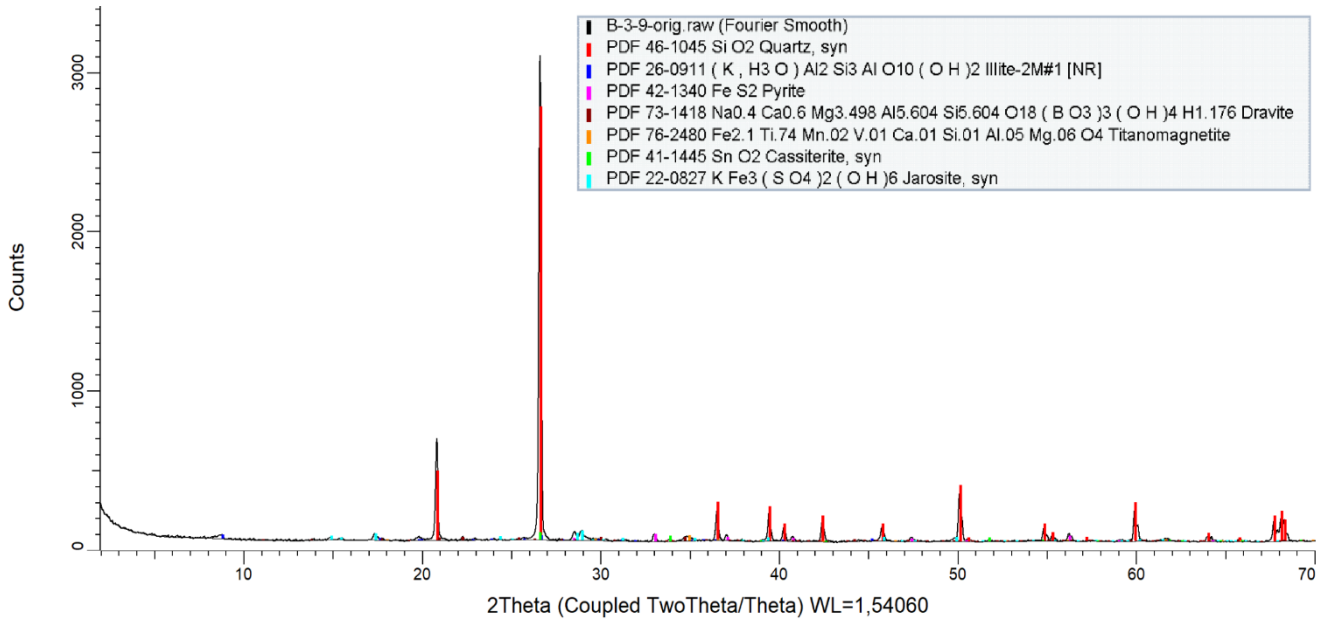

X-ray diffractogram with the identified phases of the sample BOL 3-9

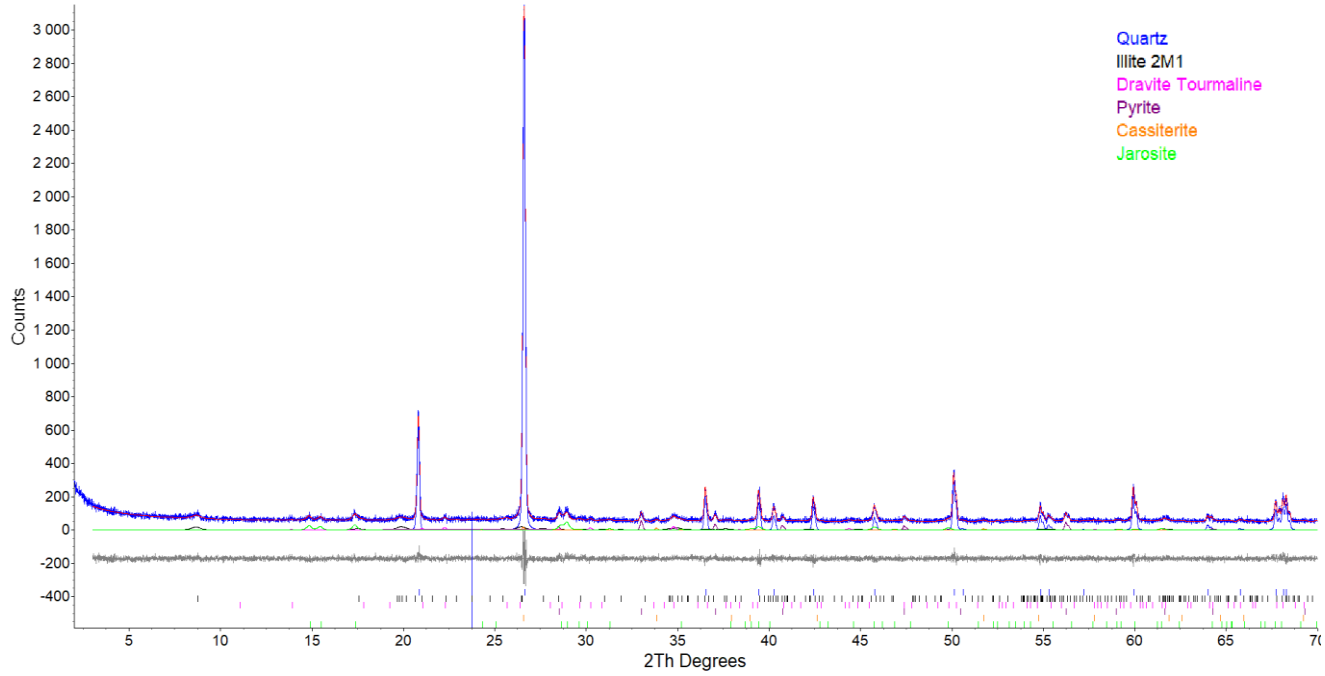

X-ray diffractogram evaluation with Rietveld refinement of the sample BOL 3-9

Mineral	***Formula***	$^{m}/_{m}\%$
Quartz	SiO_2	68.4
Illite	$(K;H_3O)Al_2Si_3AlO_{10}(OH)_2$	13.0
Dravite (schorl)	$Na(Mg_3)Al_6(Si_6O_{18})(BO_3)_3(OH)_4$	4.5
Pyrite	FeS_2	2.4
Cassiterite	SnO_2	0.2
Jarosite	$KFe_3(SO_4)_2(OH)_6$	5.6
Amorphous components		5.9

Quantitative mineralogical composition of the sample BOL 3-9

DOI: 10.14750/ME.2021.004

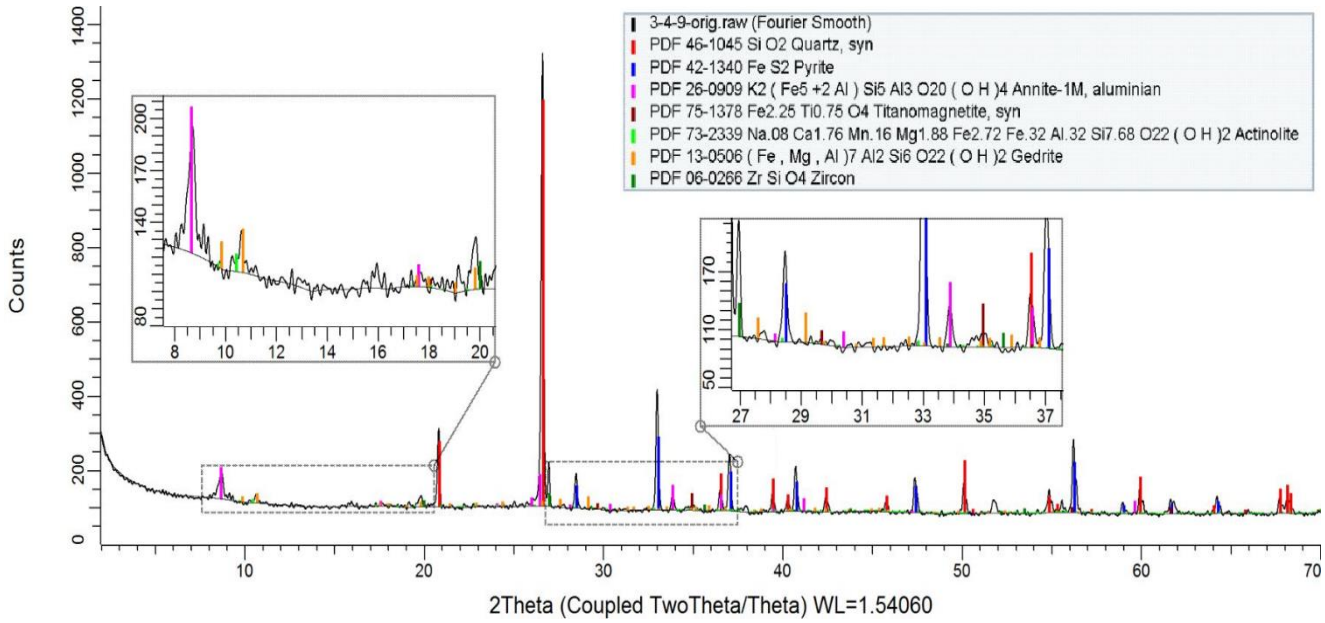

X-ray diffractogram with the identified phases of the sample BOL 4-9

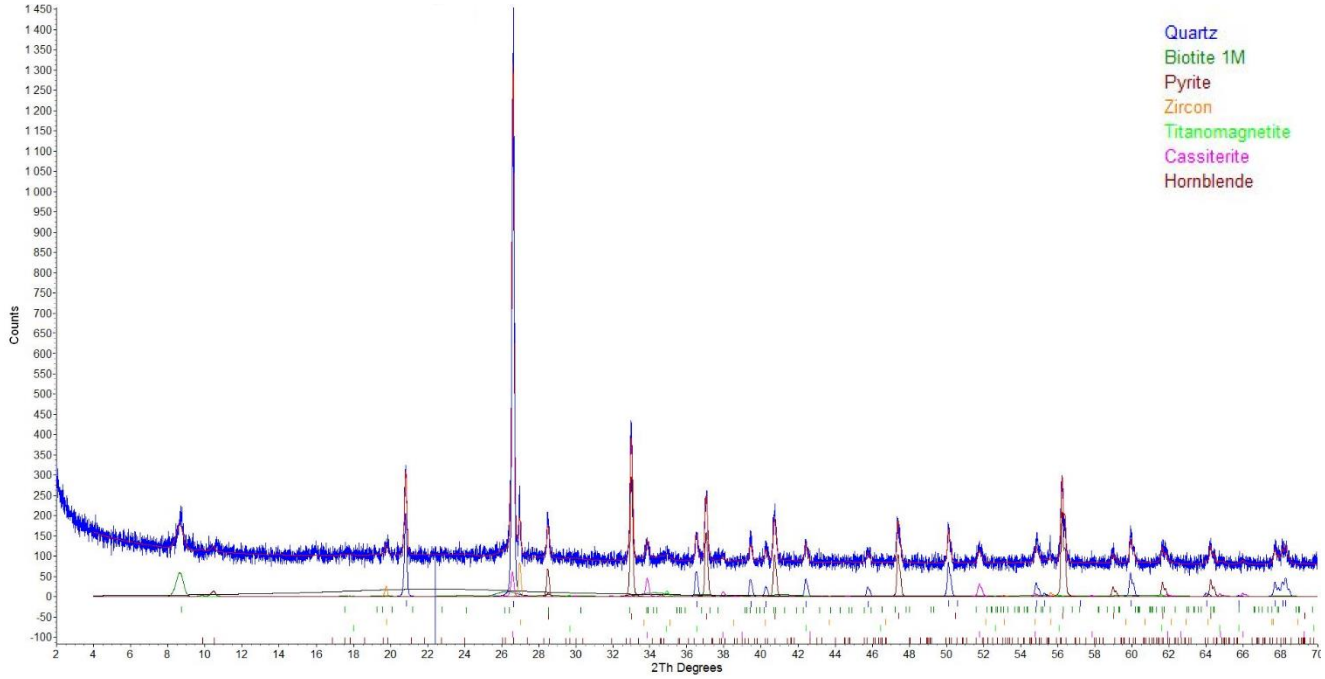

X-ray diffractogram evaluation with Rietveld refinement of the sample BOL 4-9

Mineral	***Formula***	$^{m}/_{m}\%$
Quartz	SiO_2	36.4
Biotite	$K(Mg,Fe)_3AlSi_3O_{10}(OH)_2$	13.1
Pyrite	FeS_2	15.2
Zircon	$ZrSiO_4$	0.3
Titanomagnetite	$(Fe,Ti)_3O_4$	0.9
Cassiterite	SnO_2	1.3
Hornblende	$Ca_2Mg_4(Al,Fe)Si_7AlO_{22}(OH)_2$	2.9
Amorphous components		29.9

Quantitative mineralogical composition of the sample BOL 4-9

DOI: 10.14750/ME.2021.004

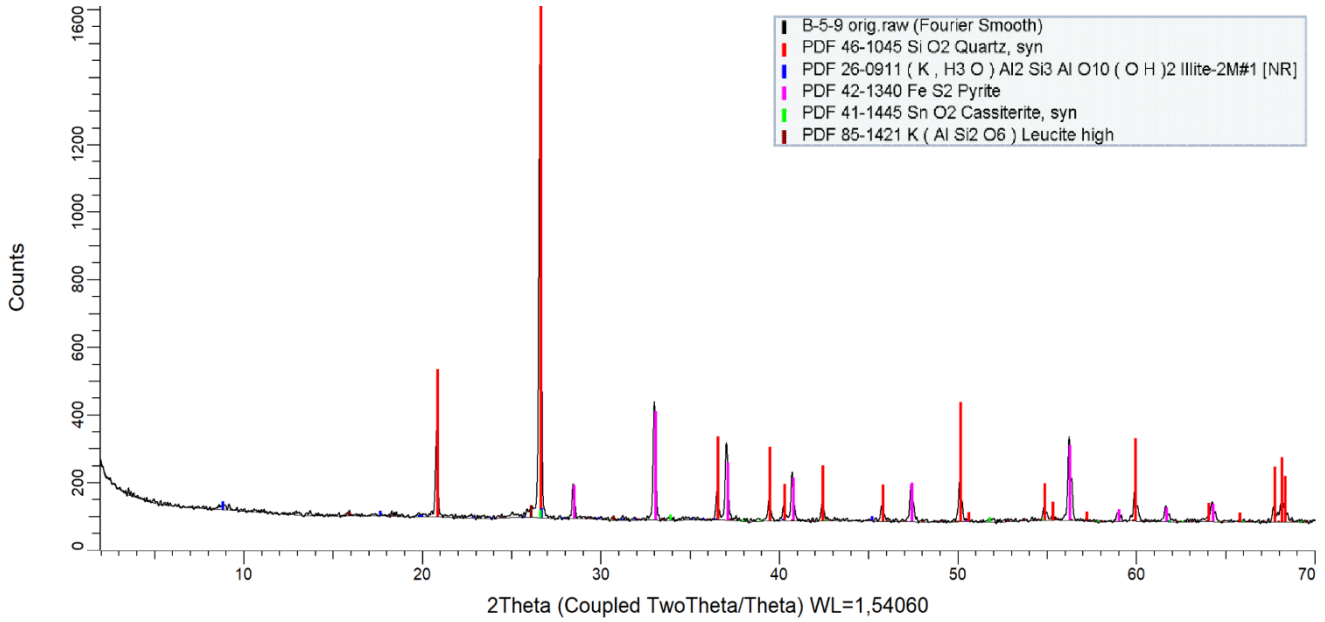

X-ray diffractogram with the identified phases of the sample BOL 5-9

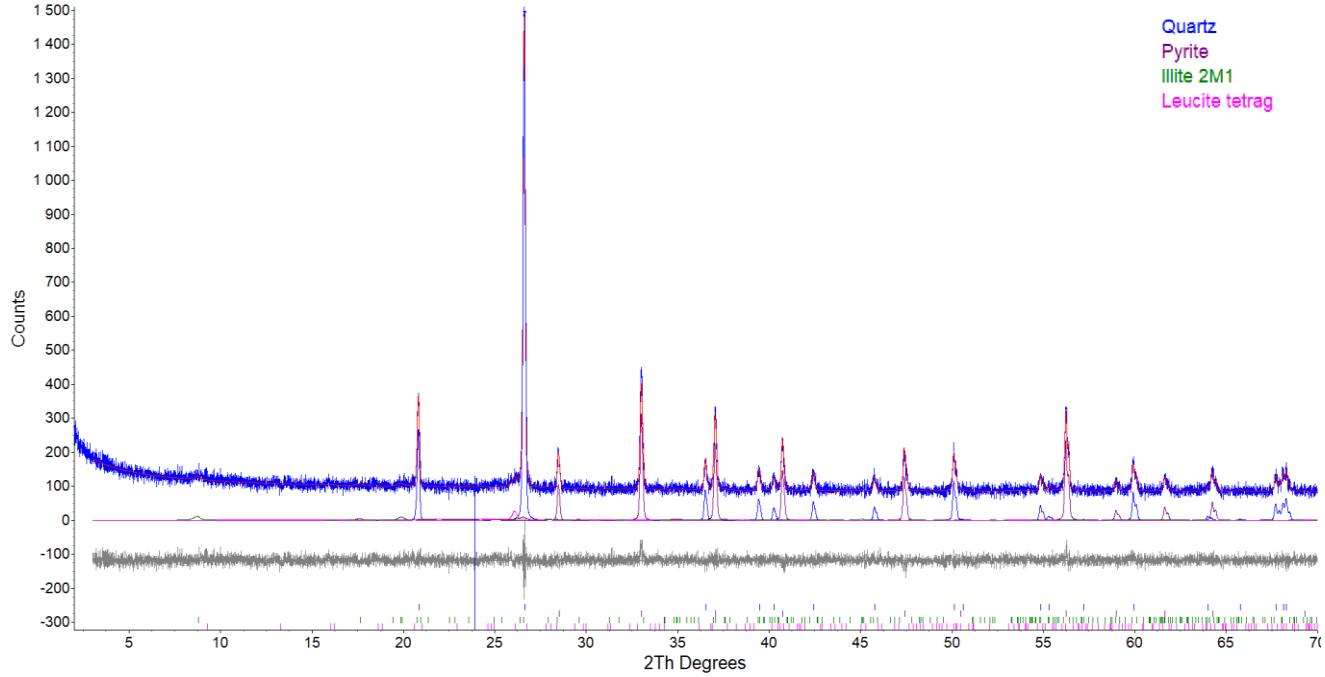

X-ray diffractogram evaluation with Rietveld refinement of the sample BOL 5-9

Mineral	***Formula***	$^{m}/_{m}\%$
Quartz	SiO_2	57.3
Pyrite	FeS_2	27.0
Illite	$(K;H_3O)Al_2Si_3AlO_{10}(OH)_2$	8.2
Leucite	$KAlSi_2O_6$	2.1
Amorphous components		5.4

Quantitative mineralogical composition of the sample BOL 5-9

DOI: 10.14750/ME.2021.004

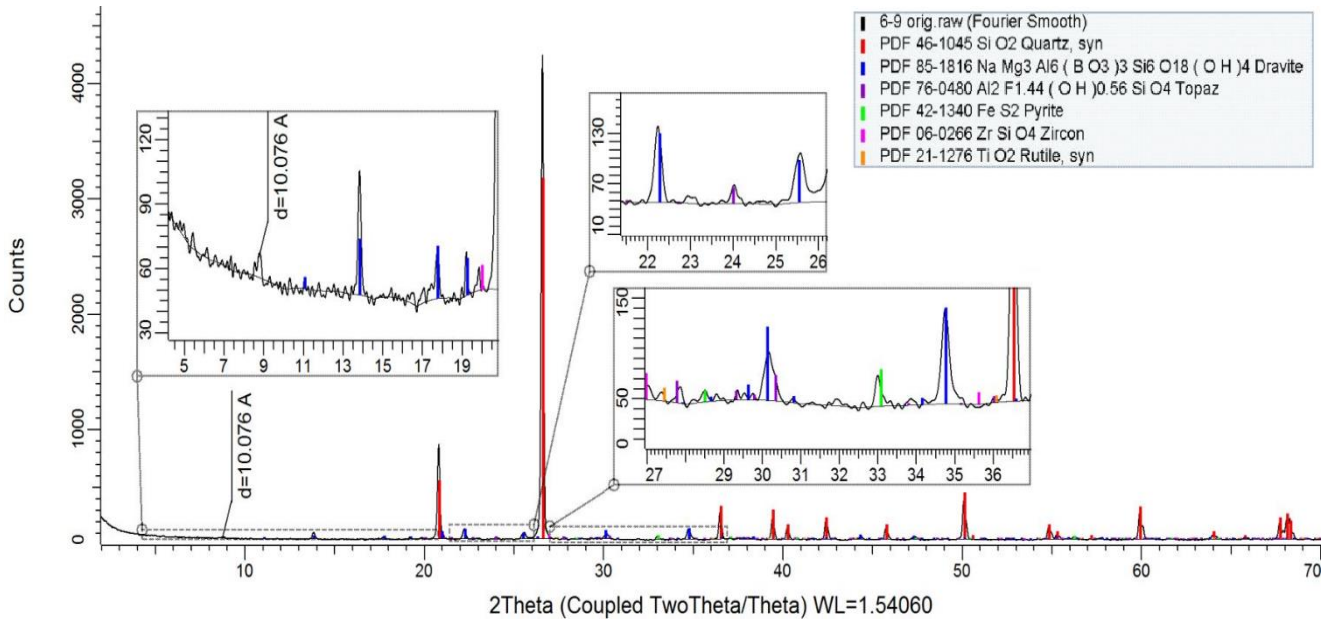

X-ray diffractogram with the identified phases of the sample BOL 6-9

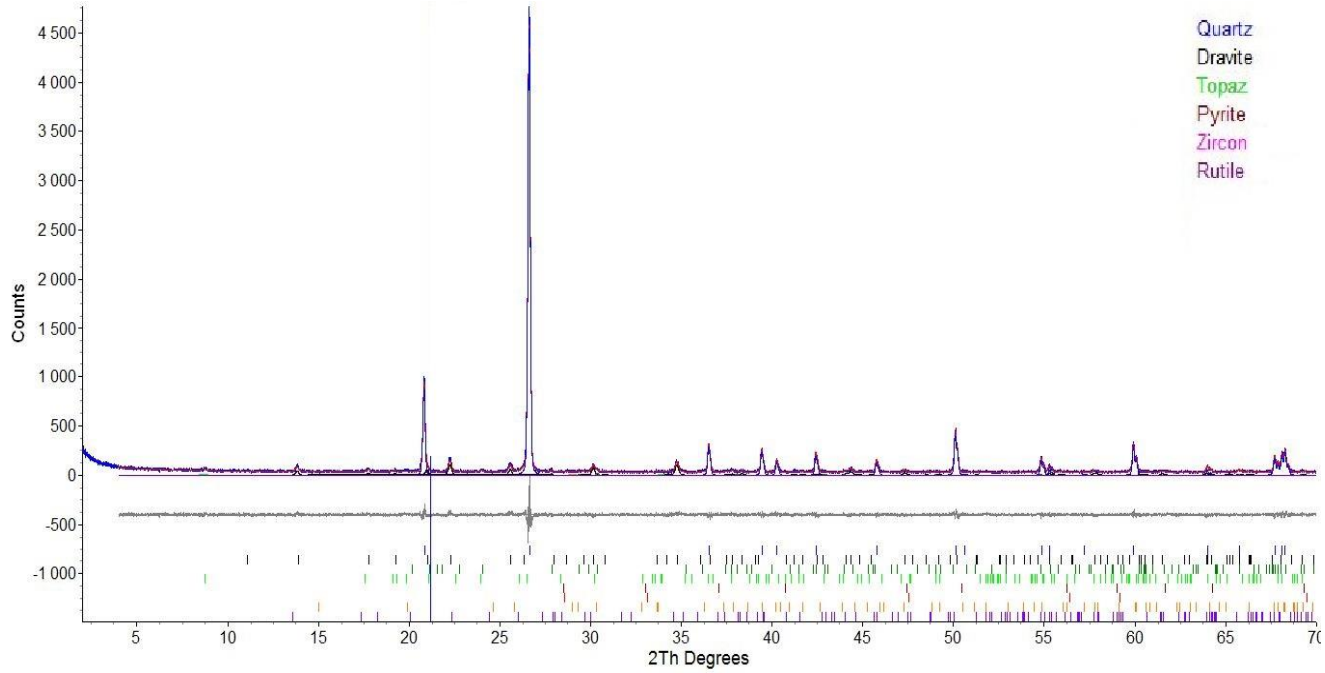

X-ray diffractogram evaluation with Rietveld refinement of the sample BOL 6-9

Mineral	***Formula***	$^{m}/_{m}\%$
Quartz	SiO_2	73.7
Dravite (schorl)	$Na(Mg_3)Al_6(Si_6O_{18})(BO_3)_3(OH)_4$	14.9
Topaz	$Al_2SiO_4(F,OH)_2$	2.4
Biotite	$K(Mg,Fe)_3AlSi_3O_{10}(OH)_2$	1.0
Pyrite	FeS_2	1.0
Amorphous components		7.0

Quantitative mineralogical composition of the sample BOL 6-9

DOI: 10.14750/ME.2021.004

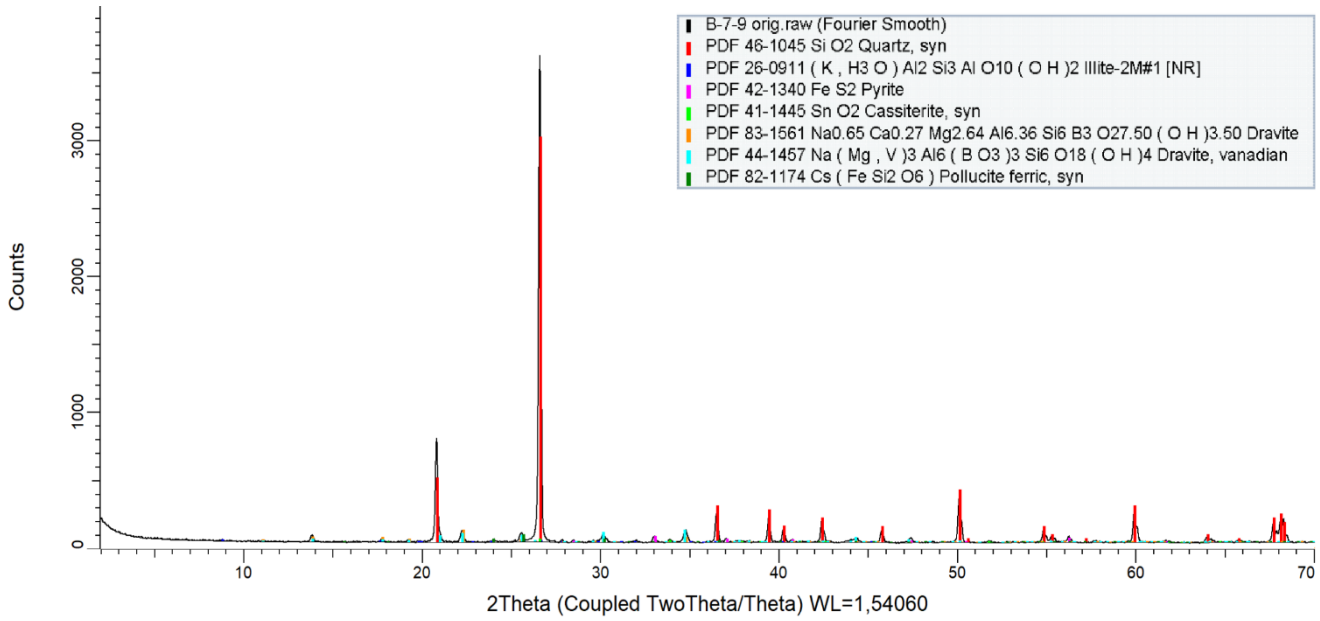

X-ray diffractogram with the identified phases of the sample BOL 7-9

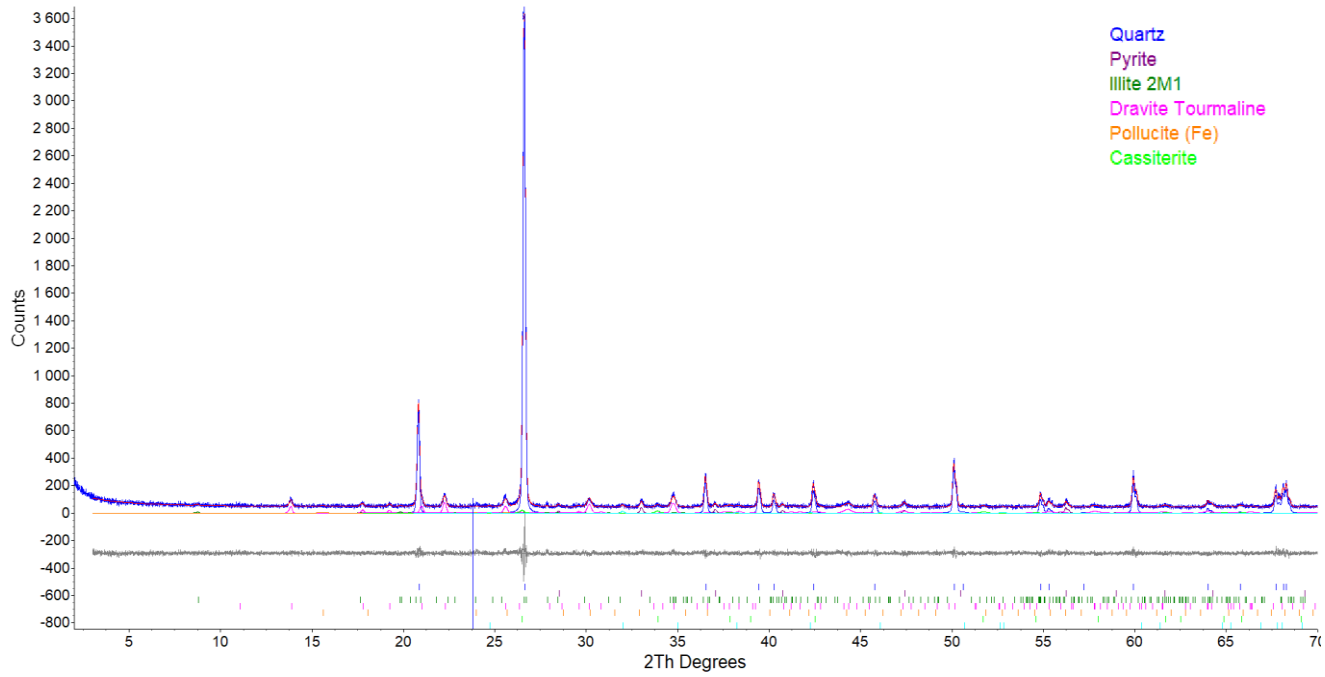

X-ray diffractogram evaluation with Rietveld refinement of the sample BOL 7-9

Mineral	***Formula***	$^{m}/_{m}\%$
Quartz	SiO_2	75.5
Pyrite	FeS_2	1.5
Illite	$(K;H_3O)Al_2Si_3AlO_{10}(OH)_2$	1.4
Dravite (schorl)	$Na(Mg_3)Al_6(Si_6O_{18})(BO_3)_3(OH)_4$	17.5
Pollucite (Fe)	$(Fe,Na)_2Al_2Si_4O_{12}*H_2O$	0.3
Cassiterite	SnO_2	0.4
Amorphous components		3.4

Quantitative mineralogical composition of the sample BOL 7-9

DOI: 10.14750/ME.2021.004

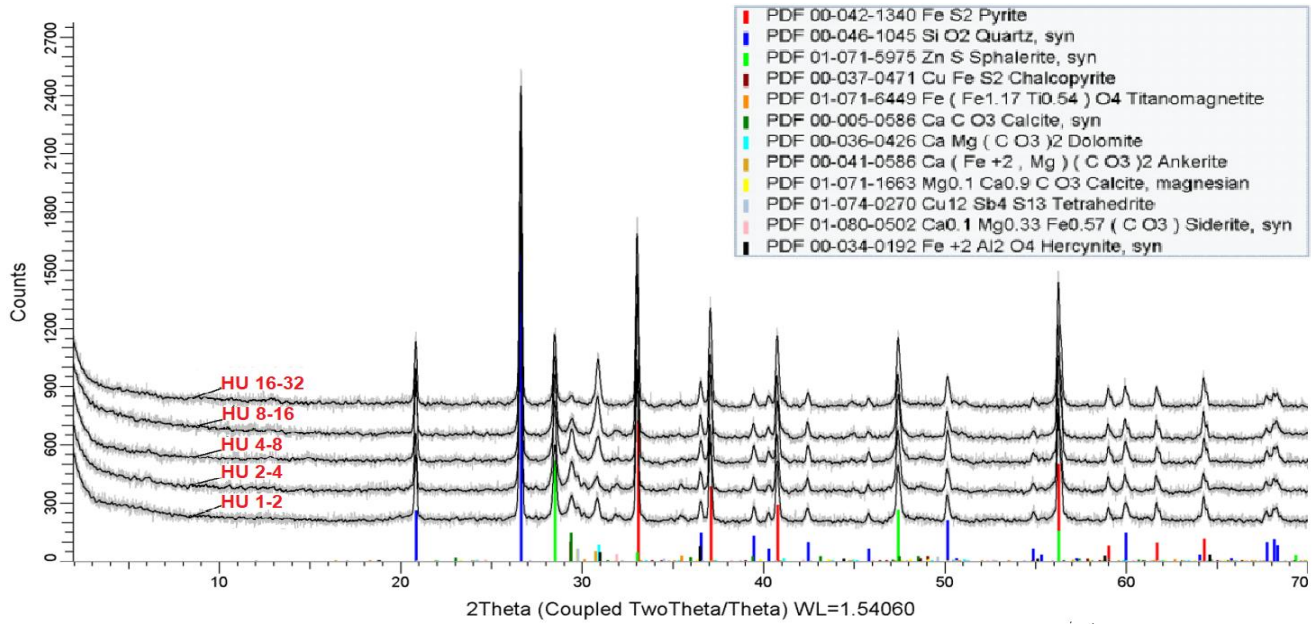

X-ray diffractogram with the identified phases of the Hungarian sample set plotted on a common x-axis chart

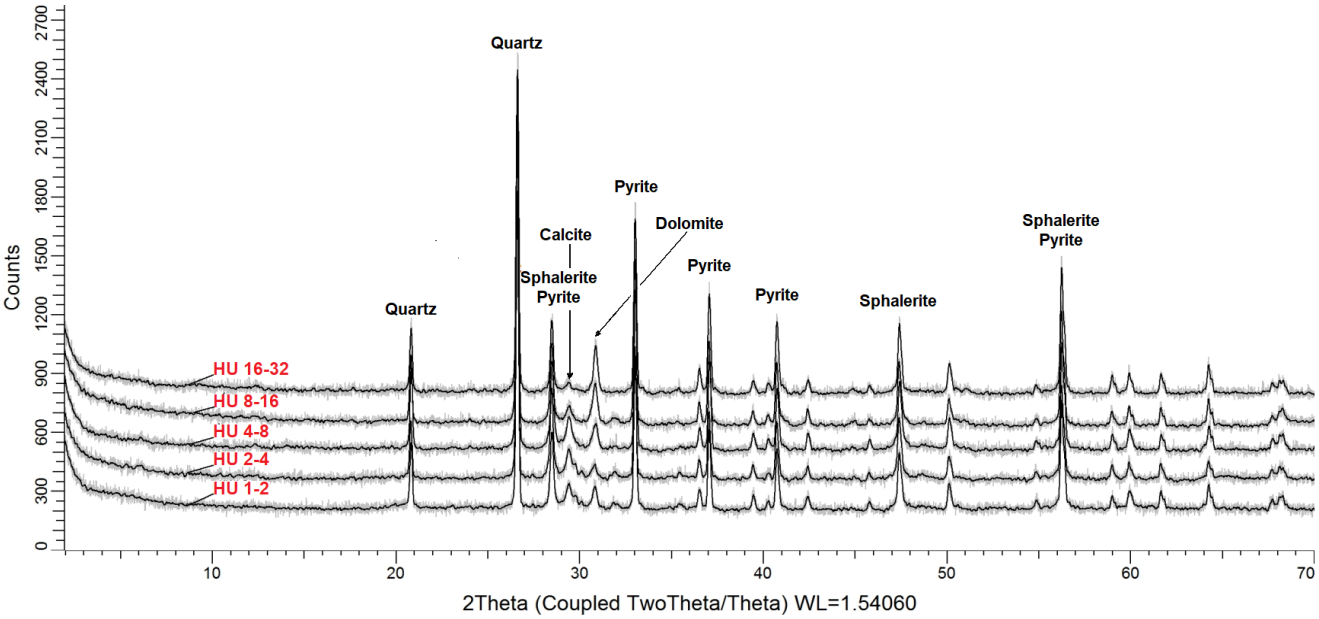

Phase indicated X-ray diffractogram of the Hungarian sample set plotted on a common x-axis chart

Mineral	***Formula***	***HU 1-2***	***HU 2-4***	***HU 4-8***	***HU 8-16***	***HU 16-32***
Pyrite	FeS_2	35.4	34.2	33.5	30.0	39.1
Quartz	SiO_2	44.7	42.1	42.3	42.4	39.2
Dolomite	$CaMg(CO_3)_2$	2.7	0.9	2.7	6.7	9.7
Ankerite ($Fe_{0.55}$)	$Ca(Fe,Mg)(CO_3)_2$	4.1	4.2	7.0	8.0	5.9
Calcite (magnesian)	$Mg_{0.1}Ca_{0.9}CO_3$	1.7	2.1	1.4	0.4	0.4
Calcite	$CaCO_3$	5.8	8.1	6.9	4.8	1.5
Chalcopyrite	$CuFeS_2$	1.6	1.9	1.9	1.2	1.0
Sphalerite iron	ZnS	3.3	5.5	3.9	6.3	2.2
Titanomagnetite	$Fe(Fe_{1.17}Ti_{0.54})O_4$	0.7	0.6	0.3	0.1	0.3
Hercynite	$FeAl_2O_4$	0.1	0.5	0.1	0.1	0.7
Siderite (Mg, Ca)	$Ca_{0.1}Mg_{0.33}Fe_{0.57}(CO_3)$	ind.	ind.	ind.	ind.	ind.
Tetrahedrite	$Cu_{12}Sb_4S_{13}$	ind.	ind.	ind.	ind.	ind.

Qualitative mineralogical composition of the Hungarian sample set

DOI: 10.14750/ME.2021.004

GEOCHEMICAL DATA SHEETS

DOI: 10.14750/ME.2021.004

JALPHA 1-7	**Analyzed years: 1st** (2008 sum.); **2nd** (2009 sum.); **3rd** (2010 aut. - 2011 spr.)

1st year	***Day***	***0***	***7***	***14***	***21***	***28***	***35***	***42***	***49***	***56***	***63***	***72***	***78***	***87***	***95***	***101***
	pH (-)	2.15	2.33	2.46	2.59	2.36	2.79	3.38	3.07	3.36	3.25	3.36	3.35	3.65	3.39	3.19
	Eh (mV)	441	449	461	444	452	401	359	448	346	348	362	364	419	402	443
	TDS (mg/l)	9120	4410	2130	1170	2120	570	170	250	140	189	139	133	72	117	220
	SO_4^{2-}	28810	24840	2500	810	426	296	61	114	-	-	-	-	-	-	-

2nd year	***Day***	***0***	***7***	***14***	***21***	***28***	***35***	***42***
	pH (-)	2.78	2.88	2.90	3.09	3.03	3.13	2.96
	Eh (mV)	434	444	427	370	391	373	382
	TDS (mg/l)	567	401	369	224	264	207	313
	SO_4^{2-}	-	-	-	-	-	-	-

3rd year	***Day***	***0***	***7***	***14***	***21***	***28***	***35***	***42***	***49***	***56***	***64***	***71***	***76***	***87***	***94***	***101***	***108***	***115***
	pH (-)	1.60	1.88	2.18	2.23	2.33	2.44	2.48	2.39	2.46	2.74	2.82	2.38	2.34	2.41	2.34	2.43	2.55
	Eh (mV)	437	454	461	454	453	456	455	450	449	462	474	454	475	475	469	471	483
	TDS (mg/l)	6130	3390	1685	1477	1041	887	865	1119	975	632	468	1518	1118	937	1100	909	694
	SO_4^{2-}	3040	1130	855	694	390	392	433	428	368	182	130	475	241	253	262	251	233

Remarks: In the 1st year the sulphate content was measured just in the first 49 days, but not further more. Also in year 1st only the first 49 days were measured by Ferenc Moricz, the further ones were completed by Dr. Ingar Walder (external consultant). In year 3rd on the 64th, 71st and 76th days the samplings were completed also by Dr. Ingar Walder.

Sequential Chemical Extraction (SCE) result

Element	***Be***	***Na***	***Mg***	***Al***	***P***	***K***	***Ca***	***Sc***	***Ti***	***V***	***Cr***	***Mn***	***Fe***	***Co***	***Ni***	***Cu***	***Zn***
Det. limit	0.5	0.01	0.01	0.01	0.01	0.01	0.01	0.5	0.01	2	1	2	0.01	1	1	0.5	0.5
unit	ppm	%	%	%	%	%	%	ppm	%	ppm	ppm	ppm	%	ppm	ppm	ppm	ppm
step 1st	<0.5	<0.01	<0.01	0.12	<0.01	<0.01	0.05	<0.5	<0.01	<2	12	17	0.51	2	3	46.4	>10000
step 2nd	<0.5	<0.01	<0.01	<0.01	<0.01	<0.01	<0.01	<0.5	<0.01	<2	13	<2	0.18	<1	<1	<0.5	435
step 3rd	<0.5	<0.01	<0.01	0.01	<0.01	0.03	<0.01	<0.5	<0.01	<2	13	<2	0.56	<1	<1	6.9	144
step 4th	<0.5	0.01	<0.01	0.03	<0.01	0.07	<0.01	<0.5	<0.01	<2	6	2	1.75	<1	<1	11.7	434
step 5th	<0.5	<0.01	<0.01	<0.01	<0.01	<0.01	<0.01	<0.5	<0.01	<2	<1	<2	0.76	<1	<1	22.6	966
step 6th	<0.5	0.01	<0.01	0.07	<0.01	N.A.	<0.01	<0.5	<0.01	<2	5	3	2.18	<1	1	10.1	1160
step 7th	1.7	0.03	0.24	5.51	0.08	2.34	0.02	5.2	0.26	39	37	153	0.23	<1	<1	0.6	28.2

Element	***As***	***Sr***	***Y***	***Zr***	***Mo***	***Ag***	***Cd***	***Sn***	***Sb***	***Ba***	***La***	***W***	***Pb***	***Bi***	***Li***	***S***	***CO_2***
Det. limit	3	0.5	0.5	0.5	1	2	1	10	5	1	0.5	10	2	5	1	0.01	0.01
unit	ppm	ppm	ppm	ppm	ppm	ppm	ppm	ppm	ppm	ppm	ppm	ppm	ppm	ppm	ppm	%	%
step 1st	<3	1	<0.5	<0.5	1	<2	358	<10	<5	<1	<0.5	<10	204	<5	1	1.44	<0.01
step 2nd	9	3.9	<0.5	<0.5	1	<2	12	<10	<5	7	<0.5	<10	>10000	<5	<1	0.21	<0.01
step 3rd	40	<0.5	<0.5	1.1	<1	<2	2	<10	29	3	<0.5	<10	759	<5	<1	0.2	
step 4th	74	1.1	<0.5	<0.5	<1	<2	1	<10	60	6	<0.5	<10	290	<5	<1	0.52	
step 5th	13	<0.5	<0.5	<0.5	<1	<2	20	<10	<5	<1	<0.5	<10	113	<5	<1	1.3	
step 6th	92	7.1	<0.5	<0.5	<1	>10	27	30	55	26	1.3	<10	>10000	<5	<1	4.17	
step 7th	7	751	4.4	32.9	<1	<2	<1	30	132	189	24.4	<10	932	<5	48	0.37	

Remarks: The Zn content in the 1st and the Pb in the 2nd and 6th step exceeded the upper detection limit (10 000 ppm). Two duplicated measuring were completed in different date than this analysis.

DOI: 10.14750/ME.2021.004

Sequential Chemical Extraction DUPLICATED 1st(SCE) result of JALPHA 1-7

Element	*Ag*	*Al*	*As*	*Ba*	*Be*	*Bi*	*Ca*	*Cd*	*Co*	*Cr*	*Cu*	*Fe*	*K*	*La*	*Li*	*Mg*	*Mn*
Det. limit	2	0.01	3	1	0.5	5	0.01	1	1	1	0.5	0.01	0.01	0.5	1	0.01	2
unit	ppm	%	ppm	ppm	ppm	ppm	%	ppm	ppm	ppm	ppm	%	%	ppm	ppm	%	ppm
step 1st	<2	0.02	<3	<1	<0.5	<5	<0.01	11	<1	<1	6.6	0.31	<0.01	<0.5	<1	<0.01	<2
step 2nd	<2	<0.01	3	6	<0.5	<5	<0.01	1	<1	<1	<0.5	0.04	<0.01	<0.5	<1	<0.01	<2
step 3rd	<2	<0.01	50	2	<0.5	<5	<0.01	2	<1	<1	16.9	0.89	0.04	<0.5	<1	<0.01	<2
step 4th	<2	0.01	51	4	<0.5	<5	<0.01	2	<1	<1	13	0.84	0.04	<0.5	<1	<0.01	<2
step 5th	<2	<0.01	48	<1	<0.5	<5	<0.01	6	<1	<1	8.9	1.75	<0.01	<0.5	<1	<0.01	<2
step 6th	>10	0.02	29	8	<0.5	<5	<0.01	18	<1	3	3.2	0.74	N.A.	0.6	<1	<0.01	<2
step 7th	>10	5.46	8	140	1.8	<5	0.03	9	<1	6	1.3	0.24	N.A.	21.8	51	0.24	140

Element	*Mo*	*Na*	*Ni*	*P*	*Pb*	*S*	*Sb*	*Sc*	*Sn*	*Sr*	*Ti*	*V*	*W*	*Y*	*Zn*	*Zr*	*CO_2*
Det. limit	1	0.01	1	0.01	2	0.01	5	0.5	10	0.5	0.01	2	10	0.5	0.5	0.5	0.01
unit	ppm	%	ppm	%	ppm	%	ppm	ppm	ppm	ppm	%	ppm	ppm	ppm	ppm	ppm	%
step 1st	<1	<0.01	<1	<0.01	162	0.49	<5	<0.5	<10	<0.5	<0.01	<2	<10	<0.5	649	<0.5	0.03
step 2nd	<1	<0.01	<1	<0.01	9510	0.17	<5	<0.5	<10	2.6	<0.01	<2	<10	<0.5	41.1	<0.5	0.02
step 3rd	<1	<0.01	<1	<0.01	493	0.43	30	<0.5	<10	<0.5	<0.01	<2	<10	<0.5	216	1.5	
step 4th	<1	<0.01	<1	<0.01	410	0.33	52	<0.5	10	0.7	<0.01	<2	<10	<0.5	356	<0.5	
step 5th	<1	<0.01	1	<0.01	76	2.07	<5	<0.5	<10	<0.5	<0.01	<2	<10	<0.5	174	<0.5	
step 6th	<1	0.06	<1	<0.01	>10000	1.19	31	<0.5	30	2	<0.01	<2	<10	<0.5	582	<0.5	
step 7th	<1	0.03	1	0.08	7000	0.52	163	5.2	30	675	0.28	40	<10	4.3	37.5	37.7	

Remarks: The Pb content in the 6th step exceeded the upper detection limit (10 000 ppm). In the same time the "duplicated 2nd" analysis was done also.

Sequential Chemical Extraction DUPLICATED 2nd(SCE) result of JALPHA 1-7

Element	*Ag*	*Al*	*As*	*Ba*	*Be*	*Bi*	*Ca*	*Cd*	*Co*	*Cr*	*Cu*	*Fe*	*K*	*La*	*Li*	*Mg*	*Mn*
Det. limit	2	0.01	3	1	0.5	5	0.01	1	1	1	0.5	0.01	0.01	0.5	1	0.01	2
unit	ppm	%	ppm	ppm	ppm	ppm	%	ppm	ppm	ppm	ppm	%	%	ppm	ppm	%	ppm
step 1st	<2	0.02	<3	<1	<0.5	<5	<0.01	12	<1	<1	5.9	0.28	<0.01	<0.5	<1	<0.01	<2
step 2nd	<2	<0.01	5	6	<0.5	<5	<0.01	2	<1	<1	<0.5	0.04	<0.01	<0.5	<1	<0.01	<2
step 3rd	<2	<0.01	41	2	<0.5	<5	<0.01	1	<1	<1	13.9	0.69	0.03	<0.5	<1	<0.01	<2
step 4th	<2	0.01	55	5	<0.5	<5	<0.01	2	<1	<1	13.8	0.92	0.04	<0.5	<1	<0.01	<2
step 5th	<2	<0.01	72	<1	<0.5	<5	<0.01	4	<1	<1	8.8	2.39	<0.01	<0.5	<1	<0.01	<2
step 6th	>10	0.02	46	7	<0.5	<5	<0.01	16	<1	2	3.1	1.05	N.A.	<0.5	<1	<0.01	<2
step 7th	9	5.15	18	136	1.6	<5	0.03	1	<1	9	1.6	0.42	N.A.	26.8	49	0.23	129

Element	*Mo*	*Na*	*Ni*	*P*	*Pb*	*S*	*Sb*	*Sc*	*Sn*	*Sr*	*Ti*	*V*	*W*	*Y*	*Zn*	*Zr*	*CO_2*
Det. limit	1	0.01	1	0.01	2	0.01	5	0.5	10	0.5	0.01	2	10	0.5	0.5	0.5	0.01
unit	ppm	%	ppm	%	ppm	%	ppm	ppm	ppm	ppm	%	ppm	ppm	ppm	ppm	ppm	%
step 1st	<1	<0.01	<1	<0.01	186	0.45	<5	<0.5	<10	<0.5	<0.01	<2	<10	<0.5	658	<0.5	0.03
step 2nd	<1	<0.01	<1	<0.01	>10000	0.19	<5	<0.5	<10	3.1	<0.01	<2	<10	<0.5	40.7	<0.5	0.02
step 3rd	<1	<0.01	<1	<0.01	506	0.36	20	<0.5	<10	<0.5	<0.01	<2	<10	<0.5	172	1.3	
step 4th	<1	<0.01	<1	<0.01	416	0.33	56	<0.5	10	1	<0.01	<2	<10	<0.5	335	<0.5	
step 5th	<1	<0.01	1	<0.01	81	2.66	<5	<0.5	<10	<0.5	<0.01	<2	<10	<0.5	171	<0.5	
step 6th	<1	0.06	<1	<0.01	>10000	2.11	37	<0.5	30	1.3	<0.01	<2	<10	<0.5	661	<0.5	
step 7th	<1	0.04	4	0.08	1930	0.6	153	4.8	30	744	0.27	35	<10	4.5	58.9	36.4	

Remarks: The Pb in the 2nd and 6th step exceeded the upper detection limit (10 000 ppm).

DOI: 10.14750/ME.2021.004

PLAYA IROCO 1-7	**Analyzed years: 1st** (2008 sum.); **2nd** (2009 sum.); **3rd** (2010 aut. - 2011 spr.)

1st year	***Day***	***0***	***7***	***14***	***21***	***28***	***35***	***42***	***49***	***56***	***63***	***72***	***78***	***87***	***95***	***101***
	pH (-)	1.17	1.39	1.59	1.99	1.81	2.16	2.91	2.68	2.91	3.00	2.86	3.18	2.68	2.55	2.47
	Eh (mV)	465	474	467	451	440	419	431	427	388	385	382	395	449	418	487
	TDS (mg/l)	37600	12800	14400	4480	7420	3250	780	700	430	335	824	942	1108	1269	1559
	SO_4^{2-}	48330	43800	7240	3105	4600	2505	345	319	-	-	-	-	-	-	-

2nd year	***Day***	***0***	***7***	***14***	***21***	***28***	***35***	***42***
	pH (-)	2.13	2.48	2.43	2.86	2.98	3.08	3.10
	Eh (mV)	450	449	432	386	398	393	386
	TDS (mg/l)	3140	999	1271	396	364	276	225
	SO_4^{2-}	-	-	-	-	-	-	-

3rd year	***Day***	***0***	***7***	***14***	***21***	***28***	***35***	***42***	***49***	***56***	***64***	***71***	***76***	***87***	***94***	***101***	***108***	***115***
	pH (-)	1.65	1.82	2.12	2.19	2.34	2.44	2.54	2.48	2.64	2.92	3.07	2.51	2.70	2.75	2.72	2.78	3.00
	Eh (mV)	452	426	421	423	423	422	425	414	414	433	455	430	435	453	445	457	467
	TDS (mg/l)	7060	3640	1705	1496	1064	969	794	960	718	447	272	962	588	474	584	448	304
	SO_4^{2-}	2565	777	641	625	393	468	388	387	304	143	83	405	146	167	186	172	170

Remarks: In the 1st year the sulphate content was measured just in the first 49 days, but not further more. Also in year 1st only the first 49 days were measured by Ferenc Moricz, the further ones were completed by Dr. Ingar Walder (external consultant). In year 3rd on the 64th, 71st and 76th days the samplings were completed also by Dr. Ingar Walder.

Sequential Chemical Extraction (SCE) result

Element	***Be***	***Na***	***Mg***	***Al***	***P***	***K***	***Ca***	***Sc***	***Ti***	***V***	***Cr***	***Mn***	***Fe***	***Co***	***Ni***	***Cu***	***Zn***
Det. limit	0.5	0.01	0.01	0.01	0.01	0.01	0.01	0.5	0.01	2	1	2	0.01	1	1	0.5	0.5
unit	ppm	%	%	%	%	%	%	ppm	%	ppm	ppm	ppm	%	ppm	ppm	ppm	ppm
step 1st	<0.5	0.07	0.02	0.28	<0.01	0.15	0.98	<0.5	<0.01	2	36	19	1.62	3	5	266	71.6
step 2nd	<0.5	<0.01	<0.01	<0.01	<0.01	0.01	0.02	<0.5	<0.01	<2	3	<2	0.17	<1	<1	4.4	1.1
step 3rd	<0.5	<0.01	<0.01	<0.01	<0.01	<0.01	<0.01	<0.5	<0.01	<2	1	<2	0.19	<1	<1	8.5	0.8
step 4th	<0.5	<0.01	<0.01	0.04	<0.01	<0.01	<0.01	<0.5	<0.01	<2	1	<2	0.04	<1	<1	2.9	1
step 5th	<0.5	<0.01	<0.01	0.01	<0.01	<0.01	<0.01	<0.5	<0.01	<2	<1	<2	2.53	3	4	4.4	0.9
step 6th	<0.5	0.01	<0.01	0.14	<0.01	N.A.	<0.01	<0.5	<0.01	<2	7	<2	0.24	<1	<1	2.4	2.2
step 7th	1.2	0.19	0.27	6.29	0.04	1.55	0.02	8.7	0.23	74	65	21	1.29	<1	2	1.3	11.4

Element	***As***	***Sr***	***Y***	***Zr***	***Mo***	***Ag***	***Cd***	***Sn***	***Sb***	***Ba***	***La***	***W***	***Pb***	***Bi***	***Li***	***S***	***CO_2***
Det. limit	3	0.5	0.5	0.5	1	2	1	10	5	1	0.5	10	2	5	1	0.01	0.01
unit	ppm	ppm	ppm	ppm	ppm	ppm	ppm	ppm	ppm	ppm	ppm	ppm	ppm	ppm	ppm	%	%
step 1st	346	10.4	0.5	<0.5	1	>10	5	<10	22	<1	<0.5	<10	185	<5	3	3.11	<0.01
step 2nd	348	41.6	<0.5	<0.5	1	<2	<1	<10	61	38	<0.5	<10	6980	<5	<1	0.2	<0.01
step 3rd	1000	0.8	<0.5	<0.5	1	<2	<1	280	1610	4	<0.5	<10	895	11	<1	<0.01	
step 4th	148	1.1	<0.5	<0.5	<1	<2	<1	100	1020	2	<0.5	<10	57	<5	<1	<0.01	
step 5th	266	<0.5	<0.5	<0.5	<1	>10	<1	<10	13	<1	<0.5	<10	<2	<5	<1	3.11	
step 6th	81	8.8	<0.5	<0.5	<1	>10	<1	50	249	10	1.8	<10	29	<5	<1	0.4	
step 7th	37	131	2.4	12.3	<1	2	<1	60	681	171	11.1	<10	31	<5	15	0.08	

Remarks: Two duplicated measuring were completed in different date than this analysis.

DOI: 10.14750/ME.2021.004

Sequential Chemical Extraction DUPLICATED 1st(SCE) result of PLAYA IROCO 1-7

Element	*Ag*	*Al*	*As*	*Ba*	*Be*	*Bi*	*Ca*	*Cd*	*Co*	*Cr*	*Cu*	*Fe*	*K*	*La*	*Li*	*Mg*	*Mn*
Det. limit	2	0.01	3	1	0.5	5	0.01	1	1	1	0.5	0.01	0.01	0.5	1	0.01	2
unit	ppm	%	ppm	ppm	ppm	ppm	%	ppm	ppm	ppm	ppm	%	%	ppm	ppm	%	ppm
step 1st	9	<0.01	16	<1	<0.5	<5	0.02	<1	<1	<1	4.9	0.12	<0.01	<0.5	<1	<0.01	<2
step 2nd	<2	<0.01	170	25	<0.5	<5	<0.01	2	<1	<1	<0.5	0.03	<0.01	0.6	<1	<0.01	<2
step 3rd	5	<0.01	716	2	<0.5	12	<0.01	4	<1	<1	3.1	0.1	<0.01	<0.5	<1	<0.01	<2
step 4th	<2	<0.01	212	1	<0.5	<5	<0.01	2	<1	<1	1.2	0.06	<0.01	<0.5	<1	<0.01	<2
step 5th	>10	<0.01	194	<1	<0.5	<5	<0.01	2	2	<1	0.8	2.05	<0.01	<0.5	<1	<0.01	<2
step 6th	>10	0.01	106	3	<0.5	<5	<0.01	1	<1	3	0.7	0.13	N.A.	0.7	<1	<0.01	<2
step 7th	4	6.18	32	153	1.3	<5	0.04	<1	<1	25	1.3	1.3	N.A.	19.5	14	0.29	22

Element	*Mo*	*Na*	*Ni*	*P*	*Pb*	*S*	*Sb*	*Sc*	*Sn*	*Sr*	*Ti*	*V*	*W*	*Y*	*Zn*	*Zr*	*CO_2*
Det. limit	1	0.01	1	0.01	2	0.01	5	0.5	10	0.5	0.01	2	10	0.5	0.5	0.5	0.01
unit	ppm	%	ppm	%	ppm	%	ppm	ppm	ppm	ppm	%	ppm	ppm	ppm	ppm	ppm	%
step 1st	<1	<0.01	<1	<0.01	189	0.31	9	<0.5	<10	3	<0.01	<2	<10	<0.5	<0.5	<0.5	0.04
step 2nd	<1	<0.01	<1	<0.01	7420	0.14	21	<0.5	<10	35.4	<0.01	<2	<10	<0.5	<0.5	<0.5	0.04
step 3rd	<1	<0.01	<1	<0.01	783	<0.01	1270	<0.5	180	0.6	<0.01	<2	<10	<0.5	<0.5	<0.5	
step 4th	<1	<0.01	<1	<0.01	144	<0.01	1090	<0.5	120	0.7	<0.01	<2	<10	<0.5	0.7	<0.5	
step 5th	<1	<0.01	4	<0.01	<2	2.31	10	<0.5	<10	<0.5	<0.01	<2	<10	<0.5	0.6	<0.5	
step 6th	<1	0.07	<1	<0.01	39	0.08	396	<0.5	70	2.2	<0.01	<2	<10	<0.5	1.8	<0.5	
step 7th	<1	0.17	2	0.04	43	0.08	595	9.9	100	113	0.28	76	10	3.9	12.7	24.5	

Remarks: In the same time the "duplicated 2nd" analysis was done also.

Sequential Chemical Extraction DUPLICATED 2nd(SCE) result of PLAYA IROCO 1-7

Element	*Ag*	*Al*	*As*	*Ba*	*Be*	*Bi*	*Ca*	*Cd*	*Co*	*Cr*	*Cu*	*Fe*	*K*	*La*	*Li*	*Mg*	*Mn*
Det. limit	2	0.01	3	1	0.5	5	0.01	1	1	1	0.5	0.01	0.01	0.5	1	0.01	2
unit	ppm	%	ppm	ppm	ppm	ppm	%	ppm	ppm	ppm	ppm	%	%	ppm	ppm	%	ppm
step 1st	5	<0.01	34	<1	<0.5	<5	0.75	<1	<1	<1	4	0.12	<0.01	<0.5	<1	<0.01	<2
step 2nd	<2	<0.01	191	28	<0.5	<5	0.03	2	<1	<1	<0.5	0.03	<0.01	0.8	<1	<0.01	<2
step 3rd	7	<0.01	944	3	<0.5	17	<0.01	5	<1	<1	3.7	0.11	<0.01	<0.5	<1	<0.01	<2
step 4th	<2	<0.01	435	2	<0.5	8	<0.01	5	<1	<1	1.6	0.07	<0.01	<0.5	<1	<0.01	<2
step 5th	>10	<0.01	284	<1	<0.5	<5	<0.01	3	3	<1	1	2.68	<0.01	<0.5	<1	<0.01	<2
step 6th	>10	0.01	106	3	<0.5	<5	<0.01	1	<1	2	1	0.2	N.A.	0.8	<1	<0.01	<2
step 7th	3	7.08	36	174	1.3	<5	0.03	<1	<1	28	0.6	1.48	N.A.	22.2	16	0.33	23

Element	*Mo*	*Na*	*Ni*	*P*	*Pb*	*S*	*Sb*	*Sc*	*Sn*	*Sr*	*Ti*	*V*	*W*	*Y*	*Zn*	*Zr*	*CO_2*
Det. limit	1	0.01	1	0.01	2	0.01	5	0.5	10	0.5	0.01	2	10	0.5	0.5	0.5	0.01
unit	ppm	%	ppm	%	ppm	%	ppm	ppm	ppm	ppm	%	ppm	ppm	ppm	ppm	ppm	%
step 1st	<1	<0.01	<1	<0.01	120	0.99	10	<0.5	<10	5.9	<0.01	<2	<10	<0.5	0.5	<0.5	0.04
step 2nd	<1	<0.01	<1	<0.01	8010	0.17	20	<0.5	<10	41	<0.01	<2	<10	<0.5	<0.5	<0.5	0.02
step 3rd	<1	<0.01	<1	<0.01	1140	<0.01	1800	<0.5	240	0.9	<0.01	<2	<10	<0.5	<0.5	<0.5	
step 4th	<1	<0.01	<1	<0.01	227	0.01	2480	<0.5	250	0.9	<0.01	<2	<10	<0.5	0.9	<0.5	
step 5th	<1	<0.01	5	<0.01	3	3.04	12	<0.5	<10	<0.5	<0.01	<2	<10	<0.5	0.7	<0.5	
step 6th	<1	0.06	<1	<0.01	39	0.2	363	<0.5	60	2.5	<0.01	<2	<10	<0.5	0.9	<0.5	
step 7th	<1	0.18	3	0.05	44	0.09	583	9.9	100	129	0.31	81	10	4.2	13.6	23.4	

DOI: 10.14750/ME.2021.004

ITOS JIG 1-7	**Analyzed years: 1st** (2008 sum.); **2nd** (2009 sum.); **3rd** (2010 aut. - 2011 spr.); **4th** year (2011 aut. - 2012 spr.)

1st year	***Day***	***0***	***3.5***	***7***	***10.5***	***14***	***17.5***	***21***	***24.5***	***28***	***31.5***	***35***	***38.5***	***42***	***45.5***	***49***	***56***	***63***	***72***	***78***	***87***	***95***	***101***
	pH (-)	1.74	1.96	2.09	2.41	2.60	2.79	2.92	2.96	2.88	2.96	3.01	3.09	3.38	3.03	2.88	2.35	2.32	2.44	2.59	2.40	2.46	2.82
	Eh (mV)	460	460	459	465	469	450	460	435	432	409	415	401	422	430	429	438	434	430	434	485	505	553
	TDS (mg/l)	8940	4750	1853	1224	623	508	377	292	280	264	213	197	195	291	346	1325	1501	1593	1167	1186	980	112
	SO_4^{2-} (mg/l)	20740	10450	11370	716	293	201	126	98	108	84	72	60	61	82	102	-	-	-	-	-	-	-

2nd year	***Day***	***0***	***7***	***14***	***21***	***28***	***35***	***42***
	pH (-)	1.68	1.89	2.25	2.36	2.45	2.41	2.46
	Eh (mV)	475	464	465	453	463	483	484
	TDS (mg/l)	6130	4010	1656	1224	1072	1159	1148
	SO_4^{2-} (mg/l)	-	-	-	-	-	-	-

3rd year	***Day***	***0***	***7***	***14***	***21***	***28***	***35***	***42***	***49***	***56***	***62***	***70***	***77***	***82***	***93***	***100***	***107***	***114***	***121***
	pH (-)	1.64	1.69	1.92	2.13	2.35	2.46	2.58	2.59	2.59	2.62	2.76	2.74	2.55	2.42	2.35	2.36	2.36	2.36
	Eh (mV)	458	459	457	446	453	448	452	458	462	467	469	467	491	502	507	517	518	519
	TDS (mg/l)	16780	5820	2610	1645	933	807	639	617	682	610	469	568	659	910	1043	1020	1137	1157
	SO_4^{2-} (mg/l)	9259	2276	1519	705	324	348	262	285	210	173	104	141	190	268	322	309	334	330

4th year	***Day***	***0***	***7***	***14***	***21***	***28***	***35***	***42***	***49***	***56***	***63***	***70***	***77***	***84***	***91***	***98***	***105***	***112***	***119***
	pH (-)	1.49	1.94	2.25	2.33	2.35	2.39	2.4	2.34	2.35	2.32	2.28	2.3	2.34	2.35	2.31	2.33	2.34	2.35
	Eh (mV)	492	487	477	490	495	506	503	504	515	511	517	517	513	509	515	515	513	529
	TDS (mg/l)	10240	3970	1606	1070	966	867	978	1013	897	1111	1251	1184	1269	1320	1331	1317	1324	1309
	SO_4^{2-} (mg/l)	21965	5359	1391	682	556	437	510	543	482	646	722	700	825	964	989	1026	1054	1030

Remarks: In the 1st year the sulphate content was measured just in the first 49 days, moreover twice a week, but not further more. Also in year 1st only the first 49 days were measured by Ferenc Moricz, the further ones were completed by Dr. Ingar Walder (external consultant). In year 3rd on the 70th, 77th and 82nd days and in year 4th on the 84th and 91st days the samplings were completed also by Dr. Ingar Walder.

O_2 content sampling in year 4th, period days 105th - 112nd				
Day	***0***	***1***	***4***	***7***
O_2 content (V/V%)	21.1	18.6	13.9	9.8

Column free volume (cm^3)	2512

Sequential Chemical Extraction (SCE) result

Element	***Be***	***Na***	***Mg***	***Al***	***P***	***K***	***Ca***	***Sc***	***Ti***	***V***	***Cr***	***Mn***	***Fe***	***Co***	***Ni***	***Cu***	***Zn***
Det. limit	0.5	0.01	0.01	0.01	0.01	0.01	0.01	0.5	0.01	2	1	2	0.01	1	1	0.5	0.5
unit	ppm	%	%	%	%	%	%	ppm	%	ppm	ppm	ppm	%	ppm	ppm	ppm	ppm
step 1st	<0.5	<0.01	<0.01	0.08	<0.01	0.03	<0.01	<0.5	<0.01	<2	8	11	0.09	<1	3	3.9	3.9
step 2nd	<0.5	<0.01	<0.01	0.02	<0.01	0.02	<0.01	<0.5	<0.01	<2	51	<2	0.06	<1	<1	0.5	<0.5
step 3rd	<0.5	<0.01	<0.01	0.06	<0.01	0.05	<0.01	<0.5	<0.01	<2	19	<2	0.36	<1	<1	4.7	1.8
step 4th	<0.5	<0.01	<0.01	0.07	<0.01	0.05	<0.01	<0.5	<0.01	<2	8	<2	0.21	<1	<1	1.3	1.5
step 5th	<0.5	<0.01	<0.01	0.02	<0.01	<0.01	<0.01	<0.5	<0.01	<2	2	<2	2.67	2	4	10.4	5.5
step 6th	<0.5	0.01	<0.01	0.15	<0.01	N.A.	<0.01	<0.5	<0.01	<2	20	<2	1.23	<1	1	2.9	3
step 7th	1.7	0.13	0.32	7.68	0.05	2.26	0.01	9.2	0.27	80	119	44	1.32	<1	2	0.9	11.6

Element	***As***	***Sr***	***Y***	***Zr***	***Mo***	***Ag***	***Cd***	***Sn***	***Sb***	***Ba***	***La***	***W***	***Pb***	***Bi***	***Li***	***S***	***CO_2***
Det. limit	3	0.5	0.5	0.5	1	2	1	10	5	1	0.5	10	2	5	1	0.01	0.01
unit	ppm	ppm	ppm	ppm	ppm	ppm	ppm	ppm	ppm	ppm	ppm	ppm	ppm	ppm	ppm	%	%
step 1st	3	4.6	<0.5	<0.5	<1	<2	1	<10	11	3	<0.5	<10	261	<5	<1	0.27	<0.01
step 2nd	20	3.7	<0.5	<0.5	1	<2	<1	<10	47	16	<0.5	<10	1450	<5	<1	0.06	<0.01
step 3rd	208	<0.5	<0.5	0.7	4	<2	<1	140	254	4	<0.5	<10	568	<5	<1	0.14	
step 4th	97	1.7	<0.5	<0.5	<1	<2	<1	150	494	5	<0.5	<10	86	<5	<1	0.08	
step 5th	255	<0.5	<0.5	<0.5	<1	>10	<1	<10	10	<1	<0.5	<10	11	<5	<1	3.39	
step 6th	156	8.4	<0.5	<0.5	<1	>10	<1	80	170	14	0.8	<10	151	<5	<1	1.76	
step 7th	26	151	2.7	15.7	2	<2	<1	90	369	304	17	10	64	<5	15	0.09	

DOI: 10.14750/ME.2021.004

ITOS JIG 2-7	**Analyzed years: 1st** (2008 sum.); **2nd** (2009 sum.); **3rd** (2010 aut. - 2011 spr.); **4th** year (2011 aut. - 2012 spr.)

1st year	***Day***	***0***	***3.5***	***7***	***10.5***	***14***	***17.5***	***21***	***24.5***	***28***	***31.5***	***35***	***38.5***	***42***	***45.5***	***49***	***56***	***63***	***72***	***78***	***87***	***95***	***101***
	pH (-)	1.70	1.66	1.96	2.10	2.30	2.49	2.61	2.54	2.47	2.48	2.52	2.58	2.86	2.76	2.75	2.66	2.68	2.71	2.69	2.67	2.61	2.81
	Eh (mV)	471	474	469	457	469	457	467	455	463	447	450	436	456	454	447	441	432	422	440	532	545	558
	TDS (mg/l)	10580	7680	3530	2170	1447	1102	864	915	1166	1019	1053	899	867	731	557	657	641	734	618	624	639	1061
	SO_4^{2-}	21660	14950	6860	1460	778	550	337	343	403	339	320	258	234	209	153	-	-	-	-	-	-	-

2nd year	***Day***	***0***	***7***	***14***	***21***	***28***	***35***	***42***
	pH (-)	2.05	2.02	2.29	2.38	2.52	2.58	2.64
	Eh (mV)	477	466	451	437	493	468	483
	TDS (mg/l)	2440	3150	1663	1249	906	805	660
	SO_4^{2-}	-	-	-	-	-	-	-

3rd year	***Day***	***0***	***7***	***14***	***21***	***28***	***35***	***42***	***49***	***56***	***62***	***70***	***77***	***82***	***93***	***100***	***107***	***114***	***121***
	pH (-)	1.72	1.67	1.83	1.96	2.13	2.24	2.45	2.46	2.53	2.72	2.92	2.89	2.70	2.53	2.53	2.59	2.59	2.62
	Eh (mV)	458	459	457	446	453	448	452	458	462	467	469	467	491	502	507	517	518	519
	TDS (mg/l)	9150	5640	3250	2580	1697	1361	904	891	740	516	375	368	488	705	682	598	608	558
	SO_4^{2-}	7040	4460	1443	1572	887	646	588	430	271	181	93	86	113	139	151	146	133	130

4th year	***Day***	***0***	***7***	***14***	***21***	***28***	***35***	***42***	***49***	***56***	***63***	***70***	***77***	***84***	***91***	***98***	***105***	***112***	***119***
	pH (-)	1.65	1.95	2.23	2.29	2.37	2.43	2.42	2.35	2.33	2.25	2.19	2.22	2.25	2.26	2.23	2.28	2.25	2.27
	Eh (mV)	473	470	474	486	490	503	512	531	545	547	565	587	566	559	568	591	568	583
	TDS (mg/l)	4830	3380	1548	1121	839	757	825	937	900	1166	1403	1341	1497	1518	1537	1451	1560	1499
	SO_4^{2-}	8209	3825	1342	857	537	472	500	533	527	742	938	928	1142	1290	1321	1275	1415	1312

Remarks: In the 1st year the sulphate content was measured just in the first 49 days, moreover twice a week, but not further more. Also in year 1st only the first 49 days were measured by Ferenc Moricz, the further ones were completed by Dr. Ingar Walder (external consultant). In year 3rd on the 70th, 77th and 82nd days and in year 4th on the 84th and 91st days the samplings were completed also by Dr. Ingar Walder.

O_2 content sampling in year 4th, period days 105th - 112nd				
Day	***0***	***1***	***4***	***7***
O_2 content ($^V/_V$%)	21.1	17.7	10.4	6.4

Column free volume (cm^3)	2500

Sequential Chemical Extraction (SCE) result

Element	***Be***	***Na***	***Mg***	***Al***	***P***	***K***	***Ca***	***Sc***	***Ti***	***V***	***Cr***	***Mn***	***Fe***	***Co***	***Ni***	***Cu***	***Zn***
Det. limit	0.5	0.01	0.01	0.01	0.01	0.01	0.01	0.5	0.01	2	1	2	0.01	1	1	0.5	0.5
unit	ppm	%	%	%	%	%	%	ppm	%	ppm	ppm	ppm	%	ppm	ppm	ppm	ppm
step 1st	<0.5	<0.01	<0.01	0.08	<0.01	0.03	<0.01	<0.5	<0.01	<2	14	6	0.16	<1	1	2.5	5.7
step 2nd	<0.5	<0.01	<0.01	<0.01	<0.01	0.01	<0.01	<0.5	<0.01	<2	24	<2	0.06	<1	<1	<0.5	<0.5
step 3rd	<0.5	<0.01	<0.01	0.03	<0.01	0.06	<0.01	<0.5	<0.01	<2	17	<2	0.45	<1	<1	2.3	1.5
step 4th	<0.5	<0.01	<0.01	0.07	<0.01	0.05	<0.01	<0.5	<0.01	<2	8	<2	0.21	<1	<1	1.3	1.5
step 5th	<0.5	<0.01	<0.01	0.01	<0.01	<0.01	<0.01	<0.5	<0.01	<2	1	<2	1.53	2	3	5.9	4.9
step 6th	<0.5	0.01	<0.01	0.13	<0.01	N.A.	<0.01	<0.5	<0.01	<2	11	<2	0.29	<1	<1	2.2	3.7
step 7th	1.7	0.19	0.39	8.71	0.05	2.3	0.02	11.8	0.31	101	108	32	1.68	<1	3	2	13.7

Element	***As***	***Sr***	***Y***	***Zr***	***Mo***	***Ag***	***Cd***	***Sn***	***Sb***	***Ba***	***La***	***W***	***Pb***	***Bi***	***Li***	***S***	***CO_2***
Det. limit	3	0.5	0.5	0.5	1	2	1	10	5	1	0.5	10	2	5	1	0.01	0.01
unit	ppm	ppm	ppm	ppm	ppm	ppm	ppm	ppm	ppm	ppm	ppm	ppm	ppm	ppm	ppm	%	%
step 1st	6	5.1	<0.5	<0.5	<1	<2	1	<10	<5	3	<0.5	<10	192	<5	<1	0.36	<0.01
step 2nd	22	4.4	<0.5	<0.5	1	<2	<1	<10	11	12	<0.5	<10	434	<5	<1	0.03	<0.01
step 3rd	345	<0.5	<0.5	<0.5	2	<2	<1	50	88	4	<0.5	<10	684	<5	<1	0.16	
step 4th	97	1.7	<0.5	<0.5	<1	<2	<1	150	494	5	<0.5	<10	86	<5	<1	0.08	
step 5th	143	<0.5	<0.5	<0.5	<1	<2	<1	<10	<5	<1	<0.5	<10	<2	<5	<1	1.95	
step 6th	64	8	<0.5	<0.5	<1	>10	<1	50	63	11	1.3	<10	46	<5	<1	0.4	
step 7th	22	152	3.2	16.8	1	<2	<1	70	207	237	17	10	27	<5	23	0.06	

DOI: 10.14750/ME.2021.004

ITOS GRANZA 1-7	**Analyzed years: 1st** (2008 sum.); **2nd** (2009 sum.); **3rd** (2010 aut. - 2011 spr.); **4th** year (2011 aut. - 2012 spr.)

1st year	***Day***	***0***	***3.5***	***7***	***10.5***	***14***	***17.5***	***21***	***24.5***	***28***	***31.5***	***35***	***38.5***	***42***	***45.5***	***49***	***56***	***63***	***72***	***78***	***87***	***95***	***101***
	pH (-)	2.21	2.09	2.31	2.42	2.62	2.83	2.91	2.94	3.01	3.01	3.11	3.12	3.34	3.35	3.05	2.76	2.55	2.48	2.44	2.35	2.32	2.42
	Eh (mV)	477	478	469	453	464	450	456	442	452	427	435	428	454	463	475	486	509	559	528	573	574	567
	TDS (mg/l)	2820	2620	1391	967	621	525	378	329	272	230	215	210	239	248	278	565	926	1371	1370	1488	1405	1274
	SO_4^{2-}	7760	7200	5755	638	349	253	148	139	107	87	70	66	78	83	102	-	-	-	-	-	-	-

2nd year	***Day***	***0***	***7***	***14***	***21***	***28***	***35***
	pH (-)	1.84	2.00	2.20	2.33	2.43	2.47
	Eh (mV)	499	494	490	503	538	561
	TDS (mg/l)	4590	3390	2020	1403	1147	1127
	SO_4^{2-}	-	-	-	-	-	-

3rd year	***Day***	***0***	***7***	***14***	***21***	***28***	***35***	***42***	***49***	***56***	***62***	***70***	***77***	***82***	***93***	***100***	***107***	***114***	***121***
	pH (-)	1.77	1.72	1.91	2.06	2.21	2.36	2.58	2.57	2.55	2.69	3.04	2.95	2.94	2.82	2.76	2.79	2.77	2.78
	Eh (mV)	496	493	491	489	499	499	505	502	508	510	490	493	505	519	515	515	523	532
	TDS (mg/l)	7540	4620	2540	1862	1238	1034	650	698	698	554	296	311	313	360	416	383	414	422
	SO_4^{2-}	6446	3906	960	914	723	630	405	399	298	231	81	77	79	77	116	89	102	100

4th year	***Day***	***0***	***7***	***14***	***21***	***28***	***35***	***42***	***49***	***56***	***63***	***70***	***77***	***84***	***91***	***98***	***105***	***112***	***119***
	pH (-)	1.66	1.86	2.17	2.25	2.3	2.37	2.4	2.41	2.43	2.36	2.35	2.4	2.47	2.48	2.4	2.49	2.51	2.5
	Eh (mV)	524	520	526	560	607	633	630	629	625	596	604	597	590	590	620	612	599	605
	TDS (mg/l)	5370	3960	1823	1280	1091	961	910	865	693	828	841	760	771	796	737	643	610	626
	SO_4^{2-}	13183	7923	2558	1557	1114	868	758	609	438	556	540	476	492	547	503	429	407	402

Remarks: In the 1st year the sulphate content was measured just in the first 49 days, moreover twice a week, but not further more. Also in year 1st only the first 49 days were measured by Ferenc Moricz, the further ones were completed by Dr. Ingar Walder (external consultant). In the year 2nd, on the 42nd day sampling was not done. In year 3rd on the 70th, 77th and 82nd days and in year 4th on the 84th and 91st days the samplings were completed also by Dr. Ingar Walder.

O_2 content sampling in year 4th, period days 105th - 112nd				
Day	***0***	***1***	***4***	***7***
O_2 content (V/V%)	21.1	19.4	17.0	14.5

Column free volume (cm^3)	2484

Sequential Chemical Extraction (SCE) result

Element	***Be***	***Na***	***Mg***	***Al***	***P***	***K***	***Ca***	***Sc***	***Ti***	***V***	***Cr***	***Mn***	***Fe***	***Co***	***Ni***	***Cu***	***Zn***
Det. limit	0.5	0.01	0.01	0.01	0.01	0.01	0.01	0.5	0.01	2	1	2	0.01	1	1	0.5	0.5
unit	ppm	%	%	%	%	%	%	ppm	%	ppm	ppm	ppm	%	ppm	ppm	ppm	ppm
step 1st	<0.5	<0.01	<0.01	0.02	<0.01	0.02	0.02	<0.5	<0.01	<2	1	7	0.03	<1	<1	<0.5	8.8
step 2nd	<0.5	<0.01	<0.01	0.03	<0.01	0.02	<0.01	<0.5	<0.01	<2	26	3	0.08	<1	<1	<0.5	2.1
step 3rd	<0.5	<0.01	<0.01	0.05	<0.01	0.03	<0.01	<0.5	<0.01	<2	45	4	0.3	<1	1	3.6	3.2
step 4th	<0.5	<0.01	<0.01	0.06	0.01	0.06	<0.01	<0.5	<0.01	<2	7	<2	0.36	<1	<1	2	2.2
step 5th	<0.5	<0.01	<0.01	0.01	<0.01	<0.01	<0.01	<0.5	<0.01	<2	1	<2	0.68	<1	1	13.8	5.6
step 6th	<0.5	0.01	<0.01	0.11	0.01	N.A.	<0.01	<0.5	<0.01	<2	11	<2	0.49	<1	<1	4.7	3.2
step 7th	2	0.17	0.29	7.25	0.05	2.3	0.03	7.5	0.2	61	105	45	1.17	<1	<1	1.8	12.2

Element	***As***	***Sr***	***Y***	***Zr***	***Mo***	***Ag***	***Cd***	***Sn***	***Sb***	***Ba***	***La***	***W***	***Pb***	***Bi***	***Li***	***S***	***CO_2***
Det. limit	3	0.5	0.5	0.5	1	2	1	10	5	1	0.5	10	2	5	1	0.01	0.01
unit	ppm	ppm	ppm	ppm	ppm	ppm	ppm	ppm	ppm	ppm	ppm	ppm	ppm	ppm	ppm	%	%
step 1st	<3	3.7	<0.5	<0.5	<1	<2	1	<10	83	4	<0.5	<10	471	<5	<1	0.12	<0.01
step 2nd	16	6.2	<0.5	<0.5	1	<2	<1	<10	377	16	<0.5	<10	3520	<5	<1	0.07	<0.01
step 3rd	137	<0.5	<0.5	2	4	<2	<1	60	1520	4	<0.5	<10	694	6	<1	0.08	
step 4th	90	1.3	<0.5	<0.5	<1	<2	<1	80	1370	7	<0.5	<10	326	5	<1	0.12	
step 5th	8	<0.5	<0.5	<0.5	<1	2	2	<10	10	<1	<0.5	<10	34	<5	<1	1.16	
step 6th	93	6.8	<0.5	<0.5	<1	>10	<1	60	1160	13	1.8	<10	963	<5	<1	0.55	
step 7th	11	123	3.2	23.8	2	<2	<1	80	430	473	15.1	<10	39	<5	13	0.14	

DOI: 10.14750/ME.2021.004

ITOS GRANZA 2-7	**Analyzed years: 1st** (2008 sum.); **2nd** (2009 sum.); **3rd** (2010 aut. - 2011 spr.); **4th** year (2011 aut. - 2012 spr.)

1st year	***Day***	***0***	***3.5***	***7***	***10.5***	***14***	***17.5***	***21***	***24.5***	***28***	***31.5***	***35***	***38.5***	***42***	***45.5***	***49***	***56***	***63***	***72***	***78***	***87***	***95***	***101***
	pH (-)	2.20	2.16	2.34	2.44	2.58	2.61	2.68	2.58	2.66	2.66	2.70	2.75	2.94	3.00	2.80	2.66	2.59	2.65	2.58	2.47	2.55	2.57
	Eh (mV)	545	548	515	514	499	507	505	503	494	485	488	479	502	501	505	502	513	530	539	548	535	555
	TDS (mg/l)	2470	1785	1063	835	670	527	703	717	711	644	675	672	755	672	642	751	828	967	952	913	893	778
	SO_4^{2-}	4830	3060	4600	463	348	419	351	359	400	370	338	363	404	390	353	-	-	-	-	-	-	-

2nd year	***Day***	***0***	***7***	***14***	***21***	***28***	***35***
	pH (-)	2.01	2.03	2.22	2.35	2.45	2.51
	Eh (mV)	540	520	515	538	551	560
	TDS (mg/l)	3120	3050	1960	1413	1149	984
	SO_4^{2-}	-	-	-	-	-	-

3rd year	***Day***	***0***	***7***	***14***	***21***	***28***	***35***	***42***	***49***	***56***	***62***	***70***	***77***	***82***	***93***	***100***	***107***	***114***	***121***
	pH (-)	1.96	1.80	1.94	2.11	2.25	2.31	2.45	2.45	2.44	2.56	2.68	2.68	2.47	2.55	2.58	2.58	2.61	2.63
	Eh (mV)	577	563	553	548	560	572	566	579	568	569	557	546	583	557	550	552	546	549
	TDS (mg/l)	3840	3890	2380	1654	1151	1204	931	953	930	770	684	595	916	738	695	755	644	648
	SO_4^{2-}	4124	4004	2117	1407	895	846	743	790	615	443	293	248	420	326	335	325	295	310

4th year	***Day***	***0***	***7***	***14***	***21***	***28***	***35***	***42***	***49***	***56***	***63***	***70***	***77***	***84***	***91***	***98***	***105***	***112***	***119***
	pH (-)	1.81	1.95	2.21	2.21	2.29	2.39	2.45	2.47	2.5	2.48	2.49	2.49	2.62	2.52	2.54	2.68	2.65	2.65
	Eh (mV)	620	607	588	614	614	621	613	614	600	576	577	561	559	555	573	575	570	575
	TDS (mg/l)	3650	2680	1612	1367	1046	850	790	701	527	614	576	574	497	581	534	409	413	408
	SO_4^{2-}	10940	9946	2501	1836	1180	833	720	521	335	412	355	356	306	392	361	260	262	261

Remarks: In the 1st year the sulphate content was measured just in the first 49 days, moreover twice a week, but not further more. Also in year 1st only the first 49 days were measured by Ferenc Moricz, the further ones were completed by Dr. Ingar Walder (external consultant). In the year 2nd, on the 42nd day sampling was not done. In year 3rd on the 70th, 77th and 82nd days and in year 4th on the 84th and 91st days the samplings were completed also by Dr. Ingar Walder.

O_2 content sampling in year 4th, period days 105th - 112nd				
Day	***0***	***1***	***4***	***7***
O_2 content ($^V/_V$%)	21.1	19.7	19.0	18.1

Column free volume (cm^3)	2634

Sequential Chemical Extraction (SCE) result

Element	***Be***	***Na***	***Mg***	***Al***	***P***	***K***	***Ca***	***Sc***	***Ti***	***V***	***Cr***	***Mn***	***Fe***	***Co***	***Ni***	***Cu***	***Zn***
Det. limit	0.5	0.01	0.01	0.01	0.01	0.01	0.01	0.5	0.01	2	1	2	0.01	1	1	0.5	0.5
unit	ppm	%	%	%	%	%	%	ppm	%	ppm	ppm	ppm	%	ppm	ppm	ppm	ppm
step 1st	<0.5	<0.01	<0.01	<0.01	<0.01	0.02	<0.01	<0.5	<0.01	<2	1	4	0.02	<1	<1	<0.5	1.2
step 2nd	<0.5	<0.01	<0.01	0.03	<0.01	0.02	<0.01	<0.5	<0.01	<2	38	4	0.1	<1	<1	<0.5	0.6
step 3rd	<0.5	<0.01	<0.01	0.05	<0.01	0.04	<0.01	<0.5	<0.01	<2	39	4	0.41	<1	1	3.2	1.8
step 4th	<0.5	0.01	<0.01	0.06	0.01	0.08	<0.01	<0.5	<0.01	<2	6	2	0.59	<1	<1	2.3	1.9
step 5th	<0.5	<0.01	<0.01	0.02	<0.01	<0.01	<0.01	<0.5	<0.01	<2	1	<2	1.98	<1	1	7.5	4
step 6th	<0.5	0.01	<0.01	0.11	<0.01	N.A.	<0.01	<0.5	<0.01	<2	13	<2	0.32	<1	<1	2.4	2.7
step 7th	1.8	0.17	0.29	6.64	0.06	2.05	0.05	6.8	0.22	58	115	75	1	<1	<1	1.6	14

Element	***As***	***Sr***	***Y***	***Zr***	***Mo***	***Ag***	***Cd***	***Sn***	***Sb***	***Ba***	***La***	***W***	***Pb***	***Bi***	***Li***	***S***	***CO_2***
Det. limit	3	0.5	0.5	0.5	1	2	1	10	5	1	0.5	10	2	5	1	0.01	0.01
unit	ppm	ppm	ppm	ppm	ppm	ppm	ppm	ppm	ppm	ppm	ppm	ppm	ppm	ppm	ppm	%	%
step 1st	<3	1.4	<0.5	<0.5	<1	<2	1	<10	6	<1	<0.5	<10	<2	<5	<1	0.06	<0.01
step 2nd	7	0.8	<0.5	<0.5	1	<2	<1	<10	21	10	<0.5	<10	35	<5	<1	0.02	<0.01
step 3rd	51	1.3	<0.5	1.2	3	<2	<1	30	103	5	<0.5	<10	155	<5	<1	0.13	
step 4th	47	3.4	<0.5	<0.5	<1	<2	<1	30	159	18	<0.5	<10	249	<5	<1	0.21	
step 5th	139	<0.5	<0.5	<0.5	<1	3	<1	<10	6	<1	<0.5	<10	<2	<5	<1	2.52	
step 6th	41	9.2	<0.5	<0.5	<1	>10	<1	40	79	16	1.4	<10	88	<5	<1	0.25	
step 7th	8	214	3.4	21.7	2	<2	<1	80	227	347	18	<10	69	<5	13	0.04	

DOI: 10.14750/ME.2021.004

BOL 1-8	**Analyzed years: 2nd** (2009 sum.); **3rd** (2010 aut. - 2011 spr.); **4th** year (2011 aut. - 2012 spr.)

2nd year	***Day***	***0***	***7***	***14***	***21***	***28***	***35***
	pH (-)	2.61	2.61	2.70	2.66	2.67	2.64
	Eh (mV)	513	494	505	537	530	552
	TDS (mg/l)	1062	1121	813	807	836	821
	SO_4^{2-}	-	-	-	-	-	-

3rd year	***Day***	***0***	***7***	***14***	***21***	***28***	***35***	***42***	***49***	***56***	***62***	***70***	***77***	***82***	***93***	***100***	***107***	***114***	***121***
	pH (-)	2.57	2.41	2.43	2.46	2.51	2.56	2.68	2.66	2.70	2.72	2.84	2.85	2.80	2.77	2.72	2.71	2.77	2.81
	Eh (mV)	594	615	602	584	592	582	582	579	581	575	523	533	540	550	565	552	563	569
	TDS (mg/l)	1616	1224	1035	793	671	616	554	552	530	473	417	428	414	461	498	454	444	431
	SO_4^{2-}	1337	739	661	550	346	327	316	295	209	185	142	147	145	146	149	131	129	127

4th year	***Day***	***0***	***7***	***14***	***21***	***28***	***35***	***42***	***49***	***56***	***63***	***70***	***77***	***84***	***91***	***98***	***105***	***112***	***119***
	pH (-)	2.31	2.51	2.54	2.5	2.62	2.63	2.65	2.63	2.66	2.65	2.66	2.69	2.83	2.86	2.81	2.83	2.82	2.84
	Eh (mV)	603	601	577	575	551	560	567	577	562	564	566	576	562	560	570	566	568	553
	TDS (mg/l)	1081	848	589	541	518	460	470	450	390	405	424	366	378	355	345	334	320	323
	SO_4^{2-}	1578	792	405	317	258	204	211	194	158	160	166	136	145	142	145	136	132	125

Remarks: In the year 2nd, on the 42nd day sampling was not done. In year 3rd on the 70th, 77th and 82nd days and in year 4th on the 84th and 91st days the samplings were completed also by Dr. Ingar Walder.

O_2 content sampling in year 4th, period days 105th - 112nd				
Day	***0***	***1***	***4***	***7***
O_2 content (V/V%)	21.1	20.1	20.1	19.9

Column free volume (cm^3)	2486

BOL 2-8	**Analyzed years: 2nd** (2009 sum.); **3rd** (2010 aut. - 2011 spr.); **4th** year (2011 aut. - 2012 spr.)

2nd year	***Day***	***0***	***7***	***14***	***21***	***28***	***35***	***42***
	pH (-)	0.98	1.77	1.97	2.59	2.83	2.94	2.93
	Eh (mV)	465	457	430	412	472	471	450
	TDS (mg/l)	30200	6160	3700	760	489	345	311
	SO_4^{2-}	-	-	-	-	-	-	-

3rd year	***Day***	***0***	***7***	***14***	***21***	***28***	***35***	***42***	***49***	***56***	***62***	***70***	***77***	***82***	***93***	***100***	***107***	***114***	***121***
	pH (-)	1.44	1.93	2.18	2.27	2.29	2.30	2.33	2.18	2.21	2.29	2.27	2.11	2.22	2.06	2.18	2.14	2.15	2.22
	Eh (mV)	441	434	422	419	428	439	455	456	455	450	455	452	457	469	461	463	464	460
	TDS (mg/l)	39800	3240	1352	1054	1021	1106	1385	1575	1514	1360	1659	1542	1610	2140	1576	1808	1829	1552
	SO_4^{2-}	29475	628	337	300	296	399	616	716	674	592	703	695	850	770	698	725	693	701

4th year	***Day***	***0***	***7***	***14***	***21***	***28***	***35***	***42***	***49***	***56***	***63***	***70***	***77***	***84***	***91***	***98***	***105***	***112***	***119***
	pH (-)	1.06	1.91	2.24	2.25	2.23	2.23	2.26	2.26	2.25	2.26	2.29	2.31	2.42	2.76	2.83	2.61	2.54	2.51
	Eh (mV)	488	470	451	462	463	461	447	446	460	454	449	449	447	424	414	452	445	452
	TDS (mg/l)	24000	4140	1583	1319	1590	1723	1392	986	1362	1362	1166	1131	1066	531	378	690	777	988
	SO_4^{2-}	46888	4490	1127	848	1055	1063	839	529	771	762	598	564	577	266	194	355	420	470

Remarks: In year 3rd on the 70th, 77th and 82nd days and in year 4th on the 84th and 91st days the samplings were completed also by Dr. Ingar Walder.

O_2 content sampling in year 4th, period days 105th - 112nd				
Day	***0***	***1***	***4***	***7***
O_2 content (V/V%)	21.1	20.1	19.5	18.7

Column free volume (cm^3)	2544

DOI: 10.14750/ME.2021.004

BOL 3-8	**Analyzed years: 2nd** (2009 sum.); **3rd** (2010 aut. - 2011 spr.); **4th** year (2011 aut. - 2012 spr.)

2nd year	***Day***	***0***	***7***	***14***	***21***	***28***	***35***	***42***
	pH (-)	2.42	2.71	2.74	2.75	2.75	2.80	2.84
	Eh (mV)	505	446	492	513	493	488	486
	TDS (mg/l)	861	749	568	534	536	518	457
	SO_4^{2-}	-	-	-	-	-	-	-

3rd year	***Day***	***0***	***7***	***14***	***21***	***28***	***35***	***42***	***49***	***56***	***62***	***70***	***77***	***82***	***93***	***100***	***107***	***114***	***121***
	pH (-)	2.35	2.35	2.40	2.51	2.55	2.63	2.72	2.72	2.73	2.77	2.95	2.83	2.79	2.74	2.75	2.73	2.73	2.78
	Eh (mV)	568	553	553	545	546	546	545	542	542	553	543	523	566	550	551	561	552	549
	TDS (mg/l)	1460	1350	1000	687	537	528	465	462	452	424	326	391	386	406	427	427	450	387
	SO_4^{2-}	890	900	350	375	243	230	238	235	129	127	90	116	124	112	124	120	116	120

4th year	***Day***	***0***	***7***	***14***	***21***	***28***	***35***	***42***	***49***	***56***	***63***	***70***	***77***	***84***	***91***	***98***	***105***	***112***	***119***
	pH (-)	1.96	2.29	2.51	2.5	2.53	2.57	2.58	2.59	2.65	2.63	2.64	2.7	2.71	2.81	2.79	2.78	2.8	2.8
	Eh (mV)	626	603	581	587	571	583	570	581	573	575	586	577	572	549	567	561	567	560
	TDS (mg/l)	1472	1198	641	555	524	482	464	446	384	406	415	368	396	375	350	337	321	319
	SO_4^{2-}	3715	1790	526	356	273	224	202	186	151	161	163	146	151	150	145	134	130	121

Remarks: In year 3rd on the 70th, 77th and 82nd days and in year 4th on the 84th and 91st days the samplings were completed also by Dr. Ingar Walder.

O_2 content sampling in year 4th, period days 105th - 112nd				
Day	***0***	***1***	***4***	***7***
O_2 content (V/V%)	21.1	20.2	19.9	19.4

Column free volume (cm^3)	2738

DOI: 10.14750/ME.2021.004

BOL 1-9	**Analyzed year: 4th** year (2011 aut. - 2012 spr.)

4th year	***Day***	***0***	***7***	***14***	***21***	***28***	***35***	***42***	***49***	***56***	***63***	***70***	***77***	***84***	***91***	***98***	***105***	***112***
	pH (-)	2.48	2.26	2.49	2.44	2.50	2.58	2.60	2.53	2.47	2.42	2.59	2.34	2.53	2.62	2.62	2.61	2.52
	Eh (mV)	522	520	548	556	564	564	567	553	553	554	557	555	565	566	562	546	568
	TDS (mg/l)	1337	1772	862	835	889	723	660	808	882	1045	660	1421	911	555	603	738	902
	SO_4^{2-}	2016	2987	1009	966	907	671	601	908	875	1134	578	1775	905	456	530	767	855

Remarks: In year 4th on the 77th and 84th days the samplings were completed also by Dr. Ingar Walder.

O_2 content sampling in year 4th, period days 105th - 112nd				
Day	***0***	***1***	***4***	***7***
O_2 content (V/V%)	21.1	20.4	19.9	19.2

Column free volume (cm^3)	2750

Sequential Chemical Extraction (SCE) result

Element	***Ag***	***Al***	***As***	***Ba***	***Be***	***Bi***	***Ca***	***Cd***	***Co***	***Cr***	***Cu***	***Fe***	***K***	***La***	***Li***	***Mg***	***Mn***
Det. limit	2	0.01	3	1	0.5	5	0.01	1	1	1	0.5	0.01	0.01	0.5	1	0.01	2
unit	ppm	%	ppm	ppm	ppm	ppm	%	ppm	ppm	ppm	ppm	%	%	ppm	ppm	%	ppm
step 1st	0.1	<3	3	<0.5	<5	0.05	<1	<1	<1	2.7	0.11	<0.01	<0.5	<1	<0.01	2	0.1
step 2nd	<0.01	10	50	<0.5	<5	<0.01	<1	<1	<1	<0.5	0.14	<0.01	<0.5	<1	<0.01	<2	<0.01
step 3rd	<0.01	16	3	<0.5	<5	<0.01	<1	<1	3	0.7	0.18	<0.01	<0.5	<1	0.02	<2	<0.01
step 4th	0.01	40	45	<0.5	6	<0.01	<1	<1	1	18.1	1.57	0.17	<0.5	<1	<0.01	<2	0.01
step 5th	<0.01	<3	1	<0.5	<5	<0.01	<1	<1	<1	<0.5	0.06	<0.01	<0.5	<1	<0.01	<2	<0.01
step 6th	0.04	11	84	<0.5	<5	<0.01	<1	<1	3	<0.5	0.17	N.A.	1.9	<1	<0.01	<2	0.04
step 7th	6.4	11	738	1.7	<5	0.13	<1	<1	24	1.1	0.32	N.A.	44.8	24	0.23	38	6.4

Element	***Mo***	***Na***	***Ni***	***P***	***Pb***	***S***	***Sb***	***Sc***	***Sn***	***Sr***	***Ti***	***V***	***W***	***Y***	***Zn***	***Zr***	***CO_2***
Det. limit	1	0.01	1	0.01	2	0.01	5	0.5	10	0.5	0.01	2	10	0.5	0.5	0.5	0.01
unit	ppm	%	ppm	%	ppm	%	ppm	ppm	ppm	ppm	%	ppm	ppm	ppm	ppm	ppm	%
step 1st	<1	<0.01	2	<0.01	44	0.49	<5	<0.5	<10	7.7	<0.01	<2	<10	<0.5	55	<0.5	0.04
step 2nd	<1	<0.01	<1	<0.01	274	0.04	<5	<0.5	<10	3.6	<0.01	<2	<10	<0.5	1.6	<0.5	0.04
step 3rd	<1	<0.01	6	<0.01	366	0.03	10	<0.5	10	0.8	<0.01	5	<10	<0.5	1.9	1.1	
step 4th	<1	0.03	<1	0.01	760	0.61	167	<0.5	40	14.1	<0.01	<2	<10	<0.5	17.1	<0.5	
step 5th	<1	<0.01	<1	<0.01	17	0.19	<5	<0.5	<10	0.6	<0.01	<2	<10	<0.5	1.2	<0.5	
step 6th	<1	0.07	<1	0.01	501	0.09	47	<0.5	70	5.7	<0.01	<2	<10	<0.5	11	<0.5	
step 7th	<1	0.28	2	0.04	348	0.04	110	8.6	180	208	0.45	64	10	5.6	28.1	43.2	

DOI: 10.14750/ME.2021.004

BOL 2-9	**Analyzed year: 4th** year (2011 aut. - 2012 spr.)

	Day	*0*	*7*	*14*	*21*	*28*	*35*	*42*	*49*	*56*	*63*	*70*	*77*	*84*	*91*	*98*	*105*	*112*
4th year	*pH (-)*	2.64	2.59	3.01	2.89	2.98	3.04	3.09	2.78	2.80	2.88	2.98	2.93	3.00	2.90	3.01	2.97	2.98
	Eh (mV)	566	573	519	544	533	543	544	556	561	566	558	543	522	580	574	574	569
	TDS (mg/l)	856	476	192	230	231	226	181	337	293	237	191	196	207	187	154	168	160
	SO_4^{2-}	960	446	122	147	134	128	114	186	145	102	76	77	83	74	60	65	58

Remarks: In year 4th on the 77th and 84th days the samplings were completed also by Dr. Ingar Walder.

O_2 content sampling in year 4th, period days 105th - 112nd				
Day	*0*	*1*	*4*	*7*
O_2 content (V/V%)	21.1	20.7	20.4	20.3

Column free volume (cm^3)	2886

Sequential Chemical Extraction (SCE) result

Element	*Ag*	*Al*	*As*	*Ba*	*Be*	*Bi*	*Ca*	*Cd*	*Co*	*Cr*	*Cu*	*Fe*	*K*	*La*	*Li*	*Mg*	*Mn*
Det. limit	2	0.01	3	1	0.5	5	0.01	1	1	1	0.5	0.01	0.01	0.5	1	0.01	2
unit	ppm	%	ppm	ppm	ppm	ppm	%	ppm	ppm	ppm	ppm	%	%	ppm	ppm	%	ppm
step 1st	<2	0.01	<3	<1	<0.5	<5	0.01	<1	<1	<1	2.4	<0.01	<0.01	<0.5	<1	<0.01	2
step 2nd	<2	0.01	73	<1	<0.5	<5	<0.01	<1	<1	<1	2.2	0.13	<0.01	<0.5	<1	<0.01	<2
step 3rd	<2	0.02	263	<1	<0.5	<5	<0.01	1	<1	<1	8.2	0.47	<0.01	<0.5	<1	<0.01	12
step 4th	<2	0.08	92	45	<0.5	<5	<0.01	1	<1	2	4.7	1.13	0.04	0.5	2	0.01	8
step 5th	<2	0.06	6	5	<0.5	<5	<0.01	<1	<1	<1	<0.5	0.03	0.01	<0.5	1	<0.01	<2
step 6th	<2	0.26	66	42	<0.5	<5	0.02	<1	<1	4	3.3	0.65	N.A.	4.3	6	0.08	21
step 7th	<2	4.94	35	454	1.7	<5	0.57	<1	<1	8	5.2	0.95	N.A.	29	39	0.2	102

Element	*Mo*	*Na*	*Ni*	*P*	*Pb*	*S*	*Sb*	*Sc*	*Sn*	*Sr*	*Ti*	*V*	*W*	*Y*	*Zn*	*Zr*	*CO_2*
Det. limit	1	0.01	1	0.01	2	0.01	5	0.5	10	0.5	0.01	2	10	0.5	0.5	0.5	0.01
unit	ppm	%	ppm	%	ppm	%	ppm	ppm	ppm	ppm	%	ppm	ppm	ppm	ppm	ppm	%
step 1st	<1	<0.01	<1	<0.01	<2	0.08	<5	<0.5	<10	<0.5	<0.01	<2	<10	<0.5	118	<0.5	0.04
step 2nd	<1	<0.01	<1	<0.01	<2	0.03	<5	<0.5	<10	<0.5	<0.01	<2	<10	<0.5	9.4	<0.5	0.04
step 3rd	<1	<0.01	<1	0.01	<2	0.09	<5	<0.5	<10	1.2	<0.01	5	<10	<0.5	5.7	3.2	
step 4th	<1	0.02	<1	<0.01	25	0.3	<5	<0.5	<10	10.5	<0.01	3	<10	<0.5	15.8	0.9	
step 5th	<1	<0.01	<1	<0.01	4	<0.01	<5	<0.5	<10	1.6	<0.01	<2	<10	<0.5	1.3	0.5	
step 6th	<1	0.07	1	0.01	42	0.02	<5	0.6	30	10.7	0.02	5	<10	0.7	19.6	0.8	
step 7th	<1	1.35	3	0.03	51	0.03	16	3.6	80	261	0.26	29	<10	5.5	30.8	42	

DOI: 10.14750/ME.2021.004

BOL 3-9	**Analyzed year: 4th** year (2011 aut. - 2012 spr.)

4th year	*Day*	*0*	*7*	*14*	*21*	*28*	*35*	*42*	*49*	*56*	*63*	*70*	*77*	*84*	*91*	*98*	*105*	*112*
	pH (-)	1.84	2.33	2.42	2.48	2.50	2.47	2.25	2.01	2.06	1.99	2.02	2.14	2.32	2.09	2.26	2.38	2.30
	Eh (mV)	486	489	513	542	555	572	580	532	509	495	495	513	523	516	548	560	563
	TDS (mg/l)	8980	1075	987	909	758	898	1316	2610	2150	2600	2440	1952	1262	2390	1498	1127	1582
	SO_4^{2-}	64790	856	686	667	449	481	600	1265	1011	1356	1154	945	633	1298	718	508	720

Remarks: In year 4th on the 77th and 84th days the samplings were completed also by Dr. Ingar Walder.

O_2 content sampling in year 4th, period days 105th - 112nd				
Day	*0*	*1*	*4*	*7*
O_2 content (V/V%)	21.1	20.5	18.9	17.4

Column free volume (cm^3)	2062

Sequential Chemical Extraction (SCE) result

Element	*Ag*	*Al*	*As*	*Ba*	*Be*	*Bi*	*Ca*	*Cd*	*Co*	*Cr*	*Cu*	*Fe*	*K*	*La*	*Li*	*Mg*	*Mn*
Det. limit	2	0.01	3	1	0.5	5	0.01	1	1	1	0.5	0.01	0.01	0.5	1	0.01	2
unit	ppm	%	ppm	ppm	ppm	ppm	%	ppm	ppm	ppm	ppm	%	%	ppm	ppm	%	ppm
step 1st	<2	0.03	12	<1	<0.5	<5	0.01	4	<1	<1	13.3	0.82	<0.01	<0.5	<1	<0.01	8
step 2nd	<2	<0.01	102	<1	<0.5	<5	<0.01	1	<1	<1	<0.5	0.31	<0.01	<0.5	<1	<0.01	<2
step 3rd	<2	<0.01	75	2	<0.5	10	<0.01	<1	<1	<1	2	0.39	0.02	<0.5	<1	<0.01	<2
step 4th	<2	<0.01	79	14	<0.5	16	<0.01	<1	<1	<1	7	0.76	0.04	<0.5	<1	<0.01	<2
step 5th	2	<0.01	28	<1	<0.5	<5	<0.01	<1	1	<1	8.2	1.73	<0.01	<0.5	<1	<0.01	<2
step 6th	>10	0.01	94	12	<0.5	6	<0.01	1	<1	3	6.6	0.78	N.A.	0.8	<1	<0.01	<2
step 7th	<2	3.22	38	212	0.9	6	0.03	<1	<1	13	4.8	0.65	N.A.	30.4	17	0.18	28

Element	*Mo*	*Na*	*Ni*	*P*	*Pb*	*S*	*Sb*	*Sc*	*Sn*	*Sr*	*Ti*	*V*	*W*	*Y*	*Zn*	*Zr*	*CO_2*
Det. limit	1	0.01	1	0.01	2	0.01	5	0.5	10	0.5	0.01	2	10	0.5	0.5	0.5	0.01
unit	ppm	%	ppm	%	ppm	%	ppm	ppm	ppm	ppm	%	ppm	ppm	ppm	ppm	ppm	%
step 1st	<1	<0.01	2	<0.01	9	1.07	<5	<0.5	<10	3.3	<0.01	<2	<10	<0.5	838	<0.5	0.03
step 2nd	<1	<0.01	<1	<0.01	45	0.07	<5	<0.5	<10	0.6	<0.01	<2	<10	<0.5	16.3	<0.5	0.04
step 3rd	<1	<0.01	<1	<0.01	282	0.13	<5	<0.5	40	1.1	<0.01	<2	<10	<0.5	7.8	<0.5	
step 4th	<1	<0.01	<1	<0.01	471	0.23	19	<0.5	70	4.3	<0.01	<2	<10	<0.5	24.4	<0.5	
step 5th	<1	<0.01	3	<0.01	<2	1.97	<5	<0.5	<10	<0.5	<0.01	<2	<10	<0.5	3.2	<0.5	
step 6th	<1	0.06	<1	<0.01	53	1.15	8	<0.5	80	3.3	<0.01	<2	<10	<0.5	14.3	<0.5	
step 7th	<1	0.1	1	0.03	47	0.07	62	4.9	170	83.4	0.3	41	<10	4.1	17.5	25.3	

DOI: 10.14750/ME.2021.004

BOL 4-9	**Analyzed year: 4th** year (2011 aut. - 2012 spr.)

4th year	*Day*	*0*	*7*	*14*	*21*	*28*	*35*	*42*	*49*	*56*	*63*	*70*	*77*	*84*	*91*	*98*	*105*	*112*
	pH (-)	1.39	1.98	1.91	1.98	2.08	2.16	2.20	2.17	2.22	2.23	2.18	2.18	2.43	2.17	2.21	2.38	2.22
	Eh (mV)	474	472	471	460	465	462	461	462	464	459	452	443	445	453	442	450	447
	TDS (mg/l)	15170	4190	4640	4500	2890	2360	1785	2140	1472	1552	1958	1980	1288	2040	1888	1152	2060
	SO_4^{2-}	58321	7342	6841	6025	2915	2086	1463	1844	1332	1494	1890	1645	1376	1840	1343	667	1234

Remarks: In year 4th on the 77th and 84th days the samplings were completed also by Dr. Ingar Walder.

O_2 content sampling in year 4th, period days 105th - 112nd				
Day	*0*	*1*	*4*	*7*
O_2 content (V/V%)	21.1	20.4	18.3	16.7

Column free volume (cm^3)	2408

Sequential Chemical Extraction (SCE) result

Element	*Ag*	*Al*	*As*	*Ba*	*Be*	*Bi*	*Ca*	*Cd*	*Co*	*Cr*	*Cu*	*Fe*	*K*	*La*	*Li*	*Mg*	*Mn*
Det. limit	2	0.01	3	1	0.5	5	0.01	1	1	1	0.5	0.01	0.01	0.5	1	0.01	2
unit	ppm	%	ppm	ppm	ppm	ppm	%	ppm	ppm	ppm	ppm	%	%	ppm	ppm	%	ppm
step 1st	4	0.31	100	2	<0.5	<5	0.01	2	1	2	4.4	1.58	0.06	<0.5	1	0.01	6
step 2nd	<2	<0.01	16	85	<0.5	16	<0.01	<1	<1	<1	<0.5	0.03	<0.01	2.1	<1	<0.01	<2
step 3rd	<2	<0.01	30	30	<0.5	5	<0.01	<1	<1	<1	<0.5	0.05	<0.01	<0.5	<1	<0.01	<2
step 4th	<2	<0.01	14	7	<0.5	<5	<0.01	<1	<1	<1	<0.5	<0.01	<0.01	<0.5	<1	<0.01	<2
step 5th	10	<0.01	267	1	<0.5	<5	<0.01	3	2	<1	2.4	3.88	<0.01	<0.5	<1	<0.01	<2
step 6th	>10	0.01	284	3	<0.5	9	<0.01	4	1	2	4.5	6.17	N.A.	<0.5	<1	<0.01	<2
step 7th	<2	5.1	36	195	0.6	<5	0.01	<1	<1	26	1.6	0.52	N.A.	45.4	15	0.14	44

Element	*Mo*	*Na*	*Ni*	*P*	*Pb*	*S*	*Sb*	*Sc*	*Sn*	*Sr*	*Ti*	*V*	*W*	*Y*	*Zn*	*Zr*	*CO_2*
Det. limit	1	0.01	1	0.01	2	0.01	5	0.5	10	0.5	0.01	2	10	0.5	0.5	0.5	0.01
unit	ppm	%	ppm	%	ppm	%	ppm	ppm	ppm	ppm	%	ppm	ppm	ppm	ppm	ppm	%
step 1st	<1	<0.01	3	<0.01	74	2.18	<5	<0.5	<10	6.7	<0.01	3	<10	<0.5	134	<0.5	0.04
step 2nd	<1	<0.01	<1	<0.01	1490	0.06	<5	<0.5	<10	56.3	<0.01	<2	<10	<0.5	2.2	<0.5	0.04
step 3rd	<1	<0.01	<1	<0.01	127	0.02	<5	<0.5	30	1.7	<0.01	<2	<10	<0.5	<0.5	<0.5	
step 4th	<1	<0.01	<1	<0.01	27	<0.01	<5	<0.5	30	0.8	<0.01	<2	<10	<0.5	0.9	<0.5	
step 5th	<1	<0.01	4	<0.01	12	4.61	<5	<0.5	<10	<0.5	<0.01	<2	<10	<0.5	16.7	<0.5	
step 6th	<1	0.06	3	<0.01	58	>5	<5	<0.5	80	0.7	<0.01	<2	<10	<0.5	66.9	<0.5	
step 7th	<1	0.05	3	0.02	159	0.47	19	5.6	110	25.9	0.39	55	10	4.9	11.6	31.9	

Remarks: The S content in the 6th step exceeded the upper detection limit (5 %).

DOI: 10.14750/ME.2021.004

BOL 5-9	**Analyzed year: 4th** year (2011 aut. - 2012 spr.)

4th year	*Day*	*0*	*7*	*14*	*21*	*28*	*35*	*42*	*49*	*56*	*63*	*70*	*77*	*84*	*91*	*98*	*105*	*112*
	pH (-)	1.44	2.26	2.20	2.34	2.55	2.79	2.89	2.79	3.02	2.99	2.90	2.85	2.97	2.98	3.03	3.17	3.08
	Eh (mV)	453	430	423	420	424	421	420	412	410	407	405	402	443	428	427	441	438
	TDS (mg/l)	20200	1415	1144	841	474	346	272	335	176	230	264	326	258	184	170	94	123
	SO_4^{2-}	55500	1713	650	477	240	170	131	158	83	132	131	151	139	88	78	42	56

Remarks: In year 4th on the 77th and 84th days the samplings were completed also by Dr. Ingar Walder.

O_2 content sampling in year 4th, period days 105th - 112nd				
Day	*0*	*1*	*4*	*7*
O_2 content (V/V%)	21.1	20.9	20.6	20.5

Column free volume (cm^3)	2240

Sequential Chemical Extraction (SCE) result

Element	*Ag*	*Al*	*As*	*Ba*	*Be*	*Bi*	*Ca*	*Cd*	*Co*	*Cr*	*Cu*	*Fe*	*K*	*La*	*Li*	*Mg*	*Mn*
Det. limit	2	0.01	3	1	0.5	5	0.01	1	1	1	0.5	0.01	0.01	0.5	1	0.01	2
unit	ppm	%	ppm	ppm	ppm	ppm	%	ppm	ppm	ppm	ppm	%	%	ppm	ppm	%	ppm
step 1st	8	0.11	501	2	<0.5	<5	0.02	5	<1	<1	2.5	1.23	0.02	<0.5	<1	<0.01	5
step 2nd	<2	<0.01	713	27	<0.5	<5	<0.01	7	<1	<1	<0.5	0.13	<0.01	<0.5	<1	<0.01	<2
step 3rd	<2	<0.01	190	1	<0.5	<5	<0.01	1	<1	<1	<0.5	0.03	<0.01	<0.5	<1	<0.01	<2
step 4th	<2	<0.01	10	1	<0.5	<5	<0.01	<1	<1	<1	<0.5	<0.01	<0.01	<0.5	<1	<0.01	<2
step 5th	>10	<0.01	376	<1	<0.5	<5	<0.01	4	<1	<1	<0.5	7.45	<0.01	<0.5	<1	<0.01	12
step 6th	>10	<0.01	338	2	<0.5	<5	<0.01	4	<1	3	<0.5	7.84	N.A.	<0.5	<1	<0.01	11
step 7th	<2	1.87	55	156	0.6	<5	<0.01	<1	<1	5	0.6	0.37	N.A.	19.5	26	0.08	36

Element	*Mo*	*Na*	*Ni*	*P*	*Pb*	*S*	*Sb*	*Sc*	*Sn*	*Sr*	*Ti*	*V*	*W*	*Y*	*Zn*	*Zr*	*CO_2*
Det. limit	1	0.01	1	0.01	2	0.01	5	0.5	10	0.5	0.01	2	10	0.5	0.5	0.5	0.01
unit	ppm	%	ppm	%	ppm	%	ppm	ppm	ppm	ppm	%	ppm	ppm	ppm	ppm	ppm	%
step 1st	<1	<0.01	1	0.01	80	1.68	<5	<0.5	<10	4.1	<0.01	<2	<10	<0.5	109	<0.5	0.03
step 2nd	<1	<0.01	<1	<0.01	1790	0.07	<5	<0.5	<10	33.9	<0.01	<2	<10	<0.5	1.9	<0.5	0.04
step 3rd	<1	<0.01	<1	<0.01	71	<0.01	5	<0.5	30	<0.5	<0.01	<2	<10	<0.5	<0.5	<0.5	
step 4th	<1	<0.01	<1	<0.01	27	<0.01	8	<0.5	<10	1.1	<0.01	<2	<10	<0.5	0.6	<0.5	
step 5th	<1	<0.01	4	<0.01	93	>5	15	<0.5	10	<0.5	<0.01	<2	<10	<0.5	20	<0.5	
step 6th	<1	0.06	3	<0.01	284	>5	38	<0.5	50	1.2	<0.01	<2	<10	<0.5	27.7	<0.5	
step 7th	<1	0.01	2	0.02	119	0.33	73	2.7	70	36.6	0.16	20	<10	3.5	36	19.9	

Sequential Chemical Extraction (SCE) DUPLICATED result

Element	*Ag*	*Al*	*As*	*Ba*	*Be*	*Bi*	*Ca*	*Cd*	*Co*	*Cr*	*Cu*	*Fe*	*K*	*La*	*Li*	*Mg*	*Mn*
Det. limit	2	0.01	3	1	0.5	5	0.01	1	1	1	0.5	0.01	0.01	0.5	1	0.01	2
unit	ppm	%	ppm	ppm	ppm	ppm	%	ppm	ppm	ppm	ppm	%	%	ppm	ppm	%	ppm
step 1st	8	0.13	403	3	<0.5	<5	0.02	4	<1	<1	2.8	1.29	0.02	<0.5	<1	<0.01	5
step 2nd	<2	<0.01	765	27	<0.5	<5	<0.01	7	<1	<1	<0.5	0.13	<0.01	<0.5	<1	<0.01	<2
step 3rd	<2	<0.01	207	<1	<0.5	<5	<0.01	1	<1	<1	<0.5	0.03	<0.01	<0.5	<1	<0.01	<2
step 4th	<2	<0.01	9	<1	<0.5	<5	<0.01	<1	<1	<1	<0.5	<0.01	<0.01	<0.5	<1	<0.01	<2
step 5th	>10	<0.01	381	<1	<0.5	<5	<0.01	4	<1	<1	<0.5	7.9	<0.01	<0.5	<1	<0.01	13
step 6th	>10	<0.01	357	2	<0.5	<5	<0.01	4	<1	2	<0.5	8.27	N.A.	<0.5	<1	<0.01	12
step 7th	<2	1.86	49	152	0.6	<5	<0.01	<1	<1	6	1.5	0.38	N.A.	18.6	25	0.08	35

Element	*Mo*	*Na*	*Ni*	*P*	*Pb*	*S*	*Sb*	*Sc*	*Sn*	*Sr*	*Ti*	*V*	*W*	*Y*	*Zn*	*Zr*	*CO_2*
Det. limit	1	0.01	1	0.01	2	0.01	5	0.5	10	0.5	0.01	2	10	0.5	0.5	0.5	0.01
unit	ppm	%	ppm	%	ppm	%	ppm	ppm	ppm	ppm	%	ppm	ppm	ppm	ppm	ppm	%
step 1st	<1	<0.01	1	<0.01	82	1.62	<5	<0.5	<10	5	<0.01	<2	<10	<0.5	101	<0.5	0.03
step 2nd	<1	<0.01	<1	0.01	1790	0.07	<5	<0.5	<10	33.2	<0.01	<2	<10	<0.5	1.4	<0.5	0.04
step 3rd	<1	<0.01	<1	<0.01	79	<0.01	6	<0.5	40	<0.5	<0.01	<2	<10	<0.5	<0.5	<0.5	
step 4th	<1	<0.01	<1	<0.01	25	0.01	9	<0.5	<10	1	<0.01	<2	<10	<0.5	0.6	<0.5	
step 5th	<1	<0.01	4	<0.01	74	>5	12	<0.5	10	<0.5	<0.01	<2	<10	<0.5	18.4	<0.5	
step 6th	<1	0.07	4	<0.01	295	>5	42	<0.5	50	1.2	<0.01	<2	<10	<0.5	28.1	<0.5	
step 7th	<1	0.01	2	0.01	113	0.34	73	2.6	70	34.6	0.17	20	<10	3.4	35.8	19.7	

DOI: 10.14750/ME.2021.004

BOL 6-9	**Analyzed years: 3rd** (2010 aut. - 2011 spr.); **4th** year (2011 aut. - 2012 spr.)

3rd year	***Day***	***0***	***7***	***14***	***21***	***28***	***35***	***42***	***49***	***56***	***64***	***71***	***76***	***87***	***94***	***101***	***108***	***115***
	pH (-)	2.38	2.71	2.83	2.96	2.87	2.88	2.90	2.91	2.88	2.81	2.79	2.71	2.43	2.56	2.46	2.61	2.54
	Eh (mV)	433	362	385	405	407	403	402	393	388	401	394	425	430	423	435	420	442
	TDS (mg/l)	4740	2210	681	456	437	466	557	635	661	858	915	943	1641	1258	1437	1302	1253
	SO_4^{2-}	9440	2020	565	336	246	300	412	433	505	486	616	778	712	771	712	801	792

4th year	***Day***	***0***	***7***	***14***	***21***	***28***	***35***	***42***	***49***	***56***	***63***	***70***	***77***	***84***	***91***	***98***	***105***	***112***	***119***
	pH (-)	1.49	2.06	2.33	2.38	2.34	2.36	2.39	2.40	2.38	2.39	2.41	2.43	2.44	2.66	2.67	2.62	2.63	2.64
	Eh (mV)	550	475	459	460	457	480	479	483	533	479	494	506	488	468	466	526	498	541
	TDS (mg/l)	10810	2450	1204	1046	1077	1156	1065	943	1007	973	848	853	818	612	524	618	593	596
	SO_4^{2-}	70640	2623	788	658	646	548	492	427	428	417	356	348	339	271	239	282	273	272

Remarks: In year 3rd on the 64th, 71st and 76th days and in year 4th on the 77th and 84th days the samplings were completed also by Dr. Ingar Walder.

O_2 content sampling in year 4th, period days 105th - 112nd				
Day	***0***	***1***	***4***	***7***
O_2 content ($^V/_V$%)	21.1	20.2	18.7	17.3

Column free volume (cm^3)	2200

Sequential Chemical Extraction (SCE) result

Element	***Ag***	***Al***	***As***	***Ba***	***Be***	***Bi***	***Ca***	***Cd***	***Co***	***Cr***	***Cu***	***Fe***	***K***	***La***	***Li***	***Mg***	***Mn***
Det. limit	2	0.01	3	1	0.5	5	0.01	1	1	1	0.5	0.01	0.01	0.5	1	0.01	2
unit	ppm	%	ppm	ppm	ppm	ppm	%	ppm	ppm	ppm	ppm	%	%	ppm	ppm	%	ppm
step 1st	<2	<0.01	9	<1	<0.5	<5	0.02	2	2	<1	88.3	0.09	<0.01	<0.5	<1	<0.01	45
step 2nd	<2	<0.01	18	<1	<0.5	25	<0.01	<1	<1	<1	2.9	0.16	<0.01	<0.5	<1	<0.01	<2
step 3rd	<2	<0.01	118	<1	<0.5	22	<0.01	<1	<1	2	11.3	0.71	<0.01	<0.5	<1	<0.01	8
step 4th	<2	<0.01	<3	<1	<0.5	<5	<0.01	<1	<1	<1	0.6	0.14	<0.01	<0.5	<1	<0.01	30
step 5th	<2	<0.01	3	<1	<0.5	<5	<0.01	<1	<1	<1	70.8	0.33	<0.01	<0.5	<1	<0.01	3
step 6th	<2	0.02	146	2	<0.5	62	0.02	2	<1	3	57.3	0.84	N.A.	0.6	<1	<0.01	12
step 7th	<2	3.43	4	64	1.3	<5	0.02	<1	<1	16	6.4	0.99	N.A.	22.5	35	0.51	30

Element	***Mo***	***Na***	***Ni***	***P***	***Pb***	***S***	***Sb***	***Sc***	***Sn***	***Sr***	***Ti***	***V***	***W***	***Y***	***Zn***	***Zr***	***CO_2***
Det. limit	1	0.01	1	0.01	2	0.01	5	0.5	10	0.5	0.01	2	10	0.5	0.5	0.5	0.01
unit	ppm	%	ppm	%	ppm	%	ppm	ppm	ppm	ppm	%	ppm	ppm	ppm	ppm	ppm	%
step 1st	<1	<0.01	3	<0.01	<2	0.16	<5	<0.5	<10	<0.5	<0.01	<2	<10	<0.5	152	<0.5	0.04
step 2nd	<1	<0.01	<1	<0.01	3	0.07	<5	<0.5	<10	<0.5	<0.01	<2	<10	<0.5	3.4	<0.5	0.04
step 3rd	<1	<0.01	<1	<0.01	12	0.05	<5	<0.5	60	<0.5	<0.01	<2	<10	<0.5	3.7	<0.5	
step 4th	<1	<0.01	<1	<0.01	3	<0.01	<5	<0.5	<10	<0.5	<0.01	<2	<10	<0.5	3.3	<0.5	
step 5th	<1	<0.01	3	<0.01	<2	0.48	<5	<0.5	<10	<0.5	<0.01	<2	<10	<0.5	57.4	<0.5	
step 6th	<1	0.06	2	0.01	13	0.99	<5	<0.5	80	1.3	<0.01	<2	<10	<0.5	41.3	<0.5	
step 7th	<1	0.24	2	0.01	5	0.09	6	6.4	60	32.3	0.26	57	30	3.4	18.5	9.5	

DOI: 10.14750/ME.2021.004

BOL 7-9	**Analyzed years: 3rd** (2010 aut. - 2011 spr.); **4th** year (2011 aut. - 2012 spr.)

	Day	***0***	***7***	***14***	***21***	***28***	***35***	***42***	***49***	***56***	***64***	***71***	***76***	***87***	***94***	***101***	***108***	***115***
3rd year	***pH (-)***	2.88	3.43	3.60	3.72	3.63	3.64	3.66	3.61	3.47	3.40	3.33	3.34	3.12	3.28	3.20	3.27	3.31
	Eh (mV)	411	324	320	327	324	322	319	334	330	352	350	369	365	356	370	372	380
	TDS (mg/l)	1000	617	275	200	195	201	200	232	340	432	438	441	654	403	417	354	300
	SO_4^{2-}	712	337	215	142	160	188	166	157	278	280	317	337	259	271	260	245	241

	Day	***0***	***7***	***14***	***21***	***28***	***35***	***42***	***49***	***56***	***63***	***70***	***77***	***84***	***91***	***98***	***105***	***112***	***119***
4th year	***pH (-)***	1.89	2.27	2.54	2.57	2.47	2.48	2.50	2.54	2.49	2.48	2.51	2.53	2.5	2.76	2.72	2.66	2.53	2.50
	Eh (mV)	478	467	498	556	525	514	523	500	558	498	511	500	497	471	475	527	512	535
	TDS (mg/l)	5760	1943	806	676	762	791	715	557	739	777	697	627	704	519	435	520	620	693
	SO_4^{2-}	23410	3167	697	519	586	505	445	317	417	430	368	315	365	274	227	271	333	367

Remarks: In year 3rd on the 64th, 71st and 76th days and in year 4th on the 77th and 84th days the samplings were completed also by Dr. Ingar Walder.

O_2 content sampling in year 4th, period days 105th - 112nd				
Day	***0***	***1***	***4***	***7***
O_2 content ($^V/_V$%)	21.1	19.2	16.6	14.1

Column free volume (cm^3)	2210

Sequential Chemical Extraction (SCE) result

Element	***Ag***	***Al***	***As***	***Ba***	***Be***	***Bi***	***Ca***	***Cd***	***Co***	***Cr***	***Cu***	***Fe***	***K***	***La***	***Li***	***Mg***	***Mn***
Det. limit	2	0.01	3	1	0.5	5	0.01	1	1	1	0.5	0.01	0.01	0.5	1	0.01	2
unit	ppm	%	ppm	ppm	ppm	ppm	%	ppm	ppm	ppm	ppm	%	%	ppm	ppm	%	ppm
step 1st	<2	<0.01	<3	<1	<0.5	<5	<0.01	3	2	<1	15.8	0.02	<0.01	<0.5	<1	<0.01	21
step 2nd	<2	<0.01	5	<1	<0.5	5	<0.01	<1	<1	<1	2.8	0.03	<0.01	<0.5	<1	<0.01	2
step 3rd	<2	<0.01	25	<1	<0.5	<5	<0.01	<1	<1	2	5	0.28	<0.01	<0.5	<1	<0.01	24
step 4th	<2	0.01	<3	<1	<0.5	<5	<0.01	<1	<1	<1	<0.5	0.28	<0.01	<0.5	<1	<0.01	70
step 5th	<2	<0.01	<3	<1	<0.5	<5	0.01	1	1	<1	81.9	0.25	<0.01	<0.5	<1	<0.01	13
step 6th	2	0.03	214	4	<0.5	18	0.03	4	1	3	216	1.35	N.A.	<0.5	<1	0.01	51
step 7th	<2	3.58	6	76	1.3	<5	0.02	<1	<1	16	14.8	1.03	N.A.	22	34	0.51	31

Element	***Mo***	***Na***	***Ni***	***P***	***Pb***	***S***	***Sb***	***Sc***	***Sn***	***Sr***	***Ti***	***V***	***W***	***Y***	***Zn***	***Zr***	***CO_2***
Det. limit	1	0.01	1	0.01	2	0.01	5	0.5	10	0.5	0.01	2	10	0.5	0.5	0.5	0.01
unit	ppm	%	ppm	%	ppm	%	ppm	ppm	ppm	ppm	%	ppm	ppm	ppm	ppm	ppm	%
step 1st	<1	<0.01	2	<0.01	<2	0.04	<5	<0.5	<10	<0.5	<0.01	<2	<10	<0.5	60.7	<0.5	0.04
step 2nd	<1	<0.01	<1	<0.01	3	0.02	<5	<0.5	<10	<0.5	<0.01	<2	<10	<0.5	5	<0.5	0.04
step 3rd	<1	<0.01	<1	<0.01	6	0.02	<5	<0.5	<10	<0.5	<0.01	<2	<10	<0.5	7.5	<0.5	
step 4th	<1	<0.01	<1	<0.01	<2	<0.01	<5	<0.5	<10	<0.5	<0.01	<2	<10	<0.5	6.8	<0.5	
step 5th	<1	<0.01	3	<0.01	<2	0.35	<5	<0.5	<10	<0.5	<0.01	<2	<10	<0.5	146	<0.5	
step 6th	<1	0.06	4	0.02	9	1.25	<5	<0.5	180	2.3	<0.01	<2	<10	<0.5	224	<0.5	
step 7th	<1	0.24	3	0.01	10	0.05	<5	6.4	70	32.9	0.28	59	20	3.5	29.8	10.8	

DOI: 10.14750/ME.2021.004

HU 1-2	**Analyzed year: 4th** year (2011 aut. - 2012 spr.)

4th year	*Day*	*0*	*7*	*14*	*21*	*28*	*35*	*42*	*49*	*56*	*63*	*70*	*77*	*84*	*91*	*98*	*105*	*112*	*119*
	pH (-)	5.81	6.80	7.12	7.15	7.13	7.14	7.15	7.16	7.18	7.19	7.22	7.15	7.19	7.19	7.14	7.16	7.19	7.09
	Eh (mV)	175	227	252	327	350	339	296	307	314	316	318	346	351	329	321	291	248	261
	TDS ($^{mg}/_{l}$)	1634	1318	1206	1112	1040	996	992	968	901	943	773	864	864	749	684	659	679	732
	Alkalinity 5.4($^{mmol}/_{l}$)	0.927	0.027	0.381	0.330	0.324	0.337	0.305	0.314	0.306	0.324	0.367	0.323	0.375	0.327	0.292	0.293	0.416	0.740
	Alkalinity 4.5($^{mmol}/_{l}$)	1.073	0.127	0.482	0.430	0.419	0.438	0.405	0.410	0.402	0.436	0.549	0.437	0.494	0.437	0.402	0.408	0.515	0.879
	SO_4^{2-} ($^{mg}/_{l}$)	2390	1740	1602	1438	1310	1259	1211	1190	1080	1158	889	1031	1037	875	781	733	759	827
	Ca^{2+} ($^{mg}/_{l}$)	585	543	530	490	460	451	450	439	402	425	335	384	379	324	297	281	292	-
	Mg^{2+} ($^{mg}/_{l}$)	181	118	74	52	41.2	35.6	24.8	22.1	15.8	17.6	11.5	15.6	15.7	10.9	10.1	9.4	12.1	-

Remarks: In year 4th on the 77th and 84th days the samplings were completed also by Dr. Ingar Walder.

O_2 content sampling in year 4th, period days 105th - 112nd				
Day	***0***	***1***	***4***	***7***
O_2 content ($^{V}/_{V}$%)	21.1	19.8	17.2	16.0

Column free volume (cm^3)	2160

HU 2-4	**Analyzed year: 4th** year (2011 aut. - 2012 spr.)

4th year	*Day*	*0*	*7*	*14*	*21*	*28*	*35*	*42*	*49*	*56*	*63*	*70*	*77*	*84*	*91*	*98*	*105*	*112*	*119*
	pH (-)	5.64	6.66	7.05	7.07	7.05	7.07	7.05	7.04	7.04	7.06	7.08	6.97	6.97	6.95	6.96	6.94	6.95	6.93
	Eh (mV)	135	235	347	322	352	320	289	303	311	315	312	332	360	340	319	317	249	357
	TDS ($^{mg}/_{l}$)	1209	1007	872	760	679	653	663	591	545	661	520	546	482	484	457	440	468	477
	Alkalinity 5.4($^{mmol}/_{l}$)	0.681	0.140	0.338	0.190	0.172	0.182	0.185	0.152	0.151	0.192	0.164	0.198	0.169	0.156	0.160	0.148	0.172	0.322
	Alkalinity 4.5($^{mmol}/_{l}$)	0.882	0.244	0.431	0.280	0.245	0.262	0.267	0.232	0.231	0.289	0.266	0.296	0.263	0.250	0.257	0.241	0.262	0.429
	SO_4^{2-} ($^{mg}/_{l}$)	1627	1254	1073	891	794	726	736	652	610	754	558	608	511	504	473	454	483	479
	Ca^{2+} ($^{mg}/_{l}$)	405	342	330	284	257	249	253	223	207	260	192	223	187	180	170	163	175	-
	Mg^{2+} ($^{mg}/_{l}$)	103	97	60	44.3	36.1	31.0	22.5	22.7	19.2	20.4	12.4	12.5	11.5	13.4	9.6	10.9	8.0	-

Remarks: In year 4th on the 77th and 84th days the samplings were completed also by Dr. Ingar Walder.

O_2 content sampling in year 4th, period days 105th - 112nd				
Day	***0***	***1***	***4***	***7***
O_2 content ($^{V}/_{V}$%)	21.1	20.1	18.4	17.7

Column free volume (cm^3)	2230

HU 4-8	**Analyzed year: 4th** year (2011 aut. - 2012 spr.)

4th year	*Day*	*0*	*7*	*14*	*21*	*28*	*35*	*42*	*49*	*56*	*63*	*70*	*77*	*84*	*91*	*98*	*105*	*112*	*119*
	pH (-)	4.83	6.00	6.38	6.36	6.37	6.41	6.27	6.26	6.23	6.26	6.31	6.30	6.21	6.04	6.06	6.05	5.99	6.17
	Eh (mV)	186	240	310	218	235	240	232	243	227	236	233	265	241	234	251	242	241	242
	TDS ($^{mg}/_{l}$)	927	651	639	564	512	516	467	490	425	540	389	462	375	403	381	339	383	394
	Alkalinity 5.4($^{mmol}/_{l}$)	0.000	0.035	0.092	0.048	0.052	0.053	0.048	0.054	0.050	0.056	0.047	0.063	0.050	0.040	0.042	0.042	0.056	0.128
	Alkalinity 4.5($^{mmol}/_{l}$)	0.080	0.105	0.161	0.126	0.115	0.120	0.113	0.125	0.122	0.141	0.131	0.152	0.136	0.121	0.124	0.129	0.146	0.220
	SO_4^{2-} ($^{mg}/_{l}$)	1178	744	735	627	522	563	474	521	435	541	389	519	433	419	389	341	392	389
	Ca^{2+} ($^{mg}/_{l}$)	240	176	202	177	160	171	151	165	143	192	133	166	141	139	132	118	134	-
	Mg^{2+} ($^{mg}/_{l}$)	74	64	49.5	42.5	32.8	33.0	25.0	26.0	17.9	17.6	16.0	17.8	15.4	11.6	10.7	8.7	10.0	-

Remarks: In year 4th on the 77th and 84th days the samplings were completed also by Dr. Ingar Walder.

O_2 content sampling in year 4th, period days 105th - 112nd				
Day	***0***	***1***	***4***	***7***
O_2 content ($^{V}/_{V}$%)	21.1	20.2	18.8	18.1

Column free volume (cm^3)	2412

DOI: 10.14750/ME.2021.004

HU 8-16	**Analyzed year: 4th** year (2011 aut. - 2012 spr.)

	Day	*0*	*7*	*14*	*21*	*28*	*35*	*42*	*49*	*56*	*63*	*70*	*77*	*84*	*91*	*98*	*105*	*112*	*119*
4th year	*pH (-)*	4.77	5.22	5.63	5.55	5.62	5.61	5.63	5.51	5.55	5.49	5.35	5.12	5.09	4.68	4.60	4.36	4.56	5.33
	Eh (mV)	191	255	293	258	215	228	218	240	232	247	267	275	258	294	309	324	281	220
	TDS (mg/l)	607	488	441	323	290	343	309	287	270	343	258	267	248	249	246	221	229	247
	Alkalinity 5.4(mmol/l)	0.000	0.000	0.007	0.000	0.010	0.019	0.010	0.012	0.014	0.012	0.007	0.000	0.006	0.000	0.000	0.000	0.000	0.021
	Alkalinity 4.5(mmol/l)	0.098	0.071	0.073	0.065	0.070	0.084	0.075	0.078	0.082	0.089	0.088	0.082	0.090	0.076	0.063	0.048	0.065	0.103
	SO_4^{2-} (mg/l)	693	524	470	320	294	345	302	279	264	349	249	275	260	238	231	200	210	227
	Ca^{2+} (mg/l)	187	120	116	84	77	95	86	79	76	100	70	83	74	69	69	60	62	-
	Mg^{2+} (mg/l)	43.8	42.3	36.6	24.5	18.8	20.9	16.6	15.5	10.5	14.9	9.6	10.5	9.4	8.3	9.3	6.5	8.3	-

Remarks: In year 4th on the 77th and 84th days the samplings were completed also by Dr. Ingar Walder.

O_2 content sampling in year 4th, period days 105th - 112nd				
Day	*0*	*1*	*4*	*7*
O_2 content ($^V/_V$%)	21.1	20.4	19.0	18.6

Column free volume (cm^3)	2562

HU 16-32	**Analyzed year: 4th** year (2011 aut. - 2012 spr.)

	Day	*0*	*7*	*14*	*21*	*28*	*35*	*42*	*49*	*56*	*63*	*70*	*77*	*84*	*91*	*98*	*105*	*112*	*119*
4th year	*pH (-)*	4.58	4.53	4.83	4.83	5.03	5.13	5.04	5.01	5.01	5.14	5.05	4.81	4.57	4.53	4.54	4.45	4.43	4.23
	Eh (mV)	204	282	278	326	242	250	235	240	260	260	261	287	312	299	301	304	285	291
	TDS (mg/l)	399	381	299	245	183	220	162	167	144	184	139	167	140	151	120	121	141	151
	Alkalinity 5.4(mmol/l)	0.000	0.000	0.000	0.000	0.000	0.000	0.000	0.000	0.000	0.000	0.000	0.000	0.000	0.000	0.000	0.000	0.000	0.000
	Alkalinity 4.5(mmol/l)	0.070	0.000	0.016	0.036	0.055	0.062	0.053	0.062	0.065	0.077	0.081	0.079	0.069	0.067	0.058	0.056	0.052	0.025
	SO_4^{2-} (mg/l)	413	392	301	233	166	206	141	144	120	165	119	149	115	131	98	99	119	123
	Ca^{2+} (mg/l)	98	62	55	56	41.8	51	38.6	39.2	33.8	43.5	31.8	40.0	32.7	35.5	28.8	28.0	33.6	-
	Mg^{2+} (mg/l)	21.0	31.3	23.2	15.0	10.8	13.2	8.6	9.4	7.0	8.7	5.7	7.8	5.7	7.5	3.5	3.3	5.3	-

Remarks: In year 4th on the 77th and 84th days the samplings were completed also by Dr. Ingar Walder.

O_2 content sampling in year 4th, period days 105th - 112nd				
Day	*0*	*1*	*4*	*7*
O_2 content ($^V/_V$%)	21.1	20.6	19.5	19.0

Column free volume (cm^3)	2686